

**A Circular Economy Approach to
Multifunctional Sandwich Structures:
Polymeric Foams for
District Heating Pre-Insulated Pipes**

Doctoral Thesis

Lucía Doyle Gutiérrez
HafenCity University

Impressum

Publisher

First published 2022

HafenCity University Hamburg

Henning-Vorscherau-Platz 1, 20457 Hamburg

Contact

Email: hola@luciadoyle.com

Copyright

Lucía Doyle Gutiérrez

2022

DOI: 10.34712/142.35

A Circular Economy Approach to Multifunctional Sandwich Structures: Polymeric Foams for District Heating Pre-Insulated Pipes.

A doctoral thesis submitted to HafenCity
University Hamburg in fulfilment of the
requirements of the “Promotionsordnung der
HafenCity Universität Hamburg” for the degree of
Doktor-Ingenieur (Dr.-Ing.)

Lucía Doyle Gutiérrez



Author:

Lucia DOYLE GUTIÉRREZ

Doctoral Examination Board:

Chairperson

Prof. Irene PETERS, PhD

HafenCity University Hamburg, Germany

Supervisors

Prof. Dr.-Ing. Ingo WEIDLICH,

HafenCity University Hamburg, Germany

Prof. Ernesto DI MAIO, PhD

University of Naples Federico II, Italy

Additional Professor

Prof. Dr.-Ing. Gesa KAPTEINA

HafenCity University Hamburg, Germany

Defense Date:

5th September 2022

Composition and layout:

Abhishek SHARMA

Acknowledgements

I would like to express my deepest gratitude to Prof. Dr.-Ing. Ingo Weidlich for accepting me in his team, encouraging and supporting my ideas and believing in multidisciplinary as a true catalyser for innovation. Thank you for your dedication, insights and advice.

I'm extremely grateful to Prof. Ernesto Di Maio for accepting the co-supervision of this thesis, generously providing knowledge and expertise. Thank you for your time and guidance.

I would like to offer my special thanks to Prof. Irene Peters, PhD, for accepting to be Chairperson of the Doctoral Examination Board and to Prof. Dr.-Ing. Gesa Kapteina for accepting to be part of the examination committee. Thank you for commitment.

I am also thankful to the HafenCity University for providing the necessary framework and infrastructure for this research to take place. Special thanks to Marcus Illguth and staff from the civil engineering laboratory for the engagement, support and patience.

I would like to extend my thanks to the Hamburg Association for Energy Research (EFH) for facilitating the network and cooperation between different Universities, allowing me access to further experimental facilities and enriching my research. Particular thanks to Prof. Irina Smirnova and Xihua Hu from the Institute of Thermal Separation Processes at TUHH, Patrick Levin from the Institute of Solids Process Engineering and Particle Technology at TUHH, and Dr. Thomas Hackl from the Department of Chemistry at UHH.

Additional thanks to Dr. Rebeca Hernandez from ICTP-CSIC for the thoughtful comments and recommendations, and to Aaron Wieland for the commitment, support and flexibility.

I'd like to recognize the input of the scientific community in general: all the authors that answered my questions and reviewers who generously provided constructive critiques, ideas and their time to improve my work.

I had the pleasure of working in a great team. Thank you to Maria, Pakdad, Violeta, Sven, Stefan and Gersena for the exchange, feedback and company along this journey.

Last but not least, to my family, for the encouragement, support and inspiration.



A Circular Economy Approach to Multifunctional Sandwich Structures: Polymeric Foams for District Heating Pre - Insulated Pipes

Lucía Doyle Gutiérrez
2022

HafenCity University, Hamburg

Abstract

District heating pre-insulated pipes are a sandwich structure of material layers. Polyurethane foam bonds the medium pipe with the casing, providing an insulating function as well as a load bearing function. The high toxicity of the di-isocyanates required for its manufacturing triggers the need for a replacement. In this work, alternatives have been researched and developed considering the requirements of the circular economy. Two technology readiness levels (TRL) were covered. The higher TRL involved the evaluation of commercially available polymeric foam alternatives. Polyethylene terephthalate foam was selected, and its ageing behaviour concerning degradation sources inherent to the application was studied in detail to confirm the fulfilment of the required service life. No degradation of the mechanical properties was found after exposure to thermal cycles or hygrothermal conditions at temperatures below its glass transition, which would correspond to the scenario of groundwater ingress. The previously determined highest service temperature of 80°C was found conservative, as annealing at 100°C increases its strength, allowing this service temperature. All results suggest it is a suitable candidate for the insulation of steel medium pipes. The fast embrittlement upon exposure to hot moisture, as would occur due to permeation of the heat carrier through a plastic pipe, prevents its recommendation for this case.

The lower TRL research involved the re-evaluation of the complete sandwich assembly, from a cradle-to-cradle perspective. The foamability of polybutene-1 was explored, with the ultimate target of allowing the manufacturing of the sandwich element out of a single material, as to facilitate its recycling. Favourable grades for foaming were identified, confirming its foamability. The relationships between process parameters and the foam's microstructure were evaluated. Foams in the required size for mechanical and insulating properties characterization were successfully produced. Mechanical properties of PU from state-of-the-art flexible plastic medium pipes fall in the prediction bands obtained from the produced PB-1 foams. This provides confidence on the suitability for the application.



A Circular Economy Approach to Multifunctional Sandwich Structures: Polymeric Foams for District Heating Pre - Insulated Pipes

Lucía Doyle Gutiérrez

2022

HafenCity Universität Hamburg

Zusammenfassung

Vorgedämmte Fernwärmerohre bestehen aus mehreren Schichten unterschiedlicher Materialien. Im Standardfall verbindet ein Polyurethanschaum das Mediumrohr aus Stahl mit der Ummantelung aus Polyethylen. Der Schaum hat die Funktion der Wärmedämmung und ist für den kraftschlüssigen Verbund zwischen den Schichten zuständig. Durch die hohe Toxizität der für die Herstellung von Polyurethan erforderlichen Di-Isocyanate ist die Nachhaltigkeit des Polyurethanschaumes in Frage gestellt und es ist zukünftig wahrscheinlich ein Ersatz erforderlich. In dieser Arbeit wurde unter Berücksichtigung der Anforderungen der Kreislaufwirtschaft untersucht, welche Alternativen möglich sind. Es wurden dabei zwei unterschiedliche Stufen des technologischen Reifegrades (engl. TRL=Technology Readiness Level) abgedeckt. Auf dem höheren Reifegrad wurden kommerziell verfügbare polymere Schaumstoffalternativen bewertet. Ausgewählt wurde der Polyethylenterephthalat-Schaumstoff, dessen Alterungsverhalten im Hinblick auf anwendungsspezifische Degradationsquellen eingehend untersucht wurde. Dabei wurde keine Verschlechterung der mechanischen Eigenschaften festgestellt, nachdem der Schaum thermischen Zyklen oder hygrothermischen Lastkollektiven bei Temperaturen unterhalb des Glasübergangs ausgesetzt war. Die in der Literatur verbreitete maximale Betriebstemperatur von 80 °C erwies sich als konservativ. Es wurde festgestellt, dass durch das Glühen des Materials im Betrieb die Festigkeit erhöht wird, wodurch eine Betriebstemperatur von 100°C ermöglicht wird. Alle Ergebnisse deuten darauf hin, dass Polyethylenterephthalat ein geeigneter Kandidat für die Dämmung von Stahlmediumrohren ist. Bei Kunststoffmediumrohren ist infolge von Dampfdiffusion in die Dämmung eine schnelle Versprödung bei Einwirkung von heißer Feuchtigkeit zu erwarten. Daher kann Polyethylenterephthalat für die Dämmung von Kunststoffrohren nicht empfohlen werden.

Auf dem niedrigeren Reifegrad wurde der gesamte mehrschichtige Aufbau von Rohrleitungen für den Wärmetransport unter dem cradle-to-cradle Prinzip neu bewertet. Die Schaumherstellung von recyclebaren Polybuten-1 wurde mit dem Ziel untersucht, eine vorgedämmte Rohrleitung für den Wärmetransport aus einem einzigen Material zu ermöglichen, um Schwierigkeiten der Materialtrennung für einen geschlossenen Materialkreislauf zu umgehen. Insbesondere wurde der Druckabfall, welcher den größten Einfluss auf die Mikrostruktur des Schaums hatte, im Herstellungsprozess eingehend untersucht. Letztlich wurden Schäume hergestellt, die alle technischen Anforderungen für den Einsatz beim leitungsgebundenen Wärmetransport erfüllten. Insbesondere liegen die mechanischen Eigenschaften der Polybuten-1-Schäume in der Größenordnung des bisher üblichen Polyurethan-Schaumes für flexible Wärmerohre.



Contents

Chapter - 1	1
Introduction	1
1.1 District Heating and District Heating Pre-Insulated Pipes	1
1.2 Sustainability and the Circular Economy in Energy Infrastructure	3
1.3 Polyurethane. A sustainability hot spot	5
1.4 Definition of the Research Problem and Research Objective	6
1.5 Research questions and hypothesis	7
1.5.1 Identification of commercial polymeric foam candidates	7
1.5.2 Concept for a cradle-to-cradle pre-insulated pipe and development of the required foam	10
1.6 List of Publications	11
Chapter - 2	13
State of the Art	13
2.1 District Heating Pre-Insulated Pipes	13
2.2 Ageing of PU District heating pre-insulated pipes. Sources of Degradation	16
2.2.1 Temperature-related ageing	16
2.2.2 Cyclic Loading	18
2.2.3 Damage due to moisture	20
2.3 Foaming of polymers	22
Chapter - 3	24
Polyethylene Terephthalate Foam	24
Evaluation of its ageing behaviour	24
3.1 Introduction	24
3.2 Effects of temperature and temperature cycling on the compressive	25

behaviour of PET foam	25
3.2.1 Behaviour under temperature	25
3.2.2 Effects of thermal cycling	26
3.4 Diffusion and moisture uptake in PET foam	27
3.4 Degradation through hygrothermal exposure	29
3.5 Conclusions and main outcomes	34
Chapter - 4	35
Foaming PB-1	35
4.1 Introduction	35
4.2 Test Set-ups and methods design and validation	36
4.2.1 Autoclave for batch foaming experiments	36
4.2.4 Microstructural characterization through image analysis	40
4.3 Characterization of PB-1 – CO ₂ solutions	41
4.3.1 Sorption - desorption	42
4.4 Screening of PB-1 grades through extrusion foaming	43
4.5 Batch Foaming – Free foaming conditions	45
4.5.1 Materials and Methods	45
4.5.2 Results and Discussion	46
4.5.3 Conclusions	50
4.6 Confined foaming in molds	50
4.6.1 Materials and Methods	50
4.6.2 Results and Discussion	51
4.6.3 Conclusions	57
4.7 Conclusions and main outcomes	57
Chapter - 5	58
Conclusions	58
5.1 Main outcomes and conclusions	58

5.1.1 Scientific outcomes and conclusions	58
5.1.2 Outcomes and conclusions with regards to the insulation of district heating pipes	59
5.1.3 Outlook and future work	59
List of Figures	62
List of Tables	64
List of Abbreviations	65
List of Symbols	67
List of Annexes	69
References	70
Annex I. Validation of the Thermal Conductivity Measurements - Steady State Heat	
Flow Meter Apparatus	85
Annex II. 12 Principles of Green Engineering	89
Annex III. Publication [J1]	90
Annex IV. Publication [J2]	100
Annex V. Publication [J3]	110
Annex VI. Publication [J4]	122
Annex VII. Publication [BJ1]	146
Annex VIII. Publication [BJ2]	159
Annex IX. Publication [CP1]	172
Annex X. Publication [CP2]	180
Annex XI. Publication [CP3]	186
Annex XII. Publication [B1]	195



Chapter - 1

Introduction

The overall objective of this thesis is to identify, develop and validate polymeric foams which could replace polyurethane foam in district heating pipes. The need is motivated by the toxicity of the di-isocyanates required for its synthesis, as well as the low recyclability of the polyurethane foam, along with the medium pipe-foam-casing sandwich structure. Polyurethane foam is the state-of-the-art insulation in district heating pipes since the 1970s. The novelty of this work is that it applies Green Engineering and Cradle to Cradle principles for the selection and development of alternatives.

1.1 District Heating and District Heating Pre-Insulated Pipes

District heating (DH) is a system for the supply and distribution of heat in an urban space. Heat may be generated through different technologies, including boilers, co-generation or heat pumps, and from different sources: non-renewables such as natural gas, or renewables such as biomass, solar, geothermal or waste or surplus heat. Thermal storage may be integrated. It can serve heat for residential and commercial space heat and hot water purposes. The common element and essence of district heating systems is the network of insulated pipes connecting the heating source with the consumers. A conceptual sketch is presented in Figure 1.

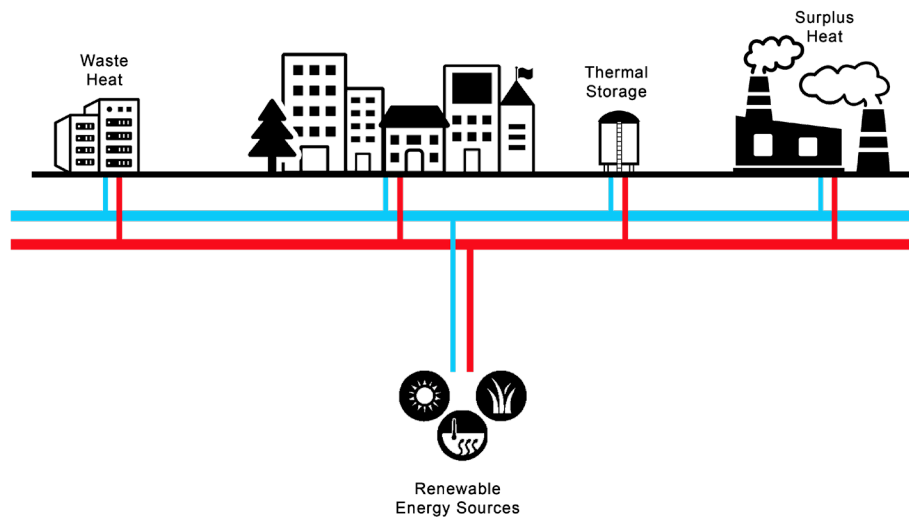


Figure 1. Conceptual sketch of a district heating network.

As a general principle, the supply line transports heat through a heat carrier from the generation plants to the consumers. The heat is transferred to the consumers through heat exchangers. The heat carrier, now colder, returns to the heating plant through the return pipe, circulating so in a closed loop.

The first example of a district heating system is often selected as the 14th century hot water distribution construction in Chaudes-Aigues in France ¹. But the development of modern district heating can be allocated to Birdsill Holly, an American hydraulic engineer, who developed the Lockport district heating in New York in 1877 ², operating with steam. He developed several patents on the topic ³⁻⁸. After this first commercial success story, many projects followed in cities such as Auburn, Detroit, ⁹ Philadelphia, ² Paris and Hamburg ¹⁰. These systems are referred to as the 1st generation DH ¹⁰, where coal-generated steam was transported and distributed through pipes in concrete ducts ¹⁰, or placed in brick or masonry tunnels, wooden tunnels, or directly buried underground ¹¹. Early descriptions of insulation for buried steam pipes include wooden tubes, asbestos or layers of asbestos and hair-felt ¹¹. The high operating temperatures and related heat losses, as well as safety issues related to steam explosions, motivated the transition to pressurized hot water as a heat carrier in the 1930s. These systems, labelled 2nd generation DH, were largely deployed in the USSR and continued to use steel pipes in concrete ducts to transport the heat carrier ¹⁰. The pipes were typically insulated on-site with mineral wool wrapped in a protective fabric layer ¹². This provided good thermal resistance as long as the mineral wool remained dry. However, if the insulation became wet, as could occur through flooding of the ducts, the thermal resistance would be significantly reduced. Deformation and sagging of the mineral wool may also occur. This contributed to the progressive energy efficiency loss of the 2nd generation DH pipes through their service life.

The 3rd generation district heating was introduced in the 1970s, fostered by the energy crisis. These systems continued to use hot water as a heat carrier but at a lower temperature than the 2nd generation ^{10,13}. A key element of this generation is the emergence and deployment of factory made pre-insulated pipes ^{10,12,13}. These pipes consisted of a steel medium pipe, a polyurethane (PU) foam layer, and a polyethylene (PE) or polyvinyl chloride (PVC) casing, being PE most common ¹³. Today, only PE is used for the casing according to the applicable standards ^{14,15}. In the United States, the Class A pre-insulated pipes were popular, which consisted of a steel medium pipe insulated by calcium silicate suspended in an oversized steel pipe providing an air gap surrounding the insulated pipe ¹³. These pipes were placed in concrete tunnels ¹³, while in Europe, polyurethane pre-insulated pipes were directly buried underground ¹⁰. Further novelties include the use of stainless steel heat exchangers in compact substations ¹⁰. The direct burial of PU pre-insulated pipes brought a great simplification and cost-efficiency to the network construction methods since it reduced the required number of compensators and U-bows ¹⁶. This is because the axial thermal expansions of the pipelines are to a certain extent counteracted by the frictional forces occurring between the bedding material and the casing ¹⁷, being the shear stresses transferred through the PU foam. The PU foam bonds the medium pipe and the casing, leading to their denomination "bonded pipes". A further advantage is the elimination of the time-consuming on-site insulation of the pipes with mineral wool and successive welding of the steel protective casing. The energy efficiency of the system is guaranteed by the superior insulating properties of the PU foam.

The concept of the 4th generation district heating (4GDH) was introduced in 2014 ¹⁰, with the ultimate target to transition to 100% renewable energy systems. In order to reach it, the concept proposes to lower the supply temperature, as to allow the integration of renewable and waste heat and lower the grid thermal losses. The networks would provide space heating, domestic hot water and cooling to renovated and non-renovated existing buildings as well as new low-energy buildings. The system should be integrated into smart energy systems and requires an institutional framework allowing for suitable planning, financing and operation of the projects. The target operating temperature of <70°C allows the use of plastic medium pipes ¹⁰. The lower heat losses and service temperature open the possibility to conceive new insulations, which is the main objective of this thesis.

The Horizon 2020 funded project FLEXYNETS¹⁸, coined the term 5th generation district heating and cooling. The main concept is the use of very low temperatures, near ambient, connected to heat pumps at the end user sites in order to boost the temperature to the required level^{19–21}. Some propose the use of a bidirectional exchange of heat and cold between connected users (prosumers), assisted by thermal storage, while other authors explore the use of a two pipe system, a hot pipe operated at comparatively low temperature and a cold pipe operated at comparatively high temperature²¹. The use of the term generation for these systems has been critiqued²², as it is not a sequential progression of the 4GDH but rather a parallel development. In any case, it is a promising technology for regions with equivalent demands of heat and cold²².

1.2 Sustainability and the Circular Economy in Energy Infrastructure

The energy supply sector is the main contributor to climate change, due to the CO₂ emissions released by the burning of fossil fuels²³. The fulfilment of international treaties to mitigate climate change, such as the Paris Agreement²⁴ requires of an energy transition, shifting from fossil fuels to renewable sources such as solar energy and wind. With heating accounting for 50% of the global energy consumption as of 2018²⁵, the decarbonization of the heating sector has a major role to play in the accomplishment of the emissions reduction committed by the European Union²⁶. District heating networks would support this transition by allowing the distribution of renewable and waste heat, in particular, that of temperature levels which can only be used for space heating.

But with the wider deployment of renewable energy technologies, as well as the arrival of the end-of-life of the first generation of renewable energy infrastructure, their sustainability is currently being questioned based on their raw material consumption and lack of recyclability or material recovery plans upon decommissioning^{27–29}. The sustainability of energy infrastructure has been traditionally understood in terms of the carbon neutrality of the fuel source. This is its use phase. But the achievement of the Paris Agreement and the Sustainable Development Goals³⁰ expand the meaning of sustainable energy to resource efficiency, where recyclability and innocuity of materials come into play, and demand an assessment of the manufacturing and end-of-life cycle phases. An example of this is the current problem of materials separation and recycling of wind blades, which may lead to their landfilling (see Figure 2). The energy transition requires as well the transition to the circular economy^{31,32}.



Figure 2. Satellite view of the landfilling of wind blades at Casper Regional Landfill in Wyoming, USA. The separation of materials in composites, used in wind blades, challenges their recycling (Image Source Google Earth. Image Date 02.09.2019).

District Heating systems have been an object of several Life Cycle Assessments (LCA). Some authors compare the environmental impacts of different heat sources or fuels for district heating systems^{33,34}, while others compare district heating with other heating technologies^{33,35,36}. The results of the heat or fuel source comparisons have been found highly sensitive to other factors such as the sources of the electricity mix^{33,34}. District heating was found to have a lower environmental impact than individual heating systems^{33,35}.

The piping network has been the object of a detailed LCA by the Chemical and Biological Engineering Department at Chalmers University, including the pipe manufacturing³⁷, network construction³⁸ and use phase³⁹. Concerning the manufacturing phase, the study concludes that the main environmental impacts arise from the manufacturing of the individual materials (i.e. steel) rather than the manufacturing of the pre-insulated pipe itself. The relative contribution of the main pre-insulated pipe materials is led by the steel pipe, followed by the PU foam and the casing, with some deviations depending on the pipe diameter and particular environmental impact considered. Included in this LCA are global warming potential, acidification potential, photo oxidation creation potential and resource depletion. Two weighting methods were used: EcoIndicator 99 and Ecoscarcity. It should be noted that the choice of impact assessment method impacts the contribution allocated to the different materials, as highlighted in the study. As for the construction phase, the environmental impacts arise mainly from the activities related to the trenches, including excavation, management of excavated materials, production and transportation of backfilling materials and asphaltting, rather than the transportation of the network components, welding of the pipes or transportation of the workers. The impacts arising from the pipe manufacturing are larger than those arising from the construction phase. The use phase was evaluated based on the heat losses of the network, related to the long-term thermal efficiency of the pre-insulated pipes. The environmental impacts arise from the extra heat generation required to compensate for the heat losses. In the study, polyurethane foam blown with cyclopentane or CO₂ was considered, which condition the thermal ageing rate of the insulation, due to differences in their diffusion coefficient. Pipes made from cyclopentane-blown PU presented 6-13% lower environmental impacts than CO₂ blown PU, due to the slower ageing of the insulating properties.

Oliver-Solá et. al. undertook an LCA of DH infrastructure, setting boundaries from a central combined heat and power plant to the heat exchangers in the dwellings⁴⁰. The objectives include the identification of the subsystems which are the main contributors to the overall environmental impact of the infrastructure and comparing DH infrastructure's environmental impact to that of the distribution network for natural gas. The chosen impact indicators were acidification, eutrophication, global warming, human toxicity, ozone layer depletion and abiotic depletion. They concluded that the main subsystem contributing to the environmental impact is the power plant. Service pipes have a higher contribution than main pipes due to their larger length. Looking into the pipes, the main contribution comes from the steel, consistent with³⁷. Other components which have a significant contribution (>15%) for at least one impact category are the trench works and the heat exchangers.

None of the cited LCAs on DH infrastructure consider the end-of-life and potential recycling of the infrastructure and materials contained. Lack of knowledge on how the decommissioning will be undertaken and available recycling technologies in the future are the main arguments why this lifecycle stage is commonly excluded. Closing the loop between a product's end of life and the manufacturing of a new one is however the key element of the circular economy.

There is no common or official definition for the circular economy. Different schools of thought and design philosophies feed into the concept, an overview of which can be found in several review papers⁴¹⁻⁴³. For this thesis, the Cradle to Cradle design philosophy⁴⁴ is selected as the main framework for circular product design. The base concept is that materials should be designed as nutrients that flow through the biological cycle or the technical cycle. These two cycles must be kept separate since mixes of the two prevent the composting of the bio-based component or the recycling of the technical component, and as long as the processes are powered by renewable energy, the number of cycles a product or process is subjected to would be irrelevant in terms of environmental impact. The concept also aims for the maximization of positive impacts, as well as tailored design for the specific niche in which the product will be used. The 12 Principles of

Green Engineering⁴⁵ concretize how to put this concept into practice⁴⁶. A strong focus on the Circular Economy, Cradle to Cradle design and the 12 Principles of Green Engineering is placed on materials, their recyclability and their innocuity to human health and the environment. Some efforts are starting to be placed in this direction by pre-insulated pipes manufacturers. Thermaflex offers Flexalen 600 flexible pre-insulated pipes⁴⁷, manufactured out of polybutene-1 service pipes, a polyolefin foam and a corrugated PE casing, which is Cradle to Cradle Certified Silver⁴⁸. The polyolefin foam is manufactured out of a metallocene PE, a flame extinguisher and a cell stabilizer⁴⁹ and manufactured as a sleeve in which the medium pipes are introduced, being so non-bonded pipes. Logstor is offering pre-insulated pipes with the casing manufactured out of recycled PE⁵⁰.

Coming back to the LCA results for the materials of pre-insulated pipes³⁷, the largest contribution was produced by the steel medium pipe. This is due to its larger mass contribution to the overall pre-insulated pipe mass, as well as the energy intensity of steel manufacturing. But when looking into innocuity to human health and recyclability, the polyurethane foam, which safeguards the energy efficiency of the networks and acts load-bearing material layer, requires hazardous raw materials which turns it into a sustainability hot spot. The environmental drawbacks of PU are described in the following section.

1.3 Polyurethane. A sustainability hot spot

Polyurethanes were first produced by Otto Bayer et. al. at IG Farben in Leverkusen, Germany, in 1937⁵¹. They are synthesized by reacting two chemicals, a polyol and a diisocyanate, in the presence of a blowing agent, and often other additives including smoke suppressants, fire retardants or surfactants⁵². Modifications in the formulation can tailor its properties, including heat resistance and thermal conductivity, resistance to chemicals, moisture and mechanical properties⁵². Over 90% of all polyurethanes are produced from either TDI (toluene diisocyanate), or MDI (methylene diphenyl diisocyanate)⁵³. TDI is mainly used in the production of low-density flexible foams and MDI for rigid foams.

While PU is chemically inert⁵⁴ and innocuous, its base material diisocyanates are toxic and present a number of health and safety hazards in varying degrees⁵⁴⁻⁵⁶ and are thought to be the trigger for a high number of cases of occupational asthma reported across all EU Member States⁵⁴⁻⁵⁶. Isocyanate wastes are classified as hazardous waste⁵⁷.

Already in 1957, cases of sensitization and strong irritation of the eyes and respiratory tract following exposure to diisocyanate have been reported in the scientific literature⁵⁵. Dernehl concluded in 1966 that "because of the irritant and sensitizing properties of the diisocyanates [...] unusual care must be taken in making the foams if undesirable toll in the illness of the workmen is to be avoided"⁵⁴.

While the market and application of PU foams based on diisocyanates has been incessantly growing in the last decades, so has the literature reporting on Human Health (HH) issues related to the use of diisocyanates. With 1.45 million exposed workers and an estimated 2900-10150 new isocyanate asthma cases per year in the EU⁵⁶, the German Federal Institute for Occupational Safety and Health (BAuA) filed a Proposal for a Restriction on diisocyanates to the European Chemicals Agency (ECHA) in 2016. The resolution of the Proposal concluded with a restriction on diisocyanates, in force since August 2020⁵⁸. This conditions the long-term viability of manufacturing PU pre-insulated pipes increases their cost and places the sustainability of the technology at stake. As included in the Restriction Proposal, and in line with the hierarchy of control measures, the very first Risk Management Measure (RMM) that should be considered is the look for substitutes for isocyanate products.

Research on non-isocyanate sources for PU production has been conducted for decades, and is still today signalized as the way to go by PU market analysts for the sector to survive⁵⁹. Figovsky et al⁶⁰ provide a patent review on non-isocyanate PU NIPU, spanning from 1954 to 2014. The chemistry of NIPU is based on the reaction between polycyclic carbonate oligomers and aliphatic or cycloaliphatic polyamines with primary amino groups⁶¹⁻⁶⁴. However, the implementation of this

route has significant shortcomings, which have disabled its commercial deployment to this date. Cited barriers are the high temperature required⁶⁰ and formation of a considerable amount⁶⁰ and toxic⁶¹ by-products formed by these reactions, need for toxic solvents⁶⁰, and lack of commercially available multifunctional cyclic carbonates⁶⁴. In a more recent review on NIPU⁶⁵, the water-based route for NIPU development is highlighted as sustainable chemistry to be pushed forwards, currently hindered by the lack of water-soluble carbonated precursors and the hydrolysis of cyclic carbonates during polymerization. Research efforts are required to improve the control of the polymerization process⁶⁵. After 70 years of research efforts, commercial manufacturing of NIPU has still not taken off, which questions the feasibility of this route.

The manufacturing phase of PU is thus hazardous and does not comply with the Circular Economy or Cradle to Cradle precepts. The end-of-life phase of PU presents hurdles as well.

The large quantities of PU foams consumed worldwide, and current restrictions on landfilling have motivated research on valorization and recycling options for PU waste⁵³. Thermo-chemical processes towards energy recovery are an important valorization pathway^{66,67} and may include incineration or decomposition by pyrolysis or hydrogenation and the combustion of the products. With a service life of 30-50 years, the composition of PU insulating foams retrieved is usually unknown, but will contain flame retardants, and often chlorofluorocarbons (CFCs) used in the past as blowing agents⁶⁶, limiting their re-use possibilities due to toxicity and ozone depletion risks. Hence, only combustion in an industrial incinerator with a state-of-the-art flue gas cleaning system complies with the need of eliminating the PU, the ozone-depleting substances as well as the fire retardants. PU has a calorific value of the same order of magnitude as coal^{68,66}. However, because of its low density, an upper limit of 2% weight is recommended for foam addition to the municipal waste mix in order to avoid problems in the combustor⁶⁶. This is however against the Circular Economy principles, which require materials to be brought back to the economy,

Alternatively, mechanical and chemical methods are proposed in the literature^{68,69}. Mechanical methods involve shredding or grinding the PU foams and then rebinding, adhesive pressing, compression molding them or their use as filler. Rebinding and adhesive pressing involve the use of diisocyanates as a binder, with the HH impacts mentioned already. Compression molding applies only to known PU waste composition as they have different conditions for molding, limiting its application.

Applications for the resulting materials include sports mats, cushioning, carpet underlay⁷⁰, but not the technical applications with key thermal and mechanical applications where PU presents its major advantages like insulation, falling into the category of down-cycling, and as mentioned, limited to the case of foams with fully known composition, which is rarely the case. The use of PU wastes as filler, in PU formulations or other construction materials i.e concrete, is reported as possible⁷¹.

Research on chemical recycling is gaining momentum^{72,73}. Alcoholysis, hydrolysis, aminolysis, glycolysis and phosphate methods have been proposed^{53,68,74}, being glycolysis the most widely used⁷⁰. Shortcomings of these methods are the involved high technical difficulty and purification costs, which compromise the industrial viability of the processes^{53,68}.

Due to the relevance of the PU sector within the plastics sector and concern on fossil raw material use, the search for bio-based alternatives has also taken place for polyurethane foams. Extensive research on the synthesis and use of polyols derived from vegetable oils such as palm, rapeseed, soybean and linseed for the production of polyurethane foams is well described in⁷⁵. The use of industrial wastes, such as crude glycerol, as substituents for polyols, is being explored. This tackles the polyol, but the use of diisocyanates still remains a burden.

1.4 Definition of the Research Problem and Research Objective

The toxicity of the di-isocyanates and the in-force restriction on their use questions the viability of the manufacturing of PU pre-insulated pipes long term, as well as the sustainability of the related infrastructure. The large deployment of DH infrastructure required by the energy transition

cannot be conceived with 2nd Generation piping technology. There is a need for research and development on alternative polymeric foams which could replace PU in DH pre-insulated pipes. They should be conceptually designed out of innocuous and recyclable materials and a safe manufacturing process.

The aim of this doctoral thesis is to develop or identify and validate polymeric foams which fulfill the technical requirements of DH pre-insulated pipes in terms of insulating properties, mechanical properties and service life, and are as well selected and conceptualized based on non-toxicity and full recyclability criteria, in line with the cradle-to-cradle design philosophy and circular economy.

1.5 Research questions and hypothesis

The overall Research Objective of this thesis can be undertaken from two angles:

- 1) Identify commercially available polymeric foams which could replace the PU foam layer and validate their fulfilment of the technical and sustainability criteria, providing a high technology readiness level (TRL) solution.
- 2) Examine the complete pre-insulated pipe sandwich structure from the cradle-to-cradle design framework, developing a polymeric foam which positively contributes to the recyclability, environmental and health and safety impacts of the assembly. This provides a low TRL proof-of concept solution.

These two research lines were followed during this doctoral thesis. During the exploratory research ⁷⁶ conducted as preparatory work, commercial polymeric foams were screened to provide candidates for research line 1, and a concept was drafted for research line two. Different research questions arise for each of them, which are described in the following sections.

1.5.1 Identification of commercial polymeric foam candidates

Common polymeric foams commercially available include polyurethane (PU), polystyrene (PS), polyethylene (PE), poly(vinyl chloride) (PVC) and polycarbonate (PC)^{77,78,53}, although the foaming of commodity polymers like polyethylene terephthalate (PET)^{79–82} or biodegradable polymers⁸³ lead by poly lactic acid (PLA)⁸⁴ have recently caught some attention.

These polymeric foams were benchmarked against the technical and sustainability criteria listed in Table 1.

Table 1. Criteria Required

<i>Technical Criteria</i>	<i>Minimum Value</i>
Service Temperature	≥ 80°C
Service Life	30 years
Thermal Conductivity	< 0.03 W/m ² K
Compressive Strength	1.3 MPa
<i>Sustainability Criteria</i>	
Health innocuity	100 %
Recyclability	100 %

There are different levels of recyclability in terms of process complexity and retainment of the product integrity and economic value. Recycling requiring minimal intervention is of best advantage. This is illustrated by Walter Stahler's Inertia Principle⁸⁵: "do not repair what is not broken, do not remanufacture something that can be repaired, do not recycle a product that can be remanufactured. Replace or treat only the smallest possible part in order to maintain the

existing economic value of the technical system". Although chemical recycling is possible for some thermoset plastics, the lowest level of recycling is aimed for in this thesis, as to minimize the environmental cost of the processes required to recover the material. Therefore, as to fulfil the recyclability criteria only thermoplastics are considered.

The results of the benchmark are summarized in Table 2.

Table 2. Benchmark of common commercial polymeric foams

Polymer	Technical Criteria	Health Innocuity	Recyclability
PS	No (thermal conductivity ^{86,87})	Residual styrene controversial ⁸⁸⁻⁹⁰	Yes ⁹¹
PE	No (thermal conductivity ⁸⁷)	Yes ⁹²	Most PE foams are cross linked ^{93,94} , which would be non-recyclable
PVC	No (service T ⁹⁵)	Controversial (dioxins ⁹⁶⁻⁹⁸ , organochlorines ⁹⁹ , phthalates ⁹⁸ , stabilizers ¹⁰⁰)	Yes ¹⁰¹
PC	Thermal conductivity unsure ^{102,103}	No (contains bisphenol A ¹⁰⁴)	Yes ¹⁰⁵
PET	Yes ^{106,107}	Yes ^{108,109}	Yes ¹¹⁰
PLA	unsure	Yes ^{111,112}	Yes ⁸⁴

From the conducted benchmark, PET and PLA obtained a better score and were evaluated in more detail.

Poly(lactic acid) (PLA) is a thermoplastic aliphatic polyester. It is a bio-based polymer derived from corn starch or sugarcane, as well as bio-degradable. It is the best-developed commercially available biopolymer ¹¹³, manufactured at low cost and in large quantities ¹¹⁴ in the form of bead foams, such as Biofoam ¹¹⁵. Extruded PLA is not yet mass produced. PLA has been reported as challenging to foam, with shortcomings including low melt strength ⁸⁴, slow crystallization kinetics⁸⁴, low toughness ⁸⁴, poor processability ⁸⁴, formability and foamability ⁸⁴, brittleness ⁸⁴, and low service temperature ⁸⁴. Substantial research is currently ongoing to overcome these challenges, an overview of which can be found in ⁸⁴. Still, PLA foam has been identified as a promising replacement for PS foams by several authors ^{113,116}. A further positive environmental impact, in line with Green Engineering Principle 9 ⁴⁵, is the PLA foam's intrinsic infrared absorbing characteristics, which arise from the ester group in the PLA molecular chain. This makes this polymer matrix a good candidate for insulation applications ¹¹³. If the service temperature of PLA foam could match the DH requirements was found uncertain. The glass transition temperature (T_g) of polymers marks the transition between the glassy to the rubbery state and is used as an indication of its highest service temperature ^{117,118}. The T_g of PLA is around 60°C ⁸⁴, which is below the required service temperature (see Table 1). However, it has been reported that PLA foams have the potential to be used above the T_g ⁸⁴, since higher crystallinity levels are reached due to the foaming process, which preserves the material's stiffness above its T_g ¹¹⁷.

Which is then the service temperature of PLA foams? This research question was experimentally evaluated with PLA bead foams, and presented in [CP1] (see section 1.6. for the full reference).

Molded expanded bead PLA foam, provided by BEWiSynbra, was used for this study. Samples were tested for compression in a universal testing machine at a constant strain rate of 2 mm/s, at 22°C, 55°C, 65°C, and 75°C. A batch of samples was tested after 2h temperature conditioning and a second batch after 48 h temperature conditioning. No difference in behavior was found, indicating no thermal crystallization occurs and no impact on the duration of the thermal conditioning. As expected for a thermoplastic, compression strength and E modulus steadily decreased with the testing temperature. However, no sudden drop in properties was observed around the T_g . Nevertheless, the mechanical properties degradation with temperature was significant. Additional drawbacks include (i) the fact that bead foams are not suitable for DH pipes, since their density and therefore mechanical properties are lower than required, and extruded PLA foam was not found

available, and (ii) fulfillment of the service life is a further research question, but its biodegradable nature combined with exposure to heat and moisture as in buried district heating pipes places it as unlikely. Because of this, the hypothesis of PLA foam as a suitable replacement for PU was discarded at an early stage.

Polyethylene terephthalate (PET) is a semi-aromatic thermoplastic polyester. PET is commonly produced through two routes: (i) the esterification reaction between terephthalic acid and ethylene glycol, yielding water as a byproduct, or (ii) the transesterification reaction between ethylene glycol and dimethyl terephthalate, producing methanol as a byproduct¹¹⁰. The widespread use of PET in other applications such as packaging opens up new possibilities of cascading use of this polymer, where practice in recycling is already in place, and would contribute to a broad consecution of Green Engineering Principle 10⁴⁵ on the macro scale. Based on its resin properties, PET is anticipated to present improved mechanical and thermal performance than polystyrene foam and higher chemical and flame resistance¹¹⁹, leading to a reduction in additives requirements. Foaming PET has been found challenging due to its low melt strength^{81,82,120}. This challenge has been overcome by the use of the breaker plate in the extruder die^{121,122}. With this manufacturing method, the foam is extruded through a breaker plate instead of a slit die, producing several individual foam strands which are then pressed together to produce a foam sheet¹²². This is represented in Figure 3.

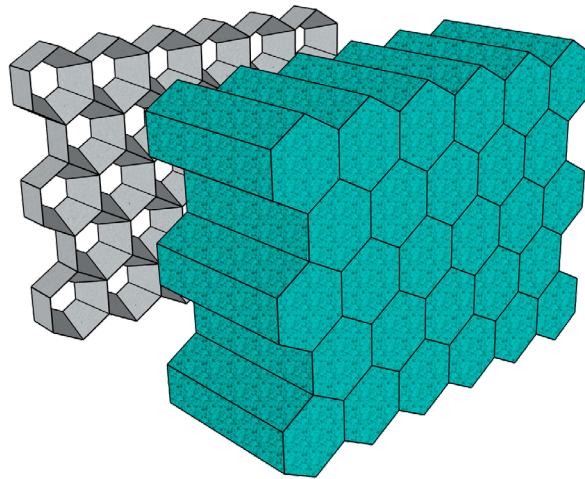


Figure 3. Representation of collided PET foam strands exiting a breaker plate.

The use of PET foam as a replacement for PU foam in district heating pipes has been explored by previous workers.

Sara Mangs studied the long term insulating properties of PET vs PU foam¹⁰⁷ by studying the transport of blowing agent gases out of the foams, and of air into the foam. The thermal conductivity of a foam (λ_{foam}) is the sum of the thermal conductivity due to conduction in the polymer matrix (λ_{pol}), the thermal conductivity due to conduction in the gas (λ_{gas}) and the thermal conductivity due to radiation (λ_{rad}). The contribution of convection is reported to only occur when the cell size exceeds a few millimeters^{75,123,124} and therefore typically disregarded, leading to:

$$\lambda_{\text{foam}} = \lambda_{\text{gas}} + \lambda_{\text{pol}} + \lambda_{\text{rad}} \quad (1)$$

Over time, the blowing agent gas diffuses out of the foam and ambient air diffuses in. The thermal conductivity of air is higher than that of typical blowing agents. As the composition of the cell gas changes over time, so does the thermal conductivity of the foam.

The effective diffusion coefficients of CO_2 , O_2 and N_2 are lower in PET foam than in PUR foam at the studied temperatures in the range of 23-90 °C¹⁰⁷. The calculated ageing of the PET foam board was circa 10 times slower than that of the PUR foam board. The initial thermal conductivity of commercial PET foam with a density of 80 kg/m³ is stated as $\lambda = 0.027 \text{ W/mK}$ ¹²⁵ which is the same

as that of PU in bonded pipes¹⁴.

If the insulating properties ageing of PET is slower than PU, the long-term energy efficiency and hence the environmental impact of the use phase of PET – insulated DH networks will be better, and further addition of diffusion barriers would not be necessary.

The IEA project Annex VI¹⁰⁶ also evaluated PET foam as a replacement for PU foam in DH pipes. The mechanical behaviour of the PET foam was evaluated based on EN 253¹⁴, with tests including compressive strength, water permeability and water resistance, water absorption, creep behaviour, bending properties and insulation performance. The study concluded that PET is a promising candidate for the replacement of PU in district heating pipes, for low temperature networks. The service temperature upper limit was designated at 80°C, coinciding with the glass transition temperature of PET.

Despite these promising reports, a decade has gone past without PET foam insulated pipes coming into the market. PET foam itself was a novel product when the cited studies were undertaken, and foam prototypes were used. PET foam boards are a commercial product today, and improvements such as the reduction of the cell size have been achieved.

An identified knowledge gap is the ageing behaviour of PET foam. This knowledge is fundamental for service life predictions, without which materials and components cannot be reliably introduced into infrastructure. This knowledge gap is addressed in the present work, constituting research line 1. Degradation sources particular to district heating pipes are analysed, and an experimental program was designed to assess their impact on the PET foam. The obtained results are presented in Chapter 3 and the related publications [J1], [J2] and [CP1] (see section 1.6 for the full references).

1.5.2 Concept for a cradle-to-cradle pre-insulated pipe and development of the required foam

As mentioned in section 1.1., district heating pipes are a sandwich assembly of different material layers. Layer separation is always a hurdle toward recycling. While the success of research line 1 would circumvent the health and safety issues and poor recyclability of PU foam, the difficulty of material layer separation would still remain.

Plastic medium pipes have emerged in the market for their use in low-temperature networks. Crosslinked polyethylene (PEX) or Polybutylene (PB-1) are used for their manufacturing^{126,127}. The cross links in PEX make it a thermoset. PB-1 however, is a recyclable thermoplastic and non-toxic¹²⁸.

Polybutylene (also known as polybutene-1 and poly(1-butene) is a polyolefin produced by the polymerisation of 1-butene using supported Ziegler–Natta catalysts¹²⁹. It is semi-crystalline, linear, isotactic and of high molecular weight. PB-1 pipes can be used up to an operating temperature of 90°C, according to ISO 15876¹³⁰. If PB-1 could be foamed, an insulated pipe could be produced out of a single recyclable material, eliminating the layer separation problem, and reaching the highest level of circular product design.

PB-1 presents useful properties for the application, such as a high heat-deflection temperature¹²⁷, contributing to the achievement of the required service temperature, low coefficient of thermal expansion, stress cracking resistance and excellent creep resistance¹⁰⁵, which could reduce degradation due to fatigue or material ratcheting, and low thermal conductivity of 0.114 W/mK¹³¹, advantageous for the production of an insulation material. This excellent insulating capacity of the polymer could counterbalance the use of environmentally friendlier and inert blowing agents such as CO₂, which have a higher thermal conductivity than the flammable cyclopentane currently used in PU foam for DH. Unlike other polyolefins, PB-1 is reported to have high melt strength and strain harden¹⁰⁵, properties frequently cited as required for foaming^{78,81,82,84,120,132–134}.

So far, no evidence of the evaluation of the foamability of PB-1 could be identified. Therefore, the main research question of this research line would be *can PB-1 be foamed, and if yes, under which conditions?* The results obtained are presented in Chapter 4 and partly in the related publications [J3], [CP2] and [B1].

1.6 List of Publications

This work corresponds to a cumulative doctoral thesis. Outcomes of the conducted research have been published in several peer reviewed Journals and Conference Proceedings, as well as disseminated in Technical Magazines, Workshops and Seminars. This thesis also includes research which has not yet been published at the time of submission.

The list of publications and oral contributions are listed below. The author's contribution is stated in each paper and confirmed by co-Authors in Annex I.

Journal Publications

- [J1] Doyle, L., & Weidlich, I. (2022a). Hydrolytic degradation of closed cell Polyethylene terephthalate foams. The role of the mobile amorphous phase in the ductile-brittle transition. *Polymer Degradation and Stability*, 110022. <https://doi.org/10.1016/j.polymdegradstab.2022.110022>
- [J2] Doyle, L., & Weidlich, I. (2022b). Moisture uptake and effects of hygrothermal exposure on closed-cell semicrystalline polyethylene terephthalate foam. *Polymer Degradation and Stability*, 202, 110009. <https://doi.org/10.1016/j.polymdegradstab.2022.110009>
- [J3] Doyle, L. (2021). Extrusion foaming behavior of polybutene-1. Toward single-material multifunctional sandwich structures. *Journal of Applied Polymer Science*, 51816. <https://doi.org/10.1002/app.51816>
- [J4] Doyle, L., Weidlich, I., & Di Maio, E. (2022). Developing Insulating Polymeric Foams: Strategies and Research Needs from a Circular Economy Perspective. *Materials (Basel, Switzerland)*, 15(18), 6212. <https://doi.org/10.3390/ma15186212>

Journal Publications – Background on state-of the art DH pre-insulated pipes

- [BJ1] Doyle, L., & Weidlich, I. (2021). Effects of Thermal and Mechanical Cyclic Loads on polyurethane Pre-Insulated Pipes // Effects of thermal and mechanical cyclic loads on polyurethane pre-insulated pipes. *Fatigue and Fracture of Engineering Materials & Structures*, 44(1), 156–168. <https://doi.org/10.1111/ffe.13347>
- [BJ2] Doyle, L., Weidlich, I., & Illguth, M. (2019). Anisotropy in Polyurethane Pre-Insulated Pipes. *Polymers*, 11(12). <https://doi.org/10.3390/polym11122074>

Conference Proceedings

- [CP1] Doyle, L., & Weidlich, I. (2021). Sustainable insulation for sustainable DHC. *Energy Reports*, 7, 150–157. <https://doi.org/10.1016/j.egy.2021.08.161>
- [CP2] Doyle, L., & Weidlich, I. (2020). Recyclable Insulating Foams for High Temperature Applications. In *Proceedings of The First International Conference on Green Polymer Materials 2020* (p. 7200). <https://doi.org/10.3390/CGPM2020-072200>
- [CP3] Doyle, L., & Weidlich, I. (2019). Mechanical Behaviour of Polylactic Acid Foam as Insulation Under Increasing Temperature. *Environmental and Climate Technologies*, 23(3), 202–210. <https://doi.org/10.2478/rtuect-2019-0090>

Book Chapters

- [B1] Doyle, L. (2022), *Determination of the melting point depression of PB-1-CO₂ solutions through image analysis*, In Technical Infrastructure management. Insights. HafenCity Universität Hamburg. <https://doi.org/10.34712/142.26>

Dissemination in Technical Magazines

Doyle, Lucía; Weidlich, Ingo (2022): Kreislaufwirtschaft für die Fernwärme durch eine nachhaltige Dämmung (Circular economy for district heating through sustainable insulation). In *bbr Leitungsbau | Brunnenbau | Geothermie* Vol. 03, 73. Jahrgang, ISSN 1611-1478, pp-20-23

Weidlich, I., Peters, I., Dochev, I. Pourbozorgi Langroudi, P. and Doyle, L. (2021), "Fernwärmeforschung an der HafenCity Universität- vom Hamburger Wärmekataster bis zum innovativen Leitungsbau. (District heating research at HafenCity University- from the Hamburg heat register to innovative pipeline construction.)", *bbr Leitungsbau | Brunnenbau | Geothermie*, Vol. 02 ISSN 1611-1478, pp. 24–27

Doyle, Lucía; Weidlich, Ingo (2020): Untersuchung zur Anisotropie gedämmter Rohre für die Wärmeund Kälteverteilung (Investigation into the anisotropy of insulated pipes for heat and cold distribution). In *Euroheat&Power* 6 (ISSN 0949-166X – D 9790F), pp. 49–52

Oral Presentations in Workshops and Seminars

- 21.06.2022 The use of diisocyanates required for polyurethane manufacturing has been restricted. Which insulation will district heating pipes use? Presentation upon collection of 3rd Student Award. Euroheat & Power Conference (Brussels, Belgium).
- 09.05.2022 Hydrolytic degradation of closed cell PET foams. Meeting of the Group Specialized in Polymers of the Spanish Royal Society of Chemistry and Spanish Royal Society of Physics (San Sebastián, Spain).
- 26.10.2021 Hygrothermal ageing of closed cell PET foam. 5th Young Polymer Scientists Seminar (Madrid, Spain)
- 08.06.2021 Insulated District Heating Pipes for the Circular Economy. PhD Researchers Day, HafenCity University Hamburg. Online.
- 28.04.2021 Rohrisolierung für die Kreislaufwirtschaft. (Pipe insulation for the circular economy). Hamburg Energieforschungskolloquium. Online.
- 29.11.2019 Insulated district heating pipes for the circular economy. Researchers meeting HafenCity University-Westküste University of Applied Sciences. Hamburg (Germany)
- 29.10.2019 Developing Insulating Foams for the Circular Economy. 4th Young Polymer Scientists Seminar. Madrid (Spain)
- 09.10.2019 Isolierung, immer nachhaltig? Entwicklung eines C2C-Isolierschaums. (Insulation, always sustainable? Development of a C2C insulation foam.) Cradle-to-Cradle Regional Group Hamburg meeting. Hamburg (Germany)

Chapter - 2

State of the Art

In this chapter, the state of the art of pre-insulated pipes is presented and described. Current knowledge of ageing and sources of damage to district heating pre-insulated pipes, with a focus on the foam, is further reviewed. Literature data were expanded with experimental studies on the cellular microstructure, compressive behaviour and thermal cycling ageing of PU pre-insulated pipes conducted in parallel to the focus of this thesis, conforming to publications [BJ1] and [BJ2]. This served as starting point and benchmark for the comparison between PU and replacement candidate PET in research line 1.

Lastly, the state of the art in polymer foaming was the object of an extensive literature review. The literature was screened and cross checked with the cradle to cradle design framework⁴⁴ and Green Principles of Green Engineering⁴⁵ in order to identify research needs and possible strategies for polymeric foam development compatible with the Circular Economy. This critical review is presented in publication [J4], and served as a starting point for the design of the research plan for research line 2.

2.1 District Heating Pre-Insulated Pipes

As introduced, the traditional and most common pre-insulated bonded pipes are composed of a steel medium pipe, a PU foam layer and a PE casing. These pipes are designed for a continuous operating temperature of up to 120°C and pressure of up to 25 bar according to EN 253¹⁴. Bonded pipes are traditionally batch manufactured. The service pipe and the casing are independently manufactured. Once placed concentric to one another, the PU is injected between the service pipe and the casing^{135,136}.



Figure 4. From left to right: DH DN40 flexible plastic medium pipe and corrugated casing, DN40 flexible plastic medium pipe with smooth casing, and bonded steel medium pipes DN20, DN100 and DN200.

Nowadays, continuous manufacturing processes for pre-insulated rigid bonded pipes have been developed, which would involve the casting of the insulation onto the service pipe in a moving mold, and the consecutive extrusion of the casing onto the insulation (axial conti process)¹³⁵, or the spraying of the PU foam around the service pipe, with the consecutive extrusion of the casing onto the insulation in a spiral movement (spiral conti process)¹³⁵. The resulting pipes from the three manufacturing processes have different thermal conductivities, stated as 0.027 W/mK for the traditionally manufactured, 0.025 W/mK for the spiral conti pipes, and 0.023 W/mK for the axial conti pipes¹³⁵. The details explaining the differences in thermal conductivity are not disclosed. The author assumes it is related to a different formulation of the PU. The individual pipes are welded together on-site. The joints, whether with shrink sleeves or electrosleeves, are insulated with PU foamed on-site¹³⁷ or by factory cast joints.

During the course of this thesis, the cellular structure and compressive behaviour of the PU foam in bonded pipes of different diameters has been studied [BJ2]. Both were found highly anisotropic, significantly higher than that typically found in PU foam sheets. The cell shape anisotropy ratio is defined as the ratio of the largest to the shortest cell diameter. The cell shape anisotropy is due to the viscous forces acting between the mold walls and the foaming melt during the volume expansion, which produces an elongation of the cells⁸⁶. Cell shape anisotropy leads to anisotropic mechanical behaviour. This knowledge is relevant since pre-insulated pipes are subjected to multiaxial loading, as will be described in more detail in section 2.2. Furthermore, cell anisotropy has been found to produce anisotropic cell thermal expansion in PU foam subjected to heat, and this deformation is only partly recovered¹³⁸ which could lead to alteration of the mechanical behaviour. The short distance between the foaming mold walls, in this case, the annular section between the medium pipe and the pipe casing, leads to high cell anisotropy ratios, with obtained values ranging between 1.8 to 2.6 depending on the pipe diameter, versus the typical values of 1.3 found in foam sheets⁸⁶. The cells present different dimensions in the three orthogonal directions, hence are orthotropic.

Flexible pipes have later emerged in the market. Their development started in the second half of the 80s with the use of plastic pipes as medium pipes, manufactured out of PEX or PB-1¹³⁹, which are still today the materials of choice according to standard EN 15632¹⁴⁰. The main advantage of PB-1 is that it is weldable^{127,139} and recyclable. PEX pipes are hardly weldable and require mechanical jointing elements such as press fittings, which posed some initial concerns about their tightness and durability¹³⁹. However positive experiences relaxed these concerns¹³⁹. Initial technical characteristics included a pipe diameter limit of DN100, and maximum operating temperatures and pressures of 90°C and 5 bars respectively¹³⁹. This initially confined it to household applications¹³⁹. However, these pipes offered a cost advantage of up to 40% depending on the country, mainly arising from the fast and flexible method of laying, despite being the material cost for the plastic pipes higher than that of steel¹³⁹. Since no welding between pipes is required, plastic pipes can be installed in narrower trenches, which can be designed to circumvent obstacles. The corrosion resistance of plastic pipes, which present no risk of rupture in case of a leak, was seen as a significant advantage¹³⁹. Further, plastic medium pipes do not require compensators, despite plastics having a larger coefficient of thermal expansion than steel¹⁴¹. This is due to their lower E modulus; thus, the thermal expansion is absorbed by elastic deformation¹⁴¹. Open questions requiring research during the incipient times of flexible plastic pipes included the creep resistance of the plastics at the DH operating temperature, the oxygen diffusion through the pipes and into the heat carrier (hot water), which could corrode circuit elements such as the heat exchangers, and water vapor diffusion from the heat carrier through the plastic pipe into the insulating foam, increasing its thermal conductivity¹³⁹. In general terms, the lack of knowledge on their long-term behaviour was the main barrier to uptake by DH project developers¹³⁹.

Lifetime predictions for the plastic medium pipes were available by 1999, when the IEA-DHC Annex V report was published¹⁴¹. These first predictions were based on the 10 years operation data together with accelerated ageing tests at different pressures and temperatures. Based on Arrhenius relationships between the accelerated ageing tests and operating temperatures, as well as the Miners rule to account for operating temperature fluctuations between summer and winter, a calculated lifetime prediction of >100 years for PEX pipes and > 60 years for PB-1 is provided,

for networks operating at 90°C in winter and 70°C in summer ¹⁴¹. These lifetime prediction data provided the necessary confidence for market uptake. More recent reports on the subject could not be found, which can be interpreted as no problems have been identified requiring research.

Some manufacturers introduced diffusion barriers, such as ethylene vinyl alcohol (EVOH) or aluminium foil layers in the early development stages, though the durability of the EVOH coating and possible debonding of the aluminium foil were still not validated ¹³⁹. Today the EVOH coating as an oxygen permeation barrier is state-of-the-art and generally included by all manufacturers ^{126,141}. The IEA-DHC Annex V report refers to laboratory results finding delamination of metal layers placed as diffusion barriers, shortening the service life of such sandwich systems, though the reference from the original source is not provided in the text. Results from permeation experiments of DH plastic pipes with and without EVOH coatings conducted in different laboratories ^{142–145} showed that the EVOH barrier reduces the oxygen permeability between a factor of 10 and 2000, depending on the temperature, pipe diameter and pipe model. The next question was if the lower O₂ permeability of EVOH coated plastic pipes is low enough to allow the mixture of steel and plastic medium pipes in the same network, with low corrosion risk for the steel pipes. The research concluded that it is safe to combine both pipe types in the same network, with different thresholds stated in different countries. In Germany, the threshold of at least 30% of the total surfaces being steel was given ¹⁴², and a lower amount of steel surfaces was required based on Scandinavian data, which would be as low as 10 % ¹⁴⁶.

The insulation of the early models of flexible plastic pipes was provided by PU foam, PEX foam or glass wool, depending on the manufacturer, but provided as sleeves or blankets, being in all cases non-bonded pipes ¹³⁹. While this variety of insulation material by different pipe manufacturers coexisted during the first decade of flexible plastic pipes, the appearance of the first models of flexible plastic medium- PU bonded pipes is reported to have appeared in this period ¹⁴¹.

PU bonded flexible pipes are state-of-the-art at present times. They are manufactured in a continuous process, in which the PU is poured into a moving casting mold, and flows around the moving pipe. The PE outer casing is then extruded in place ¹⁴⁷. Several models exist in the market. They can be found with corrugated and smooth casing. Different degrees of flexibility are attained through different formulations of the PU foam. As for the medium pipe, flexible pipes are now not only manufactured with plastic medium pipes, but also of steel, or copper ¹²⁶. State-of-the-art flexible plastic medium pipes are designed for a continuous operating temperature of 80°C and 10 bars, according to EN 15632 ¹⁴⁰, while flexible steel medium pipes allow an operating temperature of up to 120°C ¹⁴⁸.

Anisotropy and compressive behaviour of the PU foam of flexible plastic medium pipes with smooth and corrugated casing were studied and the results are reported in [BJ2]. Flexible pipes presented cell shape anisotropy of 1.7, lower than the bonded pipes, due to the continuous manufacturing process. Interestingly, while the cell anisotropy ratio was equivalent for both flexible pipe models, the E modulus ratio, defined as the ratio between the E modulus obtained when testing in the axial direction of the pipe (foam rise) and radial direction of the pipe, was not affected in the same way. This was allocated to differences in cell size and cell size variability found between the two flexible pipe models studied.

As for the development of PU foam itself, for either bonded or flexible pipes, one aspect of development during the last decades has been the change in blowing agents, common for all PU foam applications. The commonly used CFCs, favored by their soluble, volatile and non-toxic nature ¹⁴⁹, were called to be phased out by the Montreal Protocol ¹⁵⁰ due to their ozone depleting nature.

This caused a shift to the transition replacement hydrochlorofluorocarbons (HCFCs), and later to hydrofluorocarbons (HFCs). These are now called to phase out due to their high global warming potential (GWP) by the Kigali Amendment to the Montreal Protocol ¹⁵¹ in force from 1st Jan 2019. Hydrocarbons (HCs) and inert gases (N₂, CO₂) have also been used ¹⁴⁹. The phase-out programme established by the Montreal Protocol is represented in Figure 5.

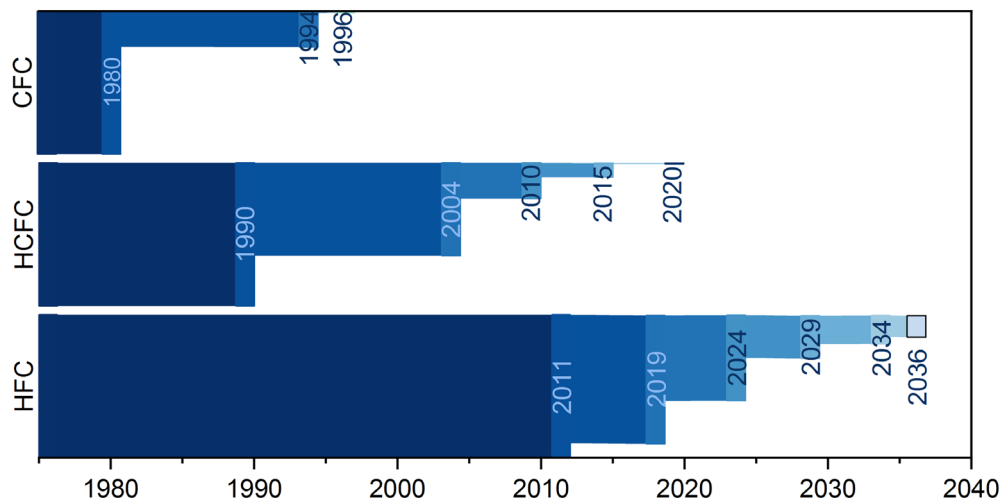


Figure 5. Sankey diagram representing the Montreal Protocol and Kigali amendment agreed blowing agents phase out programme for non-article 5 (industrialized) countries.

Within DH, the scientific evaluation of the different blowing agent candidates was focused on the diffusion of the gases through the cellular structure, in order to assess the long-term insulation performance. Initial interest was placed on CO_2 blown PU^{152,153}. HFC-365 mfc has been evaluated¹⁰⁷, as well as cyclopentane^{154,155}. Currently, all PU foam in DH pipes is cyclopentane blown, since it has a lower thermal conductivity than CO_2 , but mainly because CO_2 and other inert gases have a higher diffusivity than hydrocarbons such as pentane¹⁵⁶, leading to a worse long term insulating performance due to faster diffusion out of the foam and diffusion of ambient air into the foam, which has a higher thermal conductivity: $\lambda_{\text{cyclopentane}} = 0.0110 \text{ W/mK}$, $\lambda_{\text{CO}_2} = 0.0165 \text{ W/mK}$ and $\lambda_{\text{N}_2} = 0.0258 \text{ W/mK}$, as compiled in¹⁵⁷.

In order to hinder the thermal ageing of the foam, some manufacturers have introduced an aluminium layer as diffusion barrier¹⁵⁸, blocking the mass transport between the cell gasses and the ambient air.

As for the formulation of the PU itself, evaluation by the author has shown that different PU foam with different characteristics and properties co-exist in the different models of DH pipes [BJ2]. However, since these developments are undertaken by the industry, scientific literature reporting the advancements has not been found available.

2.2 Ageing of PU District heating pre-insulated pipes. Sources of Degradation

As introduced, the bond function of the PU foam in DH pipes has brought great simplifications and related cost-reductions to the piping laying methods. DH system's start-ups and shut downs and network operating temperature changes driven by changes in heat demand and ambient temperature lead to thermal expansions and contractions of the piping networks. These are partially counteracted by the friction between the surrounding soil and the casing, with axial shear stresses transmitted through the PU foam bond. Additionally, the surrounding soil produces compression stresses on the radial direction of the pipe. Pipes are hence subjected to multiaxial loading. Therefore, not only the ageing of the insulating properties is important, but also the changes in the mechanical behaviour of the PU foam are critical towards ensuring the pipe assembly performs as specified during its service life, as well as for lifetime predictions. Current knowledge and identified sources of degradation are summarized in this section.

2.2.1 Temperature-related ageing

Thermal degradation of the PU foam has been identified as a relevant source of degradation of DH pre-insulated pipes. The browning of the foam in contact with the medium pipe (see Figure 6)

provided a visual indication of thermal degradation of the PU, which could lead to loss of adhesion between the foam and the steel medium pipe. Therefore, previous versions of standard EN 253¹⁵⁹ focused on thermal degradation of the PU foam, with accelerated ageing tests specified at a temperature for the service pipe of 160 °C for 3600 h, or at 170 °C for 1450 h, while the casing is exposed to a temperature of 23 ± 2 °C. The equivalent lifetime of the DH pipe at the operating temperature would be linearly extrapolated using the Arrhenius equation.



*Figure 6. Section of an aged DH pipe, showing browning of the PU in the vicinity of the medium pipe.
Credit: Weidlich*

These specified accelerated ageing tests were critiqued by researchers in the field, as discrepancies were found between the results of the specified ageing tests and of real-life pipes^{160,161}. Leuteritz et al.¹⁶² argued that the specified set-up in the EN 253 standard, up to the 2009 version, did not allow for acceleration of the oxygen permeation through the casing and into the foam, underestimating so the oxidation of PU in real life pipes. They undertook tests where the service pipe was kept in a range between 160°C and 190°C depending on the tested sample, and the casing was kept at temperatures between 30 and 75°C depending on the sample, as to accelerate the gas exchange through the casing. They report that with such a procedure a maximal acceleration of 10 is possible, requiring 3 years of testing to replicate the 30 years required service life. To achieve the required acceleration, they propose to replace the 3.3 mm standard PE casing with PE film. Oxidation of the steel at the interface was also reported as a cause of failure. However, previous research by the group on Energy and Circular Economy at RISE¹⁶³ evaluated the effect of reducing the casing thickness from 3 to 0.13 mm and the rising casing temperature from 10 to 70°C, in order to accelerate the diffusion of oxygen through the casing, and concluded that thermo-oxidation was not the main mechanism producing a loss of shear strength of the foam bond, since the degradation rate of the thin and standard casing pipes was equivalent. Moreover, the degradation of the shear strength was not found linear with ageing time, but presented an initial and steep drop, after which a plateau was reached where the shear strength remained at relatively constant values for a long period of time. In a following study, the degradation mechanisms of PU aged under air and N₂ at 150°C were evaluated¹⁶⁴. Significant changes were found in the samples aged under air, including in weight, colour and dimensions. A loss of CH₂ groups together with the appearance of new carbonyl groups was detected in the FTIR spectra, showing that the changes arise for thermal oxidation. Interestingly, no change in the flexural behaviour of the foam was recorded, suggesting that thermal oxidation does not affect this property, at least in the reaction extents covered in the study. A loss of adhesion between the steel-PU foam interface was readily detected in the samples aged in N₂, from which it can be derived that the degradation of the adhesion strength is not linked to thermo-oxidation, hence different reactions govern changes in adhesion of the PU-steel interface and cohesion of the PU foam. The reactions taking place in the interface were not covered in the study, though it is known that covalent metal oxide-urethane linkages are formed at the interface between steel and isocyanate-based polymers such as PU, which explains the high performance of isocyanate-based adhesives and coatings¹⁶⁵.

The author has found that the strength of the steel-foam interphase and predominance of adhesion versus cohesion failure of the PU bond is temperature dependent, as disclosed in [BJ1]. The shear strength of unaged DH bonded pipes was evaluated at room and at 70°C. It was found that when the shear test was undertaken with the pipes at room temperature, cohesive fracture of the foam occurred, while when the pipes were at 70°C, both cohesion of the foam and adhesion of the foam-steel interface failed. This finding brings the further potential discrepancy between the laboratory accelerated ageing tests and behaviour in the field, as laboratory tests typically undertake ageing processes and then determine the loss shear strength and failure model of the bond in shear tests undertaken at room temperature, while the failure of pipes under operation will occur at the operating temperature.

A long term accelerated ageing trial conducted at 130, 150 and 170°C¹³⁶ revealed that the behavior between the three temperatures does not follow an Arrhenius relationship. An initial shear strength increase was detected with the three temperatures, which was allocated to post-curing of unreacted isocyanates, which was followed by a progressive decrease in shear strength until complete loss of adhesion at the test temperatures 150°C and 170°C. However, at 130°C, once a shear strength reduction of 65% of the initial value was reached, a plateau was attained, where the shear strength remained constant for a long period of time. This report highlighted that the temperatures proposed for the accelerated ageing altered the degradation process rather than accelerated it, leading to an underestimation of DH pipe's service life.

As an outcome of these research results, the active version of EN 253 in force¹⁴ released during the realization of this doctoral thesis collects the state of knowledge of ageing of the shear strength of the PU bond but no longer specifies accelerated ageing tests for lifetime prediction.

2.2.2 Cyclic Loading

The cyclic loading produced by the network temperature variations have been introduced. It is known that cyclic loading produces fatigue in materials. Therefore, fatigue check is included in the design guidelines for DH networks^{15,166}. However, only the steel pipe is considered, and stating lack of knowledge, it assumes that fatigue in the foam does not occur within the limits of permissible stresses. Previous projects have evaluated the effects of thermal cycling and fatigue in DH systems^{16,167}, again only covering the steel service pipe.

Polymeric foams, given their heterogeneous nature¹⁶⁸, present a complex behaviour upon thermal expansion. While the polymer skeleton has the thermal expansion of the bulk polymer, the gas inside the cells pressurizes the cell walls as it expands, distorting the cell shape^{138,169}. This is exacerbated by the fact that upon increasing temperature, the expansion of the gas coincides with the strength reduction of the polymer matrix¹³⁸. Cell size and anisotropy further come into play¹⁶⁹. It has been reported that the cells present a larger expansion in the direction parallel to the foam direction, and the original shape is not recovered to full extent¹³⁸. This might be of importance for DH pre-insulated pipes, given the fact that it presents a greater cell anisotropy than in PU foam slabs [BJ2]. The different material layers in DH pipes present different coefficients of thermal expansion (steel = $1.1 \cdot 10^{-5} \text{ K}^{-1}$ ¹⁷⁰, PE = $7.14 \cdot 10^{-4} \text{ K}^{-1}$ ¹⁷¹, PU_{foam} = $1.2 \cdot 10^{-4} \text{ K}^{-1}$ in the rise direction¹⁷²), which could be a cause of debonding upon thermal cycling. Therefore, the effects of thermal and mechanical cyclic loads on DH pre-insulated pipes were experimentally evaluated, and reported in [BJ1]. These experiments were conducted in parallel to the thermal cycling of PET foam, described in Chapter 3.

Three different cyclic loadings were executed. The parameters are stated in Table 3.

Table 3. Parameters for the executed cyclic loading trials

Trial	T interval (°C)	τ interval (MPa)	Number of cycles
T	25–100	0	250
MT-wc	25–100	0–0.12	250
MT-m	25–70	0–0.04	125

For trial T, the number of cycles was set at 250, which is the number of cycles established for fatigue check for secondary effects for distribution lines according to ¹⁵. In trial MT-wc the same number of cycles was selected as in trial T for the same reason. For the selection of the applied force, a worst-case scenario criterion was selected. Because EN 253:2019 ¹⁴ establishes aged pipes should still withstand a shear stress of 0.12 MPa at room temperature, this was the maximum shear applied.

In trial MT-m, the selected maximum shear corresponds to the acting shear stress under the network design point¹⁶⁶. The temperature was cycled between 25°C and 70°C, because buckling of the PE casing was experienced in trial MT-wc, as 100°C is too close to its heat deflecting temperature. The number of cycles conducted was 125, representing half of the established number of cycles for fatigue check for secondary effects for distribution lines according to EN 13941-1¹⁵.

The results revealed that the applied temperature cycles caused no degradation of the shear strength, meaning the free expansion and contraction of the foam itself or stresses caused by the differences in coefficient of thermal expansion between material layers are not sufficient as to produce a degradation, at least with the sample size used and applied number of cycles. However, the combination of cyclic thermal and mechanical loads reduced the strength and increased the stiffness of the foam. The foam samples were evaluated through FTIR and no change or degradation of the polymer could be identified, suggesting the loss of mechanical properties could be related to stress relaxation, material ratcheting or fatigue. The evaluation of the fractures resulting from the shear tests showed cracks initiate in Mode II, close to the foam-steel interface, and propagate in Mode I. For the definition of fracture modes, the reader is referred to Zehnder (2013) ¹⁷³. The very consistent crack pattern between samples, with a 2 cm axial displacement between each formed crack (see Figure 7 ¹⁷⁴), suggest the occurrence of strain localizations.

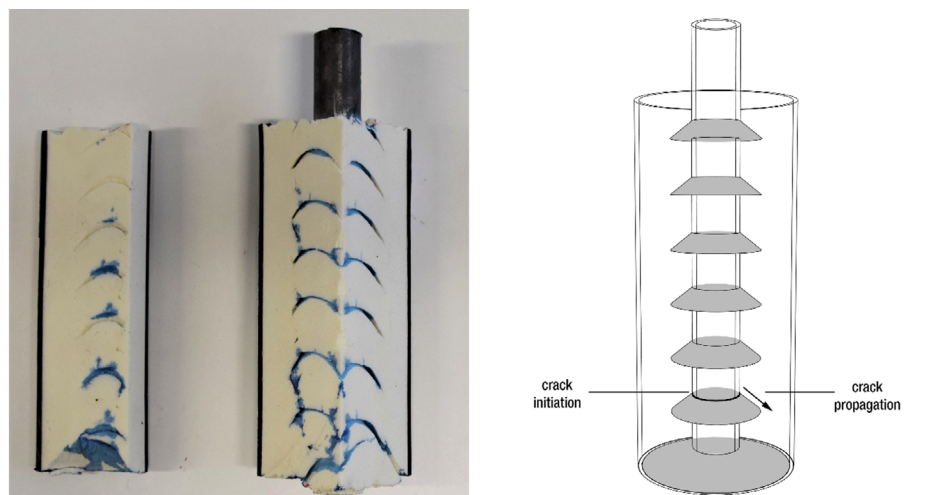


Figure 7. Right: Photograph of a tested sample, where a coloured epoxy was introduced through the cracks prior cutting to highlight the pattern. Left: proposed description of the crack initiation and propagation scheme.

Vega et al.¹⁷⁵ within Annex XII project¹⁷⁶ evaluated the effect of cyclic mechanical loads during thermal ageing of the pipes. The differences between the cited experimental program and that executed by the author are that the temperature was kept constant and at a higher level (130 and 140°C vs 70 and 100°C), the number of applied mechanical cycles was significantly higher (16000 vs 250), since the criteria for household connections was selected vs. that for distribution lines selected for the work within this doctoral thesis, and the cycle frequency and amplitude were higher. The authors of this later work conclude that the mechanical loads accelerate the chemical degradation of the PU foam, resulting in an accelerated loss of adhesion. Comparing both works, it is interesting to note that at temperatures in which thermal degradation was not detected, a degradation of the mechanical properties due to the cyclic loading could be detected, while at temperatures in which degradation of the mechanical properties takes place due to thermal degradation, the cyclic loading accelerates the degradation.

2.2.3 Damage due to moisture

Buried district heating pipelines may be located below the groundwater level. Moisture can penetrate the HDPE casing¹⁷⁷, or through the pipe ends and joints^{158,178}. Indeed damage to the PU foam due to moisture is reported in the field¹⁷⁸. In the case of plastic medium pipes, hot moisture from the heat carrier can diffuse through the medium pipe into the foam^{139,179}.

Moisture can degrade the mechanical properties of polymers in different ways, including plasticization¹⁸⁰, swelling¹⁸¹, cracking related to osmotic pressure^{182,183} or chemical degradation due to hydrolysis¹⁸⁴ in polymers subjected to this reaction. The assessment of the damage due to moisture comprises the type of degradation, the degradation rate, and the rate determining factors, such as diffusion or temperature.

Previous work on the ageing of polymeric foams upon moisture exposure conclude that diffusion is the rate determining step. Earl & Shenoj¹⁸⁵ studied the moisture uptake of PVC foams upon water immersion at 40°C and 95% RH and 40°C for over 2.5 years. A multistage absorption process was observed in the water immersion experiments, and allocated it to the progressive moisture diffusion through each layer of cells, concluding moisture reached only three layers of cells given the three plateaus observed. This equals 1-2 mm of ingress depth. The mass increase of the exposure of the samples to wet air was significantly lower. The authors interpreted the discrepancy to water accumulation in the superficial open cells, despite blotting of the sample's surface prior to weighing included in the experimental program. The lack of multistage absorption in the wet air trial could not be explained. Avilés et.al.¹⁸⁶ evaluated the ageing of PVC foam under 95 % RH and sea water immersion for 7 months. A limited degradation of the foam, based on tensile tests, was observed, which was allocated to diffusion control of the ageing process. Through microscopic observation of the foam surface and cross-sectional cuts of the foam, the authors conclude the moisture only reached the first 2-3 mm into the foam thickness, based on differences in cell diameter of the superficial cells vs internal cells, allocated to swelling caused by moisture. The number of measured cells or foam cutting methods is not provided in the study. Huo et al. evaluated the moisture uptake of PU foam upon water immersion at room temperature, for a duration of 7 months. A multistage diffusion process was observed, and interpreted again as the moisture saturation of each cell layer, resulting in 2 layers of cells over 200 days. Liu et. al.¹⁸⁷ evaluated the moisture uptake of 150 kg/m³ PET foam upon immersion in simulated sea water at 40°C. A first weight increase jump was detected at the first measurement point, allocated to water ingress in the open superficial cells, after which the weight steadily increased during the 30 days duration of the trial. Given weight stabilization was not achieved, the authors conclude moisture saturation of the foam was not achieved during the evaluated timeframe.

While these interpretations of diffusion in foams being slow and the rate determining step of the degradation conceptually fit with the macroscopic consideration of foam as a thick homogeneous material layer, where the transport involves solution at the surface, transport through the concentration gradient and desorption at the other surface^{154,188}, they differ from the notion that the availability of unoccupied volume in the polymer influence sorption and diffusion processes¹⁸⁹, increasing with increasing free volume. This is illustrated by the "foam diffusivity" model proposed by Lee¹⁹⁰, which is a function of the diffusivity of the moisture in the polymer as well as the foam

density. The foam diffusivity would increase with decreasing foam density and would be higher than the polymer diffusivity. This indicates greater mobility of the diffusant in a lower-density foam structure. This model disregards any condensation or water entrapment in the cell cavities for simplicity, assuming the diffusion occurs within the polymeric skeleton of the foam only.

Once the polymeric foam is saturated, degradation of the mechanical properties due to plasticization can be reverted with the drying of the polymer. Swelling itself can be reverted through drying, though the potential deformation of the cell's shape might not be recovered, rendering the foam case again more complex. The formation of microcracks due to swelling and osmotic pressure would be irreversible damage. As for chemical degradation, while it is known that PU is susceptible to hydrolysis¹⁹¹ and the hydrolysis of PU is a proposed chemical recycling pathway to break down the polymer and recover its constituents^{192,193}, the hydrolytical degradation of PU foam in the DH context remains widely unexplored. The hydrolytic stability of polyether PU insulation has been found reported in the context of offshore oil platforms¹⁹⁴. Though polyether PU is more stable to hydrolysis than polyester PU, the urethane bond can still undergo hydrolysis under severe conditions¹⁹⁴. The study confirmed the hydrolysis of polyether PU under sea water immersion at high temperatures, and a model was developed correlating the reaction kinetics with temperature, based on a first order reaction and an Arrhenius relationship.

Research line 1 concerns PET foam and so the chemistry of PET is to be considered. It is widely established that PET undergoes hydrolysis at high moisture and temperature levels^{184,195–200}. As such, the confirmation of its stability towards hydrolytical degradation in DH applications was stated as a subject requiring further research in the two previous works on PET foam for DH pipes^{106,107}. The study of this research question is a central element of this doctoral thesis.

From the body of knowledge created by previous research^{184,195–200} it is accepted that hydrolysis of PET produces chain scission at the ester link in the amorphous phase. The generated mobile chain fractions rearrange themselves into the crystalline phase, resulting in chemicrystallization. The ultimate consequence of the hydrolysis of PET is embrittlement, which is critical for a load bearing material. Thus, the ductile-to-brittle transition is commonly selected as end-of-life criterion^{197–199,201,202}. While it is recognized that embrittlement corresponds to a critical structural state²⁰¹, a detailed understanding of the underlying mechanism is still lacking. Many authors on the hydrolysis of PET adopt a molecular interpretation of embrittlement^{199,202,203}, where the reduction of the concentration of tie-molecules or entanglement density caused by the chain scission would be the ultimate cause of embrittlement. As such, the reaching of the critical molecular mass corresponding to the entanglement limit (M_c'), which is proportional to the molecular mass of the segment between the entanglements (M_e), would correspond to the ductile-brittle transition. Accurate lifetime predictions require specific end-life criteria, but an accurate correlation between molar mass reduction due to chain scission and specific values of M_c' and M_e has not yet been established. Ranges of M_c' between 2-3 times M_e ¹⁹⁹ to 5-10 times M_e ²⁰² can be found in the literature. Based on these ranges, an end-of-life criteria of 30% molar mass reduction has been derived²⁰³. An experimental value of $M_c' = 17$ kg/mol has been recently reported²⁰², for PET with an initial molar mass of 31.4 kg/mol and polydispersity index of 2.4. This correlates to a 45% molar mass reduction at the ductile-brittle transition.

Another proposed interpretation for embrittlement could be micromechanical, as compiled in²⁰¹. As such, stress concentrations related to the increase in crystalline content and reduction of interlamellar spacing, or lack of sufficient amorphous content to sustain deformations, would be the ultimate cause of embrittlement. The chemicrystallization resulting from PET hydrolysis has been widely reported and followed^{197,198,202–205}. Early studies on the degradation of PET¹⁸⁴ suggest that the density reduction of the amorphous fraction of PET upon crystallization, which leads to the appearance of voids at the lowest amorphous densities²⁰⁶, could be the ultimate cause of embrittlement. However, this causal chain has not been confirmed or followed in more recent work. The two possible causal chains leading to embrittlement are conceptually illustrated in Figure 8.

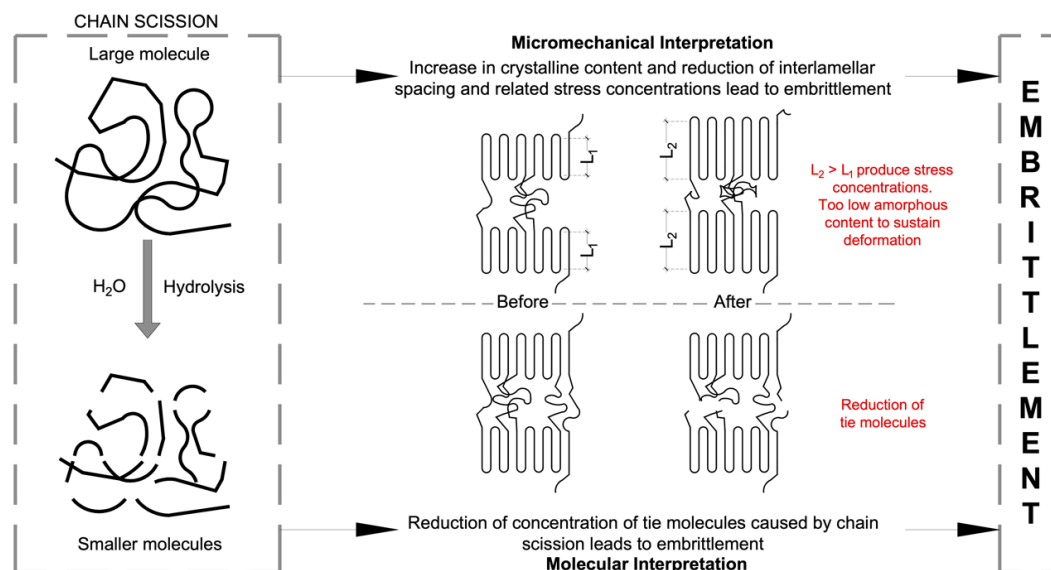


Figure 8. Possible causal chains relating chain scission to embrittlement.

Concerning the kinetics, it is accepted that it is influenced by both temperature and RH, being the temperature dependency governed by the Arrhenius law. Discrepancies arise concerning the reaction order. While many authors regard it as first order in RH, given water being largely in excess and considering no diffusion control^{184,197,199}, others report second order in RH, describing the need for two water molecules acting per chain scission²⁰⁰. A master curve with a reaction order of 0.5 has been recently proposed²⁰³, though no physical meaning is provided. Consensus on if the reaction is autocatalytic^{195,207}, or non-autocatalytic^{184,197} has not been reached.

All experimental data found in the scientific literature evaluated during the course of this work correspond to conditions in which PET is above its T_g . This is also the case for the evaluation of PET for energy^{208,209} or civil engineering^{210–212} applications, where these studies are considered accelerated ageing, since the service temperatures for these applications are around ambient temperatures. Experimental data below T_g has been thoroughly searched for by the author without success. Two identified pieces of literature claim to report data below T_g ^{184,196}, however, it was not the case as the authors did not take into account the T_g depression caused by moisture plasticization²¹³. Two further pieces of literature report that the kinetics below T_g is extremely slow^{199,202}, but do not provide experimental evidence. The importance of this is that, while modeling and extrapolation from degradation data collected at higher temperatures to lower temperatures have been undertaken^{203,212}, the validity of these Arrhenius extrapolations with activation energy (E_a) values obtained in the rubbery state to the glassy state is questionable^{202,203}.

2.3 Foaming of polymers

The foaming of polyurethane is produced by a chemical reaction simultaneously occurring when mixing an isocyanate, a polyol and water. The isocyanate reacts with water, which can be added or ambient moisture, producing carbamic acid, which then decomposes into CO_2 and amines²¹⁴. In parallel isocyanates and polyols react producing polyurethane. The formed CO_2 gas blows the polyurethane into a foam, though additional blowing agents are commonly added²¹⁴.

The foaming of thermoplastics, such as the target PB-1, is a physical process, which involves the sorption of the blowing agent into the polymer, under pressure, and the bubble nucleation and growth. This may be induced through a reduction of pressure or an increase in temperature. A mass transport from the blowing agent in the polymer-gas solution into the bubbles takes place, which ends with the vitrification or crystallization of the polymer^{149,215–217}. This last stage is critical for the success of the foaming process, as it stabilizes the cellular structure.

The selection of the polymer, blowing agent and expansion technique strongly influences the final foam morphology^{80,149}. This, together with the properties of the polymer matrix, condition the final properties of the foam⁸⁶.

As for the processing, the most broadly used techniques are batch foaming, extrusion foaming and injection molding foaming, where the first is used for research and development and the two later technologies are used for industrial manufacturing²¹⁵. In the batch foaming process, the polymer is placed in contact with the blowing agent under pressure in an autoclave, for a sufficient time to allow saturation of the polymer. Foaming can be produced by a fast decompression, which produces the nucleation of the bubbles, or by increasing the temperature. Extrusion foaming is a continuous process in which the blowing agent is mixed with the molten polymer in the extrusion barrel at high pressure. At the die exit, a pressure drop is produced, causing the foaming of the polymer. In foam injection molding, molten polymer and blowing agent are injected in a cavity, which then expands, causing a pressure drop and hence foaming²¹⁵. This technique is used mainly for producing foams with complex geometries²¹⁵.

The state of the art on physical foaming of polymers was thoroughly revised, and cross related to the Principles of Green Engineering and Cradle to Cradle design framework, in order to identify compatible strategies as well as research needs to cover during the study of the foaming of PB-1. The resulting critical review is presented in [J4].

Chapter - 3

Polyethylene Terephthalate Foam

Evaluation of its ageing behaviour

3.1 Introduction

As described in Chapter 2, sources for polymeric foam degradation occurring in DH pipelines include exposure to heat, exposure to moisture and cyclic loading. Concerning the exposure to heat, unlike for PU, literature reports that the thermal and thermoxidative degradation of PET has very low reaction rates at temperatures below its melting point of 250°C^{184,218}, and occurs mainly at or above this temperature. Since this is far from DH operating temperatures, this source of degradation was excluded from the study.

The in-situ effects of temperature, as well as the effects of temperature cycling on the compressive behaviour of PET foam was studied. The in-situ temperature effects are relevant for the calculation of the network stresses at the design point. The effects of thermal cycling are relevant for lifetime prediction. This contribution is detailed in [CP1].

The potential degradation of the PET foam due to hygrothermal exposure, as well as diffusion and moisture uptake, were experimentally evaluated. Given the fact that PET insulated DH pipes do not exist yet, the possibility to use PET as insulation for plastic or steel medium pipes was kept open. In the case of steel medium pipes, moisture ingress into the foam would be groundwater permeating through the casing or through leaks in joints. In the case of plastic insulated pipes, hot moisture from the heat carrier could diffuse through the pipe and into the foam. Therefore, the effects of moisture at ambient temperatures as well as at heat carrier temperatures were experimentally evaluated, which correspond to below and above the T_g of PET. This knowledge is relevant for confirming the validity of PET foam for the insulation of medium pipes of both materials, as well as for lifetime prediction, since the higher temperature experiments would serve as accelerated ageing. This contribution is detailed in [J1] and [J2].

For this research, commercial closed-cell PET foam boards blown with cyclopentane were used. The selected products were Kerdyn Green in 80 kg/m³ and 100 kg/m³, kindly provided by Gurit. These densities were selected because they presented the closest density to that measured for PU foam in DH pipes, ranging from 68-100 kg/m³ depending on the pre-insulated pipe type and PU formulation²¹⁹. Testing two different densities allowed to assess and compare the impact of the cellular microstructure on the different ageing processes studied.

The PET foams, unaged and throughout the different ageing processes studied were characterized through different techniques, including optical microscopy, porosimetry, Fourier transformed infrared in attenuated total reflexion mode (FTIR-ATR), nuclear magnetic resonance (NMR), differential scanning calorimetry (DSC), dynamic mechanic thermal analysis (DMTA), compression and flexural mechanical tests. The ageing of the samples was undertaken in environmental chambers. The detailed procedures are described in each contributing publication.

The largest part of the experimental programme was undertaken in the civil engineering laboratory of HafenCity University. Certain experiments were undertaken in cooperation with or as a guest researcher with the following institutions: the University of Hamburg (NMR), the Technical University of Hamburg (porosimetry), and the Institute of Polymer Science and Technology (ITCP-CSIC, Spain) (DMTA).

3.2 Effects of temperature and temperature cycling on the compressive behaviour of PET foam

It is known that temperature significantly affects the mechanical behaviour of polymers, hence polymeric foams. PET, unlike PU, is a semicrystalline polymer. Its T_g of $\sim 75^\circ\text{C}$ ²²⁰ lies in the boundaries of the service temperature. Therefore, the crystalline structure could change or degrade due to temperature or temperature cycling. The aim of this study was to observe the effects of temperature, time under temperature and temperature cycling on the mechanical behaviour of PET foams.

3.2.1 Behaviour under temperature

Static compression tests were conducted at room temperature, as well as at 70°C , 85°C and 100°C with the use of an environmental chamber (Weiss WK3-180/70/5-UKA, Reiskirchen, Germany). Five samples were tested per condition and foam density under a displacement-controlled rate of 2 mm/s. The force was measured with a 20 kN load cell (HBM, Darmstadt, Germany) and strain measured through digital image correlation using an ARAMIS 5M adjustable stereo camera system (GOM mbh, Braunschweig, Germany), with an acquisition frequency of 1 Hz. Samples were tested in the direction parallel to the extrusion, which would correspond to the radial direction of the pipes.

For the tests under temperature, two approaches were followed: conducting the tests after a short temperature stabilization time of 2 h, for which the obtained stress-strain curves are presented in Figure 9 a) and 9 d) for the foam 80 kg/m^3 and 100 kg/m^3 respectively, and conducting the tests after an overnight temperature soak at 100°C , for which the obtained stress-strain curves are presented in Figure 9 b) and 9 e) for the foam 80 kg/m^3 and 100 kg/m^3 respectively. The resulting compressive strength at 10% strain (σ_{10}) from both approaches are plotted vs temperature in Figure 9 c) and 9 f) for PET foams 80 kg/m^3 and 100 kg/m^3 respectively.

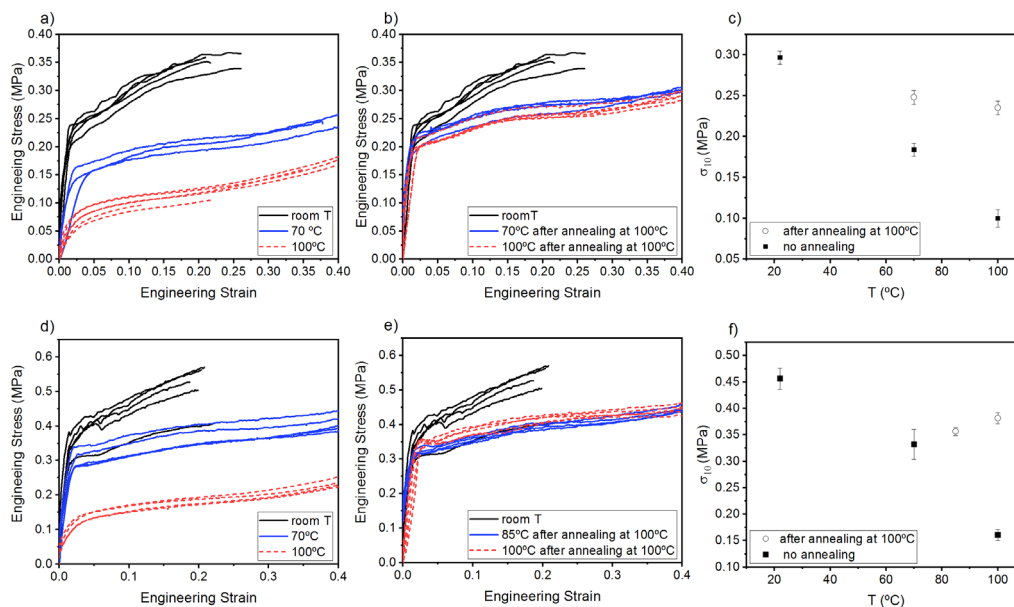


Figure 9. Compressive behaviour of PET foam under temperature, for 80 kg/m^3 (a) and 100 kg/m^3 (d); and under temperature after annealing at 100°C for PET foam 80 kg/m^3 (b) and 100 kg/m^3 (e). Evolution of the compressive strength at 100% strain (σ_{10}) with test temperature before and after annealing, for PET 80 kg/m^3 (c) and 100 kg/m^3 (f).

As viscoelastic materials, polymers exhibit time and temperature dependency on their mechanical behaviour²²⁰. The decrease of mechanical properties of the evaluated PET foams with temperature can be readily observed in Figure 9 a) and 9 d), as expected and in line with the behaviour of

PET foam previously reported by Ramnäs ¹⁰⁶. New knowledge arises from the tests conducted after an overnight temperature soak at 100°C. It can be seen in Figure 9 c) and f) how the 100°C temperature soak produces an annealing effect on the PET foam ²²¹, which partly counteracts the degradation of the mechanical properties caused by temperature.

It is known that the crystal domains in semicrystalline polymers can sustain the stiffness above T_g ¹¹⁷. The increased macromolecular flexibility and chain conformational mobility produced by temperature allows for improved crystallization ²²¹. An early definition of annealing in polymer science is the thermal treatment below the melting point which leads to crystal growth, perfection of crystals and change to more stable crystalline structures ²²². This process should lead to a lower free enthalpy under the given conditions ²²¹ which may be achieved through rotational isomerism and close packing ²²³. Indeed, different orientations are possible in PET, which arise from the rotation of the CH_2-CH_2 bond of ethylene glycol moiety, the $O-CH_2$ glycolic bond, or the $O=C-C_{aryl}$ bond ²²⁴⁻²²⁷. The *trans* and *gauche* isomers resulting from the rotation of the CH_2-CH_2 bond of ethylene glycol are represented in Figure 10.

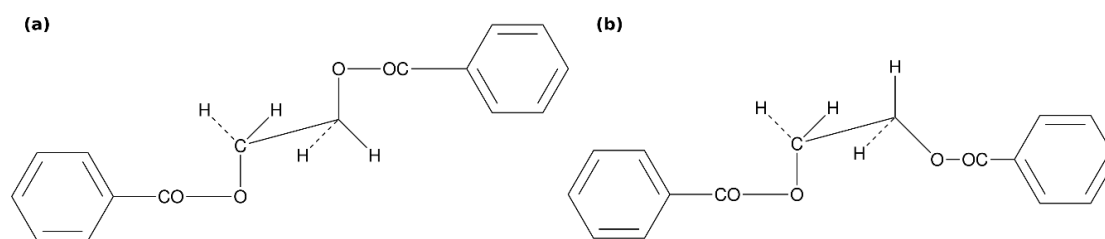


Figure 10. (a) *trans* and (b) *gauche* isomers arising from the rotation of the CH_2-CH_2 ethylenic bond of the ethylene glycol moiety

Literature reports that the T_g of PET could rise from 67°C in the amorphous state to 81°C in the semi crystalline state and up to 125°C in a crystalline and oriented state ¹¹⁰. This suggests that the ultimate cause for the enhancement of PET foam's strength and stiffness is the increase of orientation of the PET macromolecules allowed by the temperature soak.

The practical implication of this finding is that the previously determined service temperature of ~80°C for PET foam insulated DH pipes ¹⁰⁶ has been proven conservative since the DH pipelines are under temperature for long periods of time and so annealing will occur. An annealing treatment during pipe manufacturing could also be envisaged. The $\sigma_{10} = 0,3$ MPa required by EN 253 ¹⁴ can be fulfilled by PET 100 kg/m³ even at 100 °C, demonstrating that it could be used in DH networks operating at this temperature, which is commonly found in the field ²²⁸. It should be noted that the value required by the standard is at room temperature, so the achievement of the required compression strength at 10% strain at 100°C exceeds the requirement.

3.2.2 Effects of thermal cycling

Up to 250 thermal cycles were conducted, following two different temperature profiles: (a) between 25 and 100°C, and (b) between 25 and 75°C, with 30 min ramp duration and 75 min hold time for both cases. The number of cycles was selected to match those required for fatigue check for secondary effects for DH distribution lines ²²⁹ and the two temperature intervals to fluctuate around T_g (a) and below T_g (b), in order to assess potential effects on the crystalline structure and its consecutive impact on the mechanical behaviour. The effect of the applied cycles was assessed in terms of variation of mechanical properties under compression. The tests were undertaken with the same procedure as that described in the previous section.

Figure 11 presents the obtained compression stress-strain curves for foam 80 kg/m³ (a) and 100 kg/m³ (b), unaged and after the two temperature cycling trials. The applied temperature profile for both trials is represented in (c).

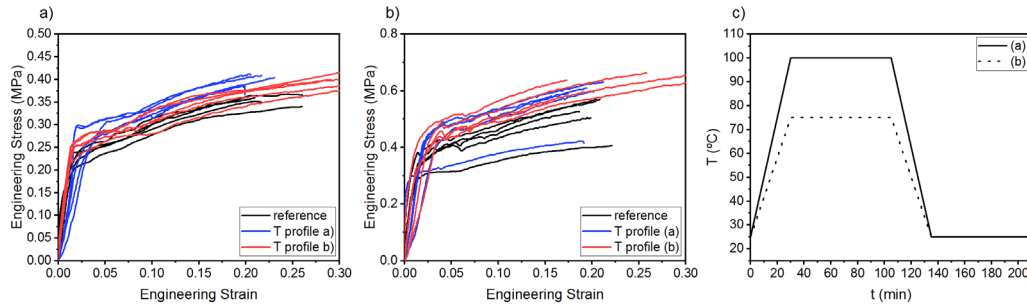


Figure 11. Compressive stress-strain curves for foam 80 kg/m³ (a) and 100 kg/m³ (b), unaged and after the two temperature cycling trials. (c) applied temperature profile for both trials.

As can be seen, no significant variation in the E modulus or σ_{10} between the unaged and the temperature cycled samples was found. The high variability between samples is allocated to heterogeneity of the cellular structure and a certain level of out-of-plane deformation. Comparing these results with the trials under temperature (section 3.2.1), we can derive that the 75 mins hold time was not long enough to induce annealing. Having this variable out, variation of the mechanical properties could occur from cracking events arising from the repetitive flexure of the cell walls caused by expansion and contraction²³⁰ or irreversible changes in the geometry of the cells, as reported by previous authors with polyurethane foam¹³⁸. In our research on PU foam [BJ1] no degradation of the shear strength of the PU bond in the pipe assembly was detected after the same number of temperature cycles and profile (a). PET foam should present a better ageing behaviour than PU foam in relation to temperature cycling, due to its low coefficient of thermal expansion, of $9.1 \cdot 10^{-5} \text{ K}^{-1}$ ²³¹ vs $15 \cdot 10^{-5} \text{ K}^{-1}$ for PU²³⁰.

It is concluded that temperature cycles in the tested amplitude and number do not cause a degradation of the mechanical properties of PET foam.

3.4 Diffusion and moisture uptake in PET foam

Knowledge of the diffusion and moisture uptake mechanisms in PET foams is fundamental for the correct understanding and interpretation of its potential degradation effects. This was studied through gravimetric experiments, under 80% RH and 40°C, and water immersion at room temperature. Samples with the larger surface corresponding to the plane perpendicular to the extrusion direction (E) and the plane perpendicular to the parallel direction (P) were evaluated, in order to observe any influence of the cellular microstructure or chain orientation arising from the extrusion stretching forces, which could increase the tortuosity¹⁸⁹ for the diffusing water molecules. The detailed experimental procedure is described in [J2].

The obtained gravimetric curves are presented in Figure 12.

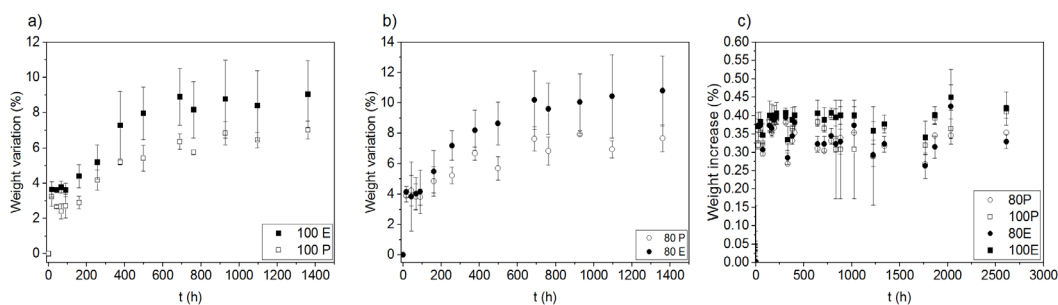


Figure 12. Weight increase foam 80 under water immersion (a), foam 100 under water immersion (b), and foams 80 and 100 at 80%RH and 40°C (c).

As can be seen, upon water immersion, a multistage absorption process can be seen, consistent with the results of previous workers on polymeric foam's moisture uptake (see section 2.2.3). However, this is not the case under wet air, where the biggest mass uptake was registered in the first measurement point conducted after 24h of exposure, after which the weight remained constant within experimental scatter during the 2600h of exposure observed. The data suggest the PET polymer was saturated within 24 hours of exposure, consistent with the saturation times reported for PET films^{232,233}. Considering that the cell walls and struts of the PET foams under study have a thickness of 5-10 μm and 20-40 μm , for the 80 and 100 kg/m^3 foam, respectively, the PET films in the literature a thickness of ~ 200 μm , and that diffusion is assumed to take place mainly through the polymer skeleton, it appears consistent that saturation times should be at least of the same order of magnitude than in films and in any case not significantly slower. In order to confirm that moisture saturation was reached within the first 24h interval, bending tests were conducted in an environmental chamber under the same conditions as the gravimetric study under wet air, thus at 80% RH and 40°C. Additional bending tests were undertaken at 0% RH and 40°C, as to derive the effect of the moisture only. The results are presented in Figure 13 (a). The lower strength and higher strain at break of the samples tested with moisture, to the point that they did not fail within the applied stresses, are a sign of plasticization due to moisture. If the moisture was only sorbed on the foam surface, such an effect would not be revealed in the mechanical tests, demonstrating saturation through the bulk of the foam.

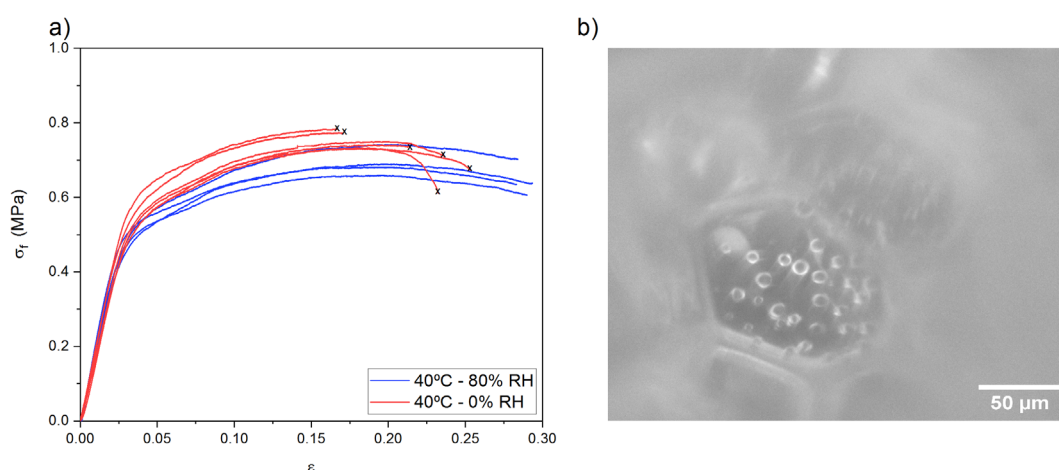


Figure 13. (a) Bending tests conducted at 40°C, with and without moisture. (b) micrograph showing water droplets inside a PET foam closed cell.

Although as for moisture diffusion, an equivalency between water immersion and wet air at 100% RH has been previously reported²³⁴, the obtained results reveal a discrepancy in the case of foams. Previous authors have interpreted the larger weight uptakes registered upon water immersion vs wet air as water accumulation in the superficial cells¹⁸⁵. But these interpretations are inconsistent with the experimental procedures followed both in the cited reference and in this work, where the sample's surfaces were blotted with paper prior weighing, precisely to remove the water collected on the surface. It appears that water passage and accumulation into the cell cavities occur. Indeed, water droplets inside the closed cells could be observed through microscopic evaluation (Figure 13 (b)), and would be the ultimate cause of the higher weight uptake. The multistage weight uptake would correspond to the progressive filling of cell cavities, cell layer by cell layer. This would be independent of the diffusion through and saturation of the polymer skeleton. These two phenomena confirm a dual moisture uptake process, conceptually illustrated in Figure 14.

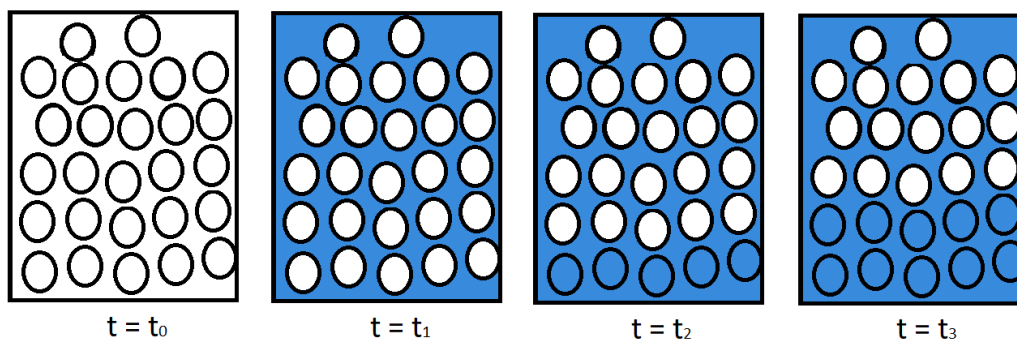


Figure 14. Conceptual scheme of dual moisture uptake of polymeric foams under water immersion through time. Blue represents moisture saturation.

The passing of liquid water into the cell cavities can occur by permeation through the cell walls, and direct flow through the open cells. The open cell content of the PET foam under study was measured and found of $\sim 20\%$, which is considered typical²³⁰. Unfortunately, the open cell content for the particular polymeric foams used in previous studies^{185,186,235} is not provided, preventing comparison.

The identification of this dual moisture uptake process would invalidate simplifications excluding the contribution of moisture entrapment in the closed cells of polymeric foams¹⁹⁰ for the case of liquid water immersion. Further, it is relevant to accurately define if “moisture saturation of the foam” refers to the polymer only, or if it includes the saturation of the cell cavities.

Both PET foams of different densities presented equivalent behaviour, despite having a different cellular microstructure. This further supports that the cellular structure does not have a significant difference in the diffusion process.

The ultimate conclusion of this study is that diffusion would not be the rate controlling step of any degradation produced by moisture.

3.4 Degradation through hygrothermal exposure

Three different ageing trials were conducted, with different moisture levels, temperatures and duration. The applied parameters are collected in Table 4.

Table 4. Parameters for the executed hygrothermal ageing trials

Trial	T (°C)	Moisture level	Duration
(1)	90	95% RH	390 h
(2)	40	80% RH	6 months
(3)	23	Water immersion	12 months

Trial (3) would correspond to conditions close to the real conditions arising from groundwater ingress.

Trial (2) would correspond to an accelerated ageing in relation to ground water ingress, but maintaining the PET foam in the same structural state as during its service life, which is the glassy state. In order to select this temperature for accelerated ageing, the T_g depression caused by moisture plasticization²¹³ has been taken into account.

Trial (1) would correspond to the typical accelerated ageing conditions applied in the study of hydrolytic stability of PET^{208–212}. These conditions are above T_g , in the rubbery state of PET. This would be also equivalent conditions to the case of hot moisture from the heat carrier permeating through the plastic pipe and into the foam, in the scenario of a plastic medium pipe insulated with

PET foam. The hydrolysis reaction of PET is represented in Figure 15.

For the details on the experimental methods applied, the reader is referred to the relevant section in [J1].

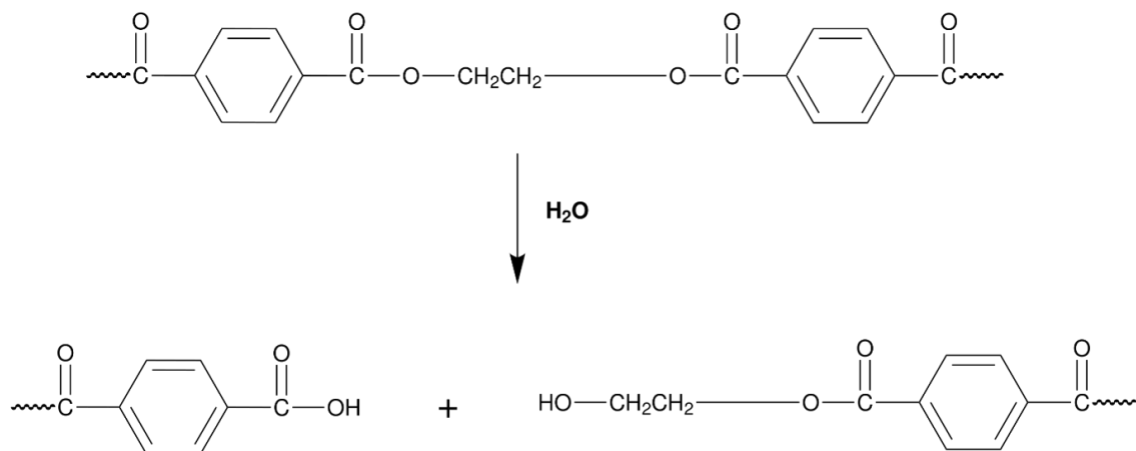


Figure 15. Hydrolysis of PET

The ageing trials (2) and (3) produced no irreversible degradation of the PET foams studied, nor in their mechanical properties, nor in their molecular or crystalline structure, as assessed through 3-point bending tests and FTIR-ATR. This shows no degradation arising from cell deformation due to swelling, or osmotic damage. This is consistent with the low moisture absorption of the PET matrix, of ~0.35%, as can be observed in Figure 12 (c). It also shows that hydrolysis did not occur within the experimental boundaries.

In trial (1), a progressive degradation of the mechanical properties with exposure time was observed, until the ductile-brittle transition was reached, slightly after 100h of exposure (Figure 16 (a) and (c)). This point represented a kink in the degradation rate, which continued, but at a different rate (Figure 16 (b) and (d)). Through FTIR-ATR and NRM it was confirmed that the degradation of the mechanical properties was due to the hydrolysis of PET: an increase in the content of the carboxylic acid was detected in the FTIR spectra, which are products of the hydrolysis reaction (Figure 16 (f)). An increase in the hydroxyl end group content was detected in the proton NMR spectra. Through end-group analysis, the rate of chain scission could be derived (Figure 16 (e)).

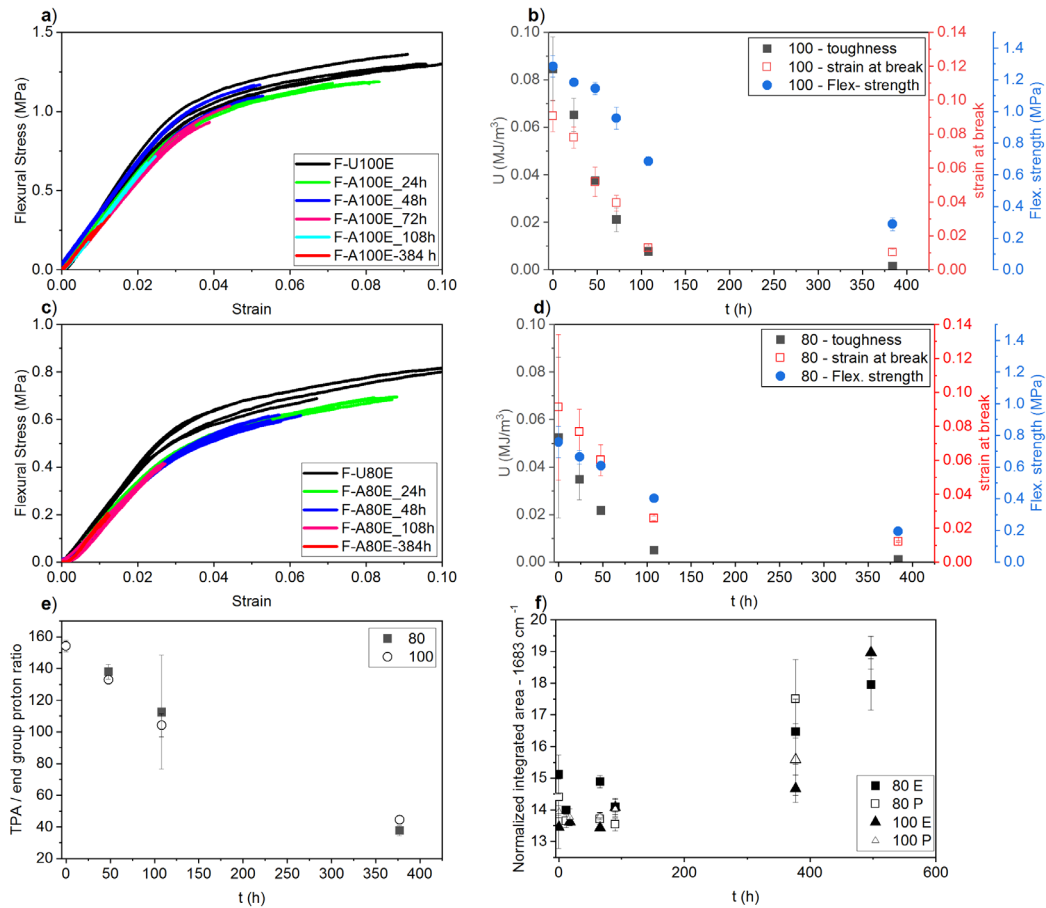


Figure 16. Flexural stress strain curves for foam 80 (a) and 100 (c) after different ageing times. Evolution of the mechanical properties with ageing time for foam 80 (b) and 100 (d). (e) Chain scission rate derived from end-group analysis of the NMR spectra. (f) Increase of carboxylic acid with time, derived from the FTIR-ATR spectra.

The well-known chemicrystallization which arises from the hydrolysis reaction^{197,198,202–205} was also identified. Firstly, a progressive shift over time between the ratio of the gauche and trans isomers was detected in the IR spectra (see Figure 17 (a)). It has been previously established that only the trans isomer is present in the crystalline region, while both trans and gauche are present in the amorphous region²³⁶. An increase in the crystallinity (X_c) was indeed confirmed with DSC (see Figure 17 (b)), where the X_c was calculated as:

$$X_c = \frac{\Delta H_f}{\Delta H_f^0} \quad (2)$$

where ΔH_f is the specific melting enthalpy measured from the second heating ramp, and ΔH_f^0 the melting enthalpy of a fully crystalline PET, taken as 140 J/g²³⁷.

Plotting the relative molecular weight with the X_c (%) a linear relationship is obtained (Figure 17 (c)), directly relating the crystallinity increase with the chain scission, consistent with the literature.

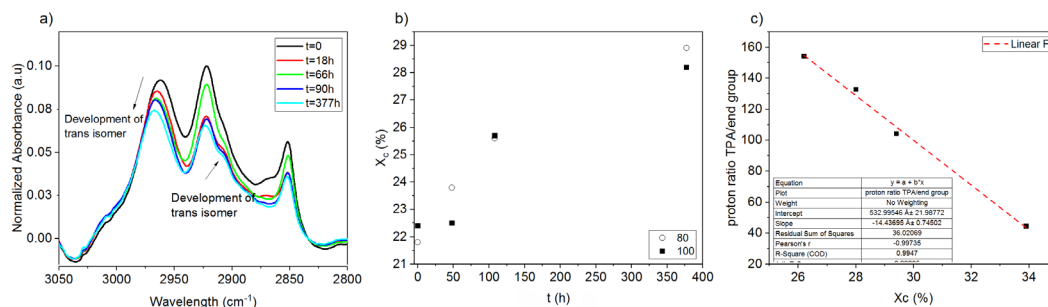


Figure 17. (a) IR spectra with ageing time, foam PET 80. (b) X_c with ageing time obtained through DCS (c) relative molecular weight (through NMR) vs X_c through ageing time

Gravimetry was also used to follow the ageing process. Samples were progressively extracted from the chamber and weighed in the wet state. The resulting gravimetric curve can be seen in Figure 18. It can be observed that, after an initial moisture uptake, a progressive weight loss was detected, reaching a minimum and then remaining constant within experimental scatter. Since the ageing was conducted under wet air and not under water immersion, loss of soluble fractions^{195,199} cannot be the cause of this weight loss. The sorbed water appears expelled with time, which could be related to structural changes in the PET. One explanation could be that the chemicrystallization upon hydrolysis produces such densification that sorbed water molecules are expelled²³⁸. But the coincidence of the attainment of minimum weight with the ductile-brittle transition suggests the existence of a structural change intimately connecting the hydrolysis reaction with the embrittlement mechanism.

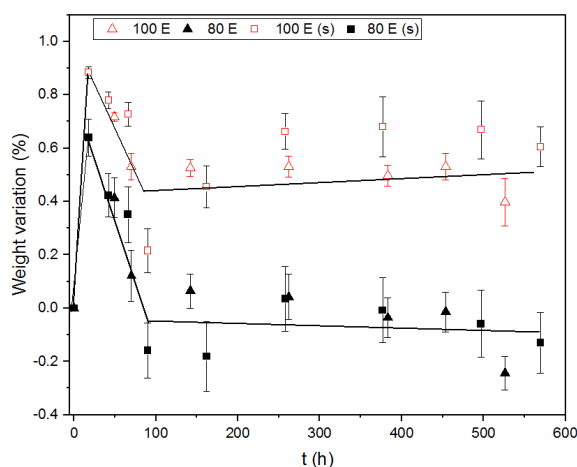


Figure 18. Samples weight variation through ageing time. Lines are added as guidance for the eye.

It has been seen that a two-phase system (crystalline/amorphous) fails to describe PET^{206,239–241}, since the different degrees of orientation can be found within the amorphous phase. Thus a three phase system has been found more suitable^{242–244}, but has never been applied in the study of the hydrolysis of PET before. These three phases consist of the crystalline (X_c), mobile amorphous fraction (X_{MAF}) and rigid amorphous fraction (X_{RAF}), where X_{MAF} and X_{RAF} are calculated as:

$$X_{MAF} = \frac{\Delta C_p}{\Delta C_p^0} \quad (3)$$

$$X_{RAF} = 1 - X_{MAF} - X_c \quad (4)$$

where ΔC_p is the jump in heat capacity at the glass transition, measured from the second heating ramp, and is the heat capacity increment of a fully amorphous PET, taken as $0.405 \text{ J} \cdot \text{g}^{-1} \cdot \text{K}^{-1}$ ²⁴⁵.

The evolution of the three fractions with ageing time is presented in Figure 19.

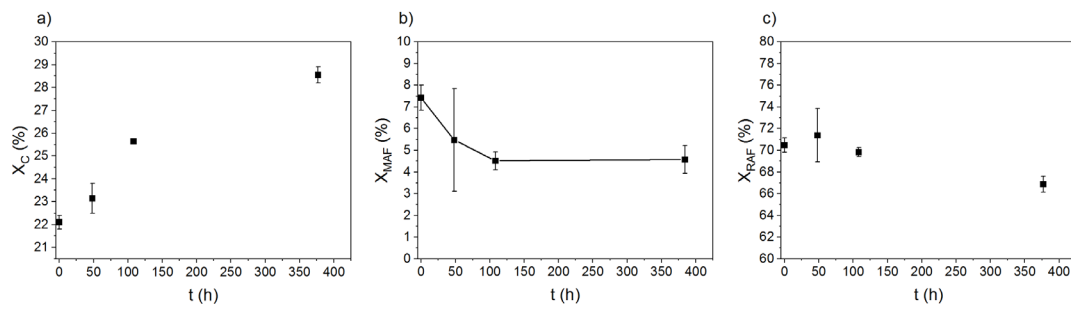


Figure 19. Total crystallinity content obtained by DSC (a), mobile amorphous fraction (b) and the RAF (c) fractions.

The evolution of the X_{MAF} fits perfectly with the weight decrease trend in the gravimetric curve. The maximum weight loss and the ductile-brittle transition point coincides with the attainment of the minimum X_{MAF} . It can be seen that the increase in the crystallinity fraction during the first 100h of ageing, until the ductile-brittle transition, occurs at the expense of the MAF fraction. From this point on, the increase in crystallinity occurs at the expense of the RAF fraction.

This finding supports the micromechanical causal chain leading to embrittlement, which would be related to the loss of MAF content in the PET, which would be providing cohesion to the material. Given these results, towards lifetime predictions, the time-to-embrittlement of PET could be more pertinently modelled as a function of MAF content than molar mass.

Since no degradation at all could be detected in the trials undertaken at room temperature or 40°C, no calculation of the E_a for the hydrolysis of PET foam could be undertaken. However, since it has been demonstrated that the cellular microstructure does not exert a significant influence on the diffusion process, previous work on the study and modelling of the hydrolysis of PET conducted in PET films can be applied to the case of PET foams. At this point, it cannot be established if the lack of degradation observed at the temperatures below T_g is related to the duration of the experimental program, with very slow reaction kinetics requiring much longer exposure times to detect the degradation, or if the hydrolysis of PET simply does not occur below its T_g .

However, the knowledge gained on the embrittlement mechanism, which appears a consequence of the consumption of the MAF and crystallinity increase during the hydrolysis reaction, requires the molecules to be mobile, this is, above T_g . Hence, even if hydrolysis would occur below T_g , at very slow rates, chemicrystallization would not occur, questioning the occurrence of embrittlement as the ultimate failure.

Towards the application of PET foam as insulation for DH pipes, applying previously developed models for PET²⁰³, service life of 30 years upon exposure to groundwater can be secured. The findings on the embrittlement mechanism suggest this service life is probably underestimated.

Given the fast embrittlement of PET at high moisture levels and temperatures above its T_g , PET foam would not be suitable for the insulation of plastic medium pipes, as the risk of degradation due to hot vapor permeation through the plastic pipe is considered high.

3.5 Conclusions and main outcomes

In this chapter, the research conducted on the ageing behaviour of polyethylene terephthalate foam upon exposure to the degradation sources occurring in DH pipelines is presented and discussed. The main outcomes of this chapter are:

- The previously determined maximal service temperature of 80°C, corresponding to the T_g of PET, has been found conservative, since an annealing effect of temperature has been constated in this work, which allows for a service temperature of at least 100°C.
- Thermal cycling does not produce any degradation of the compressive strength or E modulus of PET foam.
- Two distinct phenomena conform the moisture uptake in PET foams: (i) the diffusion and sorption of moisture by the polymer matrix, occurring at analogous rates as in films, and (ii) the progressive filling of the cell cavities by liquid water in the case of liquid water immersion, occurring at much slower rates and in a multistage manner.
- Hydrothermal degradation of PET foam is not diffusion controlled.
- The cause for hydrolysis-induced embrittlement has been found to arise from the attainment of the minimum mobile amorphous content and chemicrystallization upon hydrolysis, rather than the reduction of the concentration of tie-molecules. This questions the occurrence of hydrolysis-induced embrittlement below T_g .

Chapter - 4

Foaming PB-1

4.1 Introduction

As described in Chapter 1, the second research line pursued in this doctoral thesis is the study of the foaming of PB-1, with the goal of enabling the manufacturing of a DH pre-insulated pipe out of a single material. This chapter reports the research efforts conducted in this line, which include assessing the foamability of PB-1, deriving under which process conditions PB-1 can be successfully foamed, characterizing the resulting foams, evaluating the suitability of the characteristics of the resulting foam for the DH application and the processing-foam properties relationships which could support the further optimization of PB-1 foams for the DH application. The manufacturing of a PB-1 insulated pipe is out of the scope of this work.

- The characteristics of PB-1 known from the literature include:
- Linear, isotactic and semicrystalline ²⁴⁶.
- T_g of -25°C ¹⁰⁵

Polymorphic. PB-1 undergoes crystal-crystal transformation at room temperature. When cooling from the melt, it crystallizes into metastable Form II, characterized by a tetragonal unit cell. These crystals then progressively transform into Form I stable crystals ²⁴⁶⁻²⁴⁸. Depending on the storage conditions this process can take up to ten days ²⁴⁹. The density of Form I is much higher than the densities of the other forms. These two crystallization forms come into play under the melting and foaming conditions in this study. However, up to five crystalline forms of PB-1 have been identified, an overview is presented in ²⁵⁰.

The foaming of PB-1 has not been found reported in the open literature. From the known polymer characteristics, it is foreseen that its foaming will be challenging, arising from:

- Linear molecular structure, which is reported to involve low extensional viscosity, unfavorable for the bearing of the stretching forces during bubble growth ²⁵¹.
- Semicrystallinity. The crystalline melting temperature (T_c) marks the transition from a low viscosity (above T_c) to high viscosity (below T_c) ¹¹⁹, leading to a narrower processing window than in amorphous polymers. The processing window breadth and crystallization rate reportedly play a major role in the achievement of low density foams with fine morphology ²⁵².
- The cell stabilization step is challenging in polymers in the rubbery state at room temperature, as PB-1, resulting in difficult foaming ²¹⁵. This arises from post foaming shrinkage, resulting from blowing agent escape, or cell coalescence, induced by viscoelasticity ²¹⁵.

The research program and applied strategies were guided by the outcomes of [J4].

The lack of literature on foaming of PB-1, and of data on PB-1 melt-gas solutions required efforts on material characterization, consistent with the research needs identified in [J4]. The study of the foamability of PB-1 required an initial screening of different grades. This screening was undertaken through foam extrusion using available equipment, in cooperation with the Technical University of Hamburg. The characterization of PB-1-gas solutions conducted within this work included sorption and desorption, and plasticization effects of CO₂ in the polymer melt through the quantification of the melting point depression. These characterizations were undertaken in

parallel to the screening of grades, and so the number of grades for which the characterization was conducted was reduced as the screening progressed.

Since polymer foaming is a new research line within the HafenCity University, the conducted research involved the design and validation of test set-ups and methodologies, including the design and specification of an autoclave for batch foaming, a thermal conductivity measurement set-up, and a method for the determination of the melting point through image analysis. The structure of this Chapter is as follows:

First, the design and validation of test set-ups and measurement methods conducted within this doctoral thesis will be presented. In the subsequent section, the characterization of PB-1-CO₂ solutions will be presented, followed by a screening of the foamability of different PB-1 grades through extrusion. Batch foaming under free foaming conditions, including the evaluation of the influence of the process parameters on the expansion ratio and obtained microstructure, and the post-foaming behavior is presented in section 4.4. Batch foaming using moulds and the characterization of the resulting foams, including mechanical properties, microstructure and insulating properties is presented in section 4.5. The overall conclusions stemming from this chapter are presented in section 4.6.

Part of the outcomes of this Chapter have been published, namely the screening of different PB-1 grades through extrusion foaming, together with the CO₂ sorption/desorption characterization conform publication [J3], and the method for determination of the melting point through image analysis and validation thereof, which conforms publication [B1].

4.2 Test Set-ups and methods design and validation

This section presents the work conducted on the design and validation of specific set-ups and measurement methods required for the execution of the experimental program, which were not previously available at the HCU. Previously available set-ups and methods are not described here but in the experimental description of the respective sections.

4.2.1 Autoclave for batch foaming experiments

The autoclave was designed to cover the research needs foreseen in this doctoral thesis, as well as to allow flexibility for future applications in the scope of the research lines of the HafenCity University. The following specifications were set:

- Size: 0.5 l, with an internal diameter of 50 mm. This size was selected as to: (i) allow the possibility of foaming several samples in one batch, thus under the same foaming conditions²⁵³. (ii) Increase the time efficiency of experimental program execution, since it was foreseen that, considering the required time for heating to the melting temperature and cooling to the foaming temperature, only one foaming experiment per day can be executed. (iii) Allow the possibility of producing foam samples with a relevant size for mechanical characterization. (iv) With the available equipment, polymer sheets of 40 mm diameter could be compression molded, which would be adequate for free foaming as well as for the foaming of samples of adequate size for mechanical characterization. Therefore, the diameter was fixed as to accommodate samples with this diameter.
- View Cells: two view cells, placed opposite each other, allow the illumination and visualization of all processes occurring inside the autoclave.
- Two gas inlets to allow the foaming with CO₂ and N₂ mixtures. For environmental reasons and compatibility with the selected criteria and consistent with the outcomes of [J4], only inert gases are considered in this research. Given that the risk of post-foaming shrinkage of PB-1 had already been recognized, and the use of N₂/CO₂ mixes identified as a strategy to overcome this^{120,254,255}, as compiled in [J4], the autoclave was designed with two inlets as to allow research with blowing agent mixtures.

- Temperature up to 250°C: the upper temperature was selected to cover not only the melting temperature of PB-1, but also other of polymers of interest such as PET.
- Pressure up to 150 bars: since the strict fulfillment of the 12 Principles of Green Engineering⁴⁵ and Cradle to Cradle⁴⁴ is a goal and specification of this research, a high pressure drop was selected to support cell nucleation, consistent with the identified strategies in [J4]. The aim is to avoid the addition of nucleating agents, common in the art^{79,256–258}.
- Pressure drop rate of at least 80 bar/s. Again, in order to support cell nucleation without the use of nucleating agents, the maximization of the P drop rate²⁵⁹ was aimed for, consistent with the findings of [J4]. This was achieved with the selection of a pneumatic ball valve for automatic depressurization of the autoclave. This is a very high pressure drop rate for an autoclave with a 0.5 l volume and view cells, and was a challenge given the arising stresses in the autoclave walls. This design P drop rate was the maximal achievable. For reference, a 20 bar/s pressure drop rate for a 0.3 l standard autoclave can be reported²⁵³. Significantly higher pressure drop rates are only reported with miniature autoclaves, such as the 7 ml volume of Guo et. al, achieving 25000 bar/s²⁶⁰, or the 6000 bar/s of the 25 ml “mini-batch”²⁶¹.
- Monitorization and logging of the autoclave’s inner environment. A temperature sensor type K with a precision of $\pm 1^\circ\text{C}$ and a digital pressure sensor with a precision of 0,5% were selected. Data can be logged through a personal computer.

A schematic drawing of the autoclave set up is presented in Figure 20 and a photograph in Figure 21.

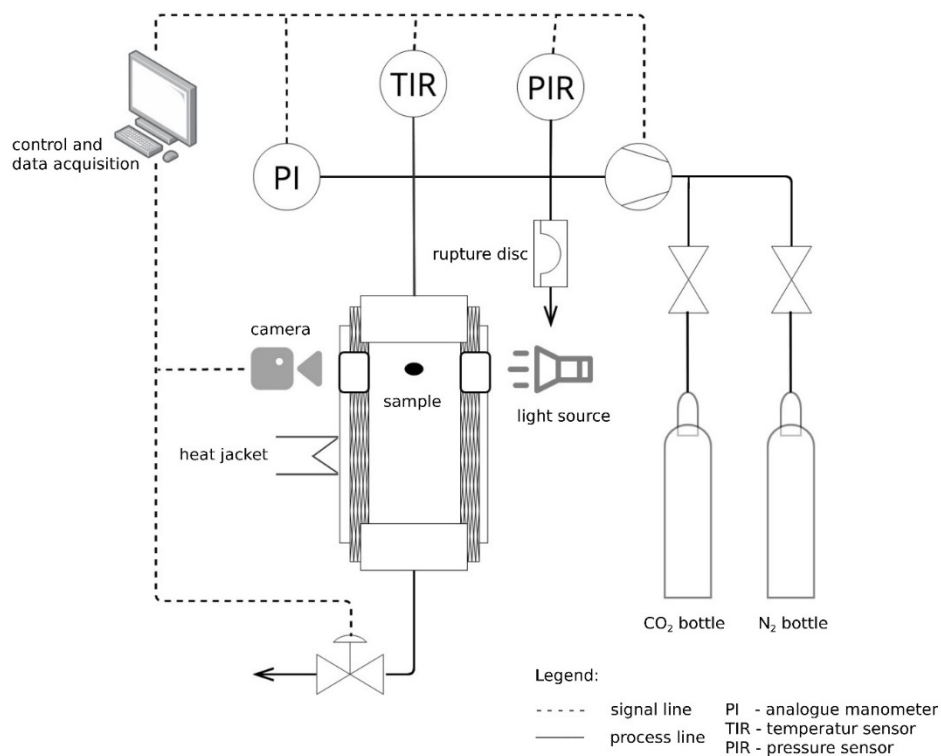


Figure 20. Schematic drawing of the autoclave set up.



Figure 21. Photograph of the autoclave set up.

4.2.2 Thermal Conductivity Measurements - Steady State Heat Flow Meter Apparatus

A steady state set-up for the measurement of thermal conductivity was developed, following ASTM C518²⁶² as far as possible. The main deviations from the standard are lower sample's thermal conductivity (λ), and that the measurement veracity was assessed in terms of bias versus data sheet values of reference foams and comparison with measurements using a commercial apparatus, and not with a calibration specimen traceable to a national standards laboratory. The design constraints included:

- Small sample size: PU foam samples extracted from DH pipes could have a maximum area of 20 mm². It was anticipated that extruded foam strands with the accessible equipment could have a cross-section area of 1 cm². This area was selected as the metering area for the set-up, which is smaller than that of the typical commercially available setups.
- ΔT required across the sample = 25°C – 40°C²⁶³
- Expected λ in the order of 0.027 W/mK.

In a heat flow meter apparatus, a steady state one-dimensional heat flux is generated through a sample placed between two parallel plates at constant but different temperatures. With a calibrated heat flux transducer, the measurement of the temperature at each plate and the sample thickness, the thermal conductivity (λ) is calculated based on Fourier's law:

$$\lambda = \phi \cdot \frac{\Delta x}{\Delta T} \quad (5)$$

where

ϕ is the heat flux

Δx is the sample thickness, which equals the distance between the hot and the cold plates.

ΔT is the temperature difference between the plates.

A heat flow meter apparatus provides a comparative, or secondary, measurement, as it requires specimens of known thermal transmission properties to calibrate the apparatus²⁶². In order to have an absolute measurement, a guarded hot plate would be required²⁶⁴.

To drive the heat flux, a Peltier element was selected. Peltier elements are thermoelectric modules that deliver solid state heat-pumping for both cooling and heating.

Heat exchange with the environment is suppressed through edge insulation. Since the test samples are insulation materials themselves, the edge insulation needs to have a lower thermal conductivity than the test samples and be significantly thicker than the sample side, as to ensure uniaxial flow across the hot and cold plates. A PU aerogel with $\lambda = 0.018\text{W/mK}$ was selected. The test sample, with dimensions 10 x 10 x 14 mm, is placed in the center of a 100 x 100 mm plate of

PU aerogel, providing 45 mm insulation on each edge.

The temperature on both sides of the sample / the hot and the cold plate is measured with thermocouples. Thin thermocouples were selected to minimize contact disruption between the samples and the plates.

The heat flux is measured through a calibrated heat flux sensor. A schematic cross-section of the set-up is presented in Figure 22 and photographs of the set up in Figure 23. The technical details of the selected components are presented in Table 5.

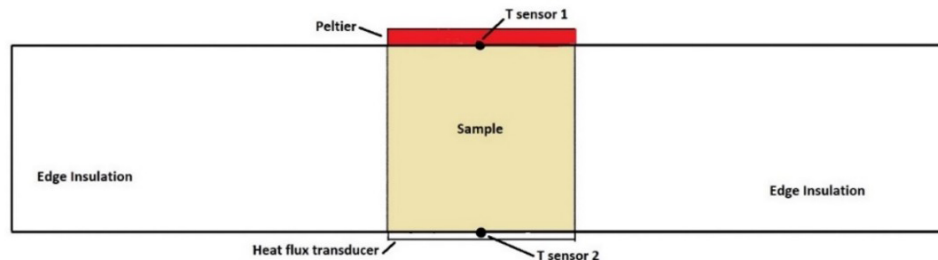


Figure 22. Cross-section schematic drawing of the heat flow meter set up.

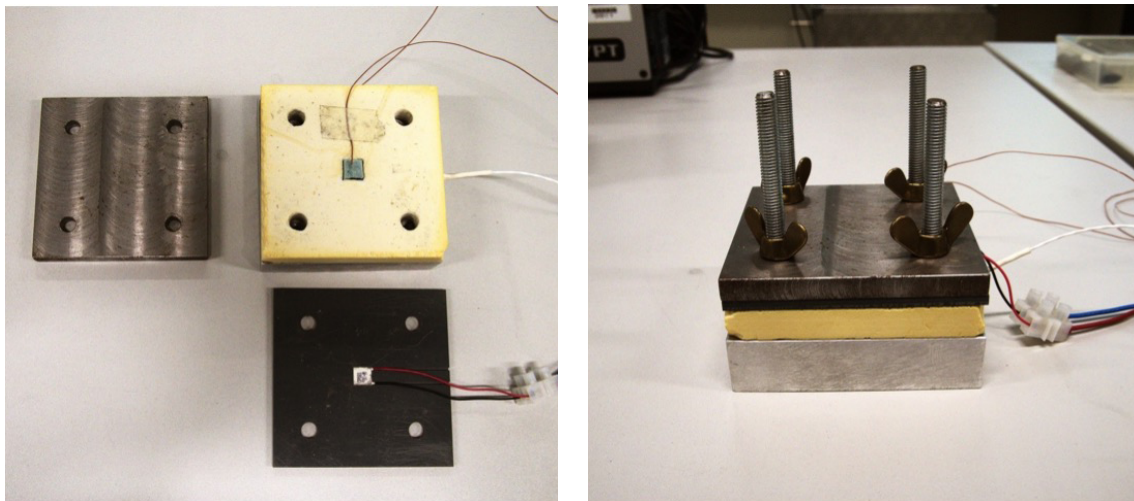


Figure 23. Left: open set up revealing the sample within the edge insulation, layer holding the Peltier element, top plate. Right: assembled set up.

Table 5. Characteristics of the selected components for the heat flow meter apparatus

Apparatus Element	Component	Characteristics
Heat source	Peltier Element CP081030-M	10x10x3mm, 3.7 W max; ΔT max 75°C
Heat Flux Sensor	gSKIN-XP (Green Teg)	10x10 mm; resolves 0.09W/m ² , calibrated according to ISO 8301
Thermocouple	Omega 5TC-TT-KI-40-1M	type K, 0.08 mm diameter
Edge insulation	BASF SLENTITE PU aerogel	14 mm thickness, $\lambda = 0.018$ W/mK according to EN 12667

The readings of the heat flux sensor and the thermocouples were displayed and logged. Once the steady state is obtained, the thermal conductivity can be derived from the measured temperatures of the hot and cold plate, the heat flux, and the sample thickness as per equation (5).

The validation of the set-up is presented in Annex I.

4.2.3 Determination of melting point through image analysis

The selection of the foaming temperature, and the relative distance between the foaming temperature and the melting and crystallization temperatures of the polymer-CO₂ dissolution under equilibrium, conditions the success of the foaming process and the expansion ratio and morphology of resulting foams²⁶⁵. The plasticization effect resulting from the dissolution of CO₂ in a polymer matrix, causing a depression of T_m , T_g and T_c , is well known^{78,265–267}. This causes a shift on the processing window. The possibility of processing at lower temperatures may also result in energy savings²⁶⁸.

Therefore, the correct setting and optimization of the foaming temperature requires the determination of the processing window under CO₂ environment. However, data on the melting point of PB-1-CO₂ mixtures could not be found in the open literature, hence required its experimental evaluation.

Previous authors have used different techniques and apparatuses for the determination of the melting point depression under CO₂, such as high pressure differential scanning calorimetry⁷⁸, infrared²⁶⁹ and near-infrared²⁶⁷ spectroscopy, or a scanning transmissometer²⁶⁸. All these are complex and expensive apparatuses not available at the HCU. It was found necessary to develop a method with the available equipment.

The view cells of the autoclave allowed for visual observation and recording of the melting process. A method for automatic digital image analysis and processing was developed as to detect the melting point from the geometrical deformation of the plastic pellets upon melting. The method and its validation through comparison with differential scanning calorimetry measurements was disclosed in publication [B1].

Summarizing, the experimental procedure requires placing a light source with variable intensity by one of the windows and a camera in the opposite window. The trigger of the camera is coupled to the autoclave control system, logging the pressure and temperature simultaneously to the image acquisition. The test temperature is set, and a pellet is placed centered in the optical path, supported on optical glass. CO₂ is then introduced with a stepwise increase in pressure, which was selected as 5 bar steps. Images are acquired in 20 s intervals and data logged accordingly.

The open-source software Cell Profiler²⁷⁰ version 4.1.3. was used for the development of the image processing and analysis pipeline. The main steps included the conversion of each image to greyscale, inverting the image intensities, segmentation of the pellet and measuring its geometrical parameters, such as eccentricity or major axis length, amongst others.

4.2.4 Microstructural characterization through image analysis

The properties of foams depend on the properties of the solid polymer and of their cellular structure⁸⁶. The fundamental role of the cellular structure on both the mechanical and the insulating properties of foams has been presented in [J4]. It is therefore of great importance to characterize it. Human scored images are tedious and time consuming²⁷¹ as well as exposed to subjectivity and bias²⁷⁰ leading to non-reproductive results. A computer-based image analysis procedure would allow to systematically process a large number of images, producing statistically representative results.

The inhomogeneous contrast of cell walls in polymeric foam images has represented a challenge for correct segmentation of the images, leading to imprecise results when applying classical computer based image analysis²⁷¹, which are mainly based on the intensity of pixels²⁷². Inherent features like broken cell walls and incomplete cells on the image borders further complicate the analysis²⁷¹.

For this purpose, a macro was developed using the open-source software Fiji²⁷³. For the image segmentation, the Trainable Weka Segmentation²⁷² plugin was used, which produces pixel-based segmentation by combining machine learning with a set of selected image features. As a first step, a classifier is trained, by adding traces of the features of the image that needs to be segmented, in this case, polymer (cell struts and walls) and cell cavities. During training, the software displays a segmented image and the result with the corresponding class colours overlaid on the original image, which allows to confirm the correct identification of the desired image features. Once the classifier is trained, it can be executed in any image. The classifier produces a probability map of the belonging of each pixel to each class. This probability can be segmented, in this case into cell cavities and cell walls. The area of the cell cavities can be then measured.

Scanned images were used, as it allowed a more systematic illumination of the samples than through optical microscopy, as well as the generation of an image of the complete sample surface. The scanning resolution was varied depending on the cell size, so as to allow the identification of the cells but not incur unnecessary computation time. Figure 24 shows an example of an original sample scan, the probability maps, and the identified cells.

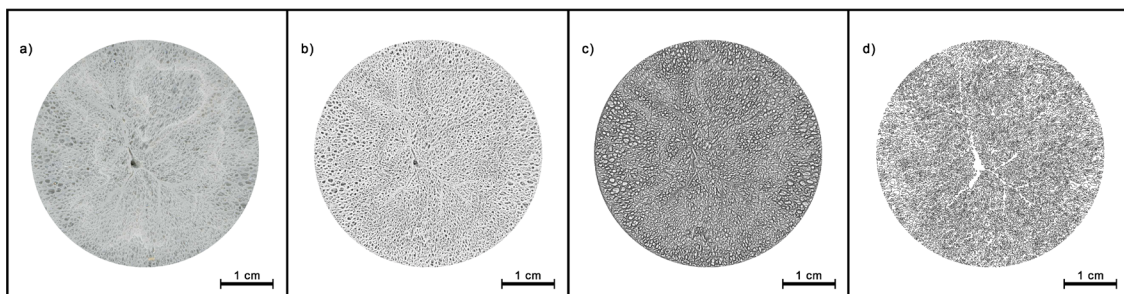


Figure 24. a) original scan of a foam sample. b) probability map of pixels belonging to cell walls (white 100% probability). c) probability map of pixels belonging to a cell cavity (white 100% probability). d) identified cell contours.

The developed classifier and macro are available at https://github.com/LuciaDoyle/Microstructure_Evaluation.

4.3 Characterization of PB-1 – CO₂ solutions

Throughout the research, four different commercial grades of PB-1 were tested, covering a range of properties and characteristics, including different chain structures, molecular weights, degree of crystallinity (X_c), melting temperature (T_m), and melt flow ratio (MFR). All resins were provided by LyondellBasell. An overview of the properties, provided by the manufacturer is presented in Table 6.

Table 6. Property overview of the evaluated PB-1 grades.

Resin	Type	Approx. molecular weight (g/mol)	X_c (%)	T_m	MFR (g/10 min @190°C/2.16 kg)
PB1-a	Homopolymer	530,000	~55	128°C	0.4
PB1-b	Homopolymer	460,000	~55	131°C	0.6
PB1-c	Thermoplastic elastomer	550,000	~25	114°C	0.5
PB1-d	Random copolymer	315,000	~35	97°C	2.5

As the research on foamability progressed, certain grades were discarded. Therefore, full characterization was not conducted for all grades.

4.3.1 Sorption - desorption

The sorption and desorption kinetics of CO₂ in PB1-a, PB1-b, and PB1-c were studied at room temperature through the gravimetric method proposed by Berens & Huvard²⁷⁴ and are reported within [J3].

PB-1 discs were saturated at room temperature and 50 bars in the autoclave. Once the defined saturation time (t_s) was reached, a rapid decompression of <30s was undertaken. The samples were placed in an analytical balance with a sensitivity of at least 1 mg and its weight decrease was logged in 5s intervals.

The CO₂ content upon desorption, $M_{t,d}$, is derived from the initial polymer weight, before sorption (W_0) and the weight of the disc with sorbed CO₂ measured during desorption (W_t), as:

$$M_{t,d} = \frac{(W_t - W_0)}{w_0} \quad (6)$$

By plotting $M_{t,d}$ with the square root of desorption time, the extrapolation to desorption time $t_d = 0$ provides $M_{t,s}$, the sorbed CO₂ at the end of the sorption period. The experiment is repeated with increasing sorption times, until a constant value of $M_{t,s}$ is reached, which corresponds to the sorption equilibrium uptake.

The desorption curves for samples sorbed up to equilibrium are presented in Figure 25 (a), and the CO₂ uptake $M_{t,s}$ versus sorption time for the three grades is presented in Figure 25 (b). Figure 25 (c) presents a close-up, to reveal the differences in CO₂ uptake for PB1-a and PB1-b.

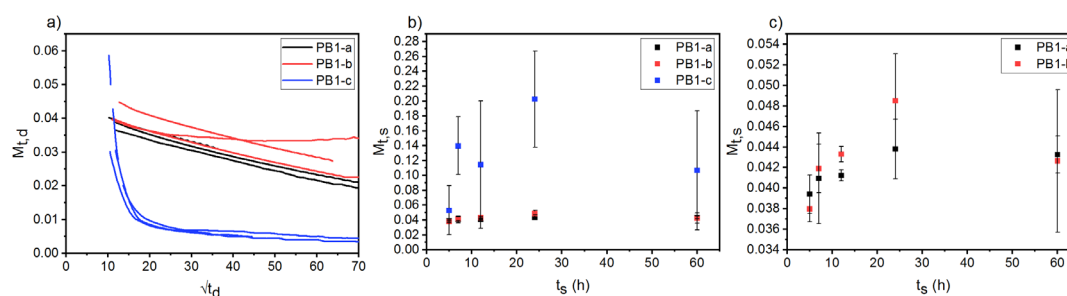


Figure 25 (a) Desorption curves after 24h sorption time (sorption equilibrium reached). (b) mass uptake versus sorption time. (c) mass uptake versus sorption time, scaled to show PB1-a and PB1-b

PB1-a and PB1-b present very similar CO₂ desorption kinetics. The desorption profile appears linear. The behaviour of PB1-c is significantly different, with an exponential decay desorption profile. For all the tested sorption times, virtually all sorbed CO₂ is desorbed in approximately 6 min. A slight combing of the PB1-c disks upon extraction from the autoclave could be also observed, in addition to a change in color from translucent to white, characteristic of lamellar thickening and recrystallization induced by CO₂²⁶⁷. Concerning the equilibrium sorption, it is observed that, despite reaching equilibrium after the same sorption time of 24h, the mass uptake of PB1-c is significantly higher, followed by PB1-b, and last PB1-a.

4.3.2 Determination of the melting point depression under CO₂ atmospheres.

The obtained melting points as a function of pressure for PB1 grades a and b (see Table 6) are given in Figure 26. As can be seen, the melting point of PB-1 decreases linearly with increasing CO₂ pressure, as commonly encountered^{265–267,275}, until a point is reached where the melting point remains approximately constant. In order to experimentally observe the values after the kink point, a cell with variable volume would be required, as to fix a temperature and progressively increase the pressure. Additional experiments at temperatures of 112°C and 105 °C were undertaken, were no melting occurred with pressures run up to 110 bars.

As can be seen in Figure 26, the melting point depression of PB1-a-CO₂ reaches 22°C, with a CO₂ pressure of 75 bars, and 14°C for PB1-b-CO₂, with a CO₂ pressure of 45 bars. The breadth of the melting point depression can be related to the amount of absorbed CO₂^{265,266,276}. The larger melting point depression in PB1-a has part of its origin in its higher melting point under ambient conditions. Interestingly, the measured melting point, of 137°C ± 3°C is well above the 128°C melting point declared on the product data sheet (see Table 6). The reported measured value is the average of five experiments.

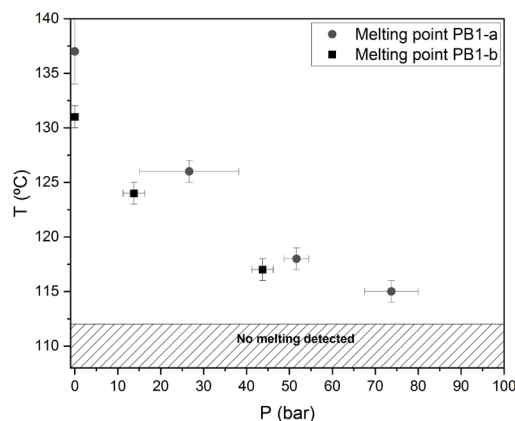


Figure 26. Melting point of PB1-a and PB1-b under different CO₂ pressures.

The observed plasticization produced by CO₂ is consistent with the depression of the crystallization temperature previously reported²⁷⁷. The measured melting points set the upper bounds for foaming for different CO₂ foaming pressures.

4.4 Screening of PB-1 grades through extrusion foaming

The study of the foamability of different PB-1 grades, conducted through extrusion experiments, is compiled and reported in publication [J3]. The extrusion experiments were conducted as a guest researcher at the Institute of Thermal Separation Processes at the Hamburg University of Technology.

The details concerning the extruder equipment and experimental procedure can be found in the publication. The main findings are summarized in this section.

The four different commercial grades of PB-1 presented in Table 6 were included in the screening. All resins were used as received.

Foaming was undertaken with a chemical blowing agent (CBA), Hydrocerol CT 550, kindly provided by Clariant. The main gas released by this CBA is CO₂, and the effective components amount to 70% according to the technical data sheet.

The main variables studied were the amount of dosed CBA, which varied between 2% and 10%, and the die exit temperature, which varied between 80 and 140°C.

Foam samples collected at each processing condition were characterized for dimensional stability, volume expansion, density, cell size and cell population density. Foamability is assessed in terms of achieved volume expansion ratio, microstructure, and processing window size.

The four different grade tests presented very different foaming behaviour, highlighting the need for broad screening of different grades in order to assess the foamability of a particular polymer. The two homopolymers, PB1-a and PB1-b presented the better foaming behaviour. Dimensionally stable foams were achieved with both, confirming foamability. A similar expansion ratio was achieved with both grades. PB1-b presents a slightly broader processing window than PB1-a, although it is narrow for both: 5°C for PB1-a and 10°C for PB1-b, with the available extrusion equipment. When comparing to PP, which would be the closest polymer PB1 can relate to, being both rubbery polyolefins, a 4°C processing window was reported in early works^{278,279}. This has

not been a barrier for the further development of PP foams, thanks to the optimization of the processing tools and use of the breaker plate ¹²¹, providing confidence in optimization possibilities for PB-1 foam.

For the case of PB1-a, larger volume expansion ratios and cell sizes were obtained with higher die temperatures. This can be explained by lower viscosity at higher temperatures, which facilitate bubble growth ²⁸⁰. Interestingly, for PB1-b, the opposite trend is encountered, with higher expansion ratios and cell sizes at the lower die temperatures. PB1-b also presented a higher die swell. It should be noted that the die swell was measured based on the diameter of the extruded strands immediately after extrusion, without the annealing required for them to be completely relaxed in a measurement of the true die swell ^{281,282}. Still, it provides adequate qualitative data. Die swell correlates with the degree of elasticity of polymer melts ^{282,283}, and it is well known that the elastic behaviour and die swell is reduced as temperature increases ^{284,285}, as evidenced in the behaviour of PB1-b. From this it can be derived that PB1-b qualitatively presents higher elasticity than PB1-a, driving its volume expansion.

The thermoplastic elastomer PB1-c foamed in a processing window between 100 and 110°C. However, it presented severe post-foaming shrinkage. This is related to the significantly higher CO₂ diffusivity in PB1-c than in the two homopolymers, as presented in section 4.3.1. The lower crystalline content of PB1-c (see Table 6) can be noted as a contributor to higher diffusivity. Further details of the chain configuration between grades are not available. Given the low dimensional stability of the resulting foams, grade PB1-c was discarded for further research.

Foaming of co-polymer PB1-d was not achieved. This could be related to its low viscosity, which cannot sustain the stretching forces required for bubble growth ¹⁴⁹ and this discarded.

The thermal conductivity of the series of PB1-a and PB1-b with at least 1 cm diameter was measured. The results are presented together with the respective sample density in Table 7 and the resulting plot in Figure 27.

Table 7. Thermal conductivity and density of PB1-a and PB1-b extruded strands

PB1-a		PB1-b	
ρ (kg/m ³)	λ (W/mK)	ρ (kg/m ³)	λ (W/mK)
740.2 ± 32.5*	0.101 ± 0.002*	502.7 ± 49.6*	0.046 ± 0.007*
500.4 ± 17.1*	0.058 ± 0.011*	480.7 ± 33.9*	0.039 ± 0.001*
492 ± 19.2*	0.051 ± 0.005*	592.7 ± 23.2*	0.055 ± 0.005*
597.8 ± 31.3*	0.074 ± 0.006*	487.1 ± 12.2*	0.053 ± 0.005*
465.2 ± 14.6*	0.062 ± 0.006*	566.7 ± 39.9*	0.056 ± 0.004*
556.8 ± 33.6*	0.040 ± 0.004*	490.2 ± 30.8*	0.059 ± 0.003*
683.6 ± 238.9*	0.065 ± 0.002*	606.1 ± 2 3.8*	0.067 ± 0.004*

* Standard deviation

No significant difference between the thermal conductivities of foams from both resins for equivalent densities is obtained.

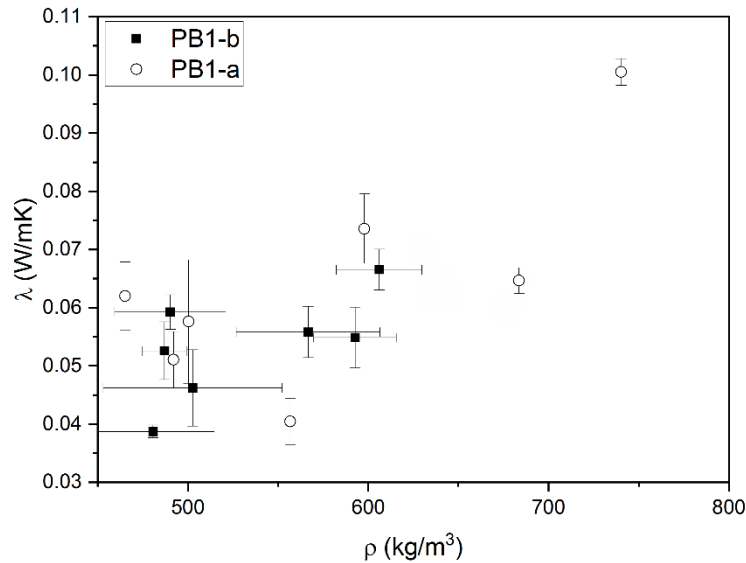


Figure 27. Thermal conductivity vs density of PB1-a and PB1-b extruded strands.

Further study of the foaming of PB-1 was conducted with PB1-a and PB1-b.

4.5 Batch Foaming – Free foaming conditions

Batch foaming experiments were conducted with the autoclave described in section 4.2.1. using CO_2 as a blowing agent.

4.5.1 Materials and Methods

In addition to PB1-a and PB1-b, CO_2 of >99.8% purity purchased from Westfalen was used. PB-1 pellets were hot pressed into discs of 40 mm diameter and 2 mm thickness and placed in a sample holder inside the autoclave. The autoclave temperature was set above the melting point of PB-1. The autoclave is purged 3 times with CO_2 before each trial. After purging, CO_2 is injected up to the selected foaming pressure.

Preliminary trials were undertaken to determine the saturation time in the molten state. For this, samples were foamed after 1h saturation time, and after overnight saturation time. Equivalent expansion ratios were obtained, indicating saturation was achieved in one hour. Nevertheless, a two-hour saturation period was established as to provide a safety margin in all executed batch foaming experiments. Once the saturation period is completed, the heating is switched off and the autoclave left to cool down until the desired foaming temperature is reached. The foaming pressure is kept to the set level by the pump. Once the foaming temperature is reached, a fast decompression of the autoclave produces the foaming of the samples.

The foaming conditions (pressure and temperature) were varied and the obtained samples were characterized in terms of observed microstructure and volume expansion ratio (V_{exp}). The V_{exp} was calculated as:

$$V_{exp} = \frac{\rho_{polymer}}{\rho_{foam}} \quad (7)$$

The density (ρ) was measured by water displacement with a glass pycnometer, demineralised water and a Sartorius MC1 LC3200 D (Goettingen, Germany) balance. Three samples per foaming condition were foamed in one batch and characterized.

The morphology of the foams was examined in an optical microscope (Leica DMLP, Wetzlar, Germany). Given PB-1's crystal-crystal transformation (see 4.1), characterization was undertaken 10 days after foaming, in order to measure the foam density in its stable condition ²⁴⁹.

Two batch foaming series were executed, according to the foaming parameters presented in Table 8. The upper temperature selected as to be below the determined melting point of PB-1-CO₂ solutions (section 4.3.2) at the relevant conditions. Foaming temperature was progressively lowered until reduced volume expansion of the obtained foams was observed.

Table 8. Foaming parameters

Foaming P (bar)		Foaming T (°C)			
50		80	85	90	95
100	75	80	85	90	95

Pressure drop rate was measured as 140 bars/s when foaming from 50 bars and 122 bars/s when foaming from 100 bars.

4.5.2 Results and Discussion

Volume Expansion Ratio

The obtained volume expansion ratios for each resin and foaming condition are presented in Figure 28.

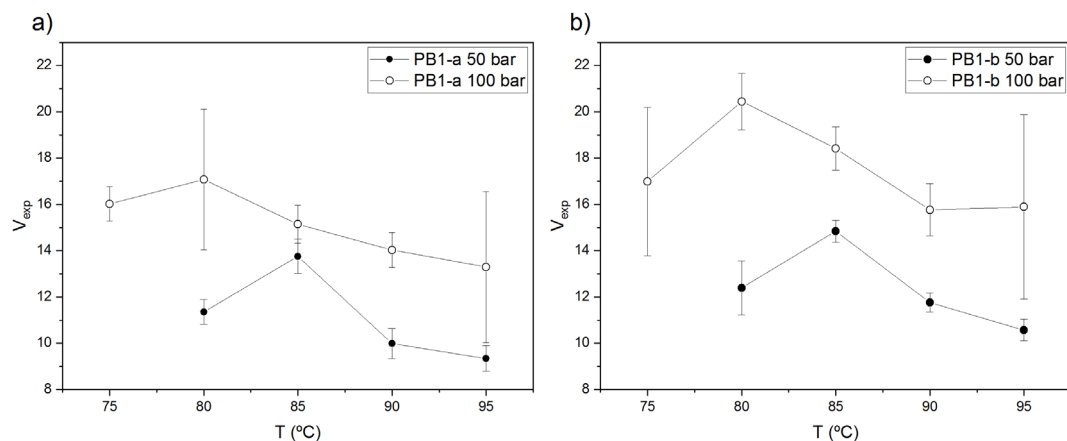


Figure 28. Obtained volume expansion with the tested foaming parameters for PB1-a (a) and PB1-b (b). Connecting lines are guidance for the eyes.

The shape of the obtained trends is commonly encountered ^{257,286}, and reveals that at higher temperatures, the gas loss is governing the foaming behaviour, related to higher gas diffusivity which conditions the achieved expansion, while the stiffness of the polymer is governing the expansion at lower temperatures. The maximum expansion is found in-between. Foaming at higher pressures shifts the maximum expansion to lower temperatures. This can be related to the plasticization effect of the CO₂ dissolved in the PB-1 matrix ²⁸⁷, and higher solubility of the CO₂ at higher pressures. A higher expansion ratio is achieved with higher pressure drops. This was expected since increasing the pressure drop increases the driving force for the cell nucleation, leading to the formation of a larger number of cells, as can be recalled from the following general expression for nucleation rate (N) ¹²⁰

$$N = M \cdot B \exp \left[-\frac{16\pi\sigma^3}{3k_B T(P_v - P_L)^2} \right] \quad (8)$$

where M and B are increasing functions of the gas concentration, and of the gas diffusivity, respectively. k_B is the Boltzmann constant, and P_v and P_L are the equilibrium gas pressure and the pressure in the liquid phase.

While the obtained trends of V_{exp} vs foaming temperature and vs foaming pressure are analogous for both resins, a higher expansion ratio is obtained with PB1-b, particularly with the higher pressure drop.

A certain level of shrinkage could be observed in the samples foamed from higher pressures.

Microstructure

The cellular structure of the different samples obtained can be seen in Figure 29 for PB1-a and Figure 30 for PB1-b.

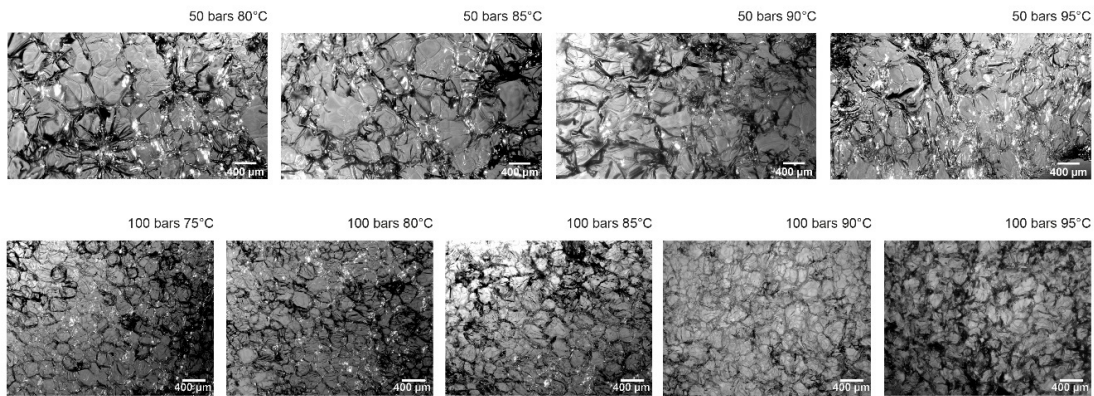


Figure 29. Representative micrographs for PB1-a foams, obtained under different process conditions.

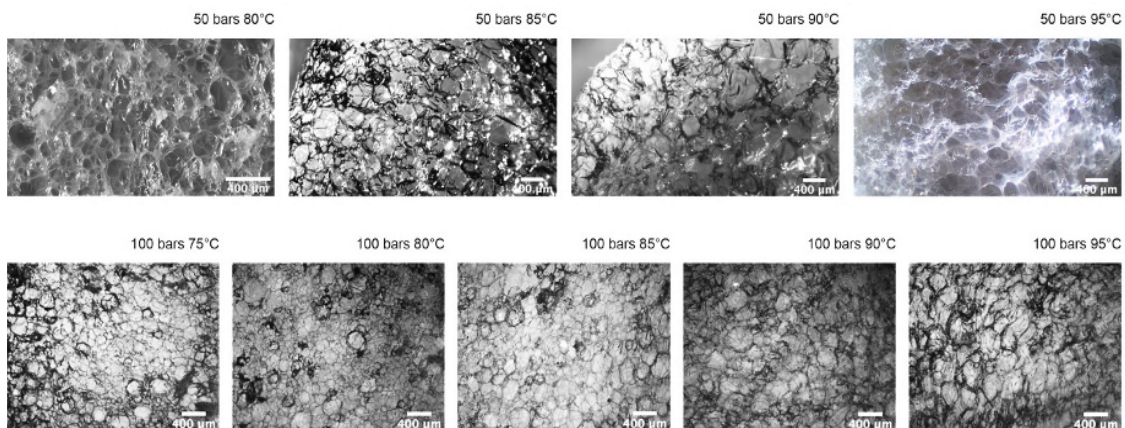


Figure 30. Representative micrographs of PB1-b foams obtained under different process conditions.

From the micrographs presented in Figure 29 and Figure 30, it can be readily observed that the cell size is significantly reduced when foaming with a higher pressure drop. When foaming from 50 bars, PB1-a foams present a diameter ranging 300- 400 μm , and PB1-b a diameter range of 150-300 μm . When foaming from 100 bars, PB1-a's cell diameters range from 140 – 200 μm , and PB1-b's 100-200 μm diameter. There is a tendency towards larger cells with PB1-a. A bi-modal cellular structure is formed when foaming from 100 bars, with a few larger cells embedded in smaller cells. The impact of the pressure drop on the obtained microstructure appears stronger than the impact of the foaming temperature, for the tested ranges. Cell wall folding can be observed, for PB1-a foamed at 100 bars, and 85°C and higher foaming temperatures, and for PB1-b foamed at 100 bars, and 90°C and higher foaming temperatures.

Post-foaming behaviour

During the characterization of the samples, shrinkage of some samples was observed, in particular, those foamed at higher temperatures. This is illustrated by the photographs in Figure 31.

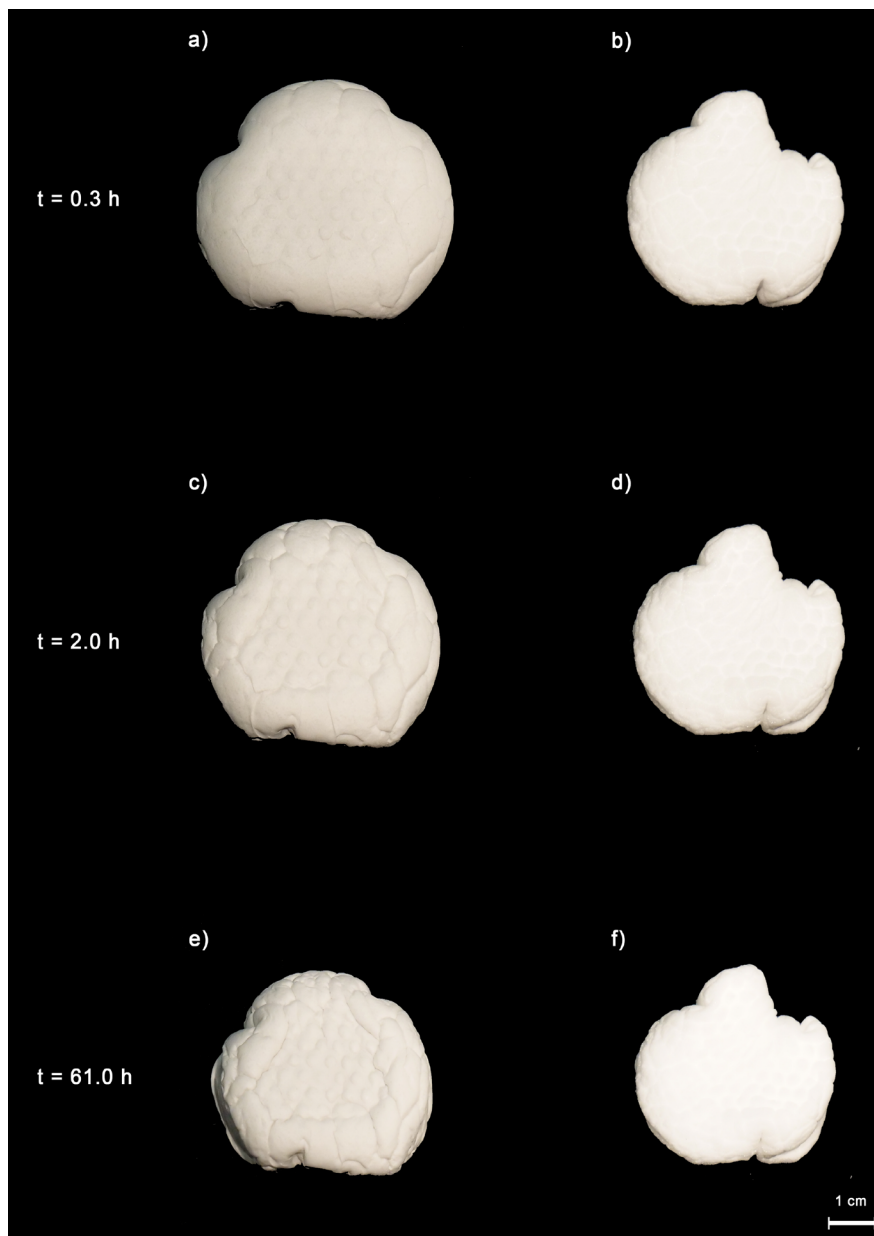


Figure 31. Photographs of taken 20 minutes, 2 hours and 61 hours after foaming, for PB1-b (a, c and e respectively) and PB1-a (b, d and f respectively).

Since dimensional stability of the resulting foams is of ultimate importance and the risk of shrinkage had been identified at an early stage, the post foaming behaviour of the produced PB-1 foams was evaluated in more detail. For this, samples were foamed under the same conditions as in Table 8, and their density was measured within the first 20 minutes after foaming, and again after 10 days. Shrinkage was quantified in terms of post-foaming density increase ($\Delta\rho_{\text{post-foaming}}$), calculated as:

$$\Delta\rho_{\text{post-foaming}} (\%) = \left(\frac{\rho_{t0} - \rho_{t10}}{\rho_{t0}} \right) \cdot 100 \quad (9)$$

where

ρ_{t0} is the initial foam density measured within 20 minutes after foaming.

ρ_{t10} is the foam density measured 10 days after foaming

The resulting plots are presented in Figure 32. It can be seen that shrinkage increases practically linearly with foaming temperature, and that it is higher for PB1-a than for PB1-b. PB1-b experiences a certain level of post-foaming expansion which is the reason for the density decrease for the 50_85 samples. It can be also seen that foaming from higher pressures produces higher expansion ratios, but also higher levels of shrinkage occur. In PB1-b shrinkage appears to peak at about 40% density reduction, which is attained with the foaming conditions of 100 bars and 90°C, and remains at an analogous level with increasing foaming temperature levels, while PB1-a's shrinkage continues to increase. Within this study, 100% post-foaming density increase was obtained for the highest tested foaming temperature and pressure.

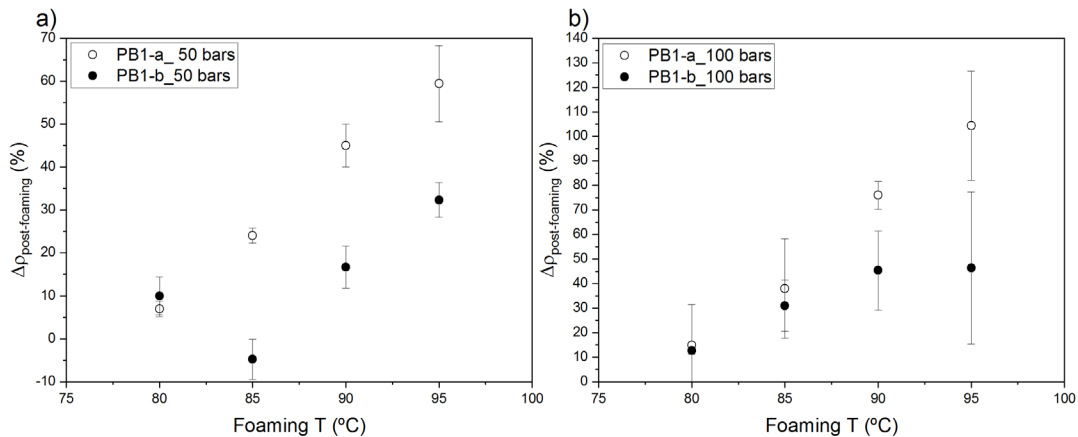


Figure 32. Post-foaming density increase (%) caused by shrinkage as a function of foaming temperature, for foams produced from 50 bars foaming pressure (a) and 100 bars foaming pressure (b).

A certain level of shrinkage was expected and consistent with the observations of previous authors working on the foaming of rubbery polymers^{254,255,265,288}. Post foaming shrinkage is commonly allocated to high blowing agent diffusion rates^{254,255,288–290} or elasticity of the polymer^{291,292}. When comparing PB1-a and PB1-b, the undertaken desorption tests (Figure 25 a) did not reveal a higher CO₂ diffusion rate in PB1-a than in PB1-b. Rheological characterization of the polymer melts was not undertaken, but the die swell measurements recorded (see section 4.4 and [J3]) pointed at a higher elasticity of PB1-b, suggesting this would not be the cause for the higher post-foaming shrinkage encountered.

Differences in the crystallization temperature and crystallization kinetics could well explain the differences in the post-foaming behaviour²¹⁵, since the crystal domains provide structural stability during the bubble growth and stabilization step, preventing cell coalescence¹¹³. The obtained data suggest that at higher foaming temperatures, the reached crystallinity degree is not high enough to sustain the overall structure. As the foaming temperature is decreased, higher levels of crystallization can be reached, leading to lower shrinkage. Slow crystallization kinetics of PB1-a would explain its poor post-foaming behaviour.

Further research on melt rheology and crystallization kinetics would be required to confirm the ultimate cause for the different post-foaming behaviour of the two resins. Different strategies can be pursued to mitigate shrinkage, such as the use of N_2/CO_2 mixes as blowing agent^{120,254,255} or the reduction of the ambient pressure, as to counterbalance negative pressure created in the cells due to the rapid CO_2 escape²⁵⁵, which drives the shrinkage. Since the scope of this doctoral thesis comprises the evaluation of the feasibility of foaming PB-1, research was continued with PB1-b only, since it presented better characteristics.

4.5.3 Conclusions

The foaming processing window for batch foaming of PB-1 with CO_2 was identified, between 75°C and 95°C. The maximum expansion ratio was obtained at 85°C when foaming from 50 bars and 80°C when foaming from 100 bars.

Higher volume expansion ratios were obtained with PB1-b. The higher levels of post-foaming shrinkage experienced by PB1-a explain the final lower level of volume expansion ratio obtained.

Given the higher final volume expansion ratios obtained, and its better post-foaming behaviour, PB1-b was selected to continue with the trials.

4.6 Confined foaming in molds

Batch foaming was undertaken in moulds, as to produce samples of adequate size for mechanical characterization and thermal conductivity measurements. These are the main properties defining the foam's suitability for the DH application.

4.6.1 Materials and Methods

Moulds of 40 mm diameter and 25 mm height were manufactured. Hot pressed PB1-b discs were placed in the moulds, saturated for 2h and foamed at the selected foaming P and T. The mould constrained the CO_2 carbon dioxide diffusion and escape path through the edges but allowed it through the faces of the samples since these were confined in perforated metal plates.

For each foaming condition, the mass of the discs was varied, based on the results of volume expansion from the free foaming experiments (section 4.5), as to obtain foams of different densities. The objective is to evaluate foaming process-foam properties relationships and compare the properties of the obtained foams with the technical requirements for DH (see Table 1).

In each batch, four samples per selected foaming conditions were produced. A photograph of the moulds and sample holder is presented in Figure 33.



Figure 33. Sample holder with four moulds. Foam samples.

Three of the samples were tested under compression in a universal testing machine at a displacement-controlled rate of 2 mm/min. The force was measured with a 2 kN load cell, accuracy class 0.5 (HBM, Darmstadt, Germany). The strain was measured by 3D digital image correlation (DIC)²⁹³ using an ARAMIS 6M adjustable stereo camera system (GOM mbh, Braunschweig, Germany). The images were acquired at a frequency of 5 Hz. From the obtained stress strain curves, the E modulus, corresponding to the slope of the initial stress strain curve, and the compressive stress at 10% strain (σ_{10}) was obtained, since they are the main mechanical properties evaluated for foams in DH, according to EN 253²⁹⁴.

From the remaining sample, specimens of 10 x 10 x 14 mm were extracted for the measurement of thermal conductivity, using the in-house heat flow meter apparatus described in section 4.2.2. Slices of each sample were scanned for the evaluation of the cellular microstructure. The complete surface of 4 slices per sample type were evaluated, using the developed macro for image analysis described in section 4.2.4. The macro provides the number of identified cells and the respective measured cell area. The cell diameter is a more common parameter found in the literature than the cell area. Given the irregularity of the cells, the equivalent cell diameter ϕ_{eq} was calculated for each cell, defined as the diameter of a circle with the same area as the measured cell area:

$$\phi_{eq} = 2 \cdot \sqrt{\frac{\text{measured area}}{\pi}} \quad (10)$$

The cell population density (N_0), defined as the number of cells per unit volume of the original unfoamed polymer, was obtained as^{78,295}:

$$N_0 = \left(\frac{n}{A}\right)^{3/2} \cdot \frac{\rho_{polymer}}{\rho_{foam}} \quad (11)$$

where n is the number of cells in the image and A the area of the image (cm²). N_0 is given in cell/cm³.

4.6.2 Results and Discussion

An overview of the produced samples is presented in Table 9. The table contains the processing parameters used for foaming, the obtained density, σ_{10} and E modulus obtained from the compression tests, and the equivalent mean and median ϕ_{eq} and N_0 obtained from the cellular microstructure characterization.

It should be noted that the obtained samples were dimensionally stable. The foams were adhered to the moulds upon extraction from the autoclave but came loose upon cooling. No shrinkage was observed, unlike the free foamed samples (section 4.5.2, Figure 32). This is consistent with recent reports of confined foaming of elastomeric polymers²⁹⁶ and can be related to the restricted CO₂ escape pathway while the foam skin is still hot.

Table 9. Characteristics of obtained PB1-b foams

Sample name	Foaming T (°C)	Foaming P (bar)	density (kg/m ³)	$\phi_{eq, mean}$ (μm)	$\phi_{eq, median}$ (μm)	N_0 (cells/cm ³)
50_80	80	50	150.29 ± 5.46*	255 ± 121*	224 ± 69 ⁺	8.9 · 10 ⁴ ± 9.2 · 10 ³
50_85	85	50	139.34 ± 2.41*	257 ± 129*	221 ± 70 ⁺	9.0 · 10 ⁴ ± 8.7 · 10 ³
50_90	90	50	138.16 ± 2.41*	303 ± 155*	270 ± 101 ⁺	5.9 · 10 ⁴ ± 5.7 · 10 ³
50_95	95	50	128.03 ± 1.08*	330 ± 177*	293 ± 118 ⁺	5.3 · 10 ⁴ ± 5.2 · 10 ³
100_85	85	100	130.53 ± 1.82*	48 ± 36*	38 ± 19 ⁺	4.3 · 10 ⁶ ± 4.2 · 10 ⁵
100_90_a	90	100	113.54 ± 1.28*	48 ± 42*	33 ± 17 ⁺	5.1 · 10 ⁶ ± 4.9 · 10 ⁵
100_90_b	90	100	122.70 ± 5.35*	47 ± 39*	33 ± 17 ⁺	5.3 · 10 ⁶ ± 5.6 · 10 ⁵
100_95	95	100	110.07 ± 8.05*	51 ± 44*	35 ± 20 ⁺	4.7 · 10 ⁶ ± 5.7 · 10 ⁵

*Standard deviation; ⁺ median absolute deviation

Cellular structure

From Table 9 it can be seen, consistently with the batch-free foaming trials, that the pressure drop is a key variable affecting the cellular microstructure, in terms of resulting cell size and cell population density. By duplicating the pressure drop, from 50 to 100 bars, the average cell size is reduced by 1/6. The cell population density is increased by a factor 66. The statistical evaluation of equivalent cell diameters for each foam sample type is presented in Figure 34 (a), which presents the mean and median values, the 25th – 75th percentile range as the box, and the kernel smooth distribution profile. A representative scan of PB-1 foam obtained from a P drop of 50 bars and P drop of 100 bars is presented in Figure 34 (b) and (c), both obtained with a foaming temperature of 85°C.

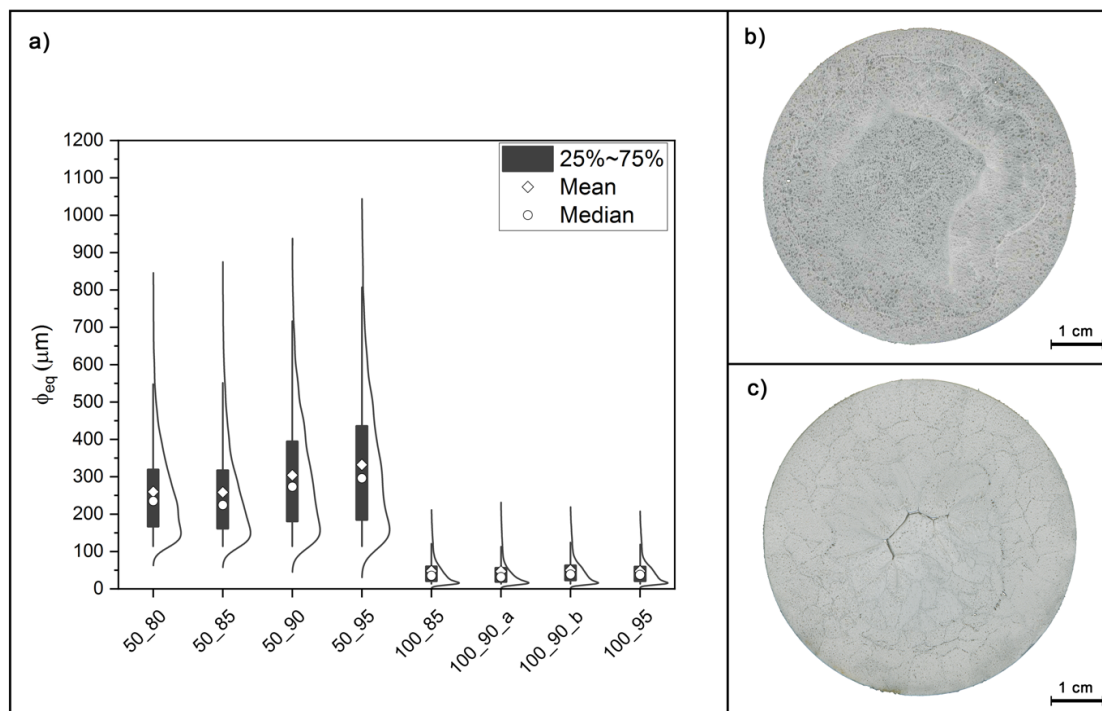


Figure 34. Statistical evaluation of the cellular microstructure per foam type (a). Representative scan of 50_85 (b) and 100_85 (c).

It can be seen that a broad range of cell sizes is obtained in all samples, but do not follow a normal distribution. Lower cell sizes occur at higher frequencies. A slight increase in cell size with foaming temperature can be seen in the 50 bar foaming pressure series, while remains constant for the 100 bar foaming pressure series. It has been previously noted that the effects of the processing temperature on cell size and cell population density are more complex to elucidate, due to the dependency with the polymer's thermal transitions²⁹⁷. The fact that the foaming was undertaken in confined conditions (moulds) with different amounts of polymer is a further variable. The target of varying the amount of polymer was to obtain foams with different densities, given that different volume expansions can be obtained at different foaming temperatures (see section 4.5). It should be also stressed that deliberately no nucleating agent was added, since tailoring properties through processing while avoiding material diversity was a specific target of this thesis, as to strictly comply with the Green Engineering Principles⁴⁵. This partly explains the heterogeneous cellular structure, since the use of nucleating agents result in more uniform cellular structures^{298–301}.

Mechanical Properties

As for the compressive behaviour of the produced PB-1 foams, the obtained engineering stress-strain curves can be seen in Figure 35. From the curves, the E modulus and σ_{10} were derived and presented in Table 10.

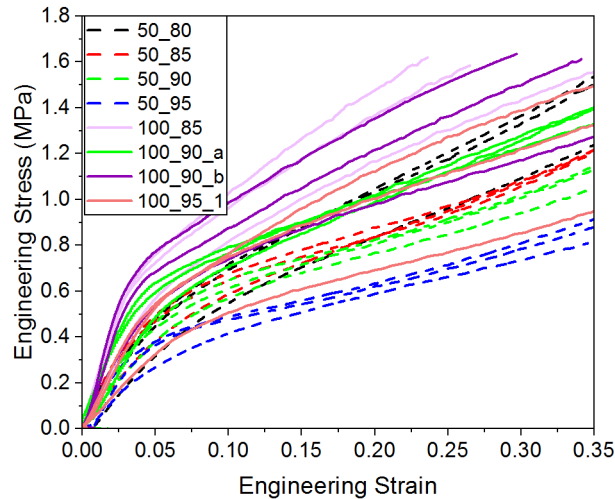


Figure 35. Engineering stress strain curves obtained under compression for the produced PB-1 foams.

Table 10. Mechanical Properties of produced foam samples

Sample name	σ_{10} (MPa)	E (Mpa)
50_80	$0.65 \pm 0.09^*$	$7.5 \pm 0.6^*$
50_85	$0.64 \pm 0.05^*$	$9.9 \pm 2.2^*$
50_90	$0.61 \pm 0.04^*$	$9.7 \pm 2.5^*$
50_95	$0.46 \pm 0.04^*$	$9.3 \pm 2.3^*$
100_85	$0.96 \pm 0.11^*$	$20.2 \pm 0.3^*$
100_90_a	$0.75 \pm 0.04^*$	$13.8 \pm 2.7^*$
100_90_b	$0.87 \pm 0.01^*$	$22.0 \pm 0.8^*$
100_95	$0.76 \pm 0.01^*$	$12.2 \pm 0.6^*$

*standard deviation

The shape of the stress-strain curves shows the elastomeric behaviour of PB-1, as a plastic yielding plateau does not occur²³⁰.

In order to observe the structure – properties relationships of the obtained foams, the cell population density, mean cell size, σ_{10} and E modulus were plotted vs the foam density, as presented in Figure 36 (a), (b), (c) and (d) respectively. This first approach was undertaken as a pioneering model for the prediction of the mechanical behaviour and concluded that the relative density of foams is the single most important variable^{302,303}.

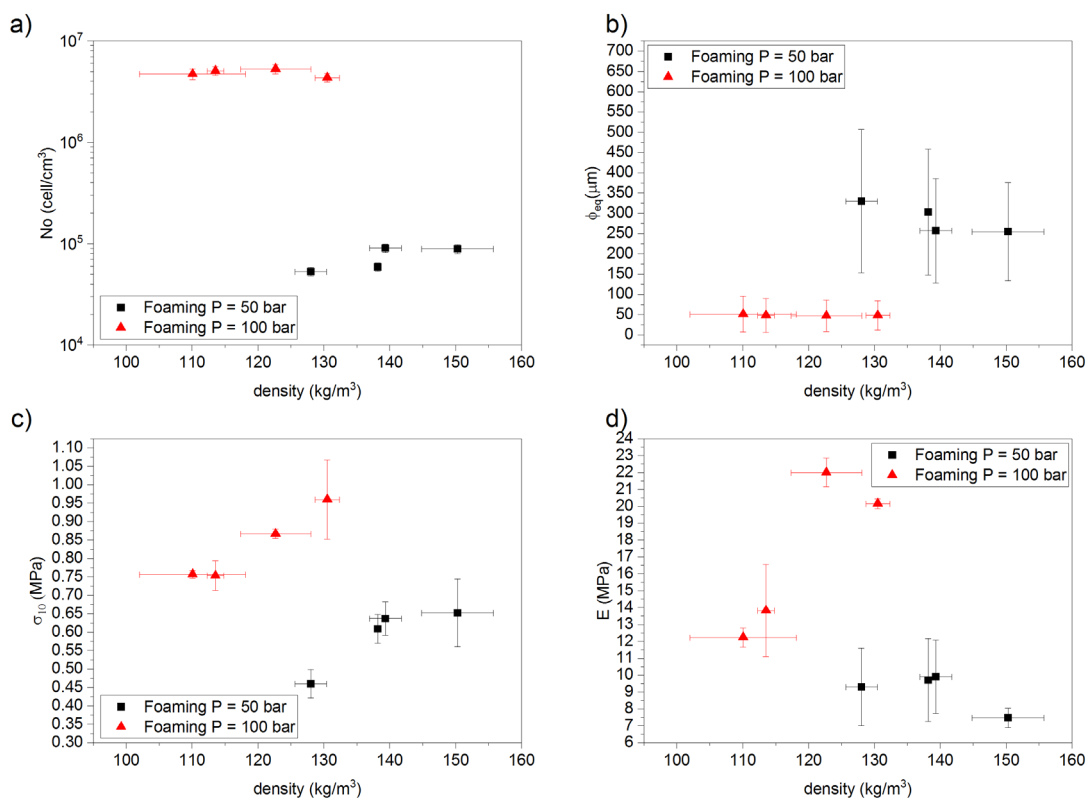


Figure 36. Cell population density (a) equivalent diameter (b), σ_{10} (c) and E modulus (d) versus foam density for the produced PB-1 foams.

From Figure 36 it can be seen that the mechanical properties are not governed mainly or at least solely by the foam density. A clear grouping per applied foaming pressure drop series appears. By varying the foaming pressure drop, foams with equivalent density but different microstructures are produced, presenting significantly different mechanical behaviour. The reduced cell size and increase in cell population density produced by increasing the pressure drop enhance the mechanical properties. For the compressive strength, it is evident that it scales with the density of foams with similar cellular structure, and the reduction of cell size and increase of cell population density causes a shift in the trend, to higher strengths. For the E modulus the trends are not as clear, but higher modulus values are obtained with the 100 bars foaming pressure series.

The inverse relationship between the cell size and the strength of foams has been observed by previous authors^{304–306}. This is explained through fracture mechanics, as the larger the cell size (hence the cell struts), the larger the probability of finding a critical flaw³⁰⁴. But not only. The shape of the cross-section of a foam strut is similar to that of a Plateau border^{304,307}, and is thicker in the area close to the interconnection points and therefore stiffer³⁰⁷. Thus, deformation occurs far from the strut interconnection points. Larger cells possess larger areas prone to deformation, impacting on the strength.

The correlation between morphological features, namely average cell size and cell population density with the mechanical properties was evaluated, as presented in Figure 37. Data point symbols are scaled with the foam density as to visualize the effect of this parameter.

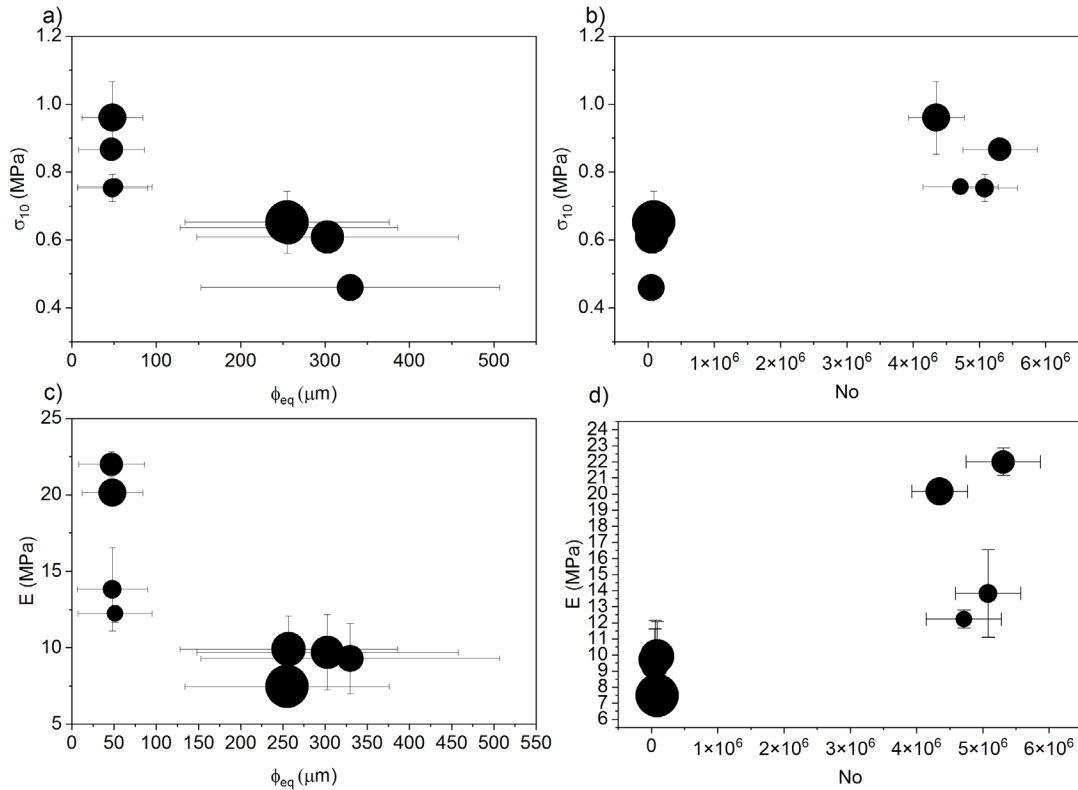


Figure 37. Obtained σ_{10} and E modulus vs mean cell equivalent diameter (a and c respectively) and versus cell population density (b and d respectively). Symbol size is scaled with the respective foam density.

The graphs display again how the E modulus and σ_{10} increase with reduced cell size and increased cell population density.

Many parameters come into play to accurately describe the mechanical behaviour of polymeric foams, including not only the cell size but also the cell geometry^{308,309}, cell size variability and cell wall thickness variability³¹⁰. More accurate modelling has been accomplished through finite element methods^{310–312}. This may be a subject of future work.

Thermal conductivity

The obtained thermal conductivity values are summarized in Table 11. Measured density and thermal conductivity for each foam batch. Sample name relates to foaming P and T.

Table 11. Measured density and thermal conductivity for each foam batch. Sample name relates to foaming P and T.

Sample	λ (W/mK)	ρ (kg/m^3)
unfoamed PB-1	0.109 ± 0.013	1008 ± 97
50_80	0.033 ± 0.003	150.3 ± 5.5
50_85	0.032 ± 0.001	139.3 ± 2.4
50_90	0.032 ± 0.003	138.2 ± 0.3
50_95	0.032 ± 0.004	128.0 ± 2.4
100_85	0.037 ± 0.003	130.5 ± 1.8
100_90_a	0.035 ± 0.002	113.5 ± 1.3
100_90_b	0.038 ± 0.004	122.7 ± 5.3
100_95	0.031 ± 0.003	110.1 ± 8.0

The variation of the measured thermal conductivity between samples was found narrow. Surprisingly the average thermal conductivity obtained for the samples with smaller cell sizes (100 bars foaming P series) appears higher than that of the larger cell size (50 bars foaming P series), contrary to literature reports ^{313,314}. Comparing the thermal conductivity of the batch foamed samples with the extruded foamed samples using a CBA (section 4.4), it can be seen how a jump in the obtained foam densities and thermal conductivities was achieved, as can be seen in Figure 38.

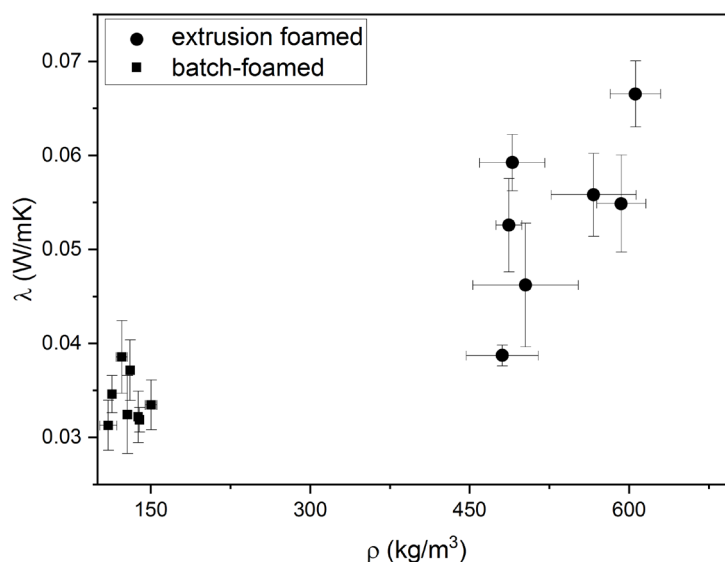


Figure 38. Thermal conductivity of PB1-b foams produced by extrusion with a CBA and by batch foaming.

Benchmark with PU in state-of-the-art DH-pipes

The technical requirements for the foam in DH pipes, in terms of mechanical properties, require a balance between strength and stiffness, as per Table 1. With the ultimate goal to evaluate the suitability of the produced PB-1 foams for the DH application, the obtained strength was plotted against their E modulus, together with the confidence and prediction bands for a 95% confidence level. As a benchmark, the properties of the PU foams extracted from DN40 flexible DH pipes with smooth casing (FSDN40) and corrugated casing (FCDN40) ²¹⁹ were added for comparison. The results are presented in Figure 39.

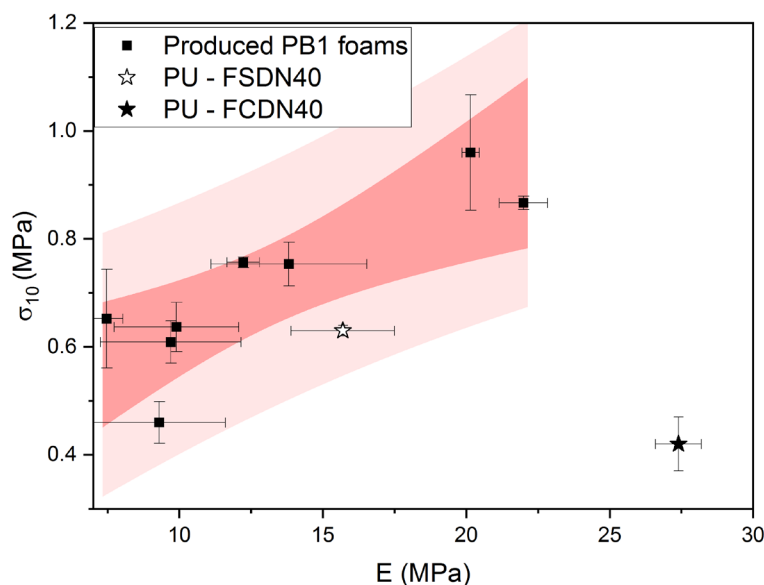


Figure 39. σ_{10} vs E modulus for the produced PB-1 foams and their confidence and prediction bands. PU foams from flexible DH pipes are added for reference.

As can be seen from the graph, the mechanical properties of the PU foam extracted from DH flexible pipes with smooth casing already fall within the prediction band for PB-1 foams. This supports the suitability of PB-1 foam as a candidate for the replacement of PU at least in this model of flexible pipes.

From Figure 39 it can also be seen that a further increase in strength and stiffness is not required by the application.

As for the thermal conductivity, obtained values are equivalent to those of polystyrene foam²³⁰ and higher than the 0.022 W/mK of state-of-the-art PU foam in flexible pipes stated reported in the product data sheet³¹⁵. Comparing with the PU from DH pipes measured in the same test in-house set-up, the mean value of the produced PB-1 foams of 0.032 would be 62% above than the 0.02 measured for PU (see Annex I).

However, it should be highlighted that neither CEN EN 15632-2:2010³¹⁶ nor its update draft³¹⁷ state a minimum requirement for λ . The lower operating temperature of the 4th generation DH¹⁰ could relax the λ requirements.

Optimization of the microstructure should be undertaken with the target to reduce the thermal conductivity while maintaining the mechanical properties in the same range.

4.6.3 Conclusions

PB1-b was successfully foamed in moulds, which allowed the obtention of samples of relevant size for mechanical and thermal characterization.

Samples displaying a range of mechanical properties were produced. The foam density as main parameter fails to describe the mechanical properties. By changing the foaming pressure drop, foams with similar density were produced, but with very different microstructure (cell size reduction factor 1/6 and cell population density increase by a factor 66 by increasing the foaming pressure from 50 to 100 bars), which lead to very different mechanical behaviour (σ_{10} increase from 0.46-0.65 MPa to 0.75-0.96 MPa).

4.7 Conclusions and main outcomes

- A screening of different PB-1 grades was undertaken, and a very different foaming and post foaming behaviour was obtained between the different tested resins. This highlights the need of a broad screening in order to assess foamability of a given polymer.
- Favourable grades for foaming have been identified, confirming the foamability of PB-1. Post-foaming shrinkage is the main problem encountered with the discarded grades.
- The pressure drop exerted the highest influence in the microstructure of the produced foams. The change in order of magnitude of the obtained cell size and cell population density results in a shift to higher compression strengths. Therefore, the mechanical properties do not correlate with the density of the foams.
- Foams in required size for mechanical characterization were successfully produced.
- Mechanical properties of PU from state-of-the-art flexible plastic medium pipes fall in the prediction bands obtained from the produced PB-1 foams. This provides confidence on the suitability for the application.

Chapter - 5

Conclusions

This doctoral thesis has evaluated different alternatives to replace PU foam in DH pipelines, which are compatible with Green Engineering and Cradle to Cradle design. This compatibility has been evaluated not only for the foam but also for the complete pipe sandwich structure.

Finding alternatives to PU foam has involved the study of polymeric foams, including polymer foaming, polymeric foam's ageing and failure. Different techniques have been used to pursue the thesis' objectives and research lines, including polymer processing, as foam extrusion and batch foaming; analytical techniques, including nuclear magnetic resonance, Fourier-transform infrared spectroscopy, gravimetry; thermal analysis, including differential scanning calorimetry and dynamic mechanical thermal analysis; mechanical tests, including bending and compression; microscopy; and image analysis.

This chapter summarizes the main outcomes and conclusions of this thesis, as well as presents an outlook and areas for future work.

5.1 Main outcomes and conclusions

5.1.1 Scientific outcomes and conclusions

- Temperature soak at 100°C produces an annealing effect in PET foams, hence PET, increasing its compressive strength and E modulus. This extends its service temperature beyond its T_g . The annealing effect has been allocated to an increase in the orientation of the PET macromolecules, allowed by the temperature soak.
- The diffusion of moisture vapor in PET foams occurs at analogous rates as in polymer films, at least for engineering timescales. The diffusion of liquid water through (PET) foams is a dual process comprising (i) the diffusion and sorption of the water molecules through the polymer skeleton, at analogous rates as in polymer films, and (ii) the progressive passage and filling of the cell cavities, which appears a multistage process. This invalidates simplifications excluding the contribution of moisture entrapment in the closed cells of polymeric foams for the case of liquid water immersion. The entrapment of liquid water in the cells did not affect the mechanical behavior of the PET foams. The contribution ratio between liquid water flow through the open cells and permeation through the cell walls could not be extracted from the experimental program.
- From the above, it can be derived that the hygrothermal degradation of PET foams is not diffusion controlled.
- The cause for hydrolysis-induced embrittlement in PET has been found to arise from the attainment of the minimum mobile amorphous fraction and chemicrystallization upon hydrolysis, rather than the reduction of the concentration of tie-molecules. This questions the occurrence of hydrolysis-induced embrittlement below T_g . The finding indicates a micromechanical causal chain for embrittlement.
- A catalogue of research needs and best practices for polymer foaming compatible with Green Engineering and C2C has been compiled.
- The foamability of PB-1 has been demonstrated, without the use of any additives. A commercial grade favorable for foaming has been identified.

5.1.2 Outcomes and conclusions with regards to the insulation of district heating pipes

The suitability of PET foam for the insulation of DH steel medium pipes has been confirmed:

- Service temperature up to at least 100°C has been confirmed, covering the common operating temperatures of district heating networks.
- No hindrance to the fulfillment of the required 30 years' service life has been detected:
- Hygrothermal or hydrolytic degradation of PET at temperatures compatible with ground moisture ingress has not been found in the experiments. Given the confirmed lack of influence of the cellular structure on the diffusion rate, available models for lifetime prediction of PET²⁰³ may be used, from which the required service life of 30 years at groundwater temperatures can be secured. The findings concerning the hydrolysis-induced embrittlement mechanism in PET suggest service life at temperatures below T_g is underestimated.
- The executed temperature cycles, with an amplitude of 75°C and 50°C, and a number of 250 in each case, corresponding to the number of cycles required for fatigue check for secondary effects for DH distribution lines²²⁹ did not produce any degradation of the mechanical properties of PET foam.
- It was previously established that thermal or thermo-oxidative degradation of PET does not occur at the DH service temperatures.
- PET foam cannot be recommended for the insulation of DH plastic pipes. The short time-to-embrittlement experienced by PET foam exposed to hot moisture, at temperatures above its T_g , indicated that any diffusion of hot vapor through the plastic pipes and into the foam would be catastrophic for its mechanical properties. It should be said that in any case, a PET foam-insulated plastic medium pipe would be a non-bonded pipe, as the melting temperature of PET is >100°C above the melting point of PEX or PB-1, preventing the direct extrusion of PET foam on a plastic pipe. The manufacturing of such a pre-insulated pipe would involve the extrusion of a PET foam sleeve, and the insertion of the plastic pipe inside the PET foam sleeve.
- The foamability of PB-1 has been confirmed, paving the way for the manufacturing of a DH pre-insulated pipe out of a single material, valid for operating temperatures $\leq 90^\circ\text{C}$.
- The produced PB-1 foam prototypes cover a range of mechanical properties in terms of E modulus and σ_{10} . Mechanical properties of PU from state-of-the-art flexible plastic medium pipes fall in the prediction bands obtained from the produced PB-1 foams. This provides confidence on the suitability for the application.
- The obtained thermal conductivity is higher than state-of-the-art PU foam and in the range of PS foam.

5.1.3 Outlook and future work

This thesis proposes two alternative polymeric foams which could replace PU in district heating pipelines: the first candidate, PET foam, for the insulation of steel medium pipes, and the second candidate, PB-1, for the insulation of plastic medium pipes.

The PB-1 candidate introduces a higher level of circular product design, since the complete pre-insulated pipe (medium pipe, foam and casing) could be manufactured out of a single material. Being a thermoplastic, this would highly simplify the recycling of the assembly, which could be simply molten and re-processed. This is an advantage not only for the end-of-life phase, but also during the manufacturing phase, since all non-conforming pipes and scrap could be recycled on site, reducing manufacturing costs and generated waste. Plastic DH pipes present a lower environmental impact than steel medium pipes, according to several LCA^{35,318}. Since the trend is to lower the network operating temperatures to accommodate large amounts of renewable and waste heat, hence operating temperatures pertinent for plastic medium pipes, 100% PB-1 DH pipes would round up the sustainability of new district heating networks.

The work on foaming PB-1 reported here can be placed as feasibility (TRL 1-3). Several aspects were not covered in this thesis and can be the subject of future work, including but not limited to:

- Crystallization kinetics of PB-1 in CO₂ atmospheres. Crystallization kinetics, which is modified by the presence of the blowing agent, has significant effects both on cell nucleation mechanisms and cell growth^{78,319}, as well as on the cell stabilization step¹¹³. Therefore, deeper knowledge and control of the kinetics would support the optimization of the resulting cellular morphology.
- Characterization of the crystallinity degree in the produced foams. A characterization of the crystallinity in the produced foam samples in this study was not undertaken. Since the crystallinity affects the mechanical behaviour, this would be valuable for the establishment of correlations between the processing parameters, obtained cellular morphology and the mechanical properties of the obtained foams.
- Thermal conductivity reduction. While DH networks operating at lower temperatures will have lower heat losses, and so the thermal conductivity requirements of their insulation could be reduced, minimizing heat losses will be always of advantage. Optimization in this regard can be undertaken. A first step would be through the reduction of the density and cell size and increasing the cell population density. In order to continue avoiding the use of additives, the pressure drop could be further increased and the use of CO₂/N₂ mixes could be explored and optimized.
- The foaming of PB-1 has been mainly studied in batch foaming. A transfer of the foaming process to continuous manufacturing processes (extrusion) is required. Concerning basic research, extrusion foaming would allow to include the study of the effects of shear on the cell nucleation process at the die. For the scaling up of the foaming of PB-1 to continuous processes, a complete research line on the design and optimization of the processing tools (screw configuration, die geometry...) could be opened.
- Manufacturing of the pipe-foam-casing assembly. So far, the foaming of PB-1 has been considered. Further research and development (R&D) efforts are required for the manufacturing of the pipe-foam-casing assembly. One possibility to be explored is the simultaneous coextrusion of foam and pipe, through a tandem extrusion and a specially developed die. Another possibility would be to foam-extrude the insulation layer, and then melt the inner and outer layer to produce a skin which would constitute the inner pipe and outer casing, as disclosed in³²⁰. Alternatively, large scale 3D printing could be envisaged to add the casing and eventually the medium pipe to the foam layer. While 3D printing has so far been mainly used for small pieces, technology for large-scale 3D printing is emerging, such as Big Area Additive Manufacturing (BAAM)³²¹ and Large Scale Additive Manufacturing (LSAM)³²².
- Diffusion and permeation of moisture and O₂. As can be recalled from section 2.1, DH plastic medium pipes typically contain a layer of EVOH to prevent the ingress of O₂ into the heat carrier and corrode carbon steel elements, and often an Al layer to prevent the diffusion of moisture into the foam. The inclusion of these layers would be against the single material sandwich assembly proposed. The extent of diffusion and permeation of O₂ and moisture in PB-1, should be evaluated, as the studies within the DH sector reported in Chapter 2 relate to PEX pipes. Most importantly, the evaluation of the damage this could produce should be revised. Concerning the risk of moisture accumulation in the foam coming from the heat carrier, reducing its insulating properties, the extent of moisture accumulation and possibilities to optimize moisture venting through the casing can be studied, including optimizing the casing thickness. As for the O₂ permeation, it has been a risk for the inclusion of plastic pipe branches in existing networks with the steel main pipes, which are carbon steel. For new low temperature district heating networks, the complete network could be built with plastic pipes, with the heat exchangers in stainless steel, making so O₂ permeation irrelevant.
- A life cycle assessment comparing 100% PB-1 pipes vs state of the art flexible plastic medium pipes could be undertaken.
- District heating networks also employ PU foams for cushioning. The suitability of PB-1 foams for this function could also be explored.

As for the PET foam candidate, while further ageing trials (longer hygrothermal exposure periods,

intermediate temperatures) could be envisaged, providing more details for accurate modelling, the main boundary conditions for the use of PET foam in DH pipes have been set.

Additional further research could include:

- Cell size and open cell content reduction. The cell size of the evaluated PET foam is of the order of magnitude of double that of the currently used PU foam. Reduction of the cell size and the reduction of the open cell content would be beneficial towards achieving lower thermal conductivity, although the data sheet value already matches that of the PU in DH pipes.
- A large part of the future work lies in the manufacturing of the pre-insulated pipe assembly. So far, PET foam is manufactured in boards using the breaker plate. The adaptation of this technology to the extrusion of PET foam around a steel pipe requires R&D efforts. If and in which way does the PET foam bond to the steel and its implications are another aspect for further research.

List of Figures

Figure 1	Conceptual sketch of a district heating network 1
Figure 2	Satellite view of the landfilling of wind blades at Casper Regional Landfill in Wyoming, USA. The separation of materials in composites, used in wind blades, challenges their recycling 3
Figure 3	Representation of collided PET foam strands exiting a breaker plate 9
Figure 4	From left to right: DH DN40 flexible plastic medium pipe and corrugated casing, DN40 flexible plastic medium pipe with smooth casing, and bonded steel medium pipes DN20, DN100 and DN200 13
Figure 5	Sankey diagram representing the Montreal Protocol and Kigali amendment agreed blowing agents phase out programme for non-article 5 (industrialized) countries 16
Figure 6	Section of an aged DH pipe, showing browning of the PU in the vicinity of the medium pipe. 17
Figure 7	Right: Photograph of a tested sample, where a coloured epoxy was introduced through the cracks prior cutting to highlight the pattern. Left: proposed description of the crack initiation and propagation scheme 19
Figure 8	Possible causal chains relating chain scission to embrittlement 22
Figure 9	Compressive behaviour of PET foam under temperature, for 80 kg/m ³ (a) and 100 kg/m ³ (d); and under temperature after annealing at 100°C for PET foam 80 kg/m ³ (b) and 100 kg/m ³ (e). Evolution of the compressive strength at 100% strain (σ_{10}) with test temperature before and after annealing, for PET 80 kg/m ³ (c) and 100 kg/m ³ (f) 25
Figure 10	(a) trans and (b) gauche isomers arising from the rotation of the CH ₂ -CH ₂ ethylenic bond of the ethylene glycol moiety 26
Figure 11	Compressive stress-strain curves for foam 80 kg/m ³ (a) and 100 kg/m ³ (b), unaged and after the two temperature cycling trials. (c) applied temperature profile for both trials 27
Figure 12	Weight increase foam 80 under water immersion (a), foam 100 under water immersion (b), and foams 80 and 100 at 80%RH and 40°C (c) 27
Figure 13	(a) Bending tests conducted at 40°C, with and without moisture. (b) micrograph showing water droplets inside a PET foam closed cell 28
Figure 14	Conceptual scheme of dual moisture uptake of polymeric foams under water immersion through time. Blue represents moisture saturation 29
Figure 15	Hydrolysis of PET 30
Figure 16	Flexural stress strain curves for foam 80 (a) and 100 (c) after different ageing times. Evolution of the mechanical properties with ageing time for foam 80 (b) and 100 (d). (e) Chain scission rate derived from end-group analysis of the NMR spectra. (f) Increase of carboxylic acid with time, derived from the FTIR-ATR spectra 31
Figure 17	(a) IR spectra with ageing time, foam PET 80. (b) X _c with ageing time obtained through DCS (c) relative molecular weight (through NMR) vs X _c through ageing time 32

Figure 18	Samples weight variation through ageing time. Lines are added as guidance for the eye 32
Figure 19	Total crystallinity content obtained by DSC (a), mobile amorphous fraction(b) and the RAF (c) fractions. 33
Figure 20	Left: PB-1 in Form I (3/1 helix). Right: PB-1 in Form II (11/3 helix) 37
Figure 21	Schematic drawing of the autoclave set up 38
Figure 22	Photograph of the autoclave set up 39
Figure 23	Cross-section schematic drawing of the heat flow meter set up 39
Figure 24	Left: open set up revealing the sample within the edge insulation, layer holding the Peltier element, top plate. Right: assembled set up 41
Figure 25	a) original scan of a foam sample. b) probability map of pixels belonging to cell calls (white 100% probability). c) probability map of pixels belonging to a cell cavity (white 100% probability). d) identified cell contours 42
Figure 26	(a) Desorption curves after 24h sorption time (sorption equilibrium reached). (b) mass uptake versus sorption time. (c) mass uptake versus sorption time, scaled to show PB1-a and PB1-b 43
Figure 27	Melting point of PB1-a and PB1-b under different CO ₂ pressures 45
Figure 28	Thermal conductivity vs density of PB1-a and PB1-b extruded strands 46
Figure 29	Obtained volume expansion with the tested foaming parameters for PB1-a (a) and PB1-b (b) 47
Figure 30	Representative micrographs for PB1-a foams, obtained under different process conditions 47
Figure 31	Representative micrographs of PB1-b foams obtained under different process conditions 48
Figure 32	Photographs of taken 20 minutes, 2 hours and 61 hours after foaming, for PB1-b (a, c and e respectably) and PB1-a (b, d and f respectably) 49
Figure 33	Post-foaming density increase (%) caused by shrinkage as a function of foaming temperature, for foams produced from 50 bars foaming pressure (a) and 100 bars foaming pressure (b) 50
Figure 34	Sample holder with four moulds. Foam samples 52
Figure 35	Statistical evaluation of the cellular microstructure per foam type (a). Representative scan of 50_85 (b) and 100_85 (c) 53
Figure 36	Engineering stress strain curves obtained under compression for the produced PB-1 foams 54
Figure 37	Cell population density (a) equivalent diameter (b), σ_{10} (c) and E modulus (d) versus foam density for the produced PB-1 foams 55
Figure 38	Obtained σ_{10} and E modulus vs mean cell equivalent diameter (a and c respectively) and versus cell population density (b and d respectively). Symbol size is scaled with the respective foam density 56
Figure 39	σ_{10} vs E modulus for the produced PB-1 foams and their confidence and prediction bands. PU foams from flexible DH pipes are added for reference 56
Figure 40	Box plot comparting the measurements of the in-house and hot disk apparatuses. Data sheet values are added for reference 87

List of Tables

Table 1	Criteria Required 7
Table 2	Benchmark of common commercial polymeric foams 9
Table 3	Parameters for the executed cyclic loading trials 19
Table 4	Parameters for the executed hygrothermal ageing trials 29
Table 5	Characteristics of the selected components for the heat flow meter apparatus 39
Table 6	Property overview of the evaluated PB-1 grades 41
Table 7	Thermal conductivity and density of PB1-a and PB1-b extruded strands 44
Table 8	Foaming parameters 46
Table 9	Characteristics of obtained PB1-b foams 51
Table 10	Mechanical Properties of produced foam samples 53
Table 11	Measured density and thermal conductivity for each foam batch. Sample name relates to foaming P and T 55
Table 12	Measurement results for the assessment of repeatability 85
Table 13	Measurement for the assessment of reproducibility 85
Table 14	Measurements for the assessment of robustness 86
Table 15	Statistical evaluation of obtained λ values for the assessment of robustness 86
Table 16	λ measured with the in-house apparatus, the Hot Disk apparatus and the data sheet values 87

List of Abbreviations

4GDH	4th generation district heating
ATR	attenuated total reflection
BAuA	Gernam Fedearl Institute for Occupational Safety and Health
CFC	chlorofluorocarbon
DH	district heating
DMTA	dynamic mechanic thermal analysis
DSC	diferencial scanninc calorimetry
E modulus	Youngs modulus
ECHA	european chemical agency
EU	european union
EVOH	ethylene vinyl alcohol
FTIR	Fourier transformed infrared
GWP	global warming potential
HC	hydrocarbons
HCFC	hydrochlorocarbons
HDPE	high density polyethylene
HFC	hydrofluorocarbons
HH	human health
IEA	international energy agency
IR	Infrared
LCA	life cycle assessment
MAF	mobile amorphous fraction
MDI	methylene diphenyl diisocyanate
MFR	melt flow ratio
min	minutes
MSc	master of science
NIPU	non-isocyanates polyurethane
NMR	nuclear magnetic resonance
PB-1	polybutene-1
PC	polycarbonate
PE	polyethylene terephthalate
PET	polyethylene terephthalate
PEX	cross linked polyethylene
PLA	poly lactic acid
PP	polypropylene
PS	polystyrene
PU	polyurethane
PVC	Polyvinyl chloride
R&D	research and development
RAF	rigid amorphous fraction
RH	relative humidiy
RMM	risk management measure

S_d	standard deviation
SE	standard error
TDI	toluene diisocyanate
TRL	technology readiness level
USA	United States of America
USSR	Union of Soviet Socialist Republics

List of Symbols

A	area of image
Al	aluminium
CO_2	carbon dioxide
E_a	activation energy
h	hour
kB	Boltzmann constant
M_c'	critical molecular mass corresponding to the entanglement limit
M_e	molecular mass of the segment between the entanglements
$M_{t,d}$	desorption rate
$M_{t,s}$	mass of sorbed CO_2 upon saturation
N	cell nucleation rate
n	number of cells
N_0	cell population density
N_2	nitrogen
P	pressure
P_L	pressure in the liquid phase
P_v	equilibrium gas pressure
T	temperature
T_c	crystallization temperature
T_g	glass transition temperature
T_m	melting temperature
t_s	saturation time
V_{exp}	volume expansion
W_0	initial polymer weight
W_t	weight of polymer with sorbed CO_2 at a given time during desorption
X_c	crystallinity fraction
X_{MAF}	mobile amorphous fraction
X_{RAF}	rigid amorphous fraction
ΔC_p	jump in heat capacity at the glass transition
ΔC_{p0}	heat capacity of a fully amorphous (PET)
ΔH_f	specific melting enthalpy
ΔH_{f0}	melting enthalpy of a fully crystalline (PET)
ΔT	temperature difference
ΔT_m	melting point depression
Δx	distance
λ	thermal conductivity
λ_{foam}	total thermal conductivity of foam
λ_{gas}	thermal conductivity due to conduction in the gas
λ_{pol}	thermal conductivity due to conduction in the polymer matrix
λ_{rad}	thermal conductivity due to radiation
ρ_{foam}	density of monolithic polymer

ρ_{polymer}	density of foam
σ	compressive strength
σ_{10}	compressive strength at 10% strain
τ	shear
ϕ	heat flux
ϕ_{eq}	equivalent diameter of a spherical cell

List of Annexes

Annex I	Validation of the Thermal Conductivity Measurements- Steady State Heat Flow Meter Apparatus
Annex II	12 Principles of Green Engineering
Annex III	Publication [J1]
Annex IV	Publication [J2]
Annex V	Publication [J3]
Annex VI	Publication [J4]
Annex VII	Publication [BJ1]
Annex VIII	Publication [BJ2]
Annex IX	Publication [CP1]
Annex X	Publication [CP2]
Annex XI	Publication [CP3]
Annex XII	Publication [B1]

References

1. Woods P, Overgaard J. Historical development of district heating and characteristics of a modern district heating system. In: Wiltshire R, ed. Advanced district heating and cooling (DHC) systems. 1st edition. Waltham MA: Elsevier; 2015:3-15.
2. Karnitz MA. Description of district heating: US history and current status. ASHRAE Richmond chapter conference. 1981. Available at: <https://www.osti.gov/servlets/purl/6801150>. Accessed March 4, 2022.
3. Holly B, inventor. Improvement in steam-generators. US53617A.
4. Holly B, inventor. Improvement in systems of water-supplies for cities. US94746A.
5. Holly B, inventor. Improvement in combined heater and condenser. US114142A.
6. Holly B, inventor. Improvement in steam-generators for warming buildings. US193085A.
7. Holly B, inventor. Improvement in street mains or pipes for supplying large districts with heat for warming buildings. US193088A.
8. Holly B, inventor. Apparatus for supplying steam in cities. US260097A.
9. Pierce MA. Summary of District Heating Systems in the United States, 1877-2020: University of Rochester; 2022.
10. Lund H, Werner S, Wiltshire R, et al. 4th Generation District Heating (4GDH). Energy. 2014;68:1-11.
11. Carpenter RC. Methods of Insulating Underground Systems of Steam Piping. Transactions of the American Society of Heating and Ventilating Engineers. 1896;2:119-143.
12. Frederiksen S, Werner S. District heating and cooling. Lund: Studentlitteratur; 2014.
13. Stonitch L. Pre-insulated piping - The state of the art 1981. Official Proceedings of seventy-second annual conference of the International District Heating Association. 1981;LXXII.
14. DIN EN 253. District heating pipes- Bonded single pipe systems for directly buried hot water networks- Factory made pipe assembly of steel service pipe, polyurethane thermal insulation and a casing of polyethylene. 2019.
15. DIN EN 13941-1. District heating pipes- Design and installation of thermal insulated bonded single and twin pipe systems for directly buried hot water networks: Part 1: Design. 2019.
16. Christensen R. Fatigue analysis of district heating systems. 1999. Available at: <http://www.iea-dhc.org/the-research/annexes/1996-1999-annex-v/annex-v-project-04.html>.
17. Weidlich I. Sensitivity Analysis On The Axial Soil Reaction Due To Temperature Induced Pipe Movements. Energy Procedia. 2017;116:365-373.
18. European Commission. Fifth generation, Low temperature, high EXergy district heating and cooling NETWORKS. 2015-2018. Available at: <https://cordis.europa.eu/project/id/649820>. Accessed April 4, 2022.
19. Boesten S, Ivens W, Dekker SC, Eijndems H. 5th generation district heating and cooling systems as a solution for renewable urban thermal energy supply. Adv. Geosci. 2019;49:129-136.
20. Suci R-A. Fifth generation district energy systems for low carbon cities: EPFL; 2019; 7332.
21. Revesz A, Jones P, Dunham C, et al. Developing novel 5th generation district energy networks. Energy. 2020;201:117389.
22. Lund H, Østergaard PA, Nielsen TB, et al. Perspectives on fourth and fifth generation district heating. Energy. 2021;227:120520.
23. IPCC. Climate Change 2014: Synthesis Report. Contribution of Working Groups I, II and III to the Fifth Assessment Report of the Intergovernmental Panel on Climate Change. IPCC. Geneva, Switzerland; 2014.
24. Paris Agreement: COP 21; 2015.
25. IEA. Renewables 2019: IEA; 2019.

26. Intended Nationally Determined Contribution of the EU and its Member States: NDC; 2015.
27. Jensen PD, Purnell P, Velenturf AP. Highlighting the need to embed circular economy in low carbon infrastructure decommissioning: The case of offshore wind. *Sustainable Production and Consumption*. 2020;24:266-280.
28. Kim H, Park H. PV Waste Management at the Crossroads of Circular Economy and Energy Transition: The Case of South Korea. *Sustainability*. 2018;10(10):3565.
29. Mulvaney D, Richards RM, Bazilian MD, Hensley E, Clough G, Sridhar S. Progress towards a circular economy in materials to decarbonize electricity and mobility. *Renewable and Sustainable Energy Reviews*. 2021;137(8):110604.
30. Transforming our world: the 2030 Agenda for Sustainable Development: A/RES/70/1; 2015.
31. Goddin JR. The role of a circular economy for energy transition. In: *The Material Basis of Energy Transitions*: Elsevier; 2020:187-197.
32. Kalchenko O, Evseeva S, Evseeva O, Plis K. Circular economy for the energy transition in Saint Petersburg, Russia. *E3S Web Conf*. 2019;110(9):2030.
33. Mahon C, Mediboyina MK, Gartland D, Murphy F. Life cycle assessment of Irish district heating systems: a comparison of waste heat pump, biomass-based and conventional gas boiler. *Clean Techn Environ Policy*. 2022;80(4):408.
34. Eriksson O, Finnveden G, Ekvall T, Björklund A. Life cycle assessment of fuels for district heating: A comparison of waste incineration, biomass- and natural gas combustion. *Energy Policy*. 2007;35(2):1346-1362.
35. Famiglietti J, Gerevini L, Spirito G, et al. Environmental Life Cycle Assessment scenarios for a district heating network. An Italian case study. *Energy Reports*. 2021;7:368-379.
36. Jeandaux C, Videau J-B, Prieur-Vernat A. Life Cycle Assessment of District Heating Systems in Europe: Case Study and Recommendations. *Sustainability*. 2021;13(20):11256.
37. Fröling M, Holmgren C, Svanström M. Life cycle assessment of the district heat distribution system: Part 1: Pipe Production. *Int J Life Cycle Assess*. 2004;9(2):130-136.
38. Fröling M, Svanström M. Life Cycle Assessment of the District Heat Distribution System- Part 2: Network Construction (11 pp). *Int J Life Cycle Assess*. 2005;10(6):425-435.
39. Persson C, Fröling M, Svanström M. Life Cycle Assessment of the District Heat Distribution System. Part 3: Use Phase and Overall Discussion (10 pp). *Int J Life Cycle Assess*. 2006;11(6):437-446.
40. Oliver-Solà J, Gabarrell X, Rieradevall J. Environmental impacts of the infrastructure for district heating in urban neighbourhoods. *Energy Policy*. 2009;37(11):4711-4719.
41. Homrich AS, Galvão G, Abadia LG, Carvalho MM. The circular economy umbrella: Trends and gaps on integrating pathways. *Journal of Cleaner Production*. 2018;175:525-543.
42. Kirchherr J, Reike D, Hekkert M. Conceptualizing the circular economy: An analysis of 114 definitions. *Resources, Conservation and Recycling*. 2017;127:221-232.
43. Murray A, Skene K, Haynes K. The Circular Economy: An Interdisciplinary Exploration of the Concept and Application in a Global Context. *J Bus Ethics*. 2017;140(3):369-380.
44. McDonough W, Braungart M. *Cradle to cradle: Remaking the way we make things*. 1. ed. New York, NY: North Point Press; 2002.
45. Anastas PT, Zimmerman JB. Design through the 12 principles of green engineering. *Environmental science & technology*. 2003;37(5):94A-101A.
46. McDonough W, Braungart M, Anastas PT, Zimmerman JB. Applying the principles of Green Engineering to cradle-to-cradle design. *Environmental science & technology*. 2003;37(23):434A-441A.
47. Thermaflex. Flexalen 600 Heating Technical Data Sheet. 2021. Available at: https://thermaflex.com/wp-content/uploads/2021/07/TDS_Flexalen600_Heating_v1.5EU_20210521.pdf. Accessed April 15, 2022.
48. Cradle to Cradle products innovation institute. Flexalen Cradle to Cradle Certificate. 2021. Available at: https://thermaflex.com/wp-content/uploads/2021/10/2021-2023_Flexalen_

- Silver_C2C.pdf. Accessed April 15, 2022.
49. Van der Ven E, Bout H, De Bell H, Baars G., inventors; Thermaflex International Holding B.V. Thermal insulation metallocene polyethylene foam and manufacturing method therefor. EP 1 336 064 B1.
 50. Laufkötter S. Logstore und Kingspan: Nachhaltigkeit und Energie-effizienz stehen im Fokus: Logstore and Kingspan: focus on sustainability and energy efficiency. EuroHeat&Power. 2022;3(ISSN 0949-166X-D 9790 F):22-25.
 51. Bayer O. Das Di-Isocyanat-Polyadditionsverfahren (Polyurethane). Angew. Chem. 1947;59(9):257-272.
 52. Orzel, Jircny, Reese. Flexible Polyurethane Foam: A Literature Review of Thermal Decomposition Products and Toxicity. Journal of the American College of Toxicity. 1981.
 53. Gama NV, Ferreira A, Barros-Timmons A. Polyurethane Foams: Past, Present, and Future. Materials (Basel, Switzerland). 2018;11(10).
 54. Dernehl CU. Health hazards associated with polyurethane foams. Journal of Occupational Medicine: official publication of the Industrial Medical Association. 1966;8(2):59-62.
 55. Zapp JA. Hazards of isocyanates in polyurethane foam plastic production. A.M.A. archives of industrial health. 1957;15(4):324-330.
 56. Federal Institute for Occupational Safety and Health. Proposal for a Restriction: Diisocyanates. [Annex XV Restriction Report]. Version 2.1; 2017.
 57. European Commission. Commission Decision of 3 May 2000 replacing Decision 94/3/EC establishing a list of wastes pursuant to Article 1(a) of Council Directive 75/442/EEC on waste and Council Decision 94/904/EC establishing a list of hazardous waste pursuant to Article 1(4) of Council Directive 91/689/EEC on hazardous waste. 2000. Available at: <https://eur-lex.europa.eu/legal-content/EN/TXT/?uri=CELEX:02000D0532-20150601>. Accessed December 11, 2019.
 58. Commission Regulation (EU) 2020/1149 of 3 August 2020 amending Annex XVII to Regulation (EC) No 1907/2006 of the European Parliament and of the Council concerning the Registration, Evaluation, Authorisation and Restriction of Chemicals (REACH) as regards diisocyanates: (EU) 2020/1149. In: Official Journal of the European Union; 2020.
 59. Utrecht Europe, 29th May 2018.
 60. Figovsky O, Leykin A, Shapovalov L. Non-Isocyanate Polyurethanes - Yesterday, Today and Tomorrow. Al'tern. ènerg. èkol. 2016(3-4):95-108.
 61. Kathalewar MS, Joshi PB, Sabnis AS, Malshe VC. Non-isocyanate polyurethanes: from chemistry to applications. RSC Adv. 2013;3(13):4110.
 62. Helou M, Carpentier J-F, Guillaume SM. Poly(carbonate-urethane): an isocyanate-free procedure from α,ω -di(cyclic carbonate) telechelic poly(trimethylene carbonate)s. Green Chem. 2011;13(2):266-271.
 63. Zhang K, Nelson AM, Talley SJ, et al. Non-isocyanate poly(amide-hydroxyurethane)s from sustainable resources. Green Chem. 2016;18(17):4667-4681.
 64. Figovsky O, Shapovalov L, Leykin A, Birukova R, Potashnikova R. Recent advances in the development of non-isocyanate polyurethanes based on cyclic carbonates. PU Magazine. 2013;10(4).
 65. Gomez-Lopez A, Elizalde F, Calvo I, Sardon H. Trends in non-isocyanate polyurethane (NIPU) development. Chemical communications (Cambridge, England). 2021;57(92):12254-12265.
 66. ISOPA. Recovery of Rigid Polyurethane Foam from Demolition Waste: Fact Sheet: ISOPA- the European Isocyanates Producers' Association; 2001.
 67. Deng Y, Dewil R, Appels L, Ansart R, Baeyens J, Kang Q. Reviewing the thermo-chemical recycling of waste polyurethane foam. Journal of environmental management. 2021;278(Pt 1):111527.
 68. Zia KM, Bhatti HN, Ahmad Bhatti I. Methods for polyurethane and polyurethane composites, recycling and recovery: A review. Reactive and Functional Polymers. 2007;67(8):675-692.
 69. Alavi Nikje MM. Recycling of polyurethane wastes. Shawbury, Shrewsbury, Shropshire, United

- Kingdom: Smithers Rapra; 2016.
70. Kemono A, Piotrowska M. Polyurethane Recycling and Disposal: Methods and Prospects. *Polymers*. 2020;12(8).
 71. Yang W, Dong Q, Liu S, Xie H, Liu L, Li J. Recycling and Disposal Methods for Polyurethane Foam Wastes. *Procedia Environmental Sciences*. 2012;16:167-175.
 72. Godinho B, Gama N, Barros-Timmons A, Ferreira A. Recycling of different types of polyurethane foam wastes via acidolysis to produce polyurethane coatings. *Sustainable Materials and Technologies*. 2021;29:e00330.
 73. Simón D, Borreguero AM, Lucas A de, Rodríguez JF. Glycolysis of viscoelastic flexible polyurethane foam wastes. *Polymer Degradation and Stability*. 2015;116(1):23-35.
 74. Akindoyo JO, Beg MDH, Ghazali S, Islam MR, Jeyaratnam N, Yuvaraj AR. Polyurethane types, synthesis and applications – a review. *RSC Adv*. 2016;6(115):114453-114482.
 75. Kurańska M, Prociak A. Bio-Based Polyurethane Foams for Heat-Insulating Applications. In: Pacheco Torgal F, Buratti C, Kalaiselvam S, Granqvist C-G, Ivanov V, eds. *Nano and Biotech Based Materials for Energy Building Efficiency*. Vol. 112. Cham: Springer International Publishing; 2016:357-373.
 76. Kothari CR, Gaurav G. *Research methodology: Methods and techniques*. Fourth multi colour edition. New Delhi: New Age International (P) Limited, Publishers; 2019.
 77. Lee L, Zeng C, Cao X., Han X, Shen J, Xu G. Polymer nanocomposite foams. *Composites Science and Technology*. 2005;65(15-16):2344-2363.
 78. Reignier J, Gendron R, Champagne MF. Autoclave Foaming of Poly(ϵ -Caprolactone) Using Carbon Dioxide: Impact of Crystallization on Cell Structure. *Journal of Cellular Plastics*. 2007;43(6):459-489.
 79. Meller M, Li J, Dolega J, inventors; Armacell Enterprise GmbH. A foam material with very low thermal conductivity and a process for manufacturing the foam material. EP2671911A1.
 80. Di Maio L, Coccorullo I, Montesano S, Incarnato L. Chain Extension and Foaming of Recycled PET in Extrusion Equipment. *Macromol. Symp*. 2005;228(1):185-200.
 81. Xanthos M, Zhang Q, Dey SK, Li Y, Yilmazer U, O'Shea M. Effects of Resin Rheology on the Extrusion Foaming Characteristics of PET. *Journal of Cellular Plastics*. 1998;34(6):498-510.
 82. Xanthos M, Dey SK, Zhang Q, Quintans J. Parameters Affecting Extrusion Foaming of PET by Gas Injection. *Journal of Cellular Plastics*. 2000;36(2):102-111.
 83. Sarver JA, Kiran E. Foaming of polymers with carbon dioxide – The year-in-review – 2019. *The Journal of Supercritical Fluids*. 2021;173:105166.
 84. Nofar M, Park CB. *Poly lactide foams: Fundamentals, manufacturing, and applications*. Oxford: Elsevier/William Andrew; 2018. *Plastics design library PDL handbook series*.
 85. Stahel WR. *The performance economy*. 2nd ed. Basingstoke, England, New York: Palgrave Macmillan; 2010.
 86. Gibson, L. J., Ashby, M.F. *Cellular Solids*. Cambridge; 1997.
 87. Spitzner M, Rudolphi A, Pfundstein M, Gellert R. *Insulating Materials: Principles, Materials, Applications*: Birkhäuser; 2012.
 88. Velichko E, Tskhovrebov E, Shevchenko A. Environmental safety providing during heat insulation works and using thermal insulation materials. *MATEC Web Conf*. 2017;106:3009.
 89. National Toxicology Program. Styrene CAS No. 100-42-5: Report on Carcinogens, Twelfth Edition: U.S. Department of Health and Human Services; 2011.
 90. Cohen JT, Carlson G, Charnley G, et al. A comprehensive evaluation of the potential health risks associated with occupational and environmental exposure to styrene. *Journal of toxicology and environmental health. Part B, Critical reviews*. 2002;5(1-2):1-265.
 91. Koerner GR, Hsuan YG, Koerner RM. The durability of geosynthetics. In: Sarsby RW, ed. *Geosynthetics in civil engineering*. Cambridge, England, Boca Raton: Woodhead; CRC Press; 2007:36-65. *Woodhead Publishing series in textiles*; 57.
 92. Tikuisis T, Phibbs MR, Sonnenberg KL. Quantitation of employee exposure to emission products

- generated by commercial-scale processing of polyethylene. *American Industrial Hygiene Association journal*. 1995;56(8):809-814.
93. Laguna-Gutierrez E, Pinto J, Kumar V, Rodriguez-Mendez ML, Rodriguez-Perez MA. Improving the extensional rheological properties and foamability of high-density polyethylene by means of chemical crosslinking. *Journal of Cellular Plastics*. 2018;54(2):333-357.
 94. Rodríguez-Pérez MA. Crosslinked Polyolefin Foams: Production, Structure, Properties, and Applications. In: *Crosslinking in Materials Science*. Vol. 184. Berlin, Heidelberg: Springer Berlin Heidelberg; 2005:97-126. *Advances in Polymer Science*.
 95. Diab. Divinycell H: Data Sheet; 2022.
 96. Zhang M, Buekens A, Jiang X, Li X. Dioxins and polyvinylchloride in combustion and fires. *Waste management & research: the journal of the International Solid Wastes and Public Cleansing Association, ISWA*. 2015;33(7):630-643.
 97. Comanita E-D, Ghinea C, Rosca M, Simion IM, Petraru M, Gavrilescu M. Environmental impacts of polyvinyl chloride (PVC) production process. In: *The 5th IEEE International Conference, E-Health and Bioengineering: EHB 2015 : Challenging Issues for Health and Biomedical Technologies : Iasi, November 19th-21st, 2015*. Piscataway, NJ: IEEE; 2015:1-4.
 98. Chong NS, Abdulramoni S, Patterson D, Brown H. Releases of Fire-Derived Contaminants from Polymer Pipes Made of Polyvinyl Chloride. *Toxics*. 2019;7(4).
 99. Akovali G. 2 - Plastic materials: polyvinyl chloride (PVC). In: Torgal FP, Jalali S, Fucic A, eds. *Toxicity of building materials*. Cambridge: Woodhead; 2012:23-53. Woodhead publishing in materials.
 100. Thomas NL. Cellular PVC-U: Current Technology and Future Challenges. *Journal of Cellular Plastics*. 2007;43(3):237-255.
 101. Patrick S. *Practical guide to polyvinyl chloride*. [Online-ausg.]. Shrewsbury, Shropshire, UK: Rapra Technology; 2005.
 102. Jahani D, Ameli A, Saniei M, Ding W, Park CB, Naguib HE. Characterization of the Structure, Acoustic Property, Thermal Conductivity, and Mechanical Property of Highly Expanded Open-Cell Polycarbonate Foams. *Macromol. Mater. Eng*. 2015;300(1):48-56.
 103. Gedler G, Antunes M, Borca-Tasciuc T, Velasco JI, Ozisik R. Effects of graphene concentration, relative density and cellular morphology on the thermal conductivity of polycarbonate-graphene nanocomposite foams. *European Polymer Journal*. 2016;75:190-199.
 104. National Center for Biotechnology Information. PubChem Compound Summary for CID 6623, bisphenol A. 2022. Available at: <https://pubchem.ncbi.nlm.nih.gov/compound/bisphenol-A>. Accessed November 6, 2022.
 105. Olabisi O, Adewale K. *Handbook of thermoplastics*. Boca Raton: CRC Press; 2016. *Plastics Engineering*; v.41.
 106. Ramnäs J. *New materials and constructions for improving the quality and lifetime of district heating pipes including joints- thermal, mechanical and environmental performance.: Annex VIII Project 1. [Final Report]*; 2008.
 107. Mangs S. *Insulation materials in district heating pipes. [Doctoral Thesis]*. Sweden: Chalmers University of Technology; 2005.
 108. Feron VJ, Jetten J, Kruijf N de, van den Berg F. Polyethylene terephthalate bottles (PRBs): a health and safety assessment. *Food additives and contaminants*. 1994;11(5):571-594.
 109. Vasami R. Polyethylene terephthalate and endocrine disruptors. *Environmental health perspectives*. 2010;118(5):A196-7; author reply A197.
 110. Lepoittevin B, Roger P. Poly(ethylene terephthalate). In: Thomas S, P.M. V, eds. *Handbook of Engineering and Speciality Thermoplastics*. Vol. 31. Hoboken, NJ, USA: John Wiley & Sons, Inc; 2011:97-126.
 111. Li R-Y, Liu Z-G, Liu H-Q, Chen L, Liu J-F, Pan Y-H. Evaluation of biocompatibility and toxicity of biodegradable poly (DL-lactic acid) films. *American Journal of Translational Research*. 2015;7(8):1357-1370.

112. Connolly M, Zhang Y, Brown DM, et al. Novel polylactic acid (PLA)-organoclay nanocomposite bio-packaging for the cosmetic industry; migration studies and in vitro assessment of the dermal toxicity of migration extracts. *Polymer Degradation and Stability*. 2019;168:108938.
113. Gong P, Zhai S, Lee R, et al. Environmentally Friendly Polylactic Acid-Based Thermal Insulation Foams Blown with Supercritical CO₂. *Ind. Eng. Chem. Res.* 2018;57(15):5464-5471.
114. Reignier J, Gendron R, Champagne MF. Extrusion Foaming of Poly(Lactic acid) Blown with CO₂: Toward 100% Green Material. *Cellular Polymers*. 2007;26(2):83-115.
115. BEWI. Biofoam: Technical Data Sheet. [D.60.03.01-102]. 2021. Available at: <https://bewi.com/products/biofoam/>. Accessed April 21, 2022.
116. Parker K, Garancher J-P, Shah S, Fernyhough A. Expanded polylactic acid - an eco-friendly alternative to polystyrene foam. *Journal of Cellular Plastics*. 2011;47(3):233-243.
117. Peelman N, Ragaert P, Ragaert K, Meulenaer B de, Devlieghere F, Cardon L. Heat resistance of new biobased polymeric materials, focusing on starch, cellulose, PLA, and PHA. *J. Appl. Polym. Sci.* 2015;132(48):n/a-n/a.
118. Auras R, Harte B, Selke S. An overview of polylactides as packaging materials. *Macromolecular bioscience*. 2004;4(9):835-864.
119. Rotter, Melquist, Chiang, Tsai, Kelly, inventors; AMOCO CORPORATION. Increased throughput in foaming and other melt fabrication of polyester. EP0636158B1. 31.03.
120. Di Maio E, Mensitieri G, Iannace S, Nicolais L, Li W, Flumerfelt RW. Structure optimization of polycaprolactone foams by using mixtures of CO₂ and N₂ as blowing agents. *Polym. Eng. Sci.* 2005;45(3):432-441.
121. Parky CP, Garcia GA. Development of Polypropylene Plank Foam Products. *Journal of Cellular Plastics*. 2002;38(3):219-228.
122. Farthi A. Mechanical Properties of Strand PET Foams at Different Length Scales. [Doctoral Thesis]: University of Bayreuth; 2018.
123. Collishaw PG, Evans JRG. An assessment of expressions for the apparent thermal conductivity of cellular materials. *Journal of Materials Science*. 1994;29(9):2261-2273.
124. Isberg J. The thermal conductivity of polyurethane foam. [PhD Dissertation]. Sweden: Chalmers University of Technology; 1988.
125. Plüger tob. Technical Information Kerdyn Green FR. 2020. Available at: <https://www.pflueger-tob.de/kerdyn-green-fst/?lang=en>. Accessed April 22, 2022.
126. Weidlich I. Mantelrohrsysteme in der Wärmeverteilung. In: Horlacher H-B, Helbig U, eds. *Rohrleitungen 1*. Vol. 38. Berlin, Heidelberg: Springer Berlin Heidelberg; 2016:475-494.
127. Nilsson SF. New developments in pipes and related network components for district heating. In: Robin Wiltshire, ed. *Advanced District Heating and Cooling (DHC) Systems*: Elsevier; 2016:191-214.
128. Bornmann G, Loeser A. Zur Toxikologie von Polybuten-(1). *Arch. Toxikol.* 1968;23(3):240-244.
129. Alger MSM. *Polymer science dictionary*. London: Chapman & Hall; 1997.
130. ISO15876-1:2017. *Plastics piping systems for hot and cold water installations — Polybutene (PB): Part 1: General*. Geneva, Switzerland: ISO. 2017.
131. Wypych G. *Handbook of plasticizers*. Third edition. Toronto: Chemtec; 2017.
132. Park CB, Cheung LK. A study of cell nucleation in the extrusion of polypropylene foams. *Polym. Eng. Sci.* 1997;37(1):1-10.
133. Spitael P, Macosko CW. Strain hardening in polypropylenes and its role in extrusion foaming. *Polym. Eng. Sci.* 2004;44(11):2090-2100.
134. Laguna-Gutierrez E, van Hooghten R, Moldenaers P, Rodriguez-Perez MA. Understanding the foamability and mechanical properties of foamed polypropylene blends by using extensional rheology. *J. Appl. Polym. Sci.* 2015;132(33):n/a-n/a.
135. Logstor. Logstor Product Catalogue. 2022. Available at: <https://www.logstor.com/media/7319/kingspan-logstor-product-catalogue-specifications-en-eur.pdf>. Accessed September 4, 2022.

- 136.Vega A, Yarahmadi N, Jakubowicz I. Determination of the long-term performance of district heating pipes through accelerated ageing. *Polymer Degradation and Stability*. 2018;153:15-22.
- 137.Bundesverband Fernwärmeleitungen e.V (Ed.). *Das praktische Montage-Handbuch für vorgedämmte Fernwärmeleitungen: Planen, prüfen und sichten*. 3. Auflage, revidierte Ausgabe. Dresden: Bundesverband Fernwärmeleitungen; 2018.
- 138.Lerch BA, Sullivan RM. Thermal Expansion of Polyurethane Foam. 43rd Annual Technical Meeting of the Society of Engineering Science. 2006.
- 139.GEF Ingenieurgesellschaft für Energietechnik und Fernwärme MBH. *District Heating Piping with Plastic Medium Pipes: Status of the development and laying costs*: Novem; 1992.
- 140.DIN EN 15632-2. *District heating pipes- Pre-insulated flexible pipe systems: Part 2: Bonded plastic service pipes*. 2015.
- 141.Klöpsch M, Zinko H. *Plastic Pipe Systems for DH, Handbook for Safe and Economic Application*: Novem; 1999.
- 142.Steinmetz H, Klopsch M. *Neuartige Verlegetechniken flexibler Fernwarmeleitungssysteme mit Kunststoff Mediumrohren: New Installation Technique with flexible Plastic Pipelines in District Heating Systems*. Volklingen: Fernwarmeverbund Saar; 1997.
- 143.Amby L. *Untersuchung der Diffusionsverhältnisse in vorgedämmten Fernwaermekunststoffrohren.: Survey on diffusion in preheated plastic pipes for district heating*. Aarhus: Danish Technology Institute; 1992. EM-Journal; 1323/88-10.
- 144.Oestergaard, L., Larsen. J., Amby. L. *Oxygen occurrence in total district heating systems with a large number of plastic district heating pipes*. Viby: Dansk Energi Management A/S; 1993; OSTI DE93794746.
- 145.Ifwarson M. *Resumed evaluation of material in GRUDIS-systems.*: Studsvik; 1990; EX-90/66.
- 146.Walletun H, Zinko H. *Medieror av plast i fjarrvarmesyslcm.: Medium pipes of plastics for district heating systems*; 1996; Report ZW-95/14.
- 147.Logstor. *New Standards for Production*. Available at: <https://www.logstor.com/about-us/hseq/production>. Accessed September 9, 2019.
- 148.DIN EN 15632-4. *District heating pipes- Pre-insulated flexible pipe systems: Part 4: Bonded system with metal service pipes; requirements and test methods*. 2020.
- 149.Lee S-T, Park CB, eds. *Foam Extrusion*: CRC Press; 2014.
- 150.Montreal Protocol on Substances that Deplete the Ozone Layer. Chapter XXVII Environment; 1987.
- 151.Chapter XXVII 2.f Amendment to the Montreal Protocol on Substances that Deplete the ozone Layer; 2016.
- 152.GEF Ingenieurgesellschaft für Energietechnik und Fernwärme MBH. *CFC-Free Plastic Jacket Pipes for District Heating*: Novem; 1992.
- 153.Eriksson D, Sundén B. *Heat and Mass Transfer in Polyurethane Insulated District Cooling and Heating Pipes*. *Journal of Thermal Envelope and Building Science*. 1998;22(1):49-71.
- 154.Persson C. *Predicting the long-term insulation performance of district heating pipes*. [Doctoral Thesis]. Göteborg; 2015.
- 155.Lemponen J-P, Kraaz M, Smidt HD. *How cellular gases influence the insulation properties of district heating pipes and the competitiveness of district energy: Annex VII I 2005:8 DHC-05.04: IEA DHC-CHP*; 2005.
- 156.Alsoy S. *Modeling of Diffusion in Closed Cell Polymeric Foams*. *Journal of Cellular Plastics*. 1999;35(3):247-271.
- 157.Pontiff T. *Foaming Agents for Foam Extrusion*. In: Lee S-T, Park CB, eds. *Foam Extrusion*: CRC Press; 2014.
- 158.Larsen CT, Tøgeskov P, Leuteritz A. *Analyses of Diffusion Rates through PE and Impact on Ageing*. *EuroHeat&Power English Edition*. 2009;6(II).
- 159.DIN EN 253. *District heating pipes: Preinsulated bonded pipe systems for directly buried hot water networks*. 2009.

160. Meigen M, Schiricht W. Preinsulated pipes age more quickly and differently than assumed. *EuroHeat&Power English Edition*. 2005;1:32-39.
161. GEF Ingenieurgesellschaft für Energietechnik und Fernwärme MBH. Zeitstandverhalten von PUR-Schäumen in praxis-gealterten Kusntstoffmantelhohren hinsichtlich Wärmedämmung und Festigkeit. [Funded by Bundesministerium für Wirtschaft und Arbeit und Technologie]; 2004; 0327272A.
162. Leuteritz A, Döring K-D, Lampke T, Kuehnert I. Accelerated ageing of plastic jacket pipes for district heating. *Polymer Testing*. 2016;51:142-147.
163. Yarahmadi N, Sällström JH. Improved Maintenance Strategies for District Heating Pipe-Lines. The 14th International Symposium on District Heating and Cooling. 2014.
164. Yarahmadi N, Vega A, Jakubowicz I. Accelerated ageing and degradation characteristics of rigid polyurethane foam. *Polymer Degradation and Stability*. 2017;138:192-200.
165. Puentes-Parodi A, Gehde M, Leuteritz A, Kuehnert I. Failure analysis and durability of preinsulating district heat pipes. *Polym Adv Technol*. 2018;29(3):1048-1055.
166. AGFW e.V. Installation and calculations of preinsulated bonded pipes for district heating networks- static design; basics of stress analysis. AGFW-Regelwerk. Frankfurt am Main; 2007. AGFW-Arbeitsblatt; FW 401- Teil 10.
167. Randlov P, Hansen KE, Penderos M. Temperature Variations in Preinsulated DH Pipes Low Cycle Fatigue. 1996. Available at: <http://www.ieadhc.org/the-research/annexes/1993-1996-annex-iv/annex-iv-project-06.html>.
168. Holliday, Y, L., THACKRAY G. Heterogeneity in Complex Materials and the Concept of the Representative Cell. *Nature*. 1964;201(4916):270-272.
169. Gaidukovs S, Gaidukova G, Ivdrē A, Cabulis U. Viscoelastic and Thermal Properties of Polyurethane Foams Obtained from Renewable and Recyclable Components. *J renew mater*. 2018.
170. Carvill J. Engineering materials. In: *Mechanical Engineer's Data Handbook*: Elsevier; 1993:218-266.
171. Mark JE, ed. *Polymer data handbook*: Oxford university Press; 1999.
172. Andersons J, Grübe R, Vēvere L, Cābulis P, Kirpluks M. Anisotropic thermal expansion of bio-based rigid low-density closed-cell polyurethane foams. *Journal of Materials Research and Technology*. 2022;16:1517-1525.
173. Zehnder AT. Modes of Fracture. In: Wang QJ, Chung Y-W, eds. *Encyclopedia of tribology: With 493 tables*. New York [u.a.]: Springer; 2013:2292-2295. Springer reference.
174. Doyle L, Weidlich I. Effects of Thermal and Mechanical Cyclic Loads on polyurethane Pre-Insulated Pipes // Effects of thermal and mechanical cyclic loads on polyurethane pre-insulated pipes. *Fatigue and Fracture of Engineering Materials & Structures*. 2021;44(1):156-168.
175. Vega A, Yarahmadi N, Sällström JH, Jakubowicz I. Effects of cyclic mechanical loads and thermal ageing on district heating pipes. *Polymer Degradation and Stability*. 2020;182:109385.
176. Weidlich I, Banushi G, Yarahmadi N, et al. Effects of Loads on Asset Management of the 4th Generation District Heating Networks: Annex XII final report. [International Energy Agency Technology Collaboration Programme on District Heating and Cooling including Combined Heat and Power]; 2020.
177. Hay S, Huther, H., Grimm, S., Heiler, D., Dony J., Nielsen, H-J., Schuchardt, G.K., et al. „EnEff: Wärme - Technische Gebrauchsdauernanalyse von Wärmenetzen unter Berücksichtigung volatiler erneuerbarer Energien“: Teil I: Untersuchungsergebnisse zur Materialdegradation. Frankfurt am Main: AGFW-Projektgesellschaft für Rationalisierung, Information; 2020.
178. Sällberg, S. E., Nilsson, S., & Bergström, G. Leakage ways for ground-water in PUR-foam. 10th International Symposium on District Heating and Cooling. 2006;September.
179. Zinko H, Bergström G, Nilsson SF, Jarfelt U. Fuktdiffusion i plaströsystem (in Swedisch): Moisture diffusion in plastic pipe systems: Svenska Fjärrvärmeföreningens Service AB; 2002; ISSN 1402-5191.

180. Immergut EH, Mark H. Plasticization and plasticizer processes: A symposium sponsored by the Division of Industrial and Engineering Chemistry at the 147th meeting of the American Chemical Society, Philadelphia, Pa., April 6-7, 1964. Washington: American Chemical Society; 1965. Advances in chemistry series; 48.
181. Vanlandingham MR, Eduljee RF, Gillespie JW. Moisture diffusion in epoxy systems. *J. Appl. Polym. Sci.* 1999;71(5):787-798.
182. Fedors RF. Osmotic effects in water absorption by polymers. *Polymer.* 1980;21(2):207-212.
183. Fedors RF. Water-treeing as an osmotic phenomenon. *Polymer.* 1980;21(8):863-865.
184. McMahon W, Birdsall HA, Johnson GR, Camilli CT. Degradation Studies of Polyethylene Terephthalate. *J. Chem. Eng. Data.* 1959;4(1):57-79.
185. Earl JS, Shenoi RA. Determination of the Moisture Uptake Mechanism in Closed Cell Polymeric Structural Foam during Hygrothermal Exposure. *Journal of Composite Materials.* 2004;38(15):1345-1365.
186. Avilés F, Aguilar-Montero M. Mechanical degradation of foam-cored sandwich materials exposed to high moisture. *Composite Structures.* 2010;92(1):122-129.
187. Liu H, He J, Xie D, Xue Q, Peng Q. Study on the hygroscopicity of PET foam sandwich structure. *Advances in Mechanical Engineering.* 2021;13(4):168781402110118.
188. Bomberg M. A Model of Aging for Gas-Filled Cellular Plastics. *Journal of Cellular Plastics.* 1988;24(4):327-347.
189. Sekelik DJ, Stepanov EV, Nazarenko S, Schiraldi D, Hiltner A, Baer E. Oxygen barrier properties of crystallized and talc-filled poly(ethylene terephthalate). *J. Polym. Sci. B Polym. Phys.* 1999;37(8):847-857.
190. Lee WM. Water Vapor Permeation In Closed Cell Foams. *Journal of Cellular Plastics.* 1973;9(3):125-129.
191. Matuszak ML, Frisch KC, Reegen SL. Hydrolysis of linear polyurethanes and model monocarbamates. *J. Polym. Sci. Polym. Chem. Ed.* 1973;11(7):1683-1690.
192. Campbell GA, Meluch WC. Polyurethane foam recycling. Superheated steam hydrolysis. *Environmental science & technology.* 1976;10(2):182-185.
193. Motokucho S, Nakayama Y, Morikawa H, Nakatani H. Environment-friendly chemical recycling of aliphatic polyurethanes by hydrolysis in a CO₂-water system. *J. Appl. Polym. Sci.* 2018;135(8):45897.
194. Le Gac PY, Choqueuse D, Melot D. Description and modeling of polyurethane hydrolysis used as thermal insulation in oil offshore conditions. *Polymer Testing.* 2013;32(8):1588-1593.
195. Ballara A, Verdu J. Physical aspects of the hydrolysis of polyethylene terephthalate. *Polymer Degradation and Stability.* 1989;26(4):361-374.
196. Edge M, Allen NS, He JH, Derham M, Shinagawa Y. Physical aspects of the thermal and hydrolytic ageing of polyester, polysulphone and polycarbonate films. *Polymer Degradation and Stability.* 1994;44(2):193-200. Available at: <https://www.sciencedirect.com/science/article/pii/0141391094901643>.
197. Launay A, ThomINETTE F, Verdu J. Hydrolysis of poly(ethylene terephthalate): a kinetic study. *Polymer Degradation and Stability.* 1994;46(3):319-324.
198. Launay A, ThomINETTE F, Verdu J. Hydrolysis of poly(ethylene terephthalate). A steric exclusion chromatography study. *Polymer Degradation and Stability.* 1999;63(3):385-389.
199. Bellenger V, Ganem M, Mortaigne B, Verdu J. Lifetime prediction in the hydrolytic ageing of polyesters. *Polymer Degradation and Stability.* 1995;49(1):91-97.
200. Pickett JE, Coyle DJ. Hydrolysis kinetics of condensation polymers under humidity aging conditions. *Polymer Degradation and Stability.* 2013;98(7):1311-1320.
201. Fayolle B, Richaud E, Colin X, Verdu J. Review: degradation-induced embrittlement in semi-crystalline polymers having their amorphous phase in rubbery state. *J Mater Sci.* 2008;43(22):6999-7012.

202. Arhant M, Le Gall M, Le Gac P-Y, Davies P. Impact of hydrolytic degradation on mechanical properties of PET- Towards an understanding of microplastics formation. *Polymer Degradation and Stability*. 2019;161:175-182.
203. Dubelley F, Planes E, Bas C, Pons E, Yrieix B, Flandin L. Predictive durability of polyethylene terephthalate toward hydrolysis over large temperature and relative humidity ranges. *Polymer*. 2018;142:285-292.
204. Sammon C, Yarwood J, Everall N. An FT-IR study of the effect of hydrolytic degradation on the structure of thin PET films. *Polymer Degradation and Stability*. 2000;67(1):149-158. Available at: <http://www.sciencedirect.com/science/article/pii/S0141391099001044>.
205. Pegoretti A, Penati A. Effects of hygrothermal aging on the molar mass and thermal properties of recycled poly(ethylene terephthalate) and its short glass fibre composites. *Polymer Degradation and Stability*. 2004;86(2):233-243.
206. THOMPSON AB, WOODS DW. Density of Amorphous Polyethylene Terephthalate. *Nature*. 1955;176(4471):78-79.
207. Sammon C, Mura C, Yarwood J, Everall N, Swart R, Hodge D. FTIR-ATR Studies of the Structure and Dynamics of Water Molecules in Polymeric Matrixes. A Comparison of PET and PVC. *J. Phys. Chem. B*. 1998;102(18):3402-3411.
208. IEC 61215:2005. Crystalline silicon terrestrial photovoltaic (PV) modules – Design qualification and type approval. Geneva, Switzerland: International Electrotechnical Commission. 2005.
209. Gok A. Degradation Pathway Models of Poly(ethylene-Terephthalate) under accelerated weathering exposures. [Doctoral Thesis]: Case Western Reserve University; 2016.
210. Mohammadian M, Allen NS, Edge M, Jones K. Environmental Degradation of Poly (ethylene Terephthalate). *Textile Research Journal*. 1991;61(11):690-696.
211. Weidner S, Kuehn G, Werthmann B, et al. A new approach of characterizing the hydrolytic degradation of poly(ethylene terephthalate) by MALDI-MS. *J. Polym. Sci. A Polym. Chem*. 1997;35(11):2183-2192.
212. Elias V, Salman A, Goulias D. The Effect of pH, Resin Properties, and Manufacturing Process on Laboratory Degradation of Polyester Geosynthetics. *Geosynthetics International*. 1998;5(5):459-490.
213. Langevin D, Grenet J, Saiter JM. Moisture sorption in pet influence on the thermokinetic parameters. *European Polymer Journal*. 1994;30(3):339-345.
214. Tesser R, Di Serio M, Sclafani A, Santacesaria E. Modeling of polyurethane foam formation. *J. Appl. Polym. Sci*. 2004;92(3):1875-1886.
215. Di Maio E, Kiran E. Foaming of polymers with supercritical fluids and perspectives on the current knowledge gaps and challenges. *The Journal of Supercritical Fluids*. 2018;134:157-166.
216. Okolieocha C, Raps D, Subramaniam K, Altstädt V. Microcellular to nanocellular polymer foams: Progress (2004–2015) and future directions – A review. *European Polymer Journal*. 2015;73:500-519.
217. Reverchon E, Cardea S. Production of controlled polymeric foams by supercritical CO₂. *The Journal of Supercritical Fluids*. 2007;40(1):144-152.
218. Marshall I, Todd A. The thermal degradation of polyethylene terephthalate. *Trans. Faraday Soc*. 1953;49:67.
219. Doyle L, Weidlich I, Illguth M. Anisotropy in Polyurethane Pre-Insulated Pipes. *Polymers*. 2019;11(12).
220. van Krevelen DW, Nijenhuis Kt. Properties of polymers: Their correlation with chemical structure ; their numerical estimation and prediction from additive group contributions / D.W. van Krevelen. 4th, completely rev. ed. / rev. by K. te Nijenhuis. Amsterdam, Boston: Elsevier; 2009.
221. Wunderlich B. The Annealing of Crystals. In: *Macromolecular Physics*: Elsevier; 1976:348-435.

222. Stuart HA. Ordnungszustände und Umwandlungserscheinungen in Festen Hochpolymeren Stoffen: Springer Berlin Heidelberg; 1955.
223. Wunderlich B. The Microscopic Structure of Crystals. In: *Macromolecular Physics*: Elsevier; 1973:21-177.
224. Cole KC, van Gheluwe P, Hébrard MJ, Leroux J. Flexible polyurethane foam. I. FTIR analysis of residual isocyanate. *J. Appl. Polym. Sci.* 1987;34(1):395-407.
225. Cole KC, Ajji A, Pellerin É. New insights into the development of ordered structure in poly(ethylene terephthalate), II Results from transmission infrared spectroscopy of thin films. *Macromol. Symp.* 2002;184(1):1-18.
226. Eslami H, Müller-Plathe F. Structure and Mobility of Poly(ethylene terephthalate): A Molecular Dynamics Simulation Study. *Macromolecules.* 2009;42(21):8241-8250.
227. Štokr J, Schneider B, Doskočilová D, Lövy J, Sedláček P. Conformational structure of poly(ethylene terephthalate). Infra-red, Raman and n.m.r. spectra. *Polymer.* 1982;23(5):714-721.
228. Pourbozorgi Langroudi P. An Analysis of the most Frequent Operational Temperature of four District Heating Networks of Germany: HafenCity Universität Hamburg; 2022.
229. EN13941-1:2019. District heating pipes- Design and installation of thermal insulated bonded single and twin pipe systems for directly buried hot water networks- Part 1: Design;
230. Gibson LJ, Ashby MF. *Cellular Solids*. Cambridge: Cambridge University Press; 1997.
231. Mark JE. *The polymer data handbook*. 2nd ed. New York, Oxford: Oxford University Press; 2009.
232. Rueda DR, Viksne A, Kajaks J, Balta-Calleja FJ, Zachmann HG. Properties of arylpolyesters with reference to water content. *Macromol. Symp.* 1995;94(1):259-268.
233. Burgess SK, Mikkilineni DS, Yu DB, et al. Water sorption in poly(ethylene furanoate) compared to poly(ethylene terephthalate). Part 2: Kinetic sorption. *Polymer.* 2014;55(26):6870-6882.
234. Loos AC, Springer GS, Sanders BA, Tung RW. Moisture Absorption of Polyester-E Glass Composites. *Journal of Composite Materials.* 1980;14(2):142-154.
235. Huo Z, Mohamed M, Nicholas JR, Wang X, Chandrashekhara K. Experimentation and simulation of moisture diffusion in foam-cored polyurethane sandwich structure. *Jnl of Sandwich Structures & Materials.* 2016;18(1):30-49.
236. Ward IM, Wilding MA. Infra-red and Raman spectra of poly(m-methylene terephthalate) polymers. *Polymer.* 1977;18(4):327-335.
237. Mehta A, Gaur U, Wunderlich B. Equilibrium melting parameters of poly(ethylene terephthalate). *J. Polym. Sci. Polym. Phys. Ed.* 1978;16(2):289-296.
238. Dubelley F, Planes E, Bas C, Pons E, Yrieix B, Flandin L. Water Vapor Sorption Properties of Polyethylene Terephthalate over a Wide Range of Humidity and Temperature. *J. Phys. Chem. B.* 2017;121(8):1953-1962.
239. Heuvel HM, Huisman R. Effect of winding speed on the physical structure of as-spun poly(ethylene terephthalate) fibers, including orientation-induced crystallization. *J. Appl. Polym. Sci.* 1978;22(8):2229-2243.
240. English AD. Macromolecular dynamics in solid poly(ethylene terephthalate): proton and carbon-13 solid-state NMR. *Macromolecules.* 1984;17(10):2182-2192.
241. Roland CM, Walton JH, Miller JB. Proton NMR determination of crystallinity in poly(ethylene terephthalate). *Magn. Reson. Chem.* 1994;32(S1):S36-S39.
242. Fu Y, Annis B, Boller A, Jin Y, Wunderlich B. Analysis of structure and properties of poly(ethylene terephthalate) fibers. *J. Polym. Sci. B Polym. Phys.* 1994;32(13):2289-2306.
243. Fu Y, Busing WR, Jin Y, Affholter KA, Wunderlich B. Structure analysis of the noncrystalline material in poly(ethylene terephthalate) fibers. *Macromol. Chem. Phys.* 1994;195(2):803-822.
244. Wunderlich B. Reversible crystallization and the rigid-amorphous phase in semicrystalline macromolecules. *Progress in Polymer Science.* 2003;28(3):383-450. Available at: <https://www.sciencedirect.com/science/article/pii/S0079670002000850>.

245. Wunderlich B. The ATHAS database on heat capacities of polymers. *Pure and Applied Chemistry*. 1995;67(6):1019-1026.
246. Natta G, Corradini P, Bassi IW. Crystal structure of isotactic poly-alpha-butene. *Nuovo Cim*. 1960;15(S1):52-67.
247. Jones AT. Polybutene-1 – type II crystalline form. *J. Polym. Sci. B Polym. Lett*. 1963;1(8):455-456.
248. Boor J, Mitchell JC. Kinetics of crystallization and a crystal-crystal transition in poly-1-butene. *J. Polym. Sci. A Gen. Pap*. 1963;1(1):59-84.
249. Hadinata C, Boos D, Gabriel C, et al. Elongation-induced crystallization of a high molecular weight isotactic polybutene-1 melt compared to shear-induced crystallization. *Journal of Rheology*. 2007;51(2):195-215.
250. Erdem HB. The Crystallization Behaviour of Isotactic Polybutene-1. [MSc.]: Bilkent University; 2002.
251. Lee S-T, Chul B. Park. *Foam Extrusion*. 2nd revised edition. Bosa Roca: Taylor & Francis Inc; 2014. *Polymeric Foams*.
252. Weingart N, Raps D, Lu M, Endner L, Altstädt V. Comparison of the Foamability of Linear and Long-Chain Branched Polypropylene-The Legend of Strain-Hardening as a Requirement for Good Foamability. *Polymers*. 2020;12(3).
253. Corre Y-M, Maazouz A, Duchet J, Reignier J. Batch foaming of chain extended PLA with supercritical CO₂: Influence of the rheological properties and the process parameters on the cellular structure. *The Journal of Supercritical Fluids*. 2011;58(1):177-188.
254. Zhang H, Liu T, Li B, et al. Foaming and dimensional stability of LDPE foams with N₂, CO₂, i-C₄H₁₀ and CO₂ - N₂ mixtures as blowing agents. *The Journal of Supercritical Fluids*. 2020;164:104930.
255. Chen Y, Li D, Zhang H, et al. Antishrinking Strategy of Microcellular Thermoplastic Polyurethane by Comprehensive Modeling Analysis. *Ind. Eng. Chem. Res*. 2021;60(19):7155-7166.
256. Colton JS, Suh NP. The nucleation of microcellular thermoplastic foam with additives: Part I: Theoretical considerations. *Polym. Eng. Sci*. 1987;27(7):485-492.
257. Kaewmesri W, Lee PC, Park CB, Pumchusak J. Effects of CO₂ and Talc Contents on Foaming Behavior of Recyclable High-melt-strength PP. *Journal of Cellular Plastics*. 2006;42(5):405-428.
258. Tabacchiera A, inventor; Point Plastic S.r.l. Concentrate of polyfunctional compounds usable for the preparation of foamed polyester materials. EP 2 009 043 A1.
259. Park CB, Baldwin DF, Suh NP. Effect of the pressure drop rate on cell nucleation in continuous processing of microcellular polymers. *Polym. Eng. Sci*. 1995;35(5):432-440.
260. Guo Q, Wang J, Park CB, Ohshima M. A Microcellular Foaming Simulation System with a High Pressure-Drop Rate. *Ind. Eng. Chem. Res*. 2006;45(18):6153-6161.
261. Tammaro D, Contaldi V, Carbone MP, Di Maio E, Iannace S. A novel lab-scale batch foaming equipment: The mini-batch. *Journal of Cellular Plastics*. 2016;52(5):533-543.
262. ASTM C518. Standard Test Method for Steady-State Thermal Transmission Properties by Means of the Heat Flow Meter Apparatus. 17th ed.
263. ASTM C1058-97. Practice for Selecting Temperatures for Evaluating and Reporting Thermal Properties of Thermal Insulation: C16 Committee. West Conshohocken, PA: ASTM International.
264. ASTM C177-19. Test Method for Steady-State Heat Flux Measurements and Thermal Transmission Properties by Means of the Guarded-Hot-Plate Apparatus: C16 Committee. West Conshohocken, PA: ASTM International.
265. Sarver JA, Sumey JL, Williams ML, Bishop JP, Dean DM, Kiran E. Foaming of poly(ethylene-co-vinyl acetate) and poly(ethylene-co-vinyl acetate-co-carbon monoxide) and their blends with carbon dioxide. *J. Appl. Polym. Sci*. 2018;135(7):45841.
266. Pasquali I, Comi L, Pucciarelli F, Bettini R. Swelling, melting point reduction and solubility of PEG 1500 in supercritical CO₂. *International journal of pharmaceutics*. 2008;356(1-2):76-81.

267. Takahashi S, Hassler JC, Kiran E. Melting behavior of biodegradable polyesters in carbon dioxide at high pressures. *The Journal of Supercritical Fluids*. 2012;72:278-287.
268. Frerich SC. Biopolymer foaming with supercritical CO₂—Thermodynamics, foaming behaviour and mechanical characteristics. *The Journal of Supercritical Fluids*. 2015;96:349-358.
269. Kelly CA, Harrison KL, Leeke GA, Jenkins MJ. Detection of melting point depression and crystallization of polycaprolactone (PCL) in scCO₂ by infrared spectroscopy. *Polym J*. 2013;45(2):188-192.
270. Carpenter AE, Jones TR, Lamprecht MR, et al. CellProfiler: image analysis software for identifying and quantifying cell phenotypes. *Genome biology*. 2006;7(10):R100.
271. Pinto J, Solórzano E, Rodríguez-Perez MA, Saja JA de. Characterization of the cellular structure based on user-interactive image analysis procedures. *Journal of Cellular Plastics*. 2013;49(6):555-575.
272. Arganda-Carreras I, Kaynig V, Rueden C, et al. Trainable Weka Segmentation: a machine learning tool for microscopy pixel classification: a machine learning tool for microscopy pixel classification.: Oxford Univ Press; 2017; 33.
273. Schindelin J, Arganda-Carreras I, Frise E, et al. Fiji: an open-source platform for biological-image analysis. *Nature methods*. 2012;9(7):676-682.
274. Berens AR, Huvad GS. Interaction of Polymers with Near-Critical Carbon Dioxide. In: Johnston KP, Penninger JML, eds. *Supercritical fluid science and technology*. Vol. 406. Washington, D. C.: American Chemical Society; 1989:207-223. ACS Symposium Series; 406.
275. Lian Z, Epstein SA, Blenk CW, Shine AD. Carbon dioxide-induced melting point depression of biodegradable semicrystalline polymers. *The Journal of Supercritical Fluids*. 2006;39(1):107-117.
276. Fukné-Kokot K, König A, Knez Ž, Škerget M. Comparison of different methods for determination of the S–L–G equilibrium curve of a solid component in the presence of a compressed gas. *Fluid Phase Equilibria*. 2000;173(2):297-310.
277. Shi J, Wu P, Li L, Liu T, Zhao L. Crystalline transformation of isotactic polybutene-1 in supercritical CO₂ studied by in-situ fourier transform infrared spectroscopy. *Polymer*. 2009;50(23):5598-5604.
278. Burt JG. The Elements of Expansion of Thermoplastics Part II. *Journal of Cellular Plastics*. 1978;14(6):341-345.
279. Xu Z-M, Jiang X-L, Liu T, et al. Foaming of polypropylene with supercritical carbon dioxide. *The Journal of Supercritical Fluids*. 2007;41(2):299-310.
280. Matuana LM, Faruk O, Diaz CA. Cell morphology of extrusion foamed poly(lactic acid) using endothermic chemical foaming agent. *Bioresource technology*. 2009;100(23):5947-5954. Available at: <http://www.sciencedirect.com/science/article/pii/S0960852409007457>.
281. Utracki LA, Bakerdjian Z, Kamal MR. A method for the measurement of the true die swell of polymer melts. *J. Appl. Polym. Sci*. 1975;19(2):481-501.
282. Münstedt H. Extensional Rheology and Processing of Polymeric Materials. *International Polymer Processing*. 2018;33(5):594-618.
283. Xanthos M, Tan V, Ponnusamy A. Measurement of melt viscoelastic properties of polyethylenes and their blends? a comparison of experimental techniques. *Polym. Eng. Sci*. 1997;37(6):1102-1112.
284. Vinogradov GV, Prozorovskaya NV. Rheology of polymers. Viscous properties of polypropylene melt. *Rheol Acta*. 1964;3(3):156-163. Available at: <https://link.springer.com/article/10.1007/bf01984759>.
285. Han CD. The effect of temperature on the elastic properties of polymer melts. *Polym. Eng. Sci*. 1971;11(3):205-210.
286. Doyle L. Extrusion foaming behavior of polybutene-1. Toward single-material multifunctional sandwich structures. *J. Appl. Polym. Sci*. 2021:51816.

287. Doyle L. Determination of the melting point depression of PB-1-CO₂ solutions through image analysis: Hafencity Universität Hamburg; 2022.
288. Zhang H, Fang Z, Liu T, et al. Dimensional Stability of LDPE Foams with CO₂ + i-C₄H₁₀ Mixtures as Blowing Agent: Experimental and Numerical Simulation. *Industrial & Engineering Chemistry Research*. 2019;58(29):13154-13162.
289. Naguib HE, Park CB, Panzer U, Reichelt N. Strategies for achieving ultra low-density polypropylene foams. *Polym. Eng. Sci.* 2002;42(7):1481-1492.
290. Park CB, Behraves AH, Venter RD. Low density microcellular foam processing in extrusion using CO₂. *Polym. Eng. Sci.* 1998;38(11):1812-1823.
291. Sharudin RWB, Ohshima M. Preparation of microcellular thermoplastic elastomer foams from polystyrene-b-ethylene-butylene-b-polystyrene (SEBS) and their blends with polystyrene. *J. Appl. Polym. Sci.* 2013;128(4):2245-2254.
292. Zhai W, Leung SN, Wang L, Naguib HE, Park CB. Preparation of microcellular poly(ethylene-co-octene) rubber foam with supercritical carbon dioxide. *J. Appl. Polym. Sci.* 2010:NA-NA.
293. Peters WH, Ranson WF. Digital Imaging Techniques In Experimental Stress Analysis. *Opt. Eng.* 1982;21(3).
294. CEN EN 253:2020-03. EN 253:2020-03, District heating pipes – Bonded single pipe systems for directly buried hot water networks – Factory made pipe assembly of steel service pipe, polyurethane thermal insulation and a casing of polyethylene;. Berlin: Beuth Verlag GmbH.
295. Liu H, Wang X, Liu W, Liu B, Zhou H, Wang W. Reactive Modification of Poly(ethylene terephthalate) and its Foaming Behavior. *Cellular Polymers*. 2014;33(4):189-212.
296. Sarver JA, Sumey JL, Whitfield RM, Kiran E. Confined batch foaming of semi-crystalline rubbery elastomers with carbon dioxide using a mold. *J. Appl. Polym. Sci.* 2021;138(26):50698.
297. Sarver JA, Hassler JC, Kiran E. Linking thermophysical and rheological properties to the selection of CO₂ foaming conditions of rubbery elastomers using the relative rigidity reduction path. *The Journal of Supercritical Fluids*. 2020;166:105015.
298. Yang C, Wang M, Xing Z, Zhao Q, Wang M, Wu G. A new promising nucleating agent for polymer foaming: effects of hollow molecular-sieve particles on polypropylene supercritical CO₂ microcellular foaming. *RSC Adv*. 2018;8(36):20061-20067.
299. Zhai W, Yu J, Wu L, Ma W, He J. Heterogeneous nucleation uniformizing cell size distribution in microcellular nanocomposites foams. *Polymer*. 2006;47(21):7580-7589.
300. Kang JW, Kim JM, Kim MS, et al. Effects of nucleating agents on the morphological, mechanical and thermal insulating properties of rigid polyurethane foams. *Macromol. Res.* 2009;17(11):856-862.
301. Yang C, Xing Z, Wang M, et al. Better scCO₂ Foaming of Polypropylene via Earlier Crystallization with the Addition of Composite Nucleating Agent. *Ind. Eng. Chem. Res.* 2018;57(46):15916-15923.
302. Gibson, L. J., Ashby M. The mechanics of three-dimensional cellular materials. *Proc. R. Soc. Lond. A*. 1982;382(1782):43-59.
303. Menges G, Knipschild F. Estimation of mechanical properties for rigid polyurethane foams. *Polym. Eng. Sci.* 1975;15(8):623-627.
304. Brezny R, Green DJ. The effect of cell size on the mechanical behavior of cellular materials. *Acta Metallurgica et Materialia*. 1990;38(12):2517-2526.
305. Saha MC, Mahfuz H, Chakravarty UK, Uddin M, Kabir ME, Jeelani S. Effect of density, microstructure, and strain rate on compression behavior of polymeric foams. *Materials Science and Engineering: A*. 2005;406(1-2):328-336.
306. Bureau MN, Gendron R. Mechanical-Morphology Relationship of PS Foams. *Journal of Cellular Plastics*. 2003;39(5):353-367.
307. Ridha M. Mechanical and Failure Properties of Rigid Polyurethane Foam Under Tension. [Doctoral Thesis]: National University of Singapore; 2007.

308. Huber AT, Gibson, L. J. Anisotropy of foams. *J Mater Sci.* 1988;23(8):3031-3040.
309. Sullivan RM, Ghosn LJ, Lerch BA. A general tetrakaidecahedron model for open-celled foams. *International Journal of Solids and Structures.* 2008;45(6):1754-1765.
310. Chen Y, Das R, Battley M. Effects of cell size and cell wall thickness variations on the stiffness of closed-cell foams. *International Journal of Solids and Structures.* 2015;52:150-164.
311. Marvi-Mashhadi M, Lopes CS, Llorca J. Modelling of the mechanical behavior of polyurethane foams by means of micromechanical characterization and computational homogenization. *International Journal of Solids and Structures.* 2018;146:154-166.
312. Fischer F, Lim GT, Handge UA, Altstädt V. Numerical Simulation of Mechanical Properties of Cellular Materials Using Computed Tomography Analysis. *Journal of Cellular Plastics.* 2009;45(5):441-460.
313. Kang MJ, Kim YH, Park GP, Han MS, Kim WN, Park SD. Liquid nucleating additives for improving thermal insulating properties and mechanical strength of polyisocyanurate foams. *J Mater Sci.* 2010;45(19):5412-5419.
314. Prociak A, Pielichowski J, Sterzynski T. Thermal diffusivity of rigid polyurethane foams blown with different hydrocarbons. *Polymer Testing.* 2000;19(6):705-712.
315. Logstor. *FlexPipe Handbook*; 2022.
316. CEN EN 15632-2:2010+A1:2014. District heating pipes - Pre-insulated flexible pipe systems - Part 2: Bonded plastic service pipes - Requirements and test methods. Brussels, Belgium. 2010.
317. CEN EN 15632-2:2020. District heating pipes – Factory made flexible pipe systems – Part 2: Bonded system with plastic service pipes; requirements and test methods; German and English version. Brussels, Belgium. 2020.
318. Abegunrin O. Life Cycle Assessment of District Heating Pipes; Comparing Polyurethane with Polyethylene Terephthalate Insulation. [MSc.]. Hamburg: HafenCity University; 2021.
319. Doroudiani S, Park CB, Kortschot MT. Effect of the crystallinity and morphology on the microcellular foam structure of semicrystalline polymers. *Polym. Eng. Sci.* 1996;36(21):2645-2662.
320. Momose Chiaki, Matsumoto Shigeo, Horiuchi Kazuya, Shigeki Isoji, Hotta Chiaki, inventors; Dainichi Nippon Cables LTD. Manufacturing Method of Heat Insulation Pipe. JPS61108540A.
321. Roschli A, Gaul KT, Boulger AM, et al. Designing for Big Area Additive Manufacturing. *Additive Manufacturing.* 2019;25:275-285.
322. Pignatelli F, Percoco G. An application- and market-oriented review on large format additive manufacturing, focusing on polymer pellet-based 3D printing. *Prog Addit Manuf.* 2022.

Annex I. Validation of the Thermal Conductivity Measurements - Steady State Heat Flow Meter Apparatus

The set-up validation procedure and results are described in this Annex.

• Precision – Repeatability

Repeatability was determined by repeating the measurement of the same sample five times under the same conditions: same operator, same apparatus, same heat supply and on the same day. This procedure was undertaken with the eight different samples of two different polymeric foams: PU and PET.

The measurement results are provided in Table 12 together with the standard deviation (SD), the standard error of the mean (SE) and the variance.

Table 12. Measurement results for the assessment of repeatability

Sample	n° measurements	Mean (W/mK)	SD (W/mK)	SE (W/mK)	Variance (W/mK) ²
PU-1	5	0.0226	$6.18 \cdot 10^{-4}$	$2.76 \cdot 10^{-4}$	$3.82 \cdot 10^{-7}$
PU-2	5	0.01908	$3.68 \cdot 10^{-4}$	$1.65 \cdot 10^{-4}$	$1.35 \cdot 10^{-7}$
PU-3	5	0.01551	$2.06 \cdot 10^{-4}$	$9.23 \cdot 10^{-5}$	$4.26 \cdot 10^{-8}$
PET-1	5	0.02153	$5.08 \cdot 10^{-4}$	$2.27 \cdot 10^{-4}$	$2.58 \cdot 10^{-7}$
PET-2	5	0.02311	0.00107	$4.80 \cdot 10^{-4}$	$1.15 \cdot 10^{-6}$
PET-3	5	0.02297	$6.52 \cdot 10^{-4}$	$2.91 \cdot 10^{-4}$	$4.25 \cdot 10^{-7}$
PET-4	5	0.02214	$3.29 \cdot 10^{-4}$	$1.47 \cdot 10^{-4}$	$1.08 \cdot 10^{-7}$
PET-5	5	0.01822	$3.42 \cdot 10^{-4}$	$1.53 \cdot 10^{-4}$	$1.17 \cdot 10^{-7}$

From these measurements it can be seen that the average standard deviation is of 0.000512 W/mK and the standard error of 0.000229 W/mK. In the worst case (PET-2) the standard deviation obtained is <5% of the mean value, and the maximum standard error obtained is $\leq 2\%$ of the mean value. Disregarding this sample, the standard deviation obtained is <3% of the mean value, and the maximum standard error obtained is $\leq 1.5\%$ of the mean value. It can be concluded that the set-up produces repetitive measurements.

• Precision - Reproducibility

To determine intralaboratory reproducibility, the measurement of a same sample was repeated in five different days, spanning over a week. The procedure was repeated with three different polymeric foams: PU, PET and XPS. The results are presented in Table 13.

Table 13. Measurement for the assessment of reproducibility.

Sample	n° measurements	Mean (W/mK)	Standard Deviation (W/mK)	SE of mean (W/mK)	Variance (W/mK) ²
PU	5	0.02444	$3.967 \cdot 10^{-4}$	$1.774 \cdot 10^{-4}$	$1.573 \cdot 10^{-7}$
PET	5	0.02099	0.00106	$4.745 \cdot 10^{-4}$	$1.125 \cdot 10^{-6}$
XPS	5	0.01954	$4.921 \cdot 10^{-4}$	$2.201 \cdot 10^{-4}$	$2.422 \cdot 10^{-7}$

The maximum standard deviation obtained is $\leq 5\%$ of the mean value, and the maximum standard error obtained is $\leq 2.5\%$ of the mean value, obtained in the case of the PET foam.

It can be concluded that the set-up produces reproducible measurements.

- **Robustness**

To assess the robustness of the measurement, a same sample was measured on the same day, but different voltages were applied to the Peltier, creating so different temperature differences across the sample. This parameter was selected as it is the main parameter that the operator has to select and could influence the measurement results. Three measurements were undertaken using the Peltier as a heat source, producing ΔT above ambient temperatures, and one using the Peltier as a cold source, producing a ΔT below ambient temperature

Table 14. Measurements for the assessment of robustness

V to Peltier	ΔT (°C)	ϕ (W/m ²)	λ (W/mK)
4,1 V (as heat source)	44.47	77.04	0.0240
3,1 V (as heat source)	30.94	53.55	0.0240
2,1 V (as heat source)	19.12	33.77	0.0245
4,1 V (as cold source)	9.89	11.36	0.0159

Mean, median, standard deviation and standard error (SE) were calculated for the total four measurements conducted, and for the three measurements conducted with the Peltier as heat source only, as presented in Table 15.

Table 15. Statistical evaluation of obtained λ values for the assessment of robustness

N total	Mean	Standard Deviation	SE of mean	Minimum	Median	Maximum
4	0.02212	0.00413	0.00206	0.01593	0.02402	0.02449
3	0.02418	0.00027	0.00016	0.02401	0.02403	0.02449

While measurement with the Peltier acting as cold source, with a ΔT across the sample of 9.9°C, is statistically not an outlier, it significantly increases the standard deviation and standard error. It is suggested that a ΔT of $\sim 10^\circ\text{C}$ is too low to provide reliable results, consistent with ²⁶³.

The data shows the set-up is robust as long as the applied ΔT is of at least 20°C.

- **Veracity**

The veracity of the produced measurements was evaluated in terms of bias. Since a calibration standard traceable to a national standard laboratory as required by ²⁶² was not available, three different foam types (PU, PET and XPS) were measured and the results compared to the values stated on the data sheet. PET and XPS samples were additionally measured in a Hot Disk TPS 2500S apparatus (Gothenburg, Sweden) for comparison. The PU sample could not be measured in the Hot Disk, as it was extracted from a DH pipe and the sample size was not large enough to conduct the measurement. Five samples of each foam were measured in the in-house apparatus, two samples measured twice each were measured with the Hot Disk. The bias is defined as:

$$\text{Bias} = \text{measured value} - \text{true value} \quad (\text{II.1})$$

Where the data sheet value is taken as true value.

The obtained results are presented in Table 16 and Figure 41.

Table 16. λ measured with the in-house apparatus, the Hot Disk apparatus and the data sheet values.

Sample	In-house measurement (W/mK)	Hot Disk measurement (W/mK)	Data Sheet value (W/mK)	Bias in-house	Bias hot plate
PU- from Logstor pipe	$0.020 \pm 9.98 \cdot 10^{-4}$	N/A	0.027 (50°C, EN 253)	-0.007	
PET Kerdyn Green 80	$0.022 \pm 2.18 \cdot 10^{-3}$	$0.0482 \pm 6.24 \cdot 10^{-3}$	0.027, EN 12667	-0.005	0.021
XPS Jackodur KF300	$0.019 \pm 1.45 \cdot 10^{-4}$	$0.036 \pm 7.64 \cdot 10^{-4}$	0.034, EN 12667	-0.015	0.001

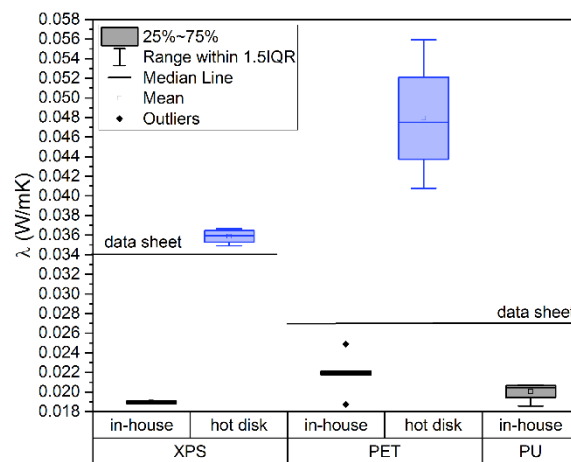


Figure 40. Box plot comparing the measurements of the in-house and hot disk apparatuses. Data sheet values are added for reference.

It can be seen that the in-house apparatus systematically under-measures the thermal conductivity. This can be related to heat losses through the edge insulation, and as anticipated by ASTM C518²⁶². This could be corrected through calibration or the installation of a heat guard. The commercial set up provides on the other side higher values than the data sheets. When comparing the in-house with the commercial set-up, the extent of the bias depends on the measured foam. The Hot Disk provides closer measurements to the data sheet values for the XPS foam, but a larger bias than the in-house set-up for the PET foam. It should be noted that nominal thermal conductivities stated in the products data sheets are defined as that that represents 90% of the production with a 90% confidence interval. It is not known if the individual samples taken from one particular foam board for this validation fulfil this criterion.

But it can be seen that the measurements provided by the in-house set-up present a bias of the same order of magnitude than commercial set-ups, and is valid for R&D purposes.

For the developed foam, in addition to the direct measurement, the % deviation from the measured PU extracted from DH pipes can be given as benchmark.

gSKIN[®] Heat Flux Sensor

gSKIN[®]-XP 26 9C calibrated

The gSKIN[®] Heat Flux Sensor measures the heat flux passing through its surface by means of ultra-sensitive thermocouples.



greenTEG AG | Technoparkstr. 1 | 8005 Zürich | Switzerland
 T +41 44 632 04 20 | F +41 44 632 14 62
 gSKIN@greenTEG.com | www.greenTEG.com

Before installing, handling, using or servicing this product consult the instruction manual at: <http://www.greenTEG.com>

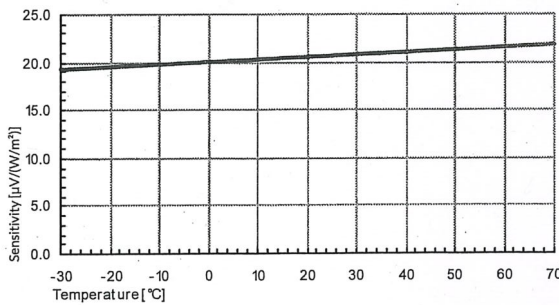
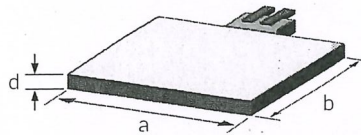
SENSOR SPECIFICATIONS

Article Number	A-044573
Serial Number	001436-H05
Sensitivity S_0 [$\mu\text{V}/(\text{W}/\text{m}^2)$]	20.70
Correction Factor S_c [$(\mu\text{V}/(\text{W}/\text{m}^2))/^\circ\text{C}$]	0.0252
Rel. Error	+/- 3%
Dimensions (a x b) [mm]	10.0 x 10.0
Thickness (d) [mm]	0.5
Electrical Resistance [Ω] at 22.5°C	<150
Temperature Range Min / Max [$^\circ\text{C}$]	-50 / +150
Calibration Range Min / Max [$^\circ\text{C}$]	-30 / +70
Cable length [cm]	100.0

CALIBRATION

The sensor is calibrated under steady state conditions with a method which is oriented towards ISO8301 standard*. A linear correction factor S_c , accounts for the temperature dependency of the sensor. To calculate the sensitivity of the sensor at temperature T the following formula is used:
 $S(T) = S_0 + (T - 22.5^\circ\text{C}) * S_c$

* E. Schwyter et al, Rev. of Sci. Instrum. 83, 074904 (2012); <http://dx.doi.org/10.1063/1.4737880>



Annex II. 12 Principles of Green Engineering

Reproduced with permission from:

Anastas PT, Zimmerman JB. Design through the 12 principles of green engineering. *Environmental science & technology*. 2003;37(5):94A-101A. DOI 10.1021/es032373g

Principle 1: Designers need to strive to ensure that all material and energy inputs and outputs are as inherently nonhazardous as possible.

Principle 2: It is better to prevent waste than to treat or clean up waste after it is formed.

Principle 3: Separation and purification operations should be designed to minimize energy consumption and materials use.

Principle 4: Products, processes and systems should be designed to maximize mass, energy, space, and time efficiency.

Principle 5: Products, processes and systems should be “output pulled” rather than “input pushed” through the use of energy and materials.

Principle 6: Embedded entropy and complexity must be viewed as an investment when making design choices on recycle, reuse, or beneficial disposition.

Principle 7: Targeted durability, not immortality, should be a design goal.

Principle 8: Design for unnecessary capacity or capability (e.g., “one size fits all”) solutions should be considered a design flaw.

Principle 9: Material diversity in multicomponent products should be minimized to promote disassembly and value retention.

Principle 10: Design of products, processes, and systems must include integration and interconnectivity with available energy and material flows.

Principle 11: Products, processes and systems should be designed for performance in a commercial “afterlife”.

Principle 12: Material and energy inputs should be renewable rather than depleting.



Contents lists available at ScienceDirect

Polymer Degradation and Stability

journal homepage: www.journals.elsevier.com/polymer-degradation-and-stability

Hydrolytic Degradation of Closed Cell Polyethylene Terephthalate Foams. The Role of the Mobile Amorphous Phase in the Ductile-Brittle Transition

Lucía Doyle^{*}, Ingo Weidlich

HafenCity University, 20457 Hamburg, Germany

ARTICLE INFO

Keywords:

PET
Hydrolysis
Embrittlement
3-phase
Cellular
Foam
Crystallinity

ABSTRACT

Polyethylene terephthalate (PET) foam is receiving increasing interest in recent years for engineering and structural applications. But for its successful and reliable implementation in real life infrastructures, knowledge on its ageing performance is critical for service life predictions. In this study the ageing of commercial closed cell PET under 90°C and 95% RH is presented and its molecular and mechanical degradation characterized. The aim of the study is to observe the impact of the cellular structure on the hydrolysis kinetics, and provide more insights on the nature of embrittlement in PET. Structural changes are evaluated based on a three-phase model with crystalline, mobile amorphous (MAF) and rigid amorphous (RAF) fractions. The hydrolytic degradation of PET foams does not appear influenced by the cellular structure. Hydrolysis and chemicrystallization appear to occur at the expense of the MAF fraction until the embrittlement occurs. The ductile-brittle transition point coincides with the achievement of the minimum MAF content. The link of embrittlement with the structural changes occurring in the mobile chains questions the occurrence of hydrolysis-induced embrittlement below T_g , which would correspond to service conditions. A micromechanical interpretation of embrittlement appears more appropriate than a molecular interpretation.

1. Introduction

Polyethylene terephthalate (PET) foam is receiving growing interest in recent years as a structural and engineering material. The need for a replacement for the commonly used polyurethane (PU) foam is triggered by the recently approved restriction on toxic di-isocyanates [1], required for its manufacturing. PET foam offers further advantages, such as its full recyclability, wide availability of recycled material and competitive cost. Its use would support the transition of the energy and construction sectors to the circular economy. Knowledge on its ageing performance is vital for service life predictions and reliable implementation in real life infrastructures.

One source of degradation is the exposure to moisture and heat, as occurring in district heating pipelines, application which motivates this study. It is known that PET undergoes a hydrolysis reaction under moisture and heat:

This reaction leads to the embrittlement of the material. Therefore, this source of degradation is of great importance for service life predictions, in particular for structural applications, and has motivated a broad number of studies of the hydrolysis of PET since early years [2–8].

These have aimed at understanding the mechanisms, kinetics of the reaction, and the extent of degradation. From these studies it is established that hydrolysis causes chain scission of the ester links in the amorphous phase, chemicrystallization, arising from the formation of chain fractions with enough mobility to join the crystalline phase, and embrittlement.

All these studies have been conducted in PET films and sheets. However, a cellular structure may cause differences that justify the experimental evaluation of foamed PET. It has been reported that the initial microstructure of PET and crystallinity content influences the hydrolysis kinetic [2, 9]. The applied stresses during the processing of PET fibres and films induces orientation of the trans and gauche rotational isomers [10–12], altering the product's permeability properties, as used for the achievement of improved barrier properties in packaging [13]. It is known that the foam extrusion process produces preferential stretching, from which the cell shape anisotropy arises [14]. The effect and extent of this on the molecular orientation of PET foam and eventual impact on the degradation kinetics remains unexplored. The cellular structure could have an impact on the diffusion rate of the moisture through the bulk of the foam, causing a different ageing state on the

^{*} Corresponding author.

E-mail address: lucia.doyle@hcu-hamburg.de (L. Doyle).

<https://doi.org/10.1016/j.polydgradstab.2022.110022>

Received 8 February 2022; Received in revised form 5 May 2022; Accepted 11 June 2022

Available online 12 June 2022

0141-3910/© 2022 Elsevier Ltd. All rights reserved.

surface than in the core of the foam. Such has been reported in previous studies of moisture uptake [15, 16] and hydrothermal ageing [17] of foams. The modelling of diffusion through cellular structures is more complex than in films [17], owing to its solid-gas heterogeneous nature [18].

In addition to the differences the cellular structure may induce, there are still open questions concerning the hydrolysis of PET which still today hinder accurate lifetime prediction.

It is widely accepted that both temperature and relative humidity (RH) influence the reaction kinetics, with the temperature dependency following the Arrhenius law. Many authors consider the reaction as first order in RH, owing to water being largely in excess and considering no diffusion control [2, 5, 6], while others report second order in RH, and explain the fit with the need of two water molecules acting per chain scission [8]. A recent model for a larger range of conditions based on literature data presents a master curve with a reaction order of 0.5 [19], though no physical meaning is provided. This later paper also highlights the large scattering of E_a available in the literature. Discussions on the reaction being autocatalytic [3, 20], or non-autocatalytic [2, 5] have been ongoing.

All the cited studies of the hydrolysis of PET have been conducted at temperatures above T_g . This is also the case for applications of energy infrastructure [21, 22] and civil engineering [23–25], which would be accelerated ageing. Service temperatures are commonly below the T_g of PET. Modelling of PET hydrolysis kinetics to temperatures below T_g has been undertaken [19, 25]. But if these Arrhenius extrapolations are valid in the glassy state, when the activation energy (E_a) has been obtained in the rubbery state, is questionable [19, 26]. And so the service life is uncertain.

Service life is determined by the degradation kinetics, and by the end-of-life criterion. For the later, the ductile-brittle transition is commonly selected [5–7, 26, 27]. It is accepted that embrittlement corresponds to a critical structural state [27]. However, the underlying mechanism is still not fully understood. The ductile-brittle transition is experimentally observed by previous authors of PET hydrolysis and commonly discussed in terms of M_c' , critical molecular mass corresponding to the entanglement limit [6, 19, 26], which is proportional to M_e (molecular mass of the segment between the entanglements). Literature provides ranges of M_c' between 2–3 times M_e [6] to 5–10 times M_e [26]. But for accurate lifetime predictions specific end-of-life-criteria need to be set. To illustrate the current uncertainty, based on literature M_c' and M_e ranges, some authors have derived a 30% molar mass reduction as end-of-life criteria [19]. Recently an experimental value of $M_c' = 17$ kg/mol has been reported [26], obtained from PET with an initial molar mass of 31.4 kg/mol and polydispersity index of 2.4. This corresponds to a 45% molar mass reduction. More insights on the underlying mechanisms for embrittlement are needed for lifetime prediction purposes, and is in the focus of this paper.

The change in crystallinity content that accompanies the hydrolysis of PET has been recognized since early studies. Ballara and Verdú

quantified the chemiscrystallization yield as about 5–6 monomer units joining the crystalline phase per chain scission [3]. Since then, authors have observed the crystallinity increase during the hydrolysis of PET [5, 7, 19, 26, 28, 29] and developed models for predicting its change with hydrolytic ageing time [19].

All the identified references on the hydrolysis of PET discuss this morphological change in the context of a two-phase system, with an amorphous and crystalline phase. However, it has been seen that such two phase system fails to describe PET and different degrees of orientation can be found within the amorphous phase [30–33] thus a three phase system has been found more suitable [34–36]. In this work the morphological changes of PET upon hydrolysis are evaluated in terms of crystalline, mobile amorphous (MAF) and rigid amorphous (RAF) fractions. The relationship between the change of these three fractions with the hydrolysis reaction and their role in the ductile-brittle transition are discussed. This brings new insights towards lifetime prediction and the validity of extrapolations to temperatures below T_g .

2. Experimental

2.1. Materials

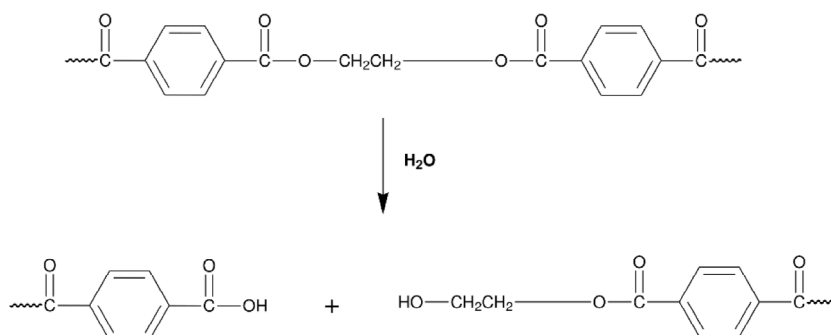
Commercial closed cell PET foam boards (Gurit Kerdyn Green) of two densities, 80 and 100 kg/m³ were used in this study. The foaming of PET is out of the scope of this work. The manufacturing of these boards includes cutting blocks of the extruded plates and gluing them in the direction parallel to the extrusion direction, in order to transfer the higher mechanical properties of the extrusion direction of the foam into the sheet surface parallel to the extrusion direction. For this study samples were always extracted from segments free from glue.

2.2. Cellular microstructure characterization

The cellular microstructure was examined in an optical microscope (Leica DMLP, Wetzlar, Germany). The cell size and shape were measured from the micrographs by adjusting the cells to an ellipse using Fiji [37]. Both extrusion foaming direction (E) and parallel direction (P) were analysed as to assess the anisotropy in the cell shape. At least 100 cells were measured for each case. Cell wall and strut thickness were additionally measured. Values presented are an average of at least 20 measurements.

2.3. Hydrolytic ageing

Foam samples were aged in an environmental chamber at 90°C and 95% relative humidity. A Weiss WK1 340 (Reiskirchen, Germany) environmental chamber was used. Samples were extracted after successive ageing times and characterized through the different techniques described below.



2.4. H^1 NMR

The chain structure of the PET was characterized through proton nuclear magnetic resonance (H^1 NMR) using a Bruker Advance II HD, 600 MHz (Billerica, USA). The solvent used was Trifluoroacetic Acid (TFA) D1 / $CDCl_3$ 16.6% v/v, both purchased to Eurisotop. Each sample was prepared and analysed in duplicate and the averages presented. The progress of the hydrolysis reaction was followed through end-group analysis as the ratio between the terephthalic acid protons and the hydroxyl end group protons.

2.5. Mechanical tests

Samples of $25 \times 25 \times 200$ mm were subjected to 3-point flexural tests. Tests were undertaken with a universal testing machine under a displacement-controlled rate of 1.5 mm/min. The force was measured with a 2 kN load cell, accuracy class 1 (HBM, Darmstadt, Germany). The strain was measured by 3D digital image correlation (DIC) [38] on the front and back surfaces of the specimen, using an ARAMIS 5M and 6M adjustable stereo camera system (GOM mbh, Braunschweig, Germany). The images were acquired at a frequency of 5 Hz. The reported strains are the averages of the measurements on both surfaces. At least 3 samples were tested for each case. The reported flexural strength (σ_f) corresponds to the maximum strength at the break point. The toughness (U) was calculated from the integral under the stress-strain curve until the strain at break is reached:

$$U = \int_0^{\varepsilon_f} \sigma_f \cdot d\varepsilon \quad (1)$$

where ε_f is the strain at break.

2.6. FTIR-ATR

Alterations in the chemical structure were evaluated through Fourier transform infrared spectroscopy (FTIR) in attenuated total reflection (ATR) mode using a Thermo Scientific Nicolet 10 FTIR spectrometer with a diamond ATR Smart Orbit accessory (Dreieich, Germany). Spectra from 32 co-added scans and 4 cm^{-1} spectral resolution were baseline corrected, and normalized to the intensity of the 1410 cm^{-1} band, which has been found insensitive to orientation and conformation [39]. Each spectrum reported is the average of 5 spectra measured in different locations of each sample. Maximum contact of the ATR crystal was applied to ensure reproducible results. The foam extrusion process produces preferential stretching which could eventually lead to molecular orientation. The conformation of the molecular chains involving both trans/gauche isomerism in the ethylene glycol unit has a significant effect on the IR spectrum of PET [40, 41]. Hence, samples were analysed both in the plane perpendicular to the foaming extrusion (E) and parallel to the extrusion (P) directions to consider orientation effects. It should be noted that the measurement of a plane is not fully in line with a cell wall. Band assignments can be found in the literature [3, 22, 28, 39, 40, 42–46] and are summarized in the Supporting Information.

2.7. DSC

Differential scanning calorimetry (DSC) analysis was conducted with a Netzsch DSC 200F3 apparatus (Selb, Germany) applying a heating/cooling/heating program in the temperature range between 20 and 310°C , with a ramp of 10 K/min and a N_2 flow rate of 20 ml/min . Approximately 5 mg of material was placed in Al open pans. The relative values of crystalline (X_c), mobile amorphous fraction (X_{MAF}) and rigid amorphous fraction (X_{RAF}), were calculated as

$$X_c = \frac{\Delta H_f}{\Delta H_f^0} \quad (2)$$

$$X_{MAF} = \frac{\Delta C_p}{\Delta C_p^0} \quad (3)$$

$$X_{RAF} = 1 - X_{MAF} - X_c \quad (4)$$

where ΔH_f is the specific melting enthalpy measured from the second heating ramp, ΔC_p is the jump in heat capacity at the glass transition, measured from the second heating ramp, ΔH_f^0 the melting enthalpy of a fully crystalline PET, taken as 140 J/g [47] and ΔC_p^0 the heat capacity increment of a fully amorphous PET, taken as $0.405 \text{ J}\cdot\text{g}^{-1}\cdot\text{K}^{-1}$ [48]. One sample per foam density and ageing time were measured. The average per each ageing time is presented.

2.8. Gravimetry

The process was gravimetrically studied. Samples of $48 \times 48 \times 25$ mm were regularly extracted from the chamber and weighed in the wet state with a Sartorius MC1 LC3200 D balance (Goettingen, Germany), and then reintroduced into the chamber. The samples remained out of the chamber for ca. 10 minutes per weight measurement, which is considered low enough to not alter the ageing process or start desorption. Specimens were always removed and weighed in the same order, to minimize variations in the results. No superficial moisture accumulation was observed on the samples by wiping with a paper tissue. The study was undertaken in duplicate. At least three samples per foam density were evaluated in each trial. Reported samples were cut with the larger surface perpendicular to the extrusion direction (E).

3. Results

3.1. Material characterization

The cellular microstructure of the foams was characterized through optical microscopy. Representative micrographs of the PET foams under consideration, in the planes perpendicular to the extrusion (E) and the parallel (P) directions are presented in Fig. 1.

The results from the cellular microstructure characterization are summarized in Table 1, where D1 is the largest diameter of the ellipse, D2 the shortest, and R the cell anisotropy ratio, defined as:

$$R = \frac{D1_p}{D2_e} \quad (5)$$

As we can see, the 100 foam presents larger cells and larger cell size anisotropy, and thicker cell walls and struts than the 80 foam. The obtained R fall into the typical values for polymeric foams, reported as around 1.3 [14].

Considering the foams under study are commercial products and details on the polymer structure and potential additives or impurities are unknown, the polymer structure was characterized through H^1 NMR as to gain this knowledge. The signal assignments were found in the literature [49–51]. A typical spectrum is presented in Fig. 2.

In addition to terephthalic acid (TPA) and ethylene glycol (EG), diethylene glycol (DEG) was found, which is a by-product of PET synthesis [52] and isophthalic acid (IA), which is one of the main co-monomers used in PET-bottle grade production [49], hence consistent with the recycled nature of this PET. The co-monomer ratio has been found the same for both foams under study (see Table 2), suggesting the same resin was used for their manufacturing. This was later confirmed by the manufacturer.

To complete the characterization of the polymeric foams under study, the initial crystallinity was determined from the second heating ramp of DSC thermograms. The integration of the melting peak yields a

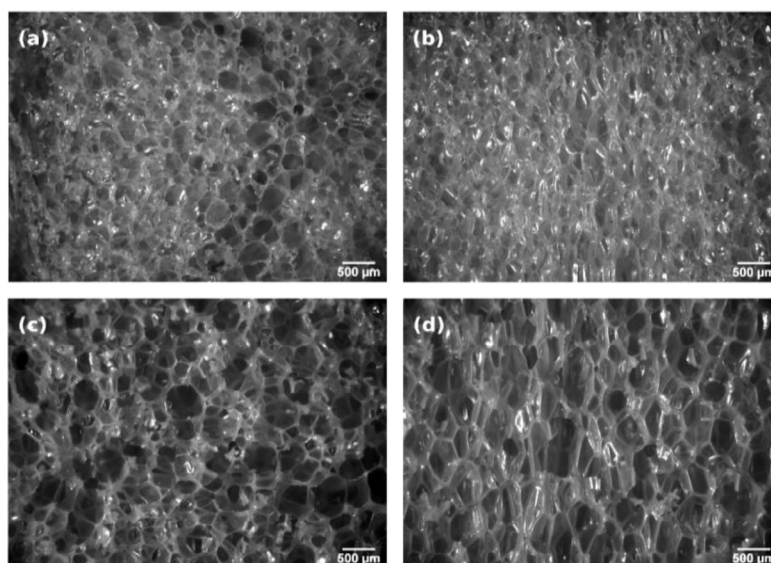


Fig. 1. Micrographs of foam 80 plane perpendicular to the extrusion direction (a) and perpendicular to the parallel direction (b), and foam 100 plane perpendicular to the extrusion direction (c) and perpendicular to the parallel direction (d).

Table 1
Measured dimensions of the cellular microstructure.

	Cell area (μm^2)	D1 (μm)	D2 (μm)	R	Strut width (μm)	Wall thickness (μm)
80E	0.07 $\pm 0.03^*$	307.8 $\pm 63.7^*$	269.6 $\pm 55.2^*$	1.35	18.5 $\pm 4.6^*$	$5.2 \pm 1.8^*$
80P	0.07 $\pm 0.03^*$	363.2 $\pm 86.8^*$	250.5 $\pm 53.2^*$			
100E	0.11 $\pm 0.06^*$	393.7 $\pm 102.1^*$	341.2 $\pm 93.2^*$	1.47	37.2 $\pm 8.7^*$	$9.1 \pm 2.1^*$
100P	0.13 $\pm 0.06^*$	501.9 $\pm 139.1^*$	322 $\pm 89.9^*$			

* Standard deviation.

crystallinity of 21.8% for PET 80 and 22.4% for PET 100. We cannot say the difference is statistically different. The reference thermograph for each foam is included in Fig. 8 (a) and (b).

3.2. Effects of ageing on the mechanical properties

Given the focus of the paper is placed in understanding the embrittlement mechanism, the effects of ageing on the mechanical properties was evaluated first, as to determine time to embrittlement and duration of the required ageing trial.

Bending tests for unaged reference samples and aged after 384 h where tested both in the E and the P direction. The bending properties did not appear to significantly differ between directions, therefore the full trial and reported tests correspond to tests in the E direction (force applied in the foam extrusion direction).

The effects of the heat and moisture exposure on the mechanical properties over ageing time can be seen in Fig. 3. The flexural stress-strain curves for foams 80 and 100 can be seen in Fig. 3 a) and c) respectively. A progressive degradation with exposure time can be observed, and the transition from ductile to brittle behavior found after 108 h of exposure.

Fig. 3 b) and d) present the flexural strength, strain at break and toughness for foams 80 and 100 respectively, derived from the stress-strain curves. A change in the degradation rate can be observed, with the inflection point at 108 h of exposure, which corresponds to the ductile-to-brittle transition point observed in the stress-strain curves.

The same behavior can be found in both foams, suggesting no diffusion-control effect related to the different cellular microstructure or wall thickness. Time to embrittlement is equivalent to previous findings in PET films [26], suggesting that the cellular structure does not create a more tortuous path for the diffusant through the PET matrix than when the matrix is in film form.

3.3. Effects of ageing in the molecular weight of PET

Typically, change in molecular weight has been used to follow the hydrolysis reaction of PET [5–7, 19, 26, 29, 53]. This is favoured by the ease of quantitative relation between molecular weight and extent of hydrolysis, since only scission at the ester link takes place, as well as the fast change in molecular weight at the early stages of hydrolytic degradation [2]. The relative concentration of end-group protons and monomer protons provide an indication of the molecular weight. This was used to follow the changes in molecular weight of the PET foams through ageing time. The monomers and the hydroxyl end group content was quantified through ^1H NMR. The low solubility of PET in commonly used NMR solvents had for long prevented the use of this technique for PET. The mixture of TFA with chloroform was found to conveniently dissolve PET at room temperature [54]. However it has also been found that the hydroxyl end groups undergo an esterification reaction with TFA [50], following the reaction:

To take this into account, each sample was measured every 24h for 5 days, in order to obtain the rate of the esterification reaction and correct for the time between sample preparation and measurement (approx. 1,5h), in a procedure analogous to that of [51]. The details of the procedure and obtained curves can be found in the Supporting Information. It was found nevertheless that the difference in that short amount of time was small.

The NMR spectra of samples with increasing ageing time show a progressive increase of the hydroxyl end group content and decreasing monomer/end group proton ratio, consistent with chain scission due to hydrolysis reaction. The ratio between the terephthalic acid monomer protons and hydroxyl end group protons with ageing time provides the chain scission rate and is presented in Fig. 4.

The cooling thermograms from the DSC analysis show that with ageing time, the crystallization occurs progressively earlier and with sharper peaks, which has been related to the presence of shorter chains [55] and provides further evidence of the chain scission. This was found

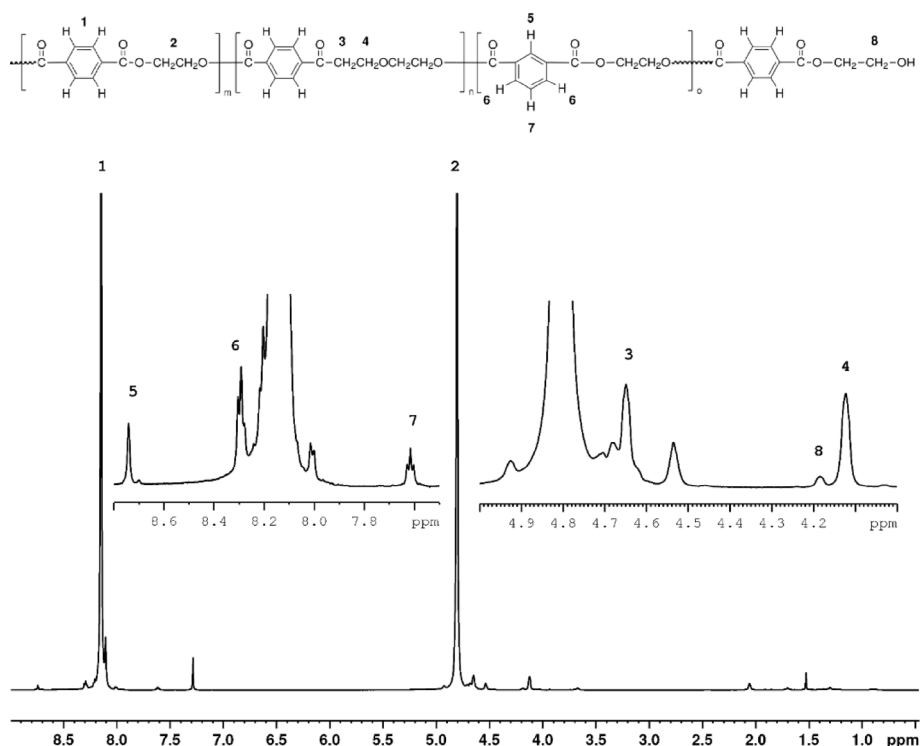


Fig. 2. Representative NMR spectra of the PET foam under study and the related peak assignments.

Table 2

Co-monomer ratios obtained from the integrated signals of the NMR spectra.

	PET foam 80 kg/m ³	PET foam 100 kg/m ³
Ratio IA/TPA	0.0113±0.0004	0.0115±0.0015
Ratio DEG/EG	0.0263±0.0018	0.0265±0.0029

equally in both foam densities, the thermograms are presented in Fig. 5.

Evidence of the chain scission could not be extracted from the FTIR-ATR spectra due to the saturation of the ester bands, as encountered by previous authors [28]. An increase of the carboxylic acid content was detected in the band at 1683 cm⁻¹, to a greater or lesser extent in both foams and directions (see Fig. 6) after longer exposures. The lack of

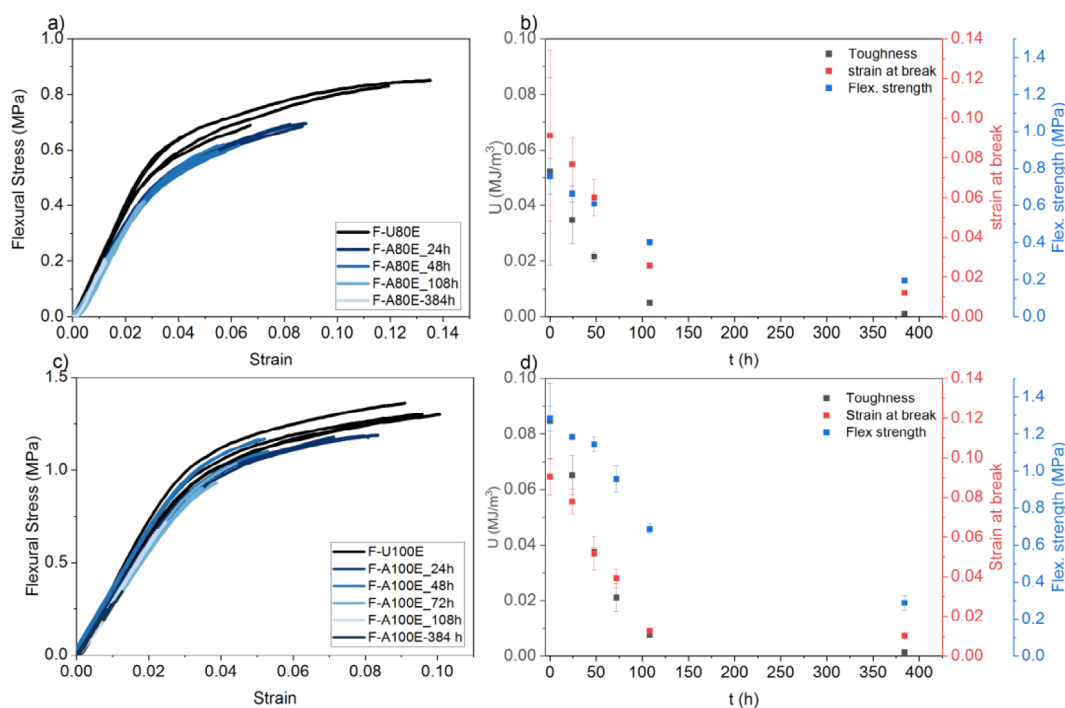


Fig. 3. Stress strain curves for foam 80 (a) and 100 (c). Flexural strength, strain at break and toughness in relation to ageing time for foams 80 (b) and 100 (d).

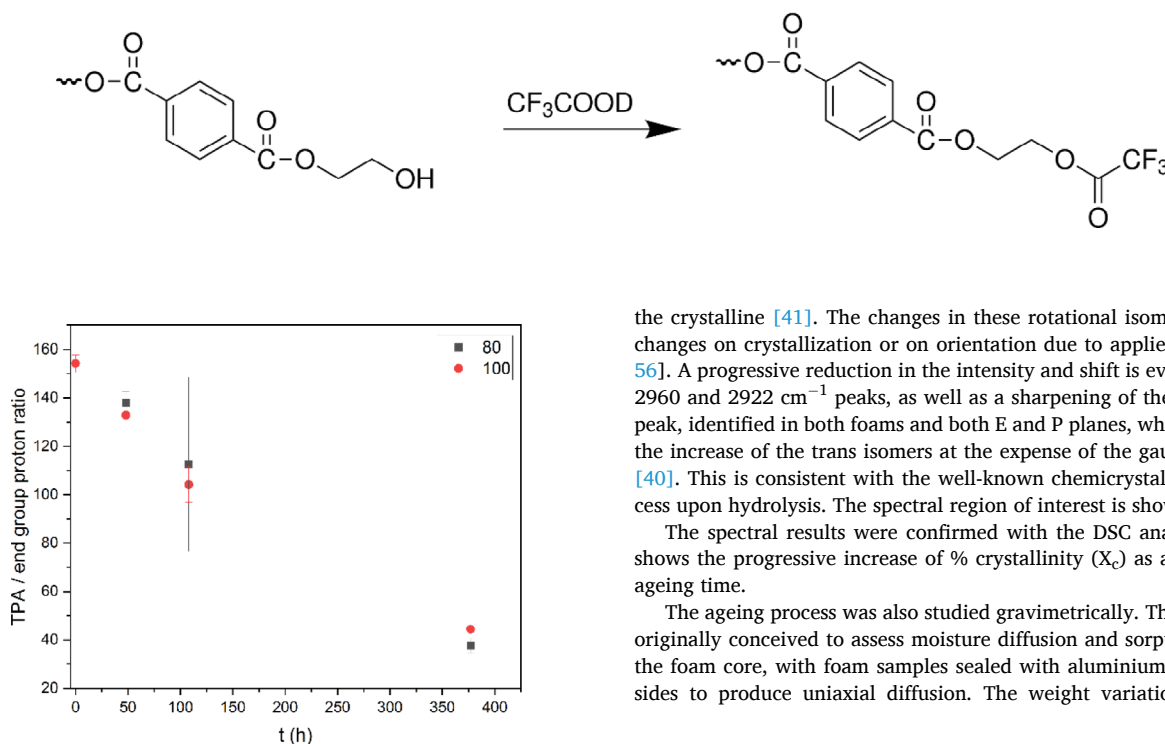


Fig. 4. TPA / hydroxyl proton ration vs ageing time.

significant increase at earlier stages of the degradation can be allocated to the sensitivity of the FTIR-ATR technique. Low resolution of the hydroxyl bands at 2800-3000 cm^{-1} prevented from detecting this end group, as previously encountered with ATR [22].

The evidence of chain scission and detection of increase of hydroxyl and carboxyl end groups through different techniques confirms the hydrolysis reaction of the PET.

3.4. Effects of ageing on the crystalline structure

A progressive increase in crystallinity could be derived from the FTIR spectra. As introduced, the conformation of the molecular chains involving both trans/gauche isomerism in the ethylene glycol unit has an impact on the IR spectrum of PET [40, 41]. While both the trans and gauche are present in the amorphous region, only the trans is present in

the crystalline [41]. The changes in these rotational isomers relate to changes on crystallization or on orientation due to applied stress [41, 56]. A progressive reduction in the intensity and shift is evident for the 2960 and 2922 cm^{-1} peaks, as well as a sharpening of the 2905 cm^{-1} peak, identified in both foams and both E and P planes, which indicates the increase of the trans isomers at the expense of the gauche isomers [40]. This is consistent with the well-known chemocrystallization process upon hydrolysis. The spectral region of interest is shown in Fig. 7.

The spectral results were confirmed with the DSC analysis. Fig. 8 shows the progressive increase of % crystallinity (X_c) as a function of ageing time.

The ageing process was also studied gravimetrically. This study was originally conceived to assess moisture diffusion and sorption through the foam core, with foam samples sealed with aluminium tape on the sides to produce uniaxial diffusion. The weight variation (%) with

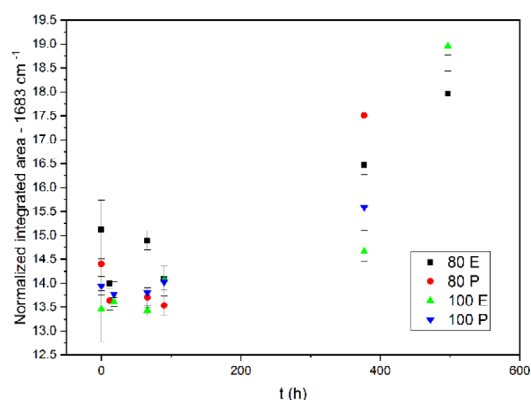


Fig. 6. Carboxylic acid content with ageing time for both foams measured in both directions, obtained from FTIR spectra.

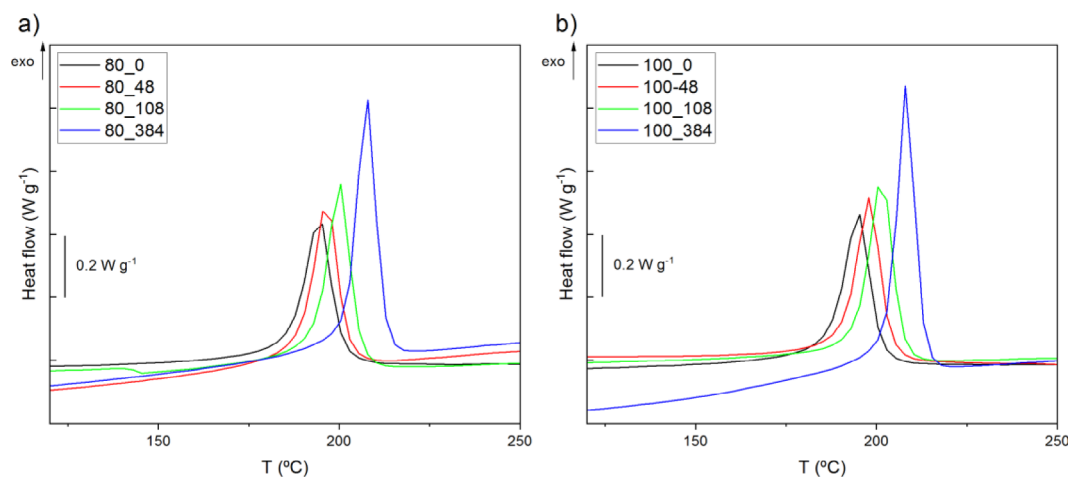


Fig. 5. Cooling DSC thermograms for PET 80 foam (a) and PET 100 foam (b) after different ageing times.

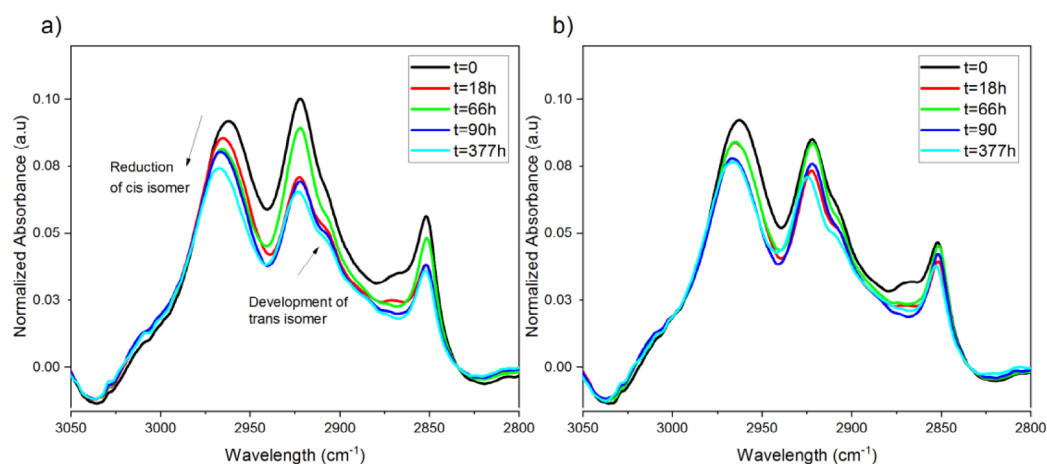


Fig. 7. FTIR spectra for PET foam 80, plane E (a) and PET foam 80, plane E (b) showing changes in the stretching mode of the aliphatic $-CH_2-$ groups in the ethylene glycol segment.

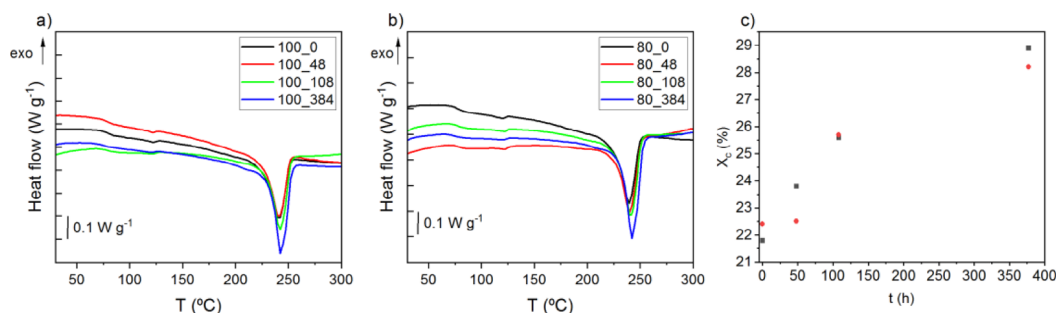


Fig. 8. Thermograms after different ageing times of (a) PET foam 100 kg/m^3 (b) PET foam 80 kg/m^3 (c) Crystallinity % as a function of ageing time. Each point corresponds to an individual measurement.

ageing time is presented in Fig. 9. An initial weight increase was observed in the first measured point after 18h, caused by moisture sorption, after which a progressive weight loss was registered until reaching a minimum point. It should be stressed that the samples were measured in the weight state. This was unexpected and therefore the study was repeated with unsealed samples. The same phenomenon was encountered, with a progressive reduction of the weight until a

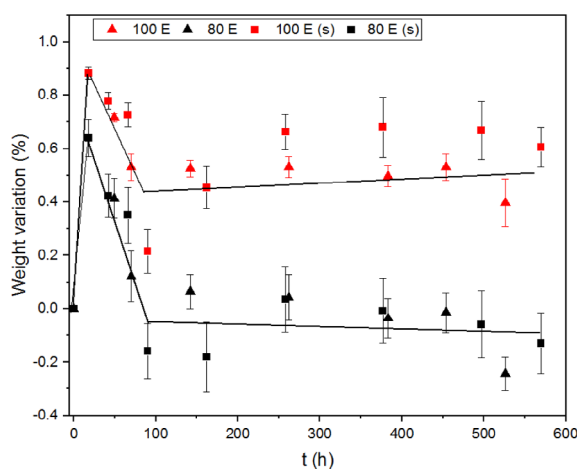


Fig. 9. Sample weight variation (%) vs ageing time for PET foams 80 and 100. Trial was repeated with sealed (s) and unsealed samples. Lines are guides for the eyes.

minimum is obtained, after which the weight remained more or less constant within experimental scatter. The slight weight increase after the minimum point observed in the first trial can be allocated to moisture sorption in the aluminium tape glue.

The coincidence of ageing time for the minimum weight point and the ductile-brittle transition obtained in the mechanical tests is striking. While weight loss has been reported in previous gravimetric studies of the hydrolysis of PET, these studies were conducted under water immersion, and the weight loss allocated to the solution of low weight molecules resulting from the chain scission to the bath water, such as isophthalic acid, terephthalic acid and/or ethylene glycol [3, 6]. However, since this study was conducted under wet air, such an extraction cannot occur.

This coincidence suggests the occurrence of a structural change intimately relating the hydrolysis reaction with the embrittlement mechanism.

This motivated a more detailed analysis of the crystallinity changes, evaluating the MAF and RAF fractions. While it is well accepted that PET follows a three-fraction model [34–36], to the best knowledge of the authors, crystallinity changes during the hydrolysis of PET have so far been analysed considering a two-fraction model only.

Fig. 10 shows the evolution of the crystalline, mobile amorphous and mobile rigid fractions with ageing time. DSC results of 80 and 100 kg/m^3 are averaged for each ageing time. It can be seen that the trend in the evolution of the X_{MAF} fits perfectly the weight decrease in the gravimetric curve, and the ductile-brittle transition point (and maximum weight loss) coincides with the attainment of the minimum X_{MAF} . Within the experimental scatter, the increase of X_c with ageing time could be considered linear, or following two different rates, with the kink point at

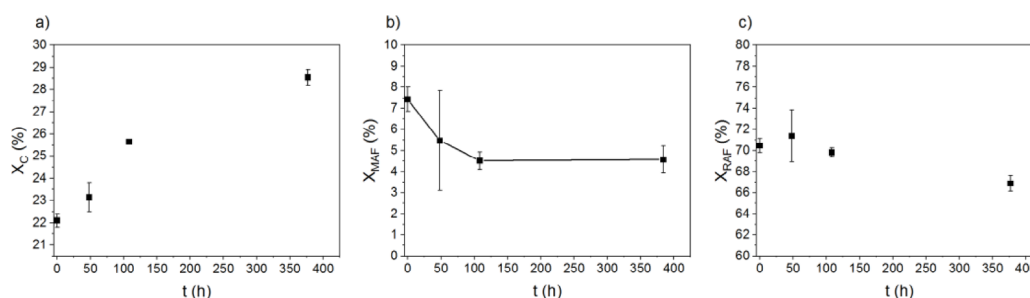


Fig. 10. Evolution of the crystalline, mobile amorphous and mobile rigid fractions with ageing time.

the same ageing time as the ductile-brittle transition point. It can be seen that the increase in the crystallinity fraction during the first 100h of ageing (ductile-brittle transition) occurs at the expense of the MAF fraction, while the increase in crystallinity from then on occurs at the expense of the RAF fraction. This suggests there is indeed a change in crystallinity increase rate.

4. Discussion

4.1. Impact of the cellular structure on the ageing process

The first question which this study aimed to answer is if and to which extent does the cellular structure impact the ageing process. When comparing both foams, made with the same polymer matrix but different cellular structure, no difference could be detected, nor in the chain scission rate, nor in the chemicrystallization rate, nor in time to embrittlement. The RAF fraction is the predominant phase, showing a high level of orientation of the PET chains, which can be allocated to the foam extrusion process. The mechanical properties are initially higher for the higher density foam, as expected [14] and degrade at a higher rate until reaching the ductile-brittle transition after the same ageing time. From this point on, the mechanical properties are residual and degrade at a very slower rate. The stress strain curves (Fig. 3) also show that the degradation occurred through the bulk of the foam. An additional FTIR-ATR study was conducted through the thickness of foam samples with sealed edges, where no differences between the layers were obtained. The obtained spectra can be found in the Supporting Information. Obtained results are consistent with previous reports of PET films, including the trend of the molecular weight decrease [7, 26], as well as the crystallinity increase [3, 26] and time-to-embrittlement [26]. Thus, it can be derived that the cellular structure does not have an effect on the degradation process and there is no diffusion control effect. The hydrolysis of PET foam can therefore be discussed in the frame of the hydrolysis of PET.

4.2. The nature of the ductile-brittle transition

The role of the two different amorphous phases on the hydrolysis of PET has not been previously discussed in the literature. From Fig 10 (b) it can be derived that the initial part of the degradation occurs at the expense of the MAF phase. Though the DSC analysis has been conducted on a small number of samples, the consistency of this trend with the gravimetry curve (Fig. 9) gives confidence on the results. The same gravimetric curve under similar temperature and moisture conditions has been reported in a moisture sorption study of PET [57]. The authors explain this weight decrease as water rejection caused by densification of the PET, suggesting a cold crystallization due to hydric plasticisation, although this suggestion could not be confirmed in their study. Though they report that this behaviour occurs for conditions close but below the T_g of PET, the reported conditions of 60°C/90% RH and 70°C and whatever RH are indeed above T_g due to its depression caused by moisture plasticization [58]. Their samples were thus hydrolysing

during the sorption experiment and confirm our finding. In our study, it can be seen that crystallinity directly correlates with molecular weight (Fig. 11), indicating that the chemicrystallization is a result of the chain scission and not of a plasticization effect of the moisture. A previous study on the plasticization effects of moisture in PET concluded that the apparent activation energy for crystal growth was weakly affected by humidity compared to the effect on the glass transition [58], supporting our interpretation.

From the gravimetric curves it can be derived that water molecules are initially sorbed in the polymer, and then lost as the hydrolysis reaction proceeds. Water sorption of PET has been linked to hydrogen bonding of the water to the polymer [20] as the end groups [58], and to ester groups by means of two H-O bonds [59]. If these bonds correspond to an induction phase of the hydrolysis reaction, or if sorbed water molecules are physically ejected as the chain segments rearrange into the crystalline phase post-scission is open for discussion. It is also seen that the hydrolysis reaction takes place particularly in the MAF fraction until the embrittlement point, and then continues in the RAF phase, at a slower rate. This could be explained through the higher accessibility of the chains in the MAF fraction. The ductile-brittle transition occurs when the MAF fraction reaches its minimum, is consumed. But the hydrolysis reaction continues. One interpretation could be that the ester links in the chains located in the RAF fraction are only accessible to moisture once microcracks are created due to the embrittlement, in line with early reports of degradation rate changing slope due to the structural changes in the polymer [2]. The reaction taking place in both phases simultaneously but at very different rates, so that the degradation in the RAF phase is negligible compared to that of the MAF phase as long as this later is ongoing, cannot be discarded at this point.

So far, the relationship between the morphological changes of PET with degradation rate and kinetics have been discussed. It is still to be determined if these changes are responsible for embrittlement. Different proposed embrittlement mechanisms for semicrystalline polymers are

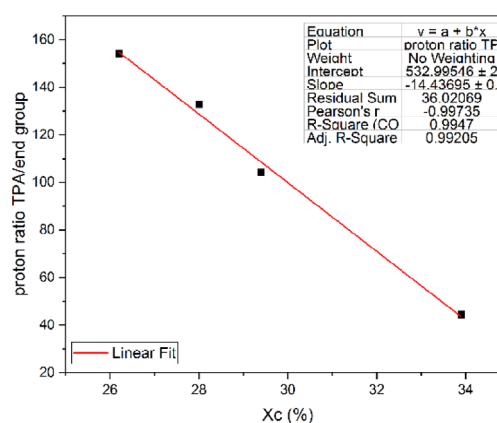


Fig. 11. Relative molecular weight vs crystallinity ratio.

reviewed in [27]. While this review focuses on polymers with the amorphous phase in the rubbery state at room temperature, such as PP, during the hydrolysis of PET above T_g , the amorphous phase is in the rubbery state, justifying the analogy. The authors hypothesize that the embrittlement could be related to the destruction of the tie-molecules, or to the chemicrystallization rather than the destruction of the entanglement network, and could be a consequence of the decrease of amorphous content to the point where deformations cannot longer be sustained or to the decrease of the interlamellar spacing. Let us look at our results. The ductile-brittle transition occurs at the point where the MAF fraction is consumed. This suggests that it is the MAF fraction which provides the cohesion of the material. Early work by Thompson and Woods [30] describe that the density of the amorphous phase decreases with crystallinity increase, until voids appear at the lowest amorphous densities. This progressive change of character of the amorphous region as crystallization progresses is the first report that the two-phase model fails to explain PET. Pioneering studies on the degradation of PET [2] point at these density changes as cause for embrittlement, suggesting that cohesive forces within the amorphous region may be great enough to inhibit void formation until the crystal growth builds up internal stress, whereupon voids and cracks suddenly appear. These interpretations are consistent with our observations, only that particularly the MAF fraction is concerned.

Previous researchers have linked tie-molecules to the RAF phase [34] and since the RAF phase is not degraded, it appears that the destruction of tie-molecules is not the immediate cause for embrittlement.

The changes of MAF and RAF content in recycled PET, arising from chain scission due to the successive reprocessing cycles have been reported [55]. The authors indicate that the degradation was induced by the separation of the MAF and rearrangement of shorter PET chains into RAF. The reduction of the MAF fraction would increase the free volume in the polymer, increasing its fragility. The increase in RAF could act as precursor of crystallinity during tensile drawing, enhancing the embrittlement of PET.

Therefore, a micromechanical interpretation of the ductile-brittle transition appears more suitable than a molecular one. This leads to the question: would it be pertinent to make lifetime predictions as a function of MAF content, rather than molecular weight? Our results suggest that the initial stages of hydrolysis and embrittlement occurs at the expense of the MAF phase, which per definition is the phase that becomes mobile above T_g . The chemicrystallization occurs when small chain fractions, with enough mobility above T_g , rearrange themselves. This brings up the question, can hydrolysis-induced embrittlement occur below T_g ? In a parallel work, no degradation of the mechanical properties of PET foam has been detected after one year moisture exposure below T_g [60].

5. Conclusions

The hydrological degradation of PET foams does not appear influenced by the cellular structure.

Considering a three-phase structure, the hydrolysis of PET and related chemicrystallization occurs at the expense of the MAF fraction until the ductile-brittle transition is reached. Embrittlement occurs when the MAF fraction is consumed. From this point on, the reaction continues at the expense of the RAF fraction. This brings new insights on the nature of the embrittlement mechanism, which appear better interpreted micromechanically than through a molecular interpretation.

CRedit authorship contribution statement

Lucía Doyle: Conceptualization, Data curation, Formal analysis, Investigation, Methodology, Software, Validation, Visualization, Writing – original draft, Writing – review & editing. **Ingo Weidlich:** Project administration, Resources, Supervision, Writing – review &

editing.

Declaration of Competing Interest

The authors declare that they have no known competing financial interests or personal relationships that could have appeared to influence the work reported in this paper.

Acknowledgements

Erik Borrs from HCU is kindly thanked for undertaking the FTIR measurements and discussions thereof. Thomas Hackl and team at UHH are kindly thanked for undertaking the NMR measurements.

This research did not receive any specific grant from funding agencies in the public, commercial, or not-for-profit sectors.

Supplementary materials

Supplementary material associated with this article can be found, in the online version, at doi:10.1016/j.polyimdegradstab.2022.110022.

References

- [1] Commission Regulation (EU) 2020/1149 of 3 August 2020 amending Annex XVII to Regulation (EC) No 1907/2006 of the European Parliament and of the Council concerning the Registration, Evaluation, Authorisation and Restriction of Chemicals (REACH) as regards diisocyanates: (EU) 2020/1149, Off. J. Eur. Union (2020).
- [2] W McMahon, HA Birdsall, GR Johnson, CT. Camilli, Degradation studies of polyethylene terephthalate, *J. Chem. Eng. Data* 4 (1) (1959) 57–79.
- [3] A Ballara, J. Verdu, Physical aspects of the hydrolysis of polyethylene terephthalate, *Polym. Degrad. Stab.* 26 (4) (1989) 361–374.
- [4] M Edge, NS Allen, JH He, M Derham, Y. Shinagawa, Physical aspects of the thermal and hydrolytic ageing of polyester, polysulphone and polycarbonate films, *Polym. Degrad. Stab.* 44 (2) (1994) 193–200.
- [5] A Launay, F Thominet, J. Verdu, Hydrolysis of poly(ethylene terephthalate): a kinetic study, *Polym. Degrad. Stab.* 46 (3) (1994) 319–324.
- [6] V Bellenger, M Ganem, B Mortaigne, J. Verdu, Lifetime prediction in the hydrolytic ageing of polyesters, *Polym. Degrad. Stab.* 49 (1) (1995) 91–97.
- [7] A Launay, F Thominet, J. Verdu, Hydrolysis of poly(ethylene terephthalate). A steric exclusion chromatography study, *Polym. Degrad. Stab.* 63 (3) (1999) 385–389.
- [8] JE Pickett, DJ. Coyle, Hydrolysis kinetics of condensation polymers under humidity aging conditions, *Polym. Degrad. Stab.* 98 (7) (2013) 1311–1320.
- [9] E Pirzadeh, A Zadhoush, M. Haghghat, Hydrolytic and thermal degradation of PET fibers and PET granule: the effects of crystallization, temperature, and humidity, *J. Appl. Polym. Sci.* 106 (3) (2007) 1544–1549.
- [10] J de Champchesnel, DI Bower, IM Ward, JF Tassin, G. Lorentz, Development of molecular orientation in sequentially drawn PET films, *Polymer* 34 (18) (1993) 3763–3770.
- [11] RM Gohil, DR. Salem, Orientation distribution in the noncrystalline regions of biaxially drawn poly(ethylene terephthalate) film: a chain-intrinsic fluorescence study, *J. Appl. Polym. Sci.* 47 (11) (1993) 1989–1998.
- [12] PM. Henrichs, Molecular orientation and structure in solid polymers with carbon-13 NMR: a study of biaxial films of poly(ethylene terephthalate), *Macromolecules* 20 (9) (1987) 2099–2112.
- [13] MT. Demeuse, *Biaxial Stretching of Film: Principles and Applications*, Woodhead Publishing, Oxford, Philadelphia, 2011.
- [14] LJ Gibson, MF. Ashby, *Cellular Solids*, Cambridge University Press, Cambridge, 1997.
- [15] Z Huo, M Mohamed, JR Nicholas, X Wang, K. Chandrashekhara, Experimentation and simulation of moisture diffusion in foam-cored polyurethane sandwich structure, *J. Sandwich Struct. Mater.* 18 (1) (2016) 30–49.
- [16] F Avilés, M. Aguilar-Montero, Mechanical degradation of foam-cored sandwich materials exposed to high moisture, *Compos. Struct.* 92 (1) (2010) 122–129.
- [17] JS Earl, RA. Shenoi, Determination of the moisture uptake mechanism in closed cell polymeric structural foam during hygrothermal exposure, *J. Compos. Mater.* 38 (15) (2004) 1345–1365.
- [18] Y.L. Holliday, G THACKRAY, Heterogeneity in complex materials and the concept of the representative cell, *Nature* 201 (4916) (1964) 270–272.
- [19] F Dubelley, E Planes, C Bas, E Pons, B Yrieix, L. Flandin, Predictive durability of polyethylene terephthalate toward hydrolysis over large temperature and relative humidity ranges, *Polymer* 142 (2018) 285–292.
- [20] C Sammon, C Mura, J Yarwood, N Everall, R Swart, D. Hodge, FTIR–ATR studies of the structure and dynamics of water molecules in polymeric matrices. A comparison of PET and PVC, *J. Phys. Chem. B* 102 (18) (1998) 3402–3411.
- [21] IEC 61215:2005, Crystalline Silicon Terrestrial Photovoltaic (PV) Modules – Design Qualification and Type Approval (IEC 61215:2005), International Electrotechnical Commission, Geneva, Switzerland, 2005.

- [22] Abdulkarim Gok, Degradation Pathway Models of Poly(ethylene-Terephthalate) under accelerated weathering exposures; 2016.
- [23] M Mohammadian, NS Allen, M Edge, K. Jones, Environmental Degradation of Poly(ethylene Terephthalate), *Text. Res. J.* 61 (11) (1991) 690–696.
- [24] S Weidner, G Kuehn, B Werthmann, H Schroeder, U Just, R Borowski, et al., A new approach of characterizing the hydrolytic degradation of poly(ethylene terephthalate) by MALDI-MS, *J. Polym. Sci. A* 35 (11) (1997) 2183–2192.
- [25] V Elias, A Salman, D. Goulias, The effect of pH, resin properties, and manufacturing process on laboratory degradation of polyester geosynthetics, *Geosynth. Int.* 5 (5) (1998) 459–490.
- [26] M Arhant, M Le Gall, P-Y Le Gac, P Davies, Impact of hydrolytic degradation on mechanical properties of PET - Towards an understanding of microplastics formation, *Polym. Degrad. Stab.* 161 (2019) 175–182.
- [27] B Fayolle, E Richaud, X Colin, J. Verdu, Review: degradation-induced embrittlement in semi-crystalline polymers having their amorphous phase in rubbery state, *J. Mater. Sci.* 43 (22) (2008) 6999–7012.
- [28] C Sammon, J Yarwood, N. Everall, An FT-IR study of the effect of hydrolytic degradation on the structure of thin PET films, *Polym. Degrad. Stab.* 67 (1) (2000) 149–158.
- [29] A Pegoretti, A. Penati, Effects of hygrothermal aging on the molar mass and thermal properties of recycled poly(ethylene terephthalate) and its short glass fibre composites, *Polym. Degrad. Stab.* 86 (2) (2004) 233–243.
- [30] AB THOMPSON, DW WOODS, Density of amorphous polyethylene terephthalate, *Nature* 176 (4471) (1955) 78–79.
- [31] HM Heuvel, R. Huisman, Effect of winding speed on the physical structure of as-spun poly(ethylene terephthalate) fibers, including orientation-induced crystallization, *J. Appl. Polym. Sci.* 22 (8) (1978) 2229–2243.
- [32] AD. English, Macromolecular dynamics in solid poly(ethylene terephthalate): proton and carbon-13 solid-state NMR, *Macromolecules* 17 (10) (1984) 2182–2192.
- [33] CM Roland, JH Walton, JB. Miller, Proton NMR determination of crystallinity in poly(ethylene terephthalate), *Magn. Reson. Chem.* 32 (S1) (1994) S36–S39.
- [34] Y Fu, B Annis, A Boller, Y Jin, B Wunderlich, Analysis of structure and properties of poly(ethylene terephthalate) fibers, *J. Polym. Sci. B* 32 (13) (1994) 2289–2306.
- [35] Y Fu, WR Busing, Y Jin, KA Affholter, B Wunderlich, Structure analysis of the noncrystalline material in poly(ethylene terephthalate) fibers, *Macromol. Chem. Phys.* 195 (2) (1994) 803–822.
- [36] B. Wunderlich, Reversible crystallization and the rigid–amorphous phase in semicrystalline macromolecules, *Prog. Polym. Sci.* 28 (3) (2003) 383–450.
- [37] J Schindelin, I Arganda-Carreras, E Frise, V Kaynig, M Longair, T Pietzsch, et al., Fiji: an open-source platform for biological-image analysis, *Nat. Methods* 9 (7) (2012) 676–682.
- [38] WH Peters, WF. Ranson, Digital Imaging techniques in experimental stress analysis, *Opt. Eng.* 21 (3) (1982).
- [39] DJ. Walls, Application of ATR-IR to the analysis of surface structure and orientation in uniaxially drawn poly(ethyleneterephthalate), *Appl. Spectrosc.* 45 (7) (1991) 1193–1198.
- [40] Z Chen, JN Hay, MJ. Jenkins, FTIR spectroscopic analysis of poly(ethylene terephthalate) on crystallization, *Eur. Polym. J.* 48 (9) (2012) 1586–1610.
- [41] IM Ward, MA. Wilding, Infra-red and Raman spectra of poly(m-methylene terephthalate) polymers, *Polymer* 18 (4) (1977) 327–335.
- [42] I Donelli, G Freddi, VA Nierstrasz, P. Taddei, Surface structure and properties of poly-(ethylene terephthalate) hydrolyzed by alkali and cutinase, *Polym. Degrad. Stab.* 95 (9) (2010) 1542–1550.
- [43] JL Koenig, MJ. Hannon, Infrared studies of chain folding in polymers. II. Polyethylene terephthalate, *J. Macromol. Sci. Part B* 1 (1) (1967) 119–145.
- [44] WH Cobbs, RL. Burton, Crystallization of polyethylene terephthalate, *J. Polym. Sci.* 10 (3) (1953) 275–290.
- [45] R Tang, JJ Liggat, WH. Siew, Partial discharge behaviour of biaxially orientated PET films: the effect of crystalline morphology, *Polym. Degrad. Stab.* 155 (2018) 122–129.
- [46] S Al-AbdulRazzak, EA Lofgren, SA Jabarin, End-group determination in poly(ethylene terephthalate) by infrared spectroscopy, *Polym. Int.* 51 (2) (2002) 174–182.
- [47] A Mehta, U Gaur, B. Wunderlich, Equilibrium melting parameters of poly(ethylene terephthalate), *J. Polym. Sci. Polym. Phys. Ed.* 16 (2) (1978) 289–296.
- [48] B. Wunderlich, The ATHAS database on heat capacities of polymers, *Pure Appl. Chem.* 67 (6) (1995) 1019–1026.
- [49] W Romão, MF Franco, YE Corilo, MN Eberlin, MA Spinacé, M-A de Paoli, Poly(ethylene terephthalate) thermo-mechanical and thermo-oxidative degradation mechanisms, *Polym. Degrad. Stab.* 94 (10) (2009) 1849–1859.
- [50] B Fox, G Moad, G van Diepen, I Willing, WD. Cook, Characterization of poly(ethylene terephthalate) and poly(ethylene terephthalate) blends, *Polymer* 38 (12) (1997) 3035–3043.
- [51] AM Kenwright, SK Peace, RW Richards, A Bunn, WA. MacDonald, End group modification in poly(ethylene terephthalate), *Polymer* 40 (8) (1999) 2035–2040.
- [52] K Ravindranath, RA. Mashelkar, Polyethylene terephthalate—I. Chemistry, thermodynamics and transport properties, *Chem. Eng. Sci.* 41 (9) (1986) 2197–2214.
- [53] B Du, R Yang, X. Xie, Investigation of hydrolysis in poly(ethylene terephthalate) by FTIR-ATR, *Chin. J. Polym. Sci.* 32 (2) (2014) 230–235.
- [54] R Hariharan, AG. Pinkus, Useful NMR solvent mixture for polyesters: Trifluoroacetic acid-d/chloroform-d, *Polym. Bull.* 30 (1) (1993) 91–95.
- [55] JD Badia, E Strömberg, S Karlsson, A. Ribes-Greus, The role of crystalline, mobile amorphous and rigid amorphous fractions in the performance of recycled poly(ethylene terephthalate) (PET), *Polym. Degrad. Stab.* 97 (1) (2012) 98–107.
- [56] I Hutchinson, I Ward, H Willis, V. Zichy, Infra-red measurements on one-way drawn poly(ethylene terephthalate) films subjected to constant strain, *Polymer* 21 (1) (1980) 55–65.
- [57] F Dubelley, E Planes, C Bas, E Pons, B Yrieix, L. Flandin, Water vapor sorption properties of polyethylene terephthalate over a wide range of humidity and temperature, *J. Phys. Chem. B* 121 (8) (2017) 1953–1962.
- [58] D Langevin, J Grenet, JM. Saiter, Moisture sorption in pet influence on the thermokinetic parameters, *Eur. Polym. J.* 30 (3) (1994) 339–345.
- [59] SO Paul, TA. Ford, Infrared spectroscopic properties of water molecules dissolved in some oxygen bases, *J. Mol. Struct.* 80 (1982) 269–278.
- [60] D Lucia, I Weidlich, Moisture uptake and effects of hygrothermal exposure on closed-cell semicrystalline polyethylene terephthalate foam, *Polym. Degrad. Stab.* 202 (2022) 110009, <https://doi.org/10.1016/j.polydegradstab.2022.110009>.

Annex IV. Publication [J2]

Polymer Degradation and Stability 202 (2022) 110009



Contents lists available at ScienceDirect

Polymer Degradation and Stability

journal homepage: www.journals.elsevier.com/polymer-degradation-and-stability

Moisture uptake and effects of hygrothermal exposure on closed-cell semicrystalline polyethylene terephthalate foam

Lucía Doyle^{*}, Ingo Weidlich

HafenCity University Hamburg, Germany

ARTICLE INFO

Keywords:

PET
Insulation
Diffusion
Cellular plastic
Foam
Sandwich structure

ABSTRACT

Polyethylene terephthalate (PET) foam is receiving increasing interest in recent years for its use in structural applications. This is favoured by its balance between mechanical properties and cost, as well as recyclability and wide availability of recycled material. Knowledge on its ageing behaviour upon hygrothermal exposure is needed to ensure the fulfilment of the required service life and foster market uptake. A six-month ageing programme under 40°C and 80% RH and a one-year water immersion ageing programme were undertaken, in order to understand the moisture uptake mechanism, and observe *in-situ* as well as irreversible degradation caused by moisture. These conditions were selected in order to ensure being below the T_g of PET, and so in the same structural state as in the use phase. No degradation of the PET foam was found after the completion of both trials. It was demonstrated that the hygrothermal degradation of the polymeric foams is not diffusion-controlled. Moisture uptake by the PET matrix was analogous to that previously reported in films. Liquid water passage into the cell cavities was progressive and much slower, but did not produce any significant additional effect on the mechanical behaviour of the PET foam.

Introduction

Polyethylene terephthalate (PET) foam is receiving increasing interest in recent years for its use in structural applications [1], including in wind industry, automotive, marine [2] and district heating piping networks [3]. While the low melt strength of PET has for long represented a hurdle for its foaming [4–6], improvements in the manufacturing process [2] by the use of the breaker plate [7] has enabled its commercial manufacturing, which has taken off in the last decade. While the balance between its mechanical properties and cost [1] encourages this interest, a further advantage is its recyclability. The widespread use of PET in many applications opens up new opportunities for the cascading use of this polymer, in line with the requirements of the Circular Economy. Construction and demolition waste (CDW) represent one third of the total waste generated in the European Union and the largest waste stream by volume [8]. As such, CDW is named as one of the key waste streams to be addressed by the First Circular Economy Action Plan of the EU [9]. Updates in the Plan include the revision of material recovery targets for CDW and considers the introduction of recycled content requirements for certain construction products [10]. The replacement of commonly used thermoset polymeric foams such as polyurethane (PU) by PET and recycled PET foam would therefore

contribute to the achievement of all the mentioned regulatory targets. The toxicity of the di-isocyanates [11,12] required for PU's manufacturing and recently approved restriction thereof [13] further highlights the need to shift to more sustainable polymeric foams.

This research is framed in the search for substitutes for PU foam in district heating (DH) pre-insulated pipes. Currently, these pipes are sandwich structures comprising a service pipe, and PU foam layer, and a protective casing of HDPE [14]. In this application, the foam undertakes a double function as thermal insulation and as load bearing element. Since the pipelines are directly buried underground, the foam supports the compression stresses of the surrounding soil and the shear stresses arising from the thermal expansion of the network. The suitability of PET foam for DH pipes has been previously assessed in terms of mechanical properties [3] and long term insulation capacity [15] and been found favourable. However, knowledge of its ageing behaviour is still lacking, and hinders its market uptake.

Reports of frequent damage in DH pipelines due to moisture can be found in the literature [16], since the groundwater level may reach the buried DH pipelines. Though the primary function of the HDPE casing is to prevent the ingress of moisture [3], it has been recently reported that moisture can penetrate it [17]. An aluminium layer between the casing and the foam has been introduced to act as diffusion barrier, and found

^{*} Corresponding author.

<https://doi.org/10.1016/j.polydegradstab.2022.110009>

Received 7 April 2022; Received in revised form 21 May 2022; Accepted 31 May 2022

Available online 1 June 2022

0141-3910/© 2022 Elsevier Ltd. All rights reserved.

efficient [18]. However, moisture can still penetrate through the pipe ends and joints [16,18].

Moisture diffusion in polymers is commonly reported as Fickian [19–23] although deviations are frequently reported due to relaxation [24], swelling [25,26], or clustering [20,25]. Timescale is a further parameter causing deviations with increasing exposure periods [25,27]. This highlights the importance of long-term experimental validation for polymeric materials for load-bearing applications.

Additionally, closed cell foams, as heterogeneous materials [28] add complexity to its correct understanding and modelling [29]. While there is consensus on the complexity of the phenomenon, different approaches have been followed for its study, leading to somewhat contradictory conclusions. When modelling transport of a solute through a cellular material, two approaches can be followed [30,31]. Some authors pursue a macroscopic point of view, where the foam is considered a homogeneous material layer [30,32]. The transport involves solution at the surface of the material, migration through the concentration gradient and desorption at the other surface of the material. Here an effective diffusion coefficient is derived. Another approach is through discrete diffusion models, treating the foam as a connection of multiple layers of cells, where a mass balance for each cell in the foam is solved [31,33,34]. From the macroscopic point of view, a foam board could be seen as a thick section, where the time required by the moisture in this case to diffuse in sufficient concentrations to the core of the foam might be the rate-determining step in the ageing process. Correct modelling of absorption and diffusion of moisture and representative experimental exposure procedures are needed for reliable lifetime predictions [35]. Indeed, a number of experimental studies on polymeric foam ageing upon moisture exposure conclude that diffusion is the rate-determining step. Earl & Shenoj [20] monitored the moisture uptake in closed cell PVC foams at 40°C and 95% relative humidity (RH) and water immersion at 40°C for over 2,5 years. The authors observed a multistage absorption process and attributed it to the progressive diffusion into each layer of cells, concluding moisture reached only the third layer of cells based on the three plateaus observed, meaning an ingress depth of only 1,2 mm. In order to confirm this attribution, the foam was cut through and an imprint blotted in a paper towel to observe the dry bulk. Avilés et al. [37] performed ageing under 95% RH and sea water immersion of PVC foam during 7 months. The authors allocated the minor reduction in tensile strength over ageing time to lack of moisture penetration into the foam core. In order to confirm this assumption, the authors undertook micrographic observations of the surface cells with ageing time as well as cross sectional cuts of the foam after the ageing period. Swelling of the surface cells was observed, but no significant sign of expansion was detected beyond 2,3 mm from the surface. No information on the number of measured cells or method for cutting the foam is provided. Huo et al. [27] undertook a 7 months water immersion ageing with PU foam at room temperature. The authors observed a multistage diffusion process as well, and interpreted each plateau as the attainment of moisture saturation by a new layer of cells, meaning 2 layers of cells after over 200 days of ageing. The authors used thermographs to assess the moisture penetration depth after immersing foam samples in hot water. Liu et al. [38] studied the moisture uptake of PET foam of 150 kg/m³ density in simulated sea water at 40°C. They observed a sharp weight increase at the first measurement point, conducted after 1.7h, and allocated it to water ingress into the surface open cells. The weight increased from then on steadily for the 30 days trial duration. Since the weight did not stabilize, the authors concluded moisture saturation was not reached during the trial.

These interpretations of moisture penetrating only on the surface of polymeric foams after long term exposures differ from the understanding that sorption and diffusion processes depend upon the availability of unoccupied volume in the polymer [39] and the increase of free volume increases diffusivity. In this line, Lee [40] proposed a model considering a “foam diffusivity”, function of the foam density and the diffusivity of the moisture in the polymer matrix. The foam diffusivity would be

higher than the polymer diffusivity and would increase with decreasing foam density, indicating greater mobility of the diffusant in a lower-density foam structure. In this model it is assumed that the diffusing water path occurs within the polymeric skeleton of the foam and any condensation or water entrapment inside the cells is disregarded for simplicity.

Towards lifetime predictions, it is critical to discern between diffusion-controlled degradation, moisture not causing degradation, or temperature-controlled degradation. It is therefore worthwhile to evaluate the reasons for this discrepancy.

Aside from the need to determine the moisture uptake rate and mechanism, the type of degradation that moisture can induce needs to be assessed. Moisture can degrade the mechanical properties of polymers and hence polymeric foams due to plasticization and swelling [36]. Plasticization would a reversible alteration, removed with the drying of the polymer. Swelling can alter the mechanical properties as well. This could be reversible. In cellular solids, it is reported the original cell shape is not recovered after cell expansion, altering the mechanical properties [41]. The absorption of moisture and related osmotic pressure can also lead to the formation of microcracks [42,43]. An additional degradation risk is hydrolysis, which has been widely reported for PET, above its glass transition temperature (T_g) [44–50]. Since hydrolysis causes irreversible embrittlement, the attainment of the ductile-brittle transition point would correspond to the end of life.

Lastly, as an insulation material, moisture ingress and entrapment in the cells is a source of degradation of the insulating properties of the foam [40], since the foam's thermal conductivity is a function of the thermal conductivity of the polymer matrix and that of the cell's inner medium [15] and water has a higher thermal conductivity than typical blowing agents.

The objective of this study is to experimentally observe the moisture uptake and effects of hygrothermal exposure on close cell PET foam at temperatures below its T_g , which correspond to the structural state encountered during its service life, and determine if the degradation is diffusion-controlled or temperature controlled. Ageing conditions of 80% RH and 40°C were selected, in order to have accelerated ageing regarding the in-service groundwater temperature of ca. 10°C, but ensure below T_g conditions. These were applied for a total duration of 6 months. Additionally, samples were aged under water immersion at room temperature for a total duration of one year.

Materials and methods

Materials

Commercial closed cell PET foam boards (Gurit Kerdyne Green) of 80 and 100 kg/m³ density were used in the study. The manufacturing of these boards includes cutting blocks of the extruded plates and gluing them in the direction parallel to the extrusion direction. The aim of this process is to transfer the higher mechanical properties of the extrusion direction of the foam (E) into the sheet surface parallel to the extrusion direction (P). For our study samples were always extracted from segments free from glue.

Microstructural characterization

Microstructure was observed in an optical microscope (Leica DMLP, Wetzlar, Germany). The cell size and shape were measured from the micrographs by adjusting the cells to an ellipse using the open source software Fiji [51]. Both surfaces perpendicular to the extrusion foaming direction (E) and perpendicular to the parallel direction (P) were analyzed as to assess the anisotropy in the cell shape. At least 100 cells were measured for each case. Cell wall and strut thickness were additionally measured. Values presented are an average of at least 20 measurements.

Open cell content O_v was determined using a Micromeritics AccyPyc

1330 Gas pycnometer (Norcross, GA, U.S.A.) operated with He, following ASTM D6226 standard [52] as far as possible. Measured samples had dimensions of approx. 35×12×12 mm. Deviation between our sample dimensions and the dimensions stated by the standard is due to the available space in the pycnometer cubicle. The pycnometer measures each specimen's density ρ_{spec} . With the mass (m) of each sample, the specimen volume V_{spec} can be calculated as

$$V_{\text{spec}} = \frac{m}{\rho_{\text{spec}}} \quad (1)$$

The geometric volume V is determined from the measurement of length, width and height.

The open cell content, expressed as the percentage of the geometric volume, is derived as:

$$O_V = \left[\frac{(V - V_{\text{spec}})}{V} \right] \cdot 100(\%) \quad (2)$$

Since a fraction of the cells are opened during the sample preparation, this was corrected by calculating the volume of surface open cells. Given the cell anisotropy, the number of cells per specimen surface was calculated dividing the surface by the surface of an ellipse with the average dimensions measured from the micrographs. The cell volume V_c was then calculated as the volume of an ellipsoid, and the volume occupied by surface cells V_s as the product of the V_c and the number of cells per surface. The corrected $O_{V, \text{corr}}$ is then calculated as:

$$O_{V, \text{corr}} = \left[\frac{(V - V_{\text{spec}} - V_s)}{V} \right] \cdot 100(\%) \quad (3)$$

Three samples with the larger surface area corresponding to the E direction and three samples corresponding to the P direction per foam density were measured. Each individual sample was measured in 6 runs. The average per foam type is reported. Pressure was capped at 20 kPa as to not distort the specimens. The crystallinity of the two foams was determined by DSC as 22% [50].

Hygrothermal ageing

Foam samples were aged in an environmental chamber (Mettler ICH-C, Schwabach, Germany) at 40°C and 80% relative humidity. Two ageing batches were conducted, with a duration of 3 and 6 months, after which samples were characterized using the techniques described in the following sections.

Ageing under water immersion

Samples were aged under water immersion at room temperature for a duration of one year. After this period samples were mechanically characterized in 3-point bending in wet state and in dry state.

Gravimetry

The process was gravimetrically studied in order to assess the long-term diffusion of moisture into the foam core and changes in the materials density. Samples of 48×48×25 mm were placed in a Weiss WK1 340 (Reiskirchen, Germany) environmental chamber at 40°C and 80% RH and regularly extracted and weighed in the wet state with a Sartorius MC1 LC3200 D balance (Göttingen, Germany), after which they were reintroduced in the chamber. The samples remained out of the chamber for ca. 10 min per weight measurement, which is considered low enough to not alter the ageing process or cause desorption. Specimens were always removed and weighed in the same order, to minimize variations in the results. No moisture accumulated in the surface of the foam, assessed by wiping the surface of the samples with paper tissue. In order to observe influence from the microstructural anisotropy in the two principal axes on the diffusion, samples were cut with the larger

surface perpendicular to the E and to the P direction. Three samples per foam density and orientation (E and P) were evaluated. Weight variation was monitored for a total duration of over 2600h.

The moisture uptake at each time point was calculated as:

$$M(t) = \frac{W(t) - W_d}{W_d} \quad (4)$$

where $W(t)$ is the wet sample's mass at time t , and W_d is the dry sample's initial mass.

Three-point flexural tests

Three-point flexural tests were undertaken on samples with dimensions 25×25×200 mm. Test were executed with a universal testing machine under a displacement-controlled rate of 1.5 mm/min. The force was measured with a 2 kN load cell, accuracy class 0.5 (HBM, Darmstadt, Germany). The strain was measured by 3D digital image correlation (DIC) [53] using an ARAMIS 6M adjustable stereo camera system (GOM mbh, Braunschweig, Germany). The images were acquired at frequency of 5 Hz.

Dynamic mechanical thermal analysis (DMTA)

The dynamic mechanical properties of samples were determined using a TA DMA Q800 analyser (TA Instruments Inc., New Castle, PA, USA) in 3-point bending at a frequency of 1 Hz and a strain amplitude of 0.05%. Measurements of the storage modulus (E'), the loss modulus (E'') and the dissipation factor ($\tan \delta$) were carried out in the temperature range of 0°C to 190°C at a heating rate of 2°C/min. Samples with dimensions 10×60×5 mm were measured unaged, after 3-months ageing and after 6-month ageing for each foam density. To assess possible differences in moisture diffusion, sorption and ageing caused by the microstructure, samples with larger surface corresponding to the plane perpendicular to the extrusion (E) direction and parallel to the E direction (P) were tested. Measurements were conducted in triplicate. Samples were dried prior testing as to assess permanent degradation.

FTIR-ATR

Fourier transform infrared spectroscopy (FTIR) in attenuated total reflection (ATR) mode was used to observe potential changes in the chemical structure. A Thermo Scientific Nicolet is 10 FTIR spectrometer with a diamond ATR Smart Orbit accessory (Dreieich, Germany) was used. Spectra from 32 co-added scans and 4 cm^{-1} spectral resolution were baseline corrected, and normalized to the intensity of the 1410 cm^{-1} band, which is reported insensitive to orientation and conformation [54]. Each spectrum reported is the average of 5 spectra measured in different locations of each sample. Maximum contact of the ATR crystal was applied to ensure reproducible results. Samples were measured in the surface parallel to the extrusion direction. In order to assess difference between the surface and the bulk of the foam, foam specimens were stamped into 20 mm diameter steel tubes, closed on one end with a steel plate sealed with butyl rubber, in order to produce uniaxial flow of the moisture through the foam. The thickness of the resulting specimens was 45 mm. After the ageing process, slices of the foam from the outer surface, the middle and the bottom were extracted and analysed through FTIR-ATR.

Results

Microstructural characterization

The results from the microstructural characterization are summarized in Table 1, where D_1 is the largest diameter of the ellipse, D_2 the shortest, and R the cell anisotropy ratio, defined as:

Table 1
Microstructural characterization

	Cell area (μm^2)	D1 (μm)	D2 (μm)	R	Strut width (μm)	Wall thickness (μm)
80E	0.07 $\pm 0.03^*$	307.8 $\pm 63.7^*$	269.6 $\pm 55.2^*$	1.35	18.5 $\pm 4.6^*$	$5.2 \pm 1.8^*$
80P	0.07 $\pm 0.03^*$	363.2 $\pm 86.8^*$	250.5 $\pm 53.2^*$			
100E	0.11 $\pm 0.06^*$	393.7 $\pm 102.1^*$	341.2 $\pm 93.2^*$	1.47	37.2 $\pm 8.7^*$	$9.1 \pm 2.1^*$
100P	0.13 $\pm 0.06^*$	501.9 $\pm 139.1^*$	322 $\pm 89.9^*$			

* Standard deviation.

$$R = \frac{D1_P}{D2_E} \quad (5)$$

This characterization has been previously reported [50] but included here for completeness.

As we can see, the 100 foam presents larger cells and larger cell size anisotropy, and thicker cell walls and struts than the 80 foam. The obtained R fall approximately into the typical values for polymeric foams of around 1.3 [55].

Table 2 presents the calculation of the open cell content. The average lies in the range of the reported typical value for closed cell foams of 20% [55].

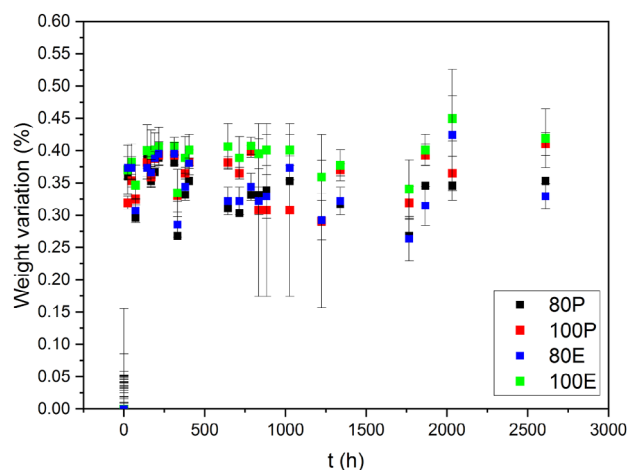
Moisture uptake

In order to assess the moisture uptake by the PET foams, the weight variation upon hydrothermal exposure was monitored for over 2600 h, and is presented in Fig. 1. The major moisture uptake step occurred during the first measurement interval, which was 24h. After this the samples weight remained stable within experimental scatter. No relaxations or multistage phenomena were observed.

It is known that the applied stresses during the processing of PET fibres and films, analogous to the preferential stretching occurring in the foam extrusion process, induces orientation of the rotational isomers [56–58].

Table 2
Calculation of open cell content

	m	Density	V_{spec}	V	V_c	O_v	$O_{v, \text{corr}}$	$O_{v, \text{corr}}^-$
	g	g/cm^3	cm^3	cm^3	cm^3	%	%	%
80 E-1	0.434	0.133	3.250	4.909	0.368	33.8	26.3	23.8 ± 2.1
80 E-2	0.412	0.114	3.606	5.192	0.386	30.5	23.1	
80 E-3	0.414	0.114	3.629	5.280	0.391	31.3	23.9	
80 P-1	0.411	0.116	3.548	5.335	0.394	33.5	26.1	
80 P-2	0.427	0.106	4.039	5.602	0.408	27.9	20.6	
80 P-3	0.387	0.102	3.795	5.429	0.387	30.1	23.0	
100 E-1	0.492	0.132	3.724	5.273	0.500	29.4	19.9	19.9 ± 1.2
100 E-2	0.473	0.134	3.517	5.089	0.487	30.9	21.3	
100 E-3	0.473	0.135	3.494	5.037	0.481	30.6	21.1	
100 P-1	0.539	0.131	4.126	5.702	0.528	27.6	18.4	
100 P-2	0.552	0.135	4.077	5.778	0.532	29.4	20.2	
100 P-3	0.556	0.133	4.176	5.415	0.222	22.9	18.8	

**Fig. 1.** Gravimetric curve of samples upon hydrothermal exposure at 40°C and 80% RH.

Preferential orientation can create a tortuous path for the diffusion species [39], leading to anisotropic diffusivity. The main-surface to edge-surface ratio of the samples was roughly 10. Comparing the E to P pairs for each foam, no concluding evidence of preferential diffusion could be found.

As can be seen, the moisture uptake is very low, in the range 0.3–0.4% weight. It should be highlighted that in this trial the moisture exposure was in vapor phase, limiting the possibilities of water accumulation in the cell cavities.

The trial was repeated with samples of three different geometries with a duration of one week, in order to discard any influence from the sample geometry on the saturation time. The sample dimensions are presented in Table 3 and the obtained gravimetric curve on Fig. 2.

It can be seen that for the three geometries, the weight uptake does not increase after 24h. It is surprising to see that the samples with the lower thickness present the lower weight increase. One possible explanation is that the cutting of the foam increases the crystallinity or orientation of the PET molecules through the produced stresses, and given the lower mass to surface ratio, this impacts the total crystallinity of the sample and so the maximum water sorption. Nevertheless, the fact that thinner samples do not absorb more moisture than the thicker samples supports the conclusion that saturation is reached within 24h.

The saturation time is in line with that reported for PET films [59, 60], but differ from the multi-stage moisture absorption process and very long saturation times reported for polymeric foams by previous authors, as described in the introduction.

An additional gravimetric study was undertaken under moisture immersion at room temperature, with a duration of nearly 1400h. The surface of the samples was blotted with paper tissue as to account only for the moisture sorbed in the foam core, and not that accumulating in the superficial open cells. The results are presented in Fig. 3. In this graph, a multistage weight uptake process can be observed indeed, with a in initial weight increase jump in the first measurement step, conducted after 18h of immersion, after which the weight remained constant until $t = 90\text{h}$. Then, a second weight increase stage is initiated, which continues until the 700h immersion are reached, when it stabilizes again. The weight increase is much higher than in the trial

Table 3
Dimensions of the three sample geometries

	mm	mm	mm
a	45.3 ± 3.4	47.9 ± 3	25.5 ± 1.2
b	50.5 ± 0.7	51.8 ± 1.3	6.2 ± 0.04
c	25.4 ± 0.1	25.2 ± 0.2	25.1 ± 0.3

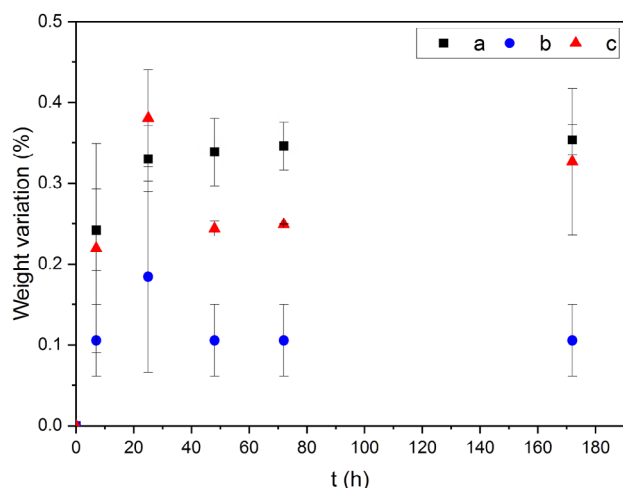


Fig. 2. Gravimetric curve of samples of different dimensions upon hygrothermal exposure, 40°C, 80% RH.

conducted with vapour.

The additional weight increase can only be explained by the filling of the cell cavities with liquid water, which occurs at a much slower rate than the moisture diffusion and saturation in the polymer matrix, and in a multistage manner. Liquid water droplets could be observed inside the cells through microscopy, as presented in Fig. 4.

The higher weight increase in the E direction could be related to the effect of the foam strands coalescence in this direction, producing larger cells and possible channels at the borders, as illustrated by Fig. 5.

To confirm if moisture saturation of the PET matrix through the bulk of the foam was reached during the first exposure day of hygrothermal exposure, three-point bending tests under the same environmental conditions (40°C and 80% RH) were undertaken after an overnight soak, as to test the samples under the same moisture saturation state of the first point of the gravimetric curve (Fig. 1). Bending tests conducted at 40°C and 0% RH were undertaken for comparison, in order to derive the effect of moisture. If the PET foam core moisture saturation is reached, its plasticization effect [61] should be evidenced by a reduction of the strength and an increase in the elongation at break. The obtained flexural stress-strain curves are shown in Fig. 6 below:

A significant plasticization effect can be readily observed. The samples tested at 40°C and 80% RH were much more ductile, to the point that they did not break within the applied stress range. Moisture also caused a reduction of the strength. Such an effect would not be

encountered if moisture had only diffused through the first layer of cells, confirming that moisture saturation had been reached through the bulk of the foam during the first hours of exposure.

Permanent effects of hygrothermal ageing on mechanical properties

Three-point bending tests were undertaken in order to assess potential changes in the mechanical properties of the PET foam after hygrothermal ageing. Samples were dried in a desiccator with silica gel after the ageing period and prior testing, in order to assess irreversible damage. The hydrolysis of PET causes chain scission of the ester link, leading to embrittlement, which would be readily identifiable from the flexural stress-strain curves. Permanent deformation of the cell shape due to swelling or cracking events would alter the mechanical behavior. Foam 80 was tested applying the force in the extrusion direction (E) and in the parallel (P) direction, in order to evaluate if differences in the cellular microstructure or chain orientation affects the moisture uptake and potential degradation. The obtained stress-strain curves of unaged and 6 months -aged samples can be seen in Fig. 7 (a), tested in the two directions. Foam 100 was tested applying the force in the E direction, after 3 and after 6 months ageing, and the obtained curves can be seen in Fig. 7 (b). These results have been presented at the 17th International Symposium on District Heating and Cooling 2021 [62].

The toughness, defined as the area below the stress-strain curve, was derived for each test, and a two-sample t-test with a significant level of 0.05 was undertaken for all aged/unaged pairs. The results showed that the behavior of the aged and unaged samples is not statistically different. No permanent degradation of the mechanical properties was detected after the 6 months hygrothermal ageing-

DMTA allowed to age and test samples with a thickness of 5 mm, with the aim to facilitate moisture diffusion through the foam thickness. Fig. 8 presents the obtained curves for PET foam 100 kg/m³, unaged and after 6 months ageing, with the load applied in the extrusion direction of the foam. The full set of curves can be found in the Supporting Information.

No change on the T_g or Storage/Loss modulus was detected in any case, showing no permanent degradation due to hygrothermal exposure even with low thickness foam samples.

As for the IR spectra, no changes were revealed by comparing unaged surface, aged surface and aged 10 mm below surface measurements. The results for PET foam with density 100 kg/m³ are presented in Fig. 9. The saturation of the ester bands in FTIR-ATR spectra have prevented previous authors from detecting chain scission due to the hydrolysis of PET [63]. FTIR-ATR spectra have been shown powerful in detecting changes in crystallinity [50,64,65], through the change in ratio between the trans and gauche isomers. A crystallinity increase could be a sign of

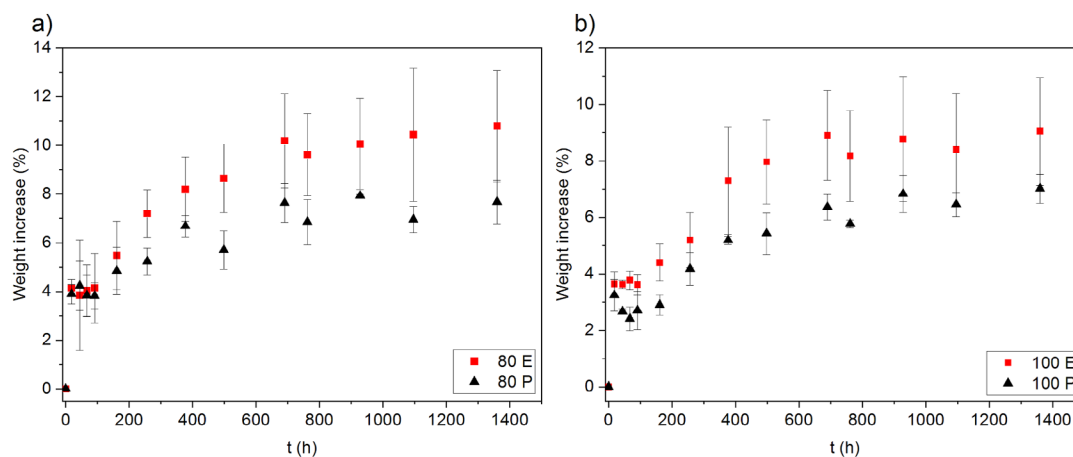


Fig. 3. Gravimetric curves for samples under water immersion at room temperature for PET foam 80 kg/m³ (a) and 100 kg/m³ (b).

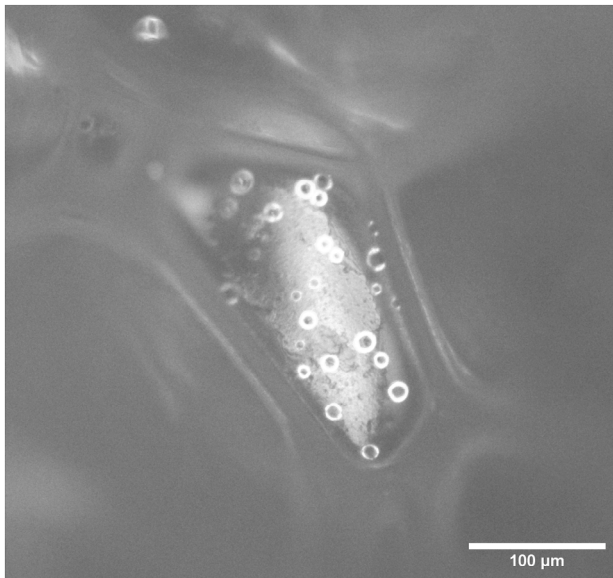


Fig. 4. Micrograph showing water droplets inside a cell

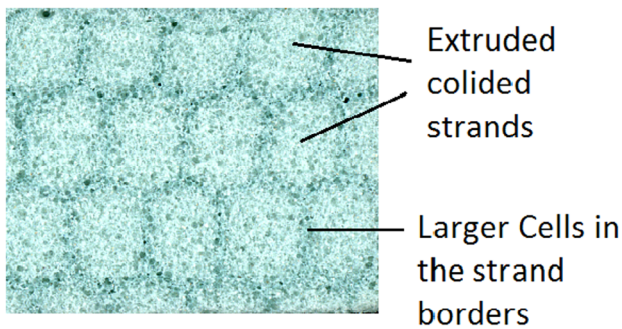


Fig. 5. Scan of the surface perpendicular to the extrusion direction of a PET 80 kg/m³ foam, where the effect of strand coalescence on the cellular structure can be observed.

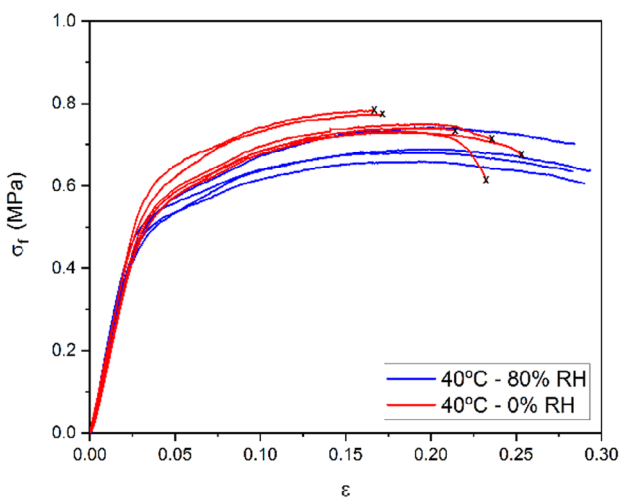


Fig. 6. Flexural stress strain curves for PET foam 80 kg/m³ tested under toom conditions, 40°C and 80% RH, and 40°C and 0% RH. Cross marks failure of the sample.

chemicrystallization upon hydrolysis [44]. This region was examined with more detail, but no significant shift between the two peaks could be derived, as illustrated by inclusion in Fig. 9.

The second ageing trial corresponds to water immersion at room temperature for a duration of one year. One batch of samples was dried in desiccators prior testing. The obtained stress-strain curves can be seen in Fig. 10. Samples were tested until failure.

After one year, no significant permanent degradation of the mechanical properties was observed.

A second batch of water immersed samples was tested without drying. The samples were kept immersed in water until they were placed in the testing machine. The goal was to observe the effects of absorbed water in the cell cavities. The obtained stress-strain curves are presented in Fig. 11.

The weight increase experienced by the samples during this 1 year water immersion was 42% for the 80 kg/m³ foam and 35% for the 100 kg/m³ foam. The stress strain curves reveal that the moisture did not produce any effect on the E modulus, but strongly increased the ductility of the foam and increased their strain at break due to plasticization. Samples from the 80 foam did not fail during under the tested stress range. These effects are analogous to those undertaken at 40°C and 80% RH (Fig. 6), revealing that the filling of the cavities with liquid water does not produce any additional effect on the mechanical properties.

Discussion

Moisture uptake and diffusion into PET foam core

In our results it can be seen that the moisture uptake into the PET foam's polymer matrix is low. This is consistent with the literature values of 8-10 water molecules absorbed per 100 PET repeating units [59,61]. The weight uptake is of the same order of magnitude than that previously reported ~1% for PET films [59,60] although lower. A crystallinity content of the tested PET foam was determined as 22% through DSC [50]. It is widely accepted that crystals are impermeable [19,23,66], therefore a 22% reduction in the weight uptake vs that reported for amorphous PET would be expected. The measured weight uptake in this study is 60% lower. While it is tempting to allocate this discrepancy to lack of saturation of the foam core, the strong plasticization effect observed in the flexural stress-strain curves under 80% RH and 40°C test versus the tests at the same temperature but 0% RH conditions show this is highly unlikely – moisture sorption on the outer surface only would not reveal such changes. In the mentioned studies of moisture sorption in PET films, saturation was achieved in 2.7-5h, being the thickness of the PET films of ~200 μm. The cell wall thickness of the foam under study is measured as 5-10 μm and the cell struts thickness as of the order of 20-40 μm, for the 80 and 100 kg/m³ foam, respectively. The thinner thickness of the polymer in the foam questions a slower diffusion process than in films. It is accepted that PET follows a 3 phase-structure [67,68], and we have found the rigid amorphous fraction (RAF) predominant in the foam under study [50]. The closer packing of the chains in the RAF fraction restricts gas diffusion and permeation [69], therefore the lower mass uptake can be related not only to the permeability of the crystalline phase but also to the reduced permeability of the RAF phase.

We are confident to conclude that moisture saturation of polymer skeleton was achieved in less than 24h through the bulk of the foam, which corresponds to the first measurement point. This is consistent with moisture diffusion studies of PET films as mentioned above, and implies that the cellular structure does not exert a significant impact on the diffusion through the polymer, at least for engineering timescales. But the filling of the cell cavities with liquid water requires longer periods of times and is a step-wise process, as revealed by the comparison with the results of moisture uptake under water immersion. While it has been previously reported that for moisture diffusion, water immersion and moisture at 100% RH are equivalent [21], this is not the case for foams, where liquid water can accumulate in the cell cavities. This

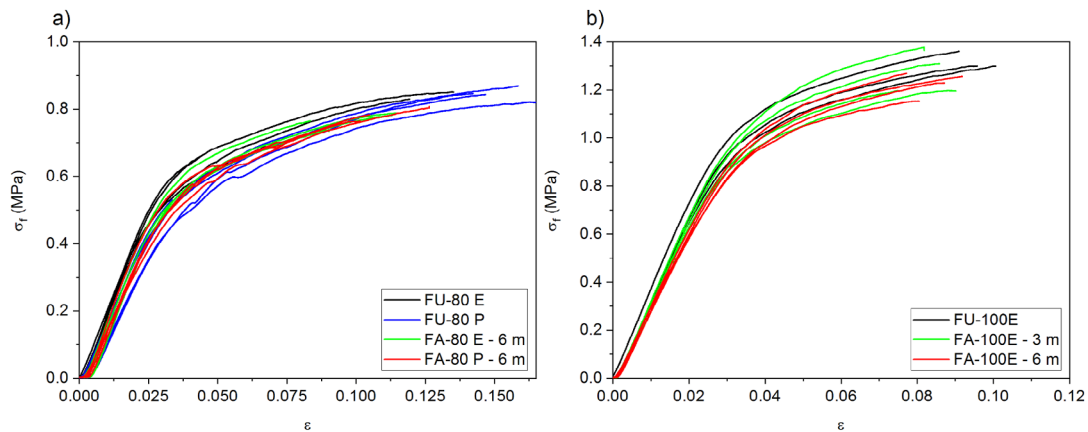


Fig. 7. (a) Flexural stress-strain curves for foam 80 kg/m³, unaged with the load on the E direction (FU-80 E) and the P direction (FU-80-E), and after 6 months ageing at 40°C and 80% RH, with the load on the E direction (FA-80 E - 6m) and the P direction (FA-80 P - 6m); and (b) 100 kg/m³ foam, unaged with the load on the E direction (FU-100 E) and after 3 (FA-100E-3m) and 6 months ageing (FA-100E-6m) at 40°C and 80% RH, both with the load in the E direction.

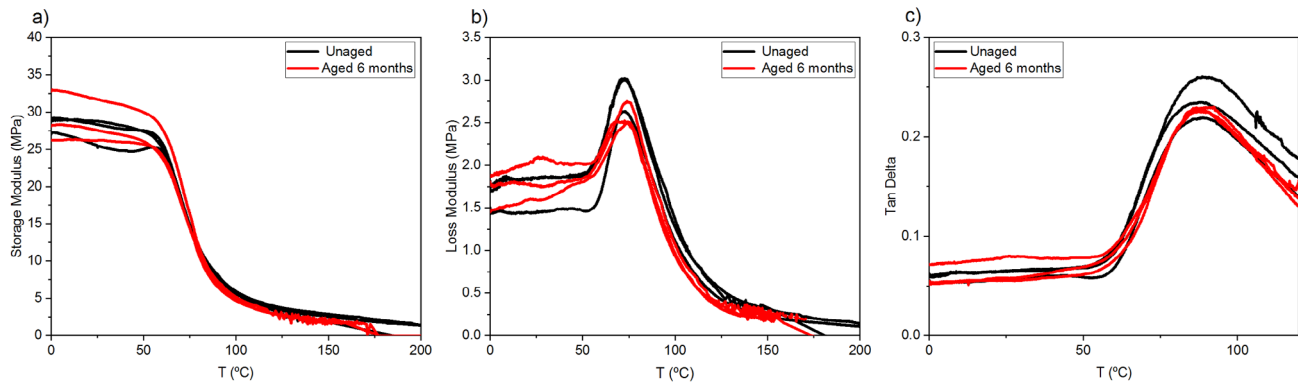


Fig. 8. Storage modulus (a), loss modulus (b) and Tan δ (c) vs temperature for PET foam 100 kg/m³, unaged and after 6 months ageing. Load applied in the extrusion direction of the foam.

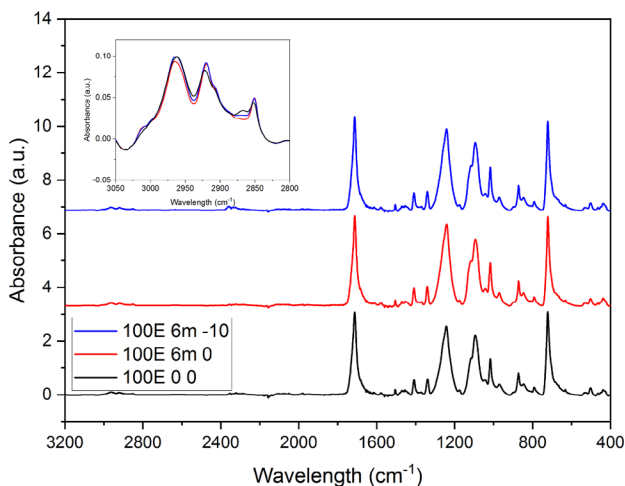


Fig. 9. Stacked IR spectra for 100 kg/m³, unaged surface sample (100E 0 0), 6 months ageing surface sample (100E 6m 0) and 6 months ageing 10 mm into the core (100E 6m -10)

passage can take place through permeation through the cell walls, and direct flow through the open cells. While our measured open cell content of ~20% is considered typical [55], the value of open cell content for the

particular polymeric foams used in previous reports of their moisture sorption is not provided [20,27,37], preventing from comparison. Previous authors have reported additional weight gain under water immersion than under moisture vapor, but this has been interpreted as water accumulation in the superficial open cells [20]. In this work as well as that of previous authors, the surface of the foams was blotted with paper tissue before weighing during the gravimetric moisture uptake experiments, making this interpretation inconsistent with the experimental procedure.

The finding that water indeed passes into the cell cavities through the bulk of the foam reveals the need for an accurate definition of “saturation of the foam”. Does this include the saturation of the cell cavities, or only of the polymer? While the models for diffusion in foams typically disregard moisture entrapment in the cell cavities for simplicity, i.e [40], experimental measurements of moisture uptake through gravimetry upon water immersion effectively measure both, the water sorbed in the polymer and the water trapped in the cell cavities. Our results show that these are two distinct phenomena which occur at different rates, as conceptually illustrated in Fig. 12.

Moisture saturation of the polymer and moisture saturation of the cavities impact different aspects of the foams function. The results of the bending tests of the wet 1 year water immersion samples (Fig. 11) show the same increase in ductility than those saturated with vapour (Fig. 6) and no degradation of the E modulus, meaning that the effect of the entrapped liquid water in the cells on the mechanical properties is limited. However, moisture entrapment in the cavities will have a strong

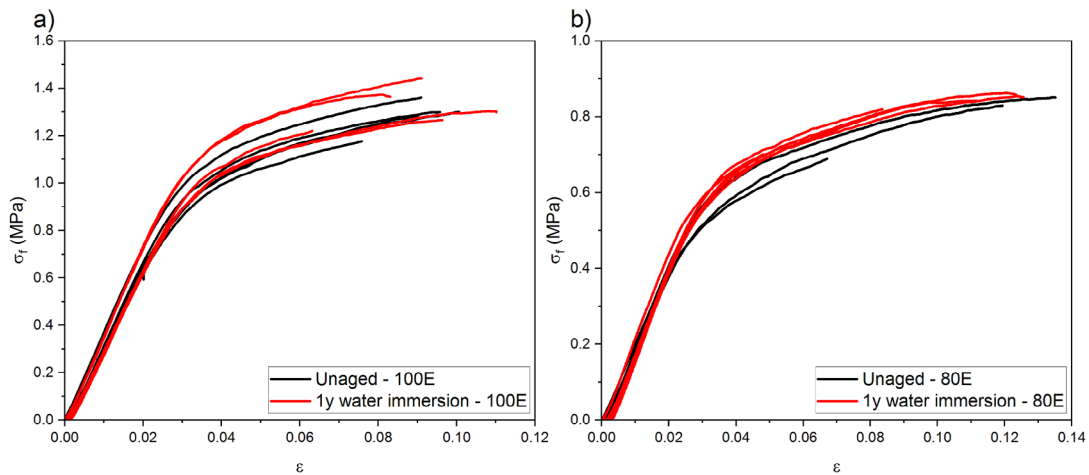


Fig. 10. Flexural stress-strain curves for PET foam 100 kg/m^3 (a) and PET foam 80 kg/m^3 , unaged and after 1 year water immersion at room temperature. Samples were dried prior testing and tested until failure.

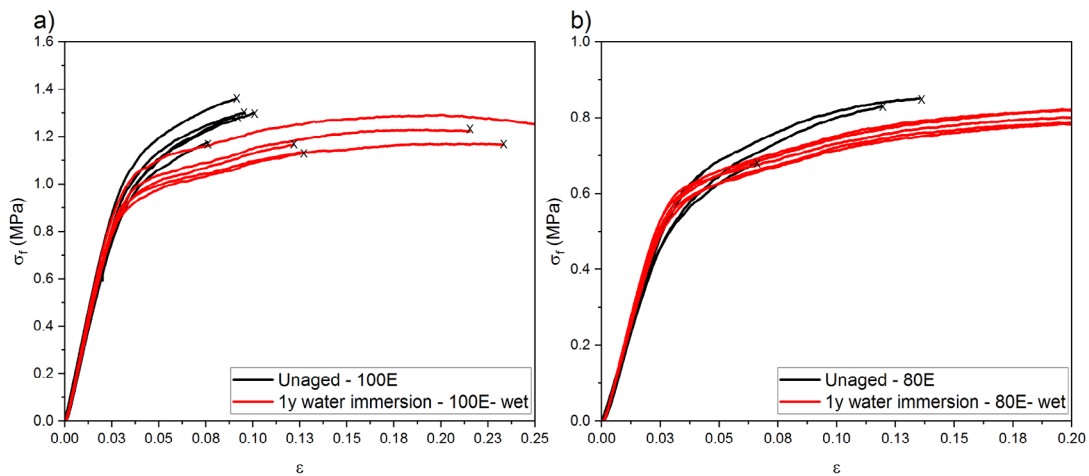


Fig. 11. Flexural stress-strain curves for PET foam 100 kg/m^3 (a) and PET foam 80 kg/m^3 , unaged and after 1 year water immersion. Samples tested wet. Cross represents the failure of the samples.

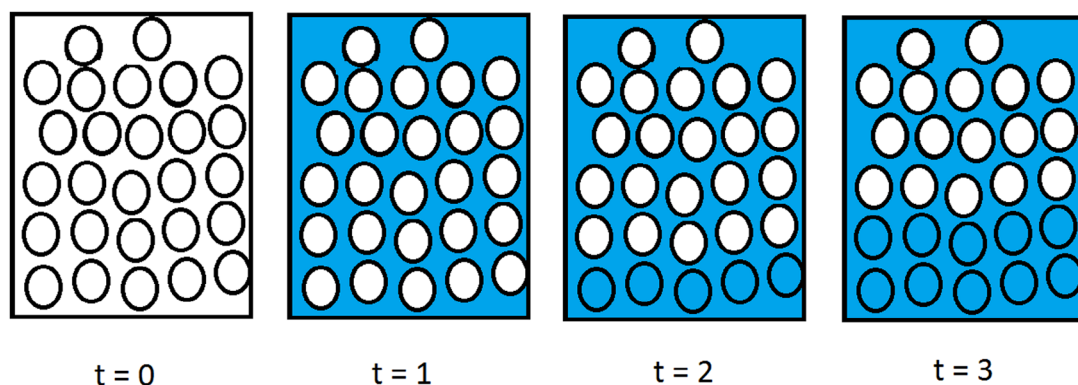


Fig. 12. Proposed scheme for moisture saturation of the polymer and cavities in a foam with time. Saturation is represented by the colour blue.

impact on the thermal conductivity hence insulating properties of the foam.

Degradation effects of hygrothermal exposure

No degradation of the PET foam has been observed after the different ageing trials, nor of its chemical structure, nor of its mechanical properties. It has been demonstrated that this lack of degradation is not

diffusion controlled. Given the low moisture uptake by PET, it is reasonable that swelling is not significant. Cracking events related to swelling or osmotic damage are also not detected, consistent with the previous.

The remaining irreversible degradation of PET which could arise from hygrothermal exposure would be embrittlement caused by hydrolysis, which has not been detected in our study. The question is, if the reaction kinetics are slow in relation to the duration of our experimental programme, if the reaction does not occur at all the temperatures under consideration, or if hydrolysis below T_g does not lead to embrittlement.

Experimental reports on the hydrolysis of PET are confined to conditions in which the polymer is above its T_g . Some early work conducted at 71°C concluded that hydrolysis does occur below T_g [46]. However, this did not take into account the depression of T_g caused by moisture plasticization [61], possibly spreading confusion. No literature reference could be found during the course of the present study providing evidence of hydrolysis of PET below T_g , with some authors citing the time length required for observing the hydrolysis of PET at lower temperatures has so far prevented its observation in laboratory experiments [49, 70]. The execution of accelerated ageing tests above the T_g of PET for energy infrastructure [65,71] and civil engineering [72–74] applications is common. According to models for service life prediction for PET upon hydrolysis [45], the required service life of 30 years for DH pipelines would be secured with high moisture at ground temperature. But the validity of these Arrhenius extrapolations to the glassy state when the activation energy (E_a) has been obtained in the rubbery state is questioned in the literature [45,49]. In this study, care was taken to select accelerated ageing condition in relation to the in-service ground moisture temperature of around 10°C, but ensuring the maintenance of the glassy state. Considering the T_g depression caused moisture [61], the selected temperature of 40°C provides an adequate $\Delta T = 20^\circ\text{C}$ below T_g . In a previous study of the hydrolysis of PET foam, above T_g [50] we have observed that the ductile-brittle transition is linked to the attainment of the minimum mobile amorphous content and crystallinity increase, leading to a micromechanical cause of embrittlement, rather than a molecular cause related to the reduction of tie-molecules concentration. The hydrolysis reaction and reduction of molecular weight continue after this point. This would question the occurrence of the hydrolysis-induced embrittlement of PET when the polymer chains are not mobile, below T_g .

Conclusions

Moisture uptake in the PET foam consists of two distinct phenomena: (i) the diffusion and sorption of moisture by the polymer matrix, at analogous rates as in films, and (ii) the progressive passage and filling of the cell cavities by liquid water in the case of liquid water immersion, which occurs much slower and in a multistage process.

The hygrothermal degradation of the PET foam is not diffusion-controlled. Plasticization of the foam is observed due to moisture sorption of the PET cellular skeleton.

The alteration of the mechanical properties due to water entrapment in the cell cavities is not significant.

The low moisture uptake of PET appears to limit degradation due to swelling or osmotic damage.

No embrittlement was observed after 6 months ageing at 40°C and 80% RH, nor after one year water immersion at room temperature. Our previous research questions the occurrence of hydrolysis-induced embrittlement at temperatures below the T_g of PET.

Author contribution

LD: Study design and conception, Data collection and analysis, Preparing the manuscript, Critical discussion of the results, Editing of the manuscript. IW: Scientific supervision, Critical discussion of the results, Editing of the manuscript.

Declaration of Competing Interest

The authors declare that they have no known competing financial interests or personal relationships that could have appeared to influence the work reported in this paper.

Acknowledgments

Rebeca Hernández from ICTP-CSIC is kindly thanked for providing the DMTA tests and interesting discussions, given the impossibility of conducting a research stay due to the COVID pandemic.

The presented research was funded by the Technical Infrastructure Management Professorship of the HafenCity University.

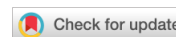
Supplementary materials

Supplementary material associated with this article can be found, in the online version, at [doi:10.1016/j.polyimdeggradstab.2022.110009](https://doi.org/10.1016/j.polyimdeggradstab.2022.110009).

References

- [1] P Mazzuca, JP Firmo, JR Correia, E. Castilho, Mechanical behaviour in shear and compression at elevated temperature of polyethylene terephthalate (PET) foam, *J. Build. Eng.* 42 (2021), 102526.
- [2] Fathi A. Mechanical Properties of Strand PET Foams at Different Length Scales; 2018.
- [3] J. Ramnäs, New Materials and Constructions For Improving The Quality And Lifetime Of District Heating Pipes Including Joints - Thermal, Mechanical And Environmental Performance, Annex VIII, 2008.
- [4] M Xanthos, Q Zhang, SK Dey, Y Li, U Yilmazer, M O'Shea, Effects of resin rheology on the extrusion foaming characteristics of PET, *J. Cell. Plast.* 34 (6) (1998) 498–510.
- [5] M Xanthos, SK Dey, Q Zhang, J. Quintans, Parameters affecting extrusion foaming of PET by gas injection, *J. Cell. Plast.* 36 (2) (2000) 102–111.
- [6] L Di Maio, I Coccorullo, S Montesano, L Incarnato, Chain Extension and foaming of recycled PET in extrusion equipment, *Macromol. Symp.* 228 (1) (2005) 185–200.
- [7] CP Parky, GA. Garcia, Development of polypropylene plank foam products, *J. Cell. Plast.* 38 (3) (2002) 219–228.
- [8] Ecorys. EU Construction & Demolition Waste Management Protocol; 2016.
- [9] European Commission. Closing the loop- an EU action plan for the circular economy: COM (2015) 614 final; 2015.
- [10] European Commission. A new Circular Economy Action Plan For a cleaner and more competitive Europe: COM(2020) 98 final; 2020.
- [11] JA. ZAPP, Hazards of isocyanates in polyurethane foam plastic production, *A.M.A. Arch. Indust. Health* 15 (4) (1957) 324–330.
- [12] European Chemical Agency, CLP Regulation: (EC) No 1272/2008, 2008.
- [13] Commission Regulation (EU) 2020/1149 of 3 August 2020 amending Annex XVII to Regulation (EC) No 1907/2006 of the European Parliament and of the Council concerning the Registration, Evaluation, Authorisation and Restriction of Chemicals (REACH) as regards diisocyanates: (EU) 2020/1149. In: Official Journal of the European Union; 2020.
- [14] I. Weidlich, Mantelrohrsysteme in der Wärmeverteilung, editors, in: H-B Horlacher, U Helbig (Eds.), *Rohrleitungen 1*, Springer Berlin Heidelberg, Berlin, Heidelberg, 2016, pp. 475–494.
- [15] Mangs S. Insulation materials in district heating pipes. PhD. Sweden; 2005.
- [16] S.E. Sällberg, S. Nilsson, G. Bergström, Leakage ways for ground-water in PUR-foam, in: Proceedings of the 10th International Symposium on District Heating and Cooling, 2006. September.
- [17] S Hay, H. Huther, S. Grimm, D. Heiler, J. Dony, H-J. Nielsen, G.K. Schuchardt, T. Grage, M. Blesl, F. Wendel, M Achmus, et al., *EnEff: Wärme - Technische Gebrauchsdaueranalyse von Wärmenetzen unter Berücksichtigung volatiler erneuerbarer Energien*: Teil I: Untersuchungsergebnisse zur Materialdegradation, AGFW-Projektgesellschaft für Rationalisierung, Frankfurt am Main, 2020. Information.
- [18] CT Larsen, P Togeskov, A. Leuteritz, Analyses of diffusion rates through PE and impact on ageing, *Euro Heat Power English Edition* 6 (II) (2009).
- [19] C Sammon, N Everall, J. Yarwood, The diffusion of water into pet followed in-situ using FT-IR ATR, *Macromol. Symp.* 119 (1) (1997) 189–196.
- [20] JS Earl, RA. Sheno, Determination of the moisture uptake mechanism in closed cell polymeric structural foam during hygrothermal exposure, *J. Compos. Mater.* 38 (15) (2004) 1345–1365.
- [21] AC Loos, GS Springer, BA Sanders, RW. Tung, Moisture absorption of polyester-glass composites, *J. Compos. Mater.* 14 (2) (1980) 142–154.
- [22] T Shigetomi, H Tsuzumi, K Toi, T. Ito, Sorption and diffusion of water vapor in poly(ethylene terephthalate) film, *J. Appl. Polym. Sci.* 76 (1) (2000) 67–74.
- [23] DR Rueda, A. Varkalis, Water sorption/desorption kinetics in poly(ethylene naphthalene-2,6-dicarboxylate) and poly(ethylene terephthalate), *J. Polym. Sci. B Polym. Phys.* 33 (16) (1995) 2263–2268.

- [24] SK Burgess, DS Mikkilineni, DB Yu, DJ Kim, CR Mubarak, RM Kriegel, et al., Water sorption in poly(ethylene furanoate) compared to poly(ethylene terephthalate). Part 1: equilibrium sorption, *Polymer* 55 (26) (2014) 6861–6869.
- [25] F Dubelley, E Planes, C Bas, E Pons, B Yrieix, L. Flandin, Water vapor sorption properties of polyethylene terephthalate over a wide range of humidity and temperature, *J. Phys. Chem. B* 121 (8) (2017) 1953–1962.
- [26] BJ Manujesh, V Rao, MS. Aan, Moisture absorption and mechanical degradation studies of polyurethane foam cored E-glass-reinforced vinyl-ester sandwich composites, *J. Reinf. Plast. Compos.* 33 (5) (2014) 479–492.
- [27] Z Huo, M Mohamed, JR Nicholas, X Wang, K. Chandrashekhara, Experimentation and simulation of moisture diffusion in foam-cored polyurethane sandwich structure, *J. Sandwich Struct. Mater.* 18 (1) (2016) 30–49.
- [28] YL Holliday, G THACKRAY, Heterogeneity in complex materials and the concept of the representative cell, *Nature* 201 (4916) (1964) 270–272.
- [29] GE Bell, J. Crank, Influence of imbedded particles on steady-state diffusion, *J. Chem. Soc., Faraday Trans. 2* (70) (1974) 1259.
- [30] Persson C. Predicting the long-term insulation performance of district heating pipes. PhD Dissertation. Göteborg; 2015.
- [31] L Pilon, AG Fedorov, R. Viskanta, Gas diffusion in closed-cell foams, *J. Cell. Plast.* 36 (6) (2000) 451–474.
- [32] M. Bomberg, A model of aging for gas-filled cellular plastics, *J. Cell. Plast.* 24 (4) (1988) 327–347.
- [33] Brodt K. Thermal insulations: Cfc-alternatives and vacuum insulation. Dissertation. Delft, Netherlands; 1995.
- [34] GCJ Bart, Du Cauzé De Nazelle GMR. Certification of thermal conductivity aging of PUR foam, *J. Cell. Plast.* 29 (1) (1993) 29–42.
- [35] Duncan BC, Broughton WR. Absorption and Diffusion of Moisture In Polymeric Materials. Measurement Good Practice Guide No. 102; 2007.
- [36] Immergut, E.H.; Mark, H.F. Plasticization and plasticizer processes. American Chemical Society, Advances in Chemistry Series ISBN 9780841222281.
- [37] F Avilés, M. Aguilar-Montero, Mechanical degradation of foam-cored sandwich materials exposed to high moisture, *Compos. Struct.* 92 (1) (2010) 122–129.
- [38] H Liu, J He, D Xie, Q Xue, Q Peng, Study on the hygroscopicity of PET foam sandwich structure, *Adv. Mech. Eng.* 13 (4) (2021), 168781402110118.
- [39] DJ Sekelik, EV Stepanov, S Nazarenko, D Schiraldi, A Hiltner, E. Baer, Oxygen barrier properties of crystallized and talc-filled poly(ethylene terephthalate), *J. Polym. Sci. B Polym. Phys.* 37 (8) (1999) 847–857.
- [40] WM. Lee, Water vapor permeation in closed cell foams, *J. Cell. Plast.* 9 (3) (1973) 125–129.
- [41] BA Lerch, RM. Sullivan, Thermal expansion of polyurethane foam, in: Proceedings of the 43rd Annual Technical Meeting of the Society of Engineering Science, 2006.
- [42] RF. Fedors, Osmotic effects in water absorption by polymers, *Polymer* 21 (2) (1980) 207–212.
- [43] RF. Fedors, Water-treeing as an osmotic phenomenon, *Polymer* 21 (8) (1980) 863–865.
- [44] A Ballara, J. Verdu, Physical aspects of the hydrolysis of polyethylene terephthalate, *Polym. Degrad. Stab.* 26 (4) (1989) 361–374.
- [45] F Dubelley, E Planes, C Bas, E Pons, B Yrieix, L. Flandin, Predictive durability of polyethylene terephthalate toward hydrolysis over large temperature and relative humidity ranges, *Polymer* 142 (2018) 285–292.
- [46] W McMahon, HA Birdsall, GR Johnson, CT. Camilli, Degradation studies of polyethylene terephthalate, *J. Chem. Eng. Data* 4 (1) (1959) 57–79.
- [47] A Launay, F Thominette, J. Verdu, Hydrolysis of poly(ethylene terephthalate): a kinetic study, *Polym. Degrad. Stab.* 46 (3) (1994) 319–324.
- [48] A Launay, F Thominette, J. Verdu, Hydrolysis of poly(ethylene terephthalate). A steric exclusion chromatography study, *Polym. Degrad. Stab.* 63 (3) (1999) 385–389.
- [49] M Arhant, M Le Gall, P-Y Le Gac, P Davies, Impact of hydrolytic degradation on mechanical properties of PET - towards an understanding of microplastics formation, *Polym. Degrad. Stab.* 161 (2019) 175–182.
- [50] Doyle L, Weidlich I. Hydrolytic degradation of closed cell Polyethylene terephthalate foams. The role of the mobile amorphous phase in the ductile-brittle transition. *Polymer Degradation and Stability* under review. 2022.
- [51] J Schindelin, I Arganda-Carreras, E Frise, V Kaynig, M Longair, T Pietzsch, et al., Fiji: an open-source platform for biological-image analysis, *Nat. Methods* 9 (7) (2012) 676–682.
- [52] D20 Committee, Test Method for Open Cell Content of Rigid Cellular Plastics, ASTM International, West Conshohocken, PA, 2022, <https://doi.org/10.1520/D6226-21>.
- [53] WH Peters, WF. Ranson, Digital imaging techniques in experimental stress analysis, *Opt. Eng.* 21 (3) (1982).
- [54] DJ. Walls, Application of ATR-IR to the analysis of surface structure and orientation in uniaxially drawn poly(ethyleneterephthalate), *Appl. Spectrosc.* 45 (7) (1991) 1193–1198.
- [55] LJ Gibson, MF. Ashby, Cellular Solids, Cambridge University Press, Cambridge, 1997.
- [56] JBF de Champchesnel, DI Bower, IM Ward, JF Tassin, G. Lorentz, Development of molecular orientation in sequentially drawn PET films, *Polymer* 34 (18) (1993) 3763–3770.
- [57] RM Gohil, DR. Salem, Orientation distribution in the noncrystalline regions of biaxially drawn poly(ethylene terephthalate) film: a chain-intrinsic fluorescence study, *J. Appl. Polym. Sci.* 47 (11) (1993) 1989–1998.
- [58] PM. Henrichs, Molecular orientation and structure in solid polymers with carbon-13 NMR: a study of biaxial films of poly(ethylene terephthalate), *Macromolecules* 20 (9) (1987) 2099–2112.
- [59] DR Rueda, A Viksne, J Kajaks, FJ Balta-Calleja, HG. Zachmann, Properties of arylpolyesters with reference to water content, *Macromol. Symp.* 94 (1) (1995) 259–268.
- [60] SK Burgess, DS Mikkilineni, DB Yu, DJ Kim, CR Mubarak, RM Kriegel, et al., Water sorption in poly(ethylene furanoate) compared to poly(ethylene terephthalate). Part 2: kinetic sorption, *Polymer* 55 (26) (2014) 6870–6882.
- [61] D Langevin, J Grenet, JM. Saiter, Moisture sorption in pet influence on the thermokinetic parameters, *Eur. Polym. J.* 30 (3) (1994) 339–345.
- [62] L Doyle, I. Weidlich, Sustainable Insulation for Sustainable DHC, in: Proceedings of the 17th International Symposium on District Heating and Cooling 7, Energy Reports 2021, Trent, UK, 2021, pp. 150–157, 6–9 September.
- [63] C Sammon, J Yarwood, N. Everall, An FT-IR study of the effect of hydrolytic degradation on the structure of thin PET films, *Polym. Degrad. Stab.* 67 (1) (2000) 149–158.
- [64] R Tang, JJ Liggat, WH. Siew, Partial discharge behaviour of biaxially orientated PET films: the effect of crystalline morphology, *Polym. Degrad. Stab.* 155 (2018) 122–129.
- [65] Abdulkarim Gok. Degradation Pathway Models of Poly(ethylene-Terephthalate) under accelerated weathering exposures; 2016.
- [66] A. Peterlin, Dependence of diffusive transport on morphology of crystalline polymers, *J. Macromol. Sci., Part B* 11 (1) (1975) 57–87.
- [67] Y Fu, WR Busing, Y Jin, KA Affholter, B. Wunderlich, Structure analysis of the noncrystalline material in poly(ethylene terephthalate) fibers, *Macromol. Chem. Phys.* 195 (2) (1994) 803–822.
- [68] Y Fu, B Annis, A Boller, Y Jin, B Wunderlich, Analysis of structure and properties of poly(ethylene terephthalate) fibers, *J. Polym. Sci. B Polym. Phys.* 32 (13) (1994) 2289–2306.
- [69] S Sato, T Nyuu, G Matsuba, K. Nagai, Correlation between interlamellar amorphous structure and gas permeability in poly(lactic acid) films, *J. Appl. Polym. Sci.* 131 (16) (2014) n/a-n/a.
- [70] V Bellenger, M Ganem, B Mortaigne, J. Verdu, Lifetime prediction in the hydrolytic ageing of polyesters, *Polym. Degrad. Stab.* 49 (1) (1995) 91–97.
- [71] IEC, 61215:2005. Crystalline silicon terrestrial photovoltaic (PV) modules – Design qualification and type approval(IEC 61215:2005) (2005).
- [72] M Mohammadian, NS Allen, M Edge, K. Jones, Environmental degradation of poly(ethylene terephthalate), *Text. Res. J.* 61 (11) (1991) 690–696.
- [73] S Weidner, G Kuehn, B Werthmann, H Schroeder, U Just, R Borowski, et al., A new approach of characterizing the hydrolytic degradation of poly(ethylene terephthalate) by MALDI-MS, *J. Polym. Sci. A Polym. Chem.* 35 (11) (1997) 2183–2192.
- [74] V Elias, A Salman, D. Goulias, The effect of pH, resin properties, and manufacturing process on laboratory degradation of polyester geosynthetics, *Geosynthetics International* 5 (5) (1998) 459–490.



Received: 12 July 2021 | Revised: 30 September 2021 | Accepted: 2 October 2021

DOI: 10.1002/app.51816

ARTICLE

Applied Polymer Science WILEY

Extrusion foaming behavior of polybutene-1. Toward single-material multifunctional sandwich structures

Lucía Doyle

Infrastructural Engineering, HafenCity University, Hamburg, Germany

CorrespondenceLucía Doyle, Infrastructural Engineering, HafenCity University, Henning-Voscherau-Platz 1, 20457 Hamburg, Germany.
Email: lucia.doyle@hcu-hamburg.de**Funding information**

HafenCity University

Abstract

Polymeric foams are a key element of many multifunctional sandwich structures. The most commonly used polymeric foam, polyurethane, presents environmental drawbacks, related to poor recyclability and the use of toxic diisocyanates for their manufacturing. The separation of layers in sandwich structures is a further unresolved hurdle toward the recyclability of these elements. There is a need for broadening the spectrum of polymeric foams. In this context, the foamability of polybutene-1 (PB-1) is studied through extrusion foaming experiments. From the application side, foaming PB-1 would allow the manufacturing of district heating pre-insulated pipes out of one single material, bringing circular product design to the energy sector. From the scientific side, there is a knowledge gap in the foaming of polymers in the rubbery state at room temperature, such as PB-1, due to difficulties in the cell stabilization step. This supports the need for research in the foaming of this polymer. In this study, four commercial grades of PB-1 were evaluated, covering different chain structures, molecular weights, and crystallinity degrees. Very different foaming behaviors were found. Dimensionally stable foams were achieved with the two homopolymers tested, demonstrating the foamability of this polymer.

KEYWORDS

extrusion, foams, polyolefins, circular economy, circular product design

1 | INTRODUCTION

Polymeric foams have experienced an increased use in recent years as a key element in multifunctional sandwich structures, which combine a structural load-bearing function with nonstructural functions like insulation. This has expanded their use in applications including aerospace,^{1–4} marine,^{5–7} civil,^{6–9} and energy infrastructure as wind blades^{10,11} and district heating piping networks.¹²

Most commonly used polymeric foams such as polyurethane (PU) are thermoset, hindering their recyclability, as well as require hazardous raw materials for

their manufacturing, such as the recently restricted diisocyanates in PU.^{13,14} Analogously to how the phasing out of chlorofluorocarbons (CFCs) enforced by the Montreal Protocol¹⁵ triggered research and development on alternative blowing agents during the 90s and 2000s,^{16–20} pressing requirements on material's recyclability and environmental impact brought by the circular economy has placed research and use of thermoplastic,^{21–28} biodegradable,^{29–31} and biobased^{32–34} foams on the current research agenda. However, the recyclability of sandwich structures is hindered by the separation of the different layers of materials, which is

This is an open access article under the terms of the Creative Commons Attribution-NonCommercial License, which permits use, distribution and reproduction in any medium, provided the original work is properly cited and is not used for commercial purposes.

© 2021 The Author. *Journal of Applied Polymer Science* published by Wiley Periodicals LLC.

still an unresolved problem. A true transition to the circular economy involves a holistic product design, evaluating the recyclability of the complete composite structure and not only of its individual layers. Best practice in green engineering includes minimization of the number of materials in an element.³⁵ This could be achieved by increasing the knowledge on foaming of a broader range of polymers, tailoring the properties of multifunctional structures not by material layers but by material processing.

Polybutene-1 (PB-1) is a polyolefin produced by the polymerization of 1-butene using supported Ziegler–Natta catalysts.³⁶ It is a high-molecular weight, linear, isotactic, and semicrystalline polymer. Properties include low coefficient of thermal expansion,¹² high-heat deflection temperature, stress cracking resistance (ESCR), and outstanding creep resistance.³⁷ It is a recyclable thermoplastic and nontoxic,³⁸ pre-requisites for circular product development.

PB-1 is one of the common materials used as service pipes for district heating networks,^{12,39} application which motivates this research. Current district heating pre-insulated pipes are sandwich components comprising a service pipe and foam layer, as for state-of-the-art of PU,³⁹ and a protective casing. The foam layer acts both as insulation and as bond between the medium pipe and the casing, supporting multiaxial stresses. Currently used PU in bonded pre-insulated pipes is required to have a thermal conductivity lower than $0.029 \text{ W}/(\text{m} \times \text{K})$,⁴⁰ and for insulated plastic pipes, an axial shear strength $>0.09 \text{ MPa}$.⁴¹ Foaming PB-1 would allow the manufacturing of a pre-insulated pipe out of only one material.

From the scientific perspective, with a glass transition temperature (T_g) of -25°C ,³⁷ PB-1 is a polymer in the rubbery state at room temperature, a polymer class for which limited studies on foaming exist, and an identified challenge in foaming.⁴² This is due to the difficulty in the cell stabilization step, as a result post-foaming shrinkage due to the escape of the blowing agent from the matrix, facilitated by being above its T_g , and cell coalescence driven by viscoelasticity. There is a need for increasing the knowledge on foam processing for this polymer class.

After an extensive literature search for PB-1 foaming, only one reference was found, where one grade of PB-1 was included in a screening of different semicrystalline polymers targeted to assess the effects of crystallinity on the morphology of foams prepared by temperature-induced batch foaming.⁴³ This highlights the need for research on the foaming behavior of this polymer.

In this study, the extrusion foaming behavior of PB-1 is studied using a chemical blowing agent (CBA). Different commercial grades were evaluated, including two homopolymers, one copolymer, and one thermoplastic elastomer. The obtained samples have been characterized for

density, expansion ratio, and microstructure. Foamability is assessed in terms of achieved volume expansion ratio, microstructure, and processing window size, using available extrusion equipment. Optimization of the foaming process is out of the scope of this study. A part of this study was presented in the First International Conference on “Green” Polymer Materials 2020⁴⁴ and included here for completeness.

Very different foaming behavior has been found between the tested grades. The two homopolymers presented the better foaming behavior. Foams with cell population density of $10^4 \text{ cells}/\text{cm}^3$ and expansion ratio of up to 1.8 were obtained, demonstrating the foamability of the polymer. The processing window was found to be narrow, as expected for a linear semicrystalline polymer. Foam shrinkage, one of the identified main risks given the rubbery nature of PB-1, was found in the thermoplastic elastomer grade only. The tested homopolymers presented good dimensional stability. The main challenge to overcome is the low-melt strength, as encountered in recent developments of polypropylene (PP),^{22,45} polyethylene terephthalate (PET),^{28,30,46} or polylactic acid (PLA) foams,³⁴ which limits volume expansion. Higher expansion ratios could be obtained through processing optimization and resin rheology improvements, through, that is, increasing the molecular weight of the polymer.

2 | EXPERIMENTAL

2.1 | Materials

Four commercial grades of PB-1 from LyondellBasell were investigated, presenting different chain structures, molecular weights, degree of crystallinity (X_c), melting temperature (T_m), and melt flow ratio (MFR). Table 1 presents an overview with the data provided by the manufacturer. Resins were used as received.

A chemical blowing agent (CBA) was used, Hydrocerol CT 550, kindly provided by Clariant. The amount of dosed CBA was varied between 2% and 10%. The main gas released by this CBA is CO_2 , and the effective components amount to 70% according to the technical data sheet.

2.2 | Sorption/desorption kinetics

Sorption and desorption kinetics of CO_2 in PB1-a, PB1-b, and PB1-c at room temperature were studied using the gravimetric method proposed by Berens & Huvar.⁴⁷ CO_2 of $>99.8\%$ purity was used. The polymer was molten and compression molded into discs of 40 mm diameter

TABLE 1 Overview of the evaluated PB-1 resins

Resin	Type	Approx. molecular weight (g/mol)	X _c (%)	T _m	MFR (g/10 min @190°C/2.16 kg)
PB1-a	Homopolymer	530,000	~55	128°C	0.4
PB1-b	Homopolymer	460,000	~55	131°C	0.6
PB1-c	Thermoplastic elastomer	550,000	~25	114°C	0.5
PB1-d	Random copolymer	315,000	~35	97°C	2.5

Abbreviation: PB1, polybutene-1.

and 2 mm thickness. PB-1 experiences crystal–crystal transformation at room temperature. When cooling from the melt, it crystallizes into metastable Form II, characterized by a tetragonal unit cell. They then gradually transform into Form I stable crystals.^{48–50} This process is completed in around 10 days depending on the storage conditions.⁵¹ Therefore 10 days were allowed between the sample molding and sorption/desorption tests, as to test in the same form as the as-received pellets in the extrusion experiments. The discs were saturated at room temperature and 50 bars in an autoclave (Eurotechnica GmbH, Bargteheide, Germany). This pressure was selected as to be close to the extruder die pressure. Once the defined saturation time (t_s) was reached, a rapid decompression of <30s was undertaken. The samples were placed in an analytical balance with sensitivity of at least 1 mg and its weight decrease logged in 5 s intervals.

From the initial disk weight before sorption, W_0 , and the weight recorded during desorption (W_t), the rate of desorbed CO₂, $M_{t,d}$, can be derived as:

$$M_{t,d} = \frac{(W_t - W_0)}{W_0}. \quad (1)$$

For Fickian diffusion from a plane sheet,⁵² the plot of $M_{t,d}$ versus $\sqrt{t_d}$ is initially linear, and extrapolation to desorption time $t_d = 0$ provides $M_{t,s}$, the sorbed CO₂ at the end of the sorption period t_s . By running consecutive tests for longer t_s , the equilibrium uptake M_∞ is found once a constant value of $M_{t,s}$ is obtained. Experiments were conducted in triplicate.

2.3 | Extrusion foaming process

A twin screw ZSE 27 MAXX extruder (Leistritz Extrusionstechnik GmbH, Nürnberg, Germany) was used, with $D = 28.3$ mm, $L/D = 48$, and 12 modular barrels with 2.1 kW heating power each and water cooling. A strand die with three strands of 4 mm diameter each was used. The feeding temperature was set as low as possible as to create a melt seal and avoid premature

degassing of the CBA, which was set between 130 and 145°C depending on the resin used. The temperature was progressively increased up to 175°C until after the CBA dosing point, as to allow its complete decomposition. From then on, it was progressively lowered. Die exit temperatures were varied between 80 and 140°C. Die pressure was monitored. Preliminary trials were conducted to determine adequate mass flow rate and screw speed for foaming with the available extruder and screw configuration. 100 rpm and 4 kg/h were found appropriate to achieve the necessary die pressure for foaming to occur.

2.4 | Foam characterization

The foam samples were randomly collected at each processing condition and characterized for dimensional stability, volume expansion, density, cell size, and cell population density.

The dimensions stability of the extrudates was evaluated by photographing the strands using a Nikon D700 camera from immediately after collection (time between collection and initial photo max 20s) up to over 2 h after extrusion, in 20 s intervals. The diameter of each strand through the sequence was then measured from the images at least three different points and the average reported.

The density of the extrudates was determined in triplicate with a 100 ml glass pycnometer, distilled water and a Sartorius AC 211 S (Göttingen, Germany) balance.

The volume expansion ratio (V_{exp}) was calculated as

$$V_{exp} = \frac{\rho_{polymer}}{\rho_{foam}}. \quad (2)$$

The morphology of the foams was examined in an optical microscope (Leica DMLP, Wetzlar, Germany). Cell size was measured from the obtained micrographs using the open-source image-processing package Fiji.⁵³ Measurements from around 100 cells and typically three micrographs per resin and process conditions are reported.

Cell population density, defined as the number of cells per unit volume of the original unfoamed polymer, was calculated as:^{29,54}

$$N_0 = \left(\frac{n}{A}\right)^{3/2} \cdot V_{\text{exp}}, \quad (3)$$

where (N_0) is the cell population density (cell/cm^3), n is the number of cells in the micrograph and A the area of the micrograph (cm^2) and V_{exp} the volume expansion ratio.

3 | RESULTS

3.1 | Sorption/desorption kinetics

Figure 1a presents the desorption curves for grades PB1-a, PB1-b, and PB1-c for samples sorbed up to equilibrium, and Figure 1b the CO_2 uptake versus sorption time. It can be readily observed that PB1-a and PB1-b present very similar CO_2 sorption/desorption kinetics, with a linear desorption profile. PB1-c presents a significantly different behavior, with an exponential decay desorption profile. Practically the totality of the sorbed CO_2 is desorbed in approximately 6 min, for all the sorption times trialed. This has a great impact on the foam dimensional stability, as will be described in the following sections. A slight combing of the PB1-c disks upon extraction from the autoclave could be also observed, as well as a change in color from translucent to white (see Figure 2).

Changes in light transmission intensity through polymer sheets have been related to lamellar thickening and recrystallization induced by CO_2 .⁵⁵

From the $M_{t,s}$ data (see Table 2) it can be also concluded that the solubility of CO_2 is higher in PB1-c. Due to the rapid desorption, the extrapolation to $t_d = 0$ is

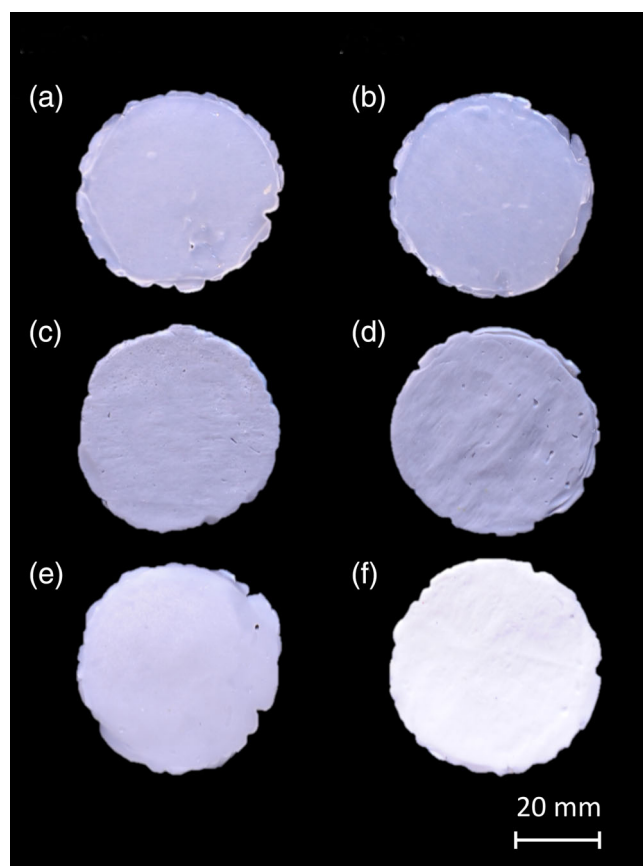


FIGURE 2 Samples of PB1-a before (a) and after (b) sorption/desorption, PB1-b before (c) and after (d), and PB1-c before (e) and after (f) sorption/desorption test. PB1, polybutene-1 [Color figure can be viewed at wileyonlinelibrary.com]

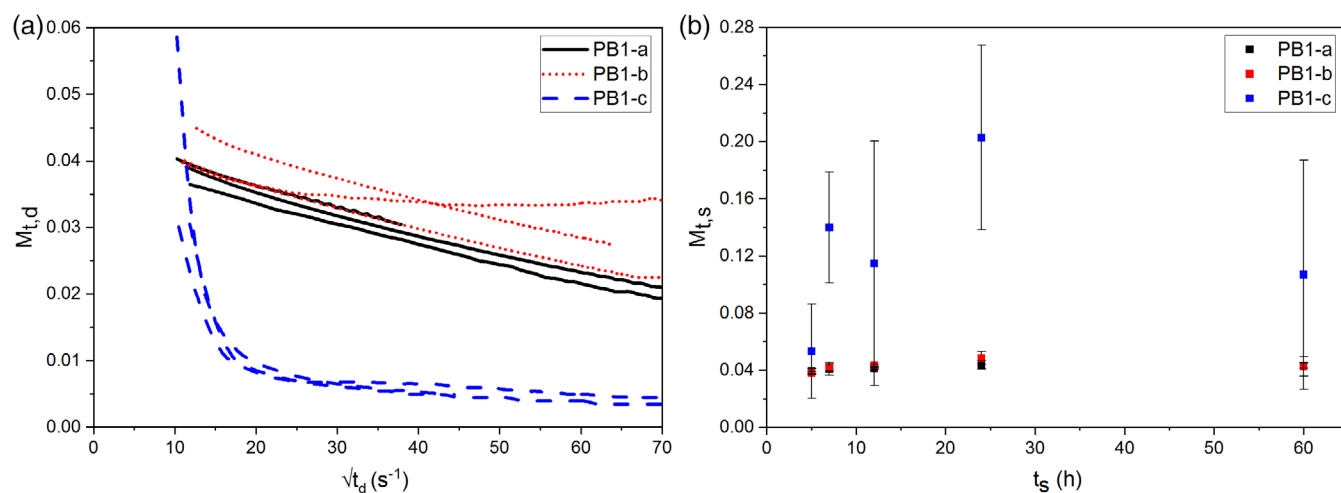


FIGURE 1 (a) Desorption curves after 24 h sorption time (sorption equilibrium reached) and (b) mass uptake versus sorption time [Color figure can be viewed at wileyonlinelibrary.com]

more imprecise than for resins PB1-a and PB1-b, and therefore the higher variability in the results. For a higher precision, an in situ measurement would be required, such as a magnetic suspension balance. The obtained results allow to explain the dimensional stability behavior of the post-extruded foam strands.

3.2 | Foaming behavior

PB1-a and PB1-b produced dimensionally stable foam extrudates. Processing temperature window was narrow in both cases. For resin PB1-a, above 115°C die temperature, rupture of the extrudate's skin and limited expansion could be visually observed, implying low-melt strength to withstand bubble growth above that temperature. The lower operating temperature was found to be 110°C, temperature below which the extrudates would solidify at the die exit. A relatively high-CBA dose was needed to visually obtain a significant volume expansion.

Resin PB1-b presented a slightly wider processing temperature window, with an equivalent behavior than PB1-a on the low end, but the upper temperature could be increased to 120°C, temperature above which gas escape from the extrudate's skin could be visually observed. A higher die swell could be observed with this resin, and its implications covered in Section 4.

The processing window for resin PB1-c was very narrow, limited by the high viscosity on the low end and high-gas diffusivity on the high end. With die temperature from 110°C onwards, gas escaping from the extrudate skin could be visually observed, leading to very low-expansion ratio, and below 100°C high-viscosity prevented processing. Foam extrudates with visually acceptable expansion ratio were obtained with a die

TABLE 2 Rate of CO₂ desorption after different saturation times

t_s (h)	$M_{t,s}$		
	PB1-a	PB1-b	PB1-c
5	0.039 ± 0.002 ^a	0.038 ± 0.001 ^a	0.053 ± 0.033 ^a
7	0.041 ± 0.004 ^a	0.042 ± 0.002 ^a	0.140 ± 0.039 ^a
12	0.041 ± 0.001 ^a	0.043 ± 0.001 ^a	0.115 ± 0.086 ^a
24	0.044 ± 0.003 ^a	0.049 ± 0.005 ^a	0.203 ± 0.065 ^a
60	0.043 ± 0.002 ^a	0.043 ± 0.007 ^a	0.107 ± 0.080 ^a

Abbreviation: PB1, polybutene-1.

^aSD.

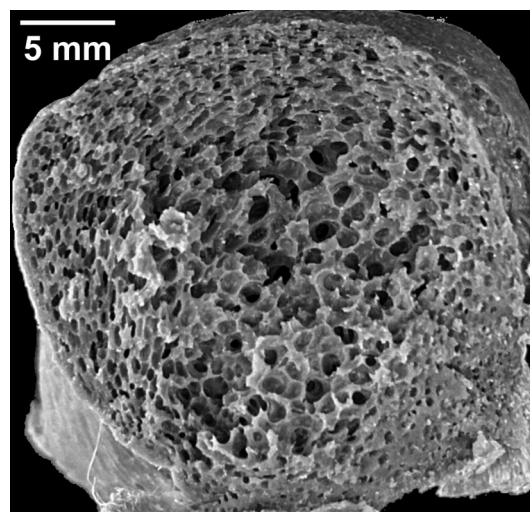


FIGURE 4 Photograph of extrudate section, corresponding to PB1-b, die T = 110°C. PB1, polybutene-1

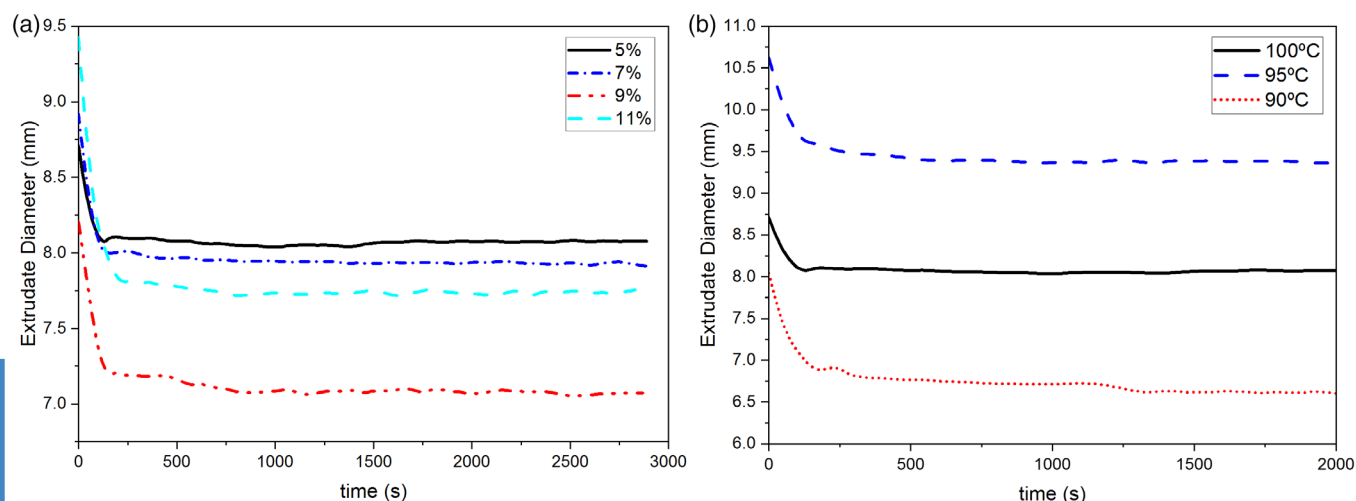


FIGURE 3 Extrudate diameter of PB1-c versus time, for different CBA concentrations at die T = 100°C (a) and 5% CBA and different die T (b). CBA, chemical blowing agent; PB1, polybutene-1 [Color figure can be viewed at wileyonlinelibrary.com]

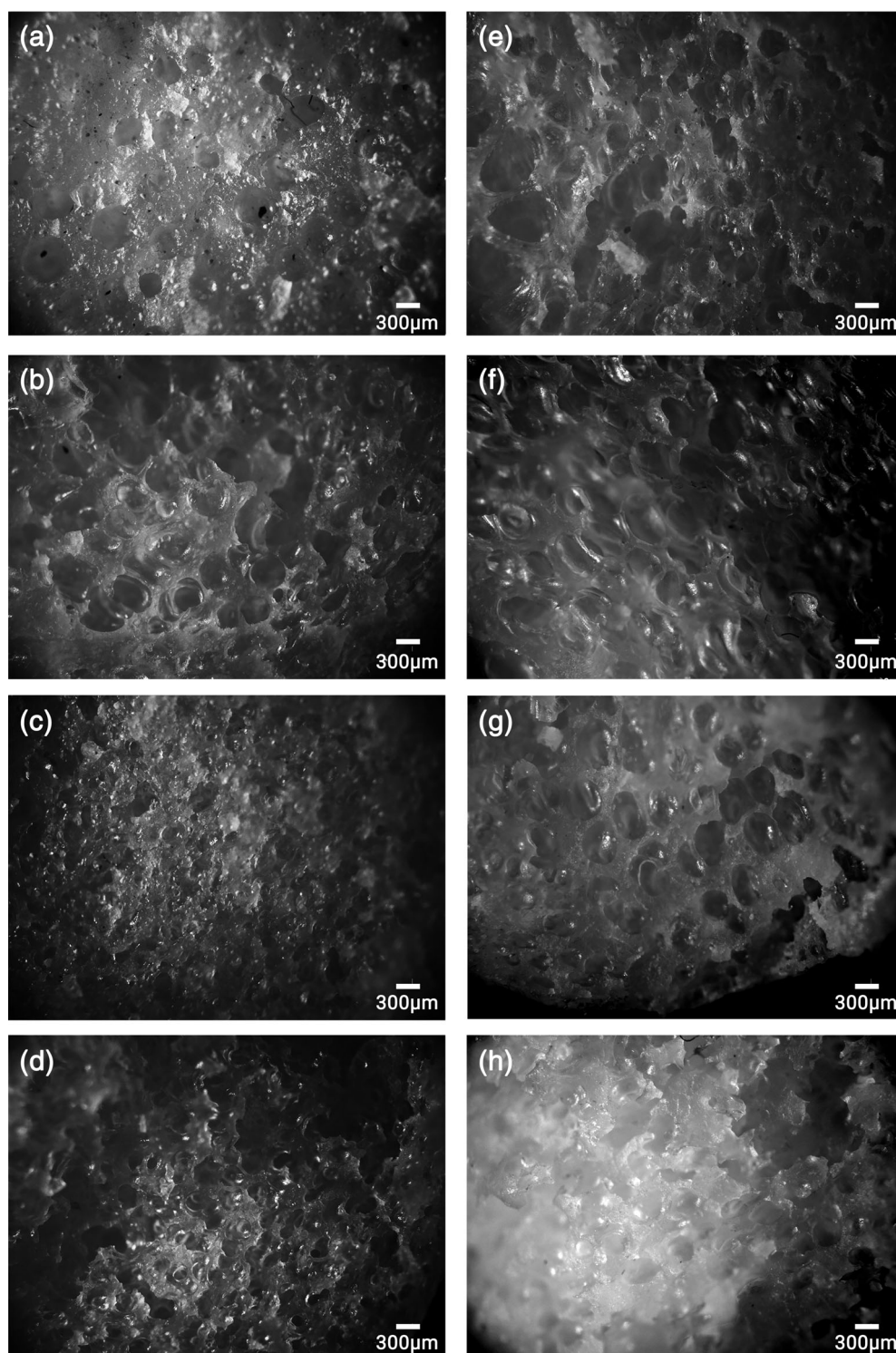


FIGURE 5 Micrographs obtained from PB1-a: (a) die $T = 110^{\circ}\text{C}$ and 4.2% CBA, (b) 7.15%, (c) 8.6%, and (d) 10% CBA; (e) die $T^{\circ} = 115^{\circ}\text{C}$ and 4.2%, (f) 7.15%, (g) 8.6%, (h) 10%. CBA, chemical blowing agent; PB1, polybutene-1

temperature of 100°C . However, severe post-foaming shrinkage was observed. Figure 3 shows the evolution of the diameter width with time after extrusion, for different CBA concentrations at 100°C die temperature (a) and for 5% CBA and different die temperature (b).

As can be seen, most of the shrinkage occurred in the first 2.5 min after foaming, irrespective of the CBA concentration used. This can be directly related to the CO_2

diffusivity of PB1-c, see Figure 2a). Given the poor dimensional stability, this grade was excluded from further characterization.

The foam extrusion of PB1-d was screened with die temperature between 80 and 110°C . Foaming was not achieved, and obtained extrudates presented low viscosity and dimensional stability. Therefore, this grade was excluded from further analysis.

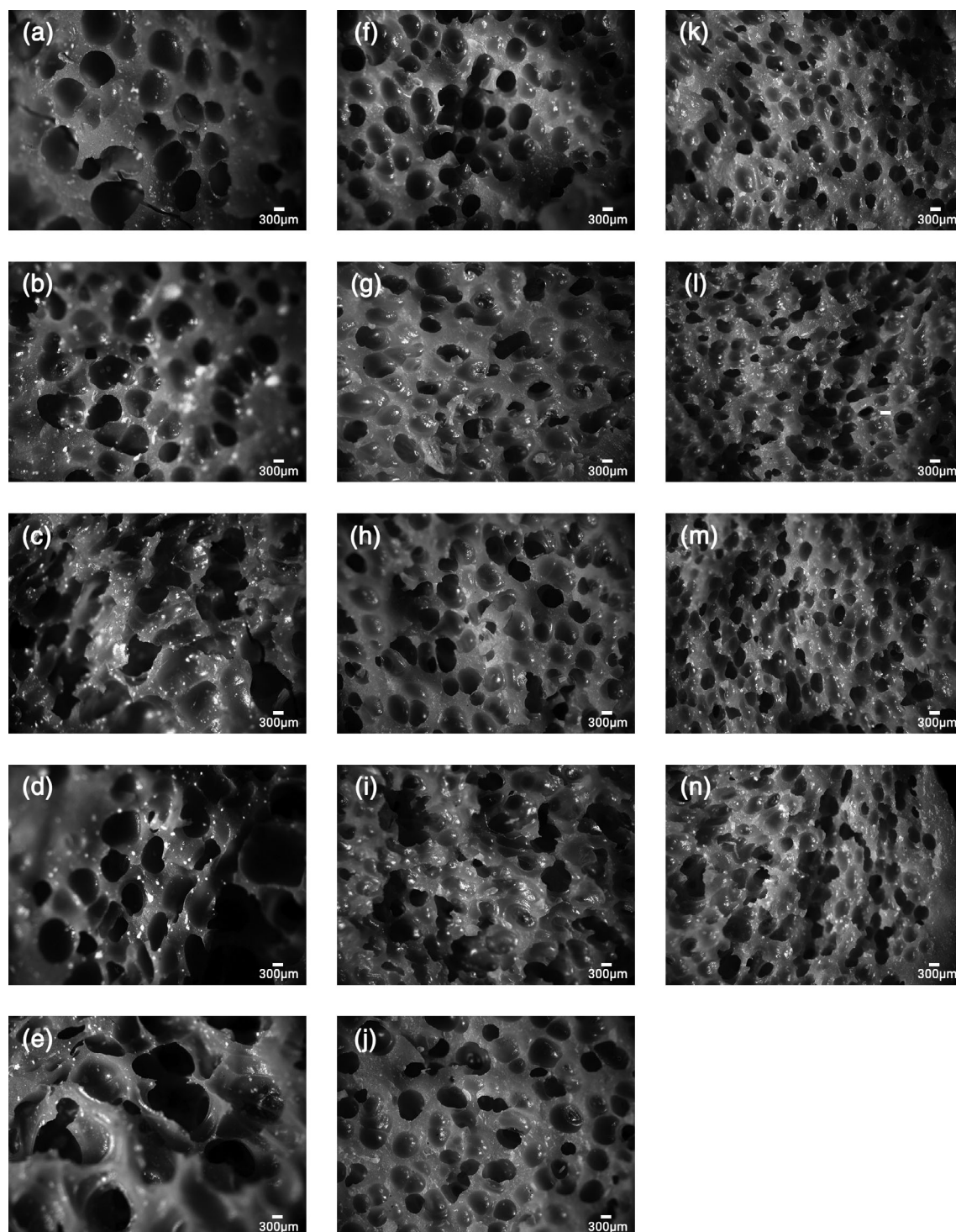


FIGURE 6 Micrographs obtained from PB1-b: (a) die $T = 110^{\circ}\text{C}$ and 2%, (b) 3%, (c) 4.2%, (d) 5.5%, and (e) 7% CBA; (f) die $T^{\circ} = 115^{\circ}\text{C}$ and 2%, (g) 3%, (h) 4.2%, (i) 5.5%, and (j) 7% CBA; and (k) die $T^{\circ} = 120^{\circ}\text{C}$ 2% CBA, (l) 4.2%, (m) 5.5%, and (n) 7% CBA. CBA, chemical blowing agent; PB1, polybutene-1

3.3 | Foam characterization

The obtained foam extrudates present a skin and a gradient in cell size. This is due to the low-die temperatures used, which solidifies the skin and produces a Joule-Thompson

like cooling at the outer surface.⁵⁶ A photograph of an example extrudate section is presented in Figure 4.

Representative micrographs for each process condition for grades PB1-a can be found in Figure 5 and for PB1-b in Figure 6.

The determined volume expansion ratio, cell diameter and cell population density their relation with the process conditions are presented in Figure 7a–c for PB1-a and Figure 7d–f for PB1-b. It should be noted that given the shape irregularity, the reported diameter is the equivalent diameter, defined as the diameter of a circle with the same area as the measured cell area.

The obtained foam densities can be found in Table 3. It should be noted that a CBA is used, for which the effective foaming components amount to 70% weight (wt). Therefore, some mass is added due to the decomposition products, contributing to the density of the obtained foam. The calculated expansion ratio is therefore slightly underestimated.

As can be observed in Figures 5, 6, and 7b,e, foams present large pores with significant cell size variability.

For PB1-a, the two die temperatures set did not produce any difference in the obtained cell size for CBA concentrations of 4.2 and 7.1% wt. Cell size decreased for 8.5% wt as cell population density increased. This inverse relationship is consistent with the reports of previous authors.^{57,58} This effect is particularly notorious for the 110°C die temperature trial, where the average cell size was reduced by more than 50%. After this point N_0 decreased again and cell size increased. This can be explained as the increase of CBA provides more available gas for cell nucleation, until a maximum is reached. With further gas increase and cell growth, cells collide against each other, reducing the number of cells and increasing their size,⁵⁹ as can be observed in the trends of Figure 7b,

c. As for the expansion ratio, as can be seen in Figure 7a); with the die temperature of 110°C, it increased until a maximum and then decreased. This indicated that at this temperature the expansion behavior is governed by the polymer melt's stiffness. The expansion increase with increasing CBA concentration can be related to the plasticization effect of the gas.⁵⁷ After reaching a maximum, the gas starts diffusing out of the polymer's hot skin, leading to a reduced expansion. For the 115°C die temperature series, the maximum expansion was achieved with the lowest concentration of CBA tested, remaining at constant levels until the last CBA concentration tested, of 10%, where the expansion decreased. It can be derived that above that dosage the increased level of gas just increased the diffusion out of the hot skin of the extrudates, thus the volume expansion remained at constant levels. The final expansion reduction together with reduction of N_0 is an indication of cell coalescence.

For PB1-b, the same inverse relationship between cell size and N_0 can be observed. With this resin, foaming could be visually observed at lower CBA doses than for PB1-a. In Table 1 it can be seen that the MFR is lower for PB1-a than for PB1-b. MFR is an indirect measurement of viscosity, being the two parameters inversely proportional. Therefore, this difference could be related to the higher viscosity of PB1-a, requiring higher CBA concentration to achieve expansion. It can be seen in Figure 7f) that the cell population density is in general higher with higher die temperatures. This could be related to reduced stiffness with higher temperatures, which favors cell nucleation and growth.

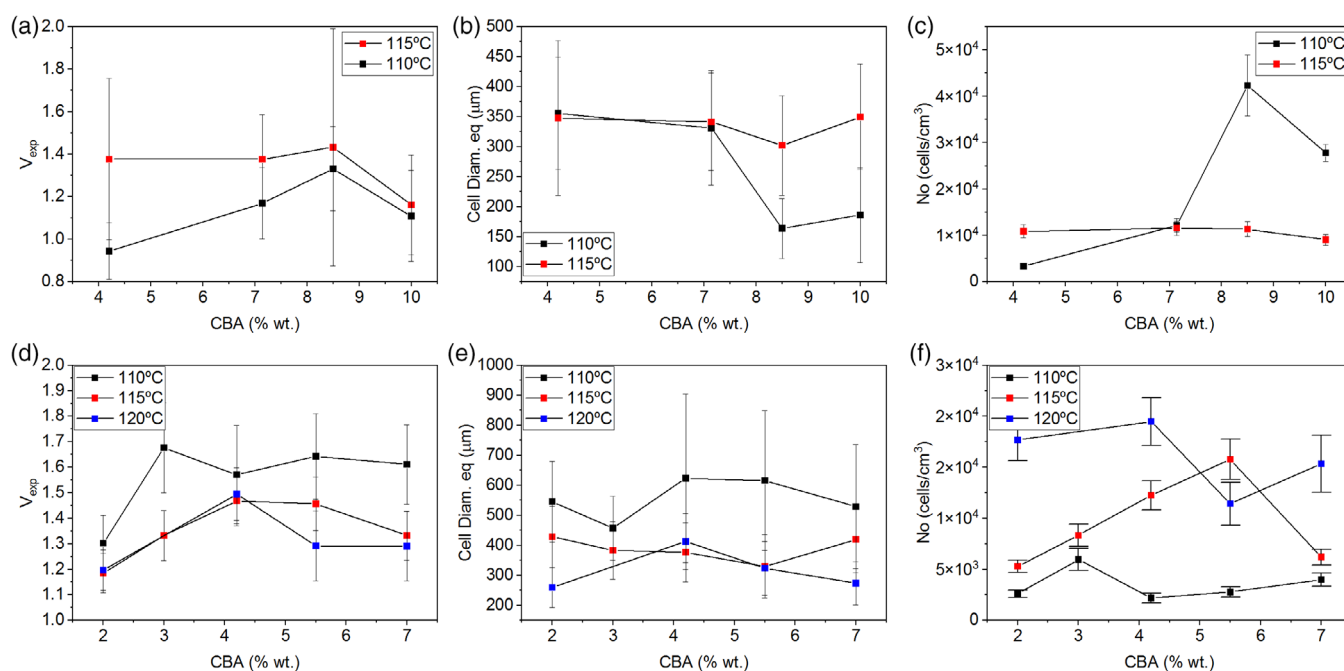


FIGURE 7 Relationship of the processing conditions with volume expansion ratio (a), cell equivalent diameter (b) and cell population density (c) for PB1-a, and same in (d), (e), and (f) for PB1-b. PB1, polybutene-1 [Color figure can be viewed at wileyonlinelibrary.com]

TABLE 3 Density of the obtained foams

	(CBA) % wt	Die T° (°C)	Density (g/cm ³)
PB1-a	4.2	110	0.74 ± 0.03
	7.1	110	0.50 ± 0.02
	8.5	110	0.60 ± 0.03
	10.0	110	0.52 ± 0.03
	11.2	110	0.63 ± 0.09
	4.3	115	0.51 ± 0.12
	7.2	115	0.51 ± 0.04
	8.6	115	0.49 ± 0.18
	10.1	115	0.60 ± 0.09
	PB1-b	2	110
3		110	0.47 ± 0.04
4.2		110	0.50 ± 0.05
5.5		110	0.48 ± 0.03
7		110	0.49 ± 0.03
2		115	0.67 ± 0.01
3		115	0.59 ± 0.02
4.2		115	0.54 ± 0.01
5.5		115	0.54 ± 5.5
7		115	0.59 ± 0.08
2		120	0.60 ± 0.01
4.2		120	0.48 ± 0.01
5.5		120	0.56 ± 0.05
7		120	0.56 ± 0.05

Abbreviations: CBA, chemical blowing agent; PB1, polybutene-1.

TABLE 4 Die swell

	d (cm)	B _{exp}
PB1-a	0.99 ± 0.06	2.48 ± 0.15
PB1-b	1.09 ± 0.06	2.73 ± 0.15

Abbreviation: PB1, polybutene-1.

As for volume expansion ratio, the highest level for this grade is achieved with the lowest die temperature. Expansion ratio is related to both cell size and cell population density. In this case, it can be seen that the volume expansion is driven by a low number of very large cells.

4 | DISCUSSION

4.1 | Effect of resin type in foaming behavior

A very different foaming behavior was found between the four different grades tested. This highlights how a

broad screening of different grades is required in order to assess the foamability of a particular polymer. Of the four grades tested, the two homopolymers PB1-a and PB1-b present better foaming behavior. The thermoplastic elastomer PB1-c failed in terms of dimensional stability, severely suffering from post-foaming shrinkage. This was an identified risk,⁴² related to the rubbery state of PB-1, which was however found in this grade only. From the study of the CO₂ desorption kinetics, it is clear that this shrinkage is related to the high diffusivity, leading to a quick gas escape before the matrix can solidify. Further information on the chain configuration would be required to explain the significantly different desorption kinetics between PB1-c and the two homopolymers. The lower crystalline content (see Table 1) can be pointed out as a contributor toward higher solubility and diffusivity.

The lack of foaming ability of PB1-d can be related to its low viscosity, which hinders the matrix from withstanding the stretching forces required for bubble growth.⁶⁰

A similar volume expansion ratio was achieved with PB1-a and PB1-b. Both grades allowed the foaming of dimensionally stable foam extrudates, which was one of the main research questions of this study. The CO₂ diffusivity has been found equivalent for both resins. PB1-b presents a slightly broader processing temperature window than PB1-a.

For PB1-a, cell size is larger for higher die temperatures. This is consistent with the report of previous authors.⁶¹ Interestingly, for PB1-b, the opposite trend is found, with significantly larger cell sizes obtained with the lower die temperatures. It has been noticed that the die swell of PB1-b is higher than for PB1-a, and higher for lower temperatures, where the die swell B_{exp} is defined as:⁶²

$$B_{\text{exp}} = \frac{d}{d_0}, \quad (4)$$

where d is the measured diameter of the extruded strand and d₀ the diameter of the die.

While for the measurement of the true die swell d should be measured in a complete relaxed strand, requiring some annealing,^{62,63} the measurement of the extruded strand diameters provides qualitative data on the die swell, which can be correlated to the degree of elasticity of different samples.^{63,64} Therefore, we can see that the PB1-b qualitatively presents higher elasticity than PB1-a, and that lower temperatures allow for a higher melt elasticity, which in turn supports the bubble growth. Table 4 presents the comparison of B_{exp} for PB1-a and PB1-b, obtained with a die temperature of 110°C.

The found correlation between die swell and foaming ability is consistent with the observations of previous authors.²⁸ It can be seen how multiple variables affect the foaming process, leading to the complexity of its optimization.

4.2 | Foamability of PB-1 versus other polymers

The foaming processing window for PB-1 has been found narrow. This was expected, as PB-1 presents characteristics which have been previously identified as challenging for foaming, such as (a) linear molecular structure, which typically involves the lack of required extensional viscosity to withstand the stretching forces during bubble growth;⁶⁰ (b) semicrystallinity, which limits the processing window due to crystallization-induced stiffness on the lower temperatures and insufficient melt strength on the higher temperatures⁴² as well as hinders the blowing agent's solubility and diffusivity,^{29,43,65} and (c) rubbery state at room temperature, which facilitates the escape of the gas, impacting on the dimensional stability of the foam.⁴² It should be noted that some of these features can also be used to the advantage of foaming. For example, while crystallization has significant effects both on cell nucleation mechanisms and cell growth,^{29,43} it has been found an effective way to improve the foaming ability of polymers with low-melt strength, as the rigid crystalline structure will help restrict the foam's cell coalescence.⁶⁵ An optimal crystallization degree during processing is needed to ensure the foam has a high expansion ratio and a large cell density, and so knowledge on its kinetics. The closest polymer that PB-1 can relate to is PP, as member of the polyolefin family, semicrystalline, and with a T_g below room temperature. Early research on foaming of PP has found the same hurdles described above^{22,45} related to the low-melt strength of PP. There is a need to find a processing optimum between allowing for bubble growth and preventing gas loss through the extrudate's hot skin. A successful strategy reported is to keep the die temperature as low as possible as to reduce gas loss during expansion,²⁴ in common to the findings of our study, where a lower temperature than the recommended processing temperature was used.

It should be noted that the objective of this study is to assess foamability and identify favorable grades for foaming using available extrusion equipment. Hence, optimization of the process conditions is not in the scope of this work. There is room for improving the obtained foam through modifications of both the resin and the extrusion equipment and process.

Early work estimated that the operable temperature range for producing an acceptable PP foam spanned a mere 4°C,⁶⁶ range which has been confirmed by later authors.⁶⁷ This is narrower than the 10°C found in our study for PB-1. Despite this, successful foaming of PP is reported though the use of branched^{24,57} or linear/branched PP blends,⁶⁸ reduction of the melt temperature and use of high-molecular weight blowing agents for minimizing gas loss during expansion, adaptation of the processing conditions at the die to match crystallization kinetics²⁴ and the use of nanoparticles.^{69,70} Commercial breakthrough has come with the optimization of processing tools, with the use of strand foam extrusion technology.⁷¹ This method involves the use of a breaker plate, a multi-orifice die producing several individual foam strands, which are then pressed together to yield low-density foam sheets.⁷² This enables expanding and stabilizing low-melt strength polymers, and is currently the state-of-the-art technology for commercial PET foam,⁷² for which low-melt strength was for long a hurdle toward successful foaming.^{28,46,73} There are therefore multiple strategies and pathways open for further optimization and successful development of a PB-1 foam.

5 | CONCLUSIONS

The foam extrusion behavior of four commercial grades of PB-1 was evaluated, including a thermoplastic elastomer, two homopolymers and a random copolymer. Very different behaviors were encountered, highlighting the importance of careful screening with different grades. The two homopolymers were successfully foamed, presenting good dimensional stability and achieving cell population densities of up to 10⁴ cells/cm³ and an expansion ratio of up to 1.8. Foamability was hence confirmed and most promising commercial resins identified. An identified challenge is low-melt strength. Possible optimization strategies to increase the expansion ratio include resin rheology improvements, tailoring processing conditions to the crystallization kinetics and optimizing the extrusion equipment, which will be part of future research.

ACKNOWLEDGMENTS

Prof. Ingo Weidlich is kindly thanked for the discussions and advice during the execution of the research and preparation of the manuscript. Xihua Hu and Prof. Irina Smirnova, from the Technical University of Hamburg, are gratefully thanked for making the extruder available. The Hamburg Energy Research Network (EFH) is kindly acknowledged for facilitating the cooperation. The work reported is self-funded by the HafenCity University. Open Access funding enabled and organized by Projekt DEAL.

ORCID

Lucia Doyle  <https://orcid.org/0000-0001-8697-8621>

REFERENCES

- [1] L. R. Lankston, J. A. Wrede, Encapsulated foam for aerospace support applications: Dayton, Ohio, 1964.
- [2] E. S. Weiser, F. F. Baillif, B. W. Grimsley, J. M. Marchello, High Temperature Structural Foam, The NASA Headquarters are located in Washington DC, USA **1997**. <https://ntrs.nasa.gov/citations/20040110267>
- [3] E. S. Weiser, T. F. Johnson, T. L. St Clair, Y. Echigo, H. Kaneshiro, B. W. Grimsley, *High Perform. Polym.* **2000**, *12*, 1.
- [4] H. F. Seibert, *Reinf. Plast.* **2006**, *50*, 44.
- [5] X. Li, Y. Weitsman, *Compos. Part B: Eng.* **2004**, *35*, 451.
- [6] L. Hollaway, P. R. Head, *Advanced Polymer Composites and Polymers in the Civil Infrastructure*, Elsevier Science, Amsterdam, London **2001**.
- [7] H. Tuwair, J. Volz, M. ElGawady, M. Mohamed, K. Chandrashekhara, V. Birman, *Structures* **2016**, *5*, 141.
- [8] A. Manalo, T. Aravinthan, A. Fam, B. Benmokrane, *J. Compos. Constr.* **2017**, *21*, 4016068.
- [9] M. Garrido, J. R. Correia, T. Keller, *Constr. Build. Mater.* **2015**, *76*, 150.
- [10] O. T. Thomsen, *J. Sandwich Struct. Mater.* **2009**, *11*, 7.
- [11] A. Fathi, F. Wolff-Fabris, V. Altstädt, R. Gätzi, *J. Sandwich Struct. Mater.* **2013**, *15*, 487.
- [12] R. Wiltshire Ed., *Advanced District Heating and Cooling (DHC) Systems*, Woodhead Publishing Series in Energy, Sawston, United Kingdom **2016**.
- [13] European Commission (EU), Commission Regulation (EU) 2020/1149 of 3 August 2020 Amending Annex XVII to Regulation (EC) No 1907/2006 of the European Parliament and of the Council Concerning the Registration, Evaluation, Authorisation and Restriction of Chemicals (REACH) as Regards Diisocyanates **2020**.
- [14] J. A. Zapp, *AMA Arch. Ind. Health* **1957**, *15*, 324.
- [15] Montreal Protocol on Substances that Deplete the Ozone Layer: Chapter XXVII 2.a, 1987.
- [16] W. M. Lamberts, *J. Cell. Plast.* **1992**, *28*, 584.
- [17] P. P. Barthelemy, A. Leroy, J. A. Franklin, L. Zipfel, W. Krücke, *J. Cell. Plast.* **1995**, *31*, 513.
- [18] P. Howard, J. Tunkel, *Identification of CFC and HCFC substitutes for blowing polyurethane foam insulation products*. Washington, DC, **1995**.
- [19] Y. Ohara, K. Tanaka, T. Hayashi, H. Tomita, S. Motani, *BCSJ* **2004**, *77*, 599.
- [20] P. Ashford, M. W. Q. Guzman, *J. Cell. Plast.* **2004**, *40*, 255.
- [21] J. Grünwald, P. Parlevliet, V. Altstädt, *J. Thermoplast. Compos. Mater.* **2017**, *30*, 437.
- [22] C. B. Park, L. K. Cheung, *Polym. Eng. Sci.* **1997**, *37*, 1.
- [23] G. J. Nam, J. H. Yoo, J. W. Lee, *J. Appl. Polym. Sci.* **2005**, *96*, 1793.
- [24] H. E. Naguib, C. B. Park, U. Panzer, N. Reichelt, *Polym. Eng. Sci.* **2002**, *42*, 1481.
- [25] G. Petrone, V. D'Alessandro, F. Franco, B. Mace, S. de Rosa, *Compos. Struct.* **2014**, *113*, 362.
- [26] B. Jeong, M. Xanthos, Y. Seo, *J. Cell. Plast.* **2006**, *42*, 165.
- [27] S.-T. Lee, M. Xanthos, S. K. Dey, *Foam Extrusion*, CRC Press, Boca Raton **2014**, p. 506.
- [28] M. Xanthos, Q. Zhang, S. K. Dey, Y. Li, U. Yilmazer, M. O'Shea, *J. Cell. Plast.* **1998**, *34*, 498.
- [29] J. Reignier, R. Gendron, M. F. Champagne, *J. Cell. Plast.* **2007**, *43*, 459.
- [30] E. Di Maio, G. Mensitieri, S. Iannace, L. Nicolais, W. Li, R. W. Flumerfelt, *Polym. Eng. Sci.* **2005**, *45*, 432.
- [31] P. Li, X. Zhu, M. Kong, Y. Lv, Y. Huang, Q. Yang, G. Li, *Int. J. Biol. Macromol.* **2021**, *183*, 222.
- [32] X. Chen, J. Li, A. Pizzi, E. Fredon, C. Gerardin, X. Zhou, G. Du, *Ind. Crops Prod.* **2021**, *168*, 113607.
- [33] X. Ye, A. J. Capezza, V. Gowda, R. T. Olsson, C. Lendel, M. S. Hedenqvist, *Adv. Sustainable Syst.* **2021**, *5*, 2100063.
- [34] M. Nofar, C. B. Park, *Poly lactide Foams: Fundamentals, Manufacturing, and Applications*, William Andrew, Norwich **2017**.
- [35] P. T. Anastas, J. B. Zimmerman, *Environ. Sci. Technol.* **2003**, *37*, 94A.
- [36] M. S. M. Alger, *Polymer Science Dictionary*, Chapman & Hall, London **1997**.
- [37] O. Olabisi, K. Adewale, *Handbook of Thermoplastics*, CRC Press, Boca Raton **2016**.
- [38] G. Bornmann, A. Loeser, *Arch. Toxikol.* **1968**, *23*, 240.
- [39] I. Weidlich, in *Rohrleitungen 1* (Eds: H.-B. Horlacher, U. Helbig), Springer Berlin Heidelberg, Berlin, Heidelberg **2016**, p. 475.
- [40] CEN. EN 253:2020-03, District heating pipes—bonded single pipe systems for directly buried hot water networks—factory made pipe assembly of steel service pipe, polyurethane thermal insulation and a casing of polyethylene; Beuth Verlag GmbH: Berlin.
- [41] CEN. District heating pipes—pre-insulated flexible pipe systems—part 2: Bonded plastic service pipes—requirements and test methods: Brussels, Belgium: **2010**.
- [42] E. Di Maio, E. Kiran, *J. Supercrit. Fluids* **2018**, *134*, 157.
- [43] S. Doroudiani, C. B. Park, M. T. Kortschot, *Polym. Eng. Sci.* **1996**, *36*, 2645.
- [44] L. Doyle, I. Weidlich, Recyclable insulating foams for high temperature applications. In Proc. of The First Int. Conf. on “Green” Polymer Materials **2020**; MDPI: Basel, Switzerland, May 2020–11/25/2020, p 7200.
- [45] H. E. Naguib, C. B. Park, N. Reichelt, *J. Appl. Polym. Sci.* **2004**, *91*, 2661.
- [46] M. Xanthos, S. K. Dey, Q. Zhang, J. Quintans, *J. Cell. Plast.* **2000**, *36*, 102.
- [47] A. R. Berens, G. S. Huvard, in *Supercritical Fluid Science and Technology*, Vol. 406 (Eds: K. P. Johnston, J. M. L. Penninger), American Chemical Society, Washington, DC **1989**, p. 207.
- [48] G. Natta, P. Corradini, I. W. Bassi, *Nuovo Cimento* **1960**, *15*, 52.
- [49] A. T. Jones, *J. Polym. Sci. B Polym. Lett.* **1963**, *1*, 455.
- [50] J. Boor, J. C. Mitchell, *J. Polym. Sci. A Gen. Pap.* **1963**, *1*, 59.
- [51] C. Hadinata, D. Boos, C. Gabriel, E. Wassner, M. Rüllmann, N. Kao, M. Laun, *J. Rheol.* **2007**, *51*, 195.
- [52] J. Crank, G. S. Park Eds., *Diffusion in Polymers*, Academic Press, London **1981**.
- [53] J. Schindelin, I. Arganda-Carreras, E. Frise, V. Kaynig, M. Longair, T. Pietzsch, S. Preibisch, C. Rueden, S. Saalfeld, B. Schmid, J.-Y. Tinevez, D. J. White, V. Hartenstein, K. Eliceiri, P. Tomancak, A. Cardona, *Nat. Methods* **2012**, *9*, 676.
- [54] H. Liu, X. Wang, W. Liu, B. Liu, H. Zhou, W. Wang, *Cell. Polym.* **2014**, *33*, 189.

- [55] S. Takahashi, J. C. Hassler, E. Kiran, *J. Supercrit. Fluids* **2012**, 72, 278.
- [56] M. T. Ngo, J. S. Dickmann, J. C. Hassler, E. Kiran, *J. Supercrit. Fluids* **2016**, 109, 1.
- [57] W. Kaewmesri, P. C. Lee, C. B. Park, J. Pumchusak, *J. Cell. Plast.* **2006**, 42, 405.
- [58] E. Laguna-Gutierrez, J. Escudero, V. Kumar, M. A. Rodriguez-Perez, *J. Cell. Plast.* **2018**, 54, 257.
- [59] L. M. Matuana, O. Faruk, C. A. Diaz, *Bioresour. Technol.* **2009**, 100, 5947.
- [60] S.-T. Lee, B. P. Chul, *Foam Extrusion*, Taylor & Francis Inc, Bosa Roca **2014**.
- [61] E. Kiran, *J. Supercrit. Fluids* **2010**, 54, 296.
- [62] L. A. Utracki, Z. Bakerdjian, M. R. Kamal, *J. Appl. Polym. Sci.* **1975**, 19, 481.
- [63] H. Münstedt, *Int. Polym. Process.* **2018**, 33, 594.
- [64] M. Xanthos, V. Tan, A. Ponnusamy, *Polym. Eng. Sci.* **1997**, 37, 1102.
- [65] P. Gong, S. Zhai, R. Lee, C. Zhao, P. Buahom, G. Li, C. B. Park, *Ind. Eng. Chem. Res.* **2018**, 57, 5464.
- [66] J. G. Burt, *J. Cell. Plast.* **1978**, 14, 341.
- [67] Z.-M. Xu, X.-L. Jiang, T. Liu, G.-H. Hu, L. Zhao, Z.-N. Zhu, W.-K. Yuan, *J. Supercrit. Fluids* **2007**, 41, 299.
- [68] P. Spitael, C. W. Macosko, *Polym. Eng. Sci.* **2004**, 44, 2090.
- [69] M. Antunes, J. I. Velasco, V. Realinho, E. Solórzano, *Polym. Eng. Sci.* **2009**, 49, 2400.
- [70] J. Zhao, Q. Zhao, C. Wang, B. Guo, C. B. Park, G. Wang, *Mater. Des.* **2017**, 131, 1.
- [71] C. P. Parky, G. A. Garcia, *J. Cell. Plast.* **2002**, 38, 219.
- [72] A. Farthi, *Mechanical Properties of Strand PET Foams at Different Length Scales*, Universität Bayreuth, Bayreuth **2018**. <https://epub.uni-bayreuth.de/4286/>.
- [73] L. Di Maio, I. Coccorullo, S. Montesano, L. Incarnato, *Macromol. Symp.* **2005**, 228, 185.

How to cite this article: L. Doyle, *J. Appl. Polym. Sci.* **2022**, 139(12), e51816. <https://doi.org/10.1002/app.51816>



Review

Developing Insulating Polymeric Foams: Strategies and Research Needs from a Circular Economy Perspective

Lucia Doyle ^{1,*} , Ingo Weidlich ¹ and Ernesto Di Maio ²

¹ Technical Infrastructure Management, HafenCity University, 20457 Hamburg, Germany

² Dipartimento di Ingegneria Chimica, dei Materiali e della Produzione Industriale, University of Naples Federico II, 80138 Naples, Italy

* Correspondence: lucia.doyle@hcu-hamburg.de

Abstract: Insulating polymeric foams have an important role to play in increasing energy efficiency and therefore contributing to combating climate change. Their development in recent years has been driven towards the reduction of thermal conductivity and achievement of the required mechanical properties as main targets towards sustainability. This perception of sustainability has overseen the choice of raw materials, which are often toxic, or has placed research efforts on optimizing one constituent while the other necessary reactants remain hazardous. The transition to the circular economy requires a holistic understanding of sustainability and a shift in design methodology and the resulting research focus. This paper identifies research needs and possible strategies for polymeric foam development compatible with Circular Product Design and Green Engineering, based on an extensive literature review. Identified research needs include material characterization of a broader spectrum of polymer melt–gas solutions, ageing behavior, tailoring of the polymer chains, detailed understanding and modeling of the effects of shear on cell nucleation, and the upscaling of processing tools allowing for high and defined pressure drop rates.

Keywords: insulation; polymer; foaming; circular economy; cradle2cradle; green engineering; circular design



Citation: Doyle, L.; Weidlich, I.; Di Maio, E. Developing Insulating Polymeric Foams: Strategies and Research Needs from a Circular Economy Perspective. *Materials* **2022**, *15*, 6212. <https://doi.org/10.3390/ma15186212>

Academic Editors: Volker Altstädt and Merve Aksit

Received: 20 July 2022

Accepted: 2 September 2022

Published: 7 September 2022

Publisher's Note: MDPI stays neutral with regard to jurisdictional claims in published maps and institutional affiliations.



Copyright: © 2022 by the authors. Licensee MDPI, Basel, Switzerland. This article is an open access article distributed under the terms and conditions of the Creative Commons Attribution (CC BY) license (<https://creativecommons.org/licenses/by/4.0/>).

1. Introduction

Insulation materials are covered by the European Eco-design Directive [1]. Eco-design, from the design process standpoint, can be referred to as a relative approach. It “starts with the present state of affairs and identifies existing problems, which people subsequently attempt to solve” [2]. Although bringing improvement, this approach has been criticized for limiting the search for truly sustainable innovations, as it only proposes optimizations from what is existing [3]. The focus of this relative approach is ‘not the good, but the less bad’ [4]. Eco-design strives for a wide implementation of insulation materials, seeking energy efficiency. Under the assumption that ‘the major environmental impacts of insulation lie in the environmental benefits it provides during the use phase’ [5], research has been driven by the objective of reducing thermal conductivity and matching the required mechanical properties as the only viewpoint, assuming that this is sustainable as such.

This has led, for example, to the selection of chlorofluorocarbon (CFC) first and flammable hydrocarbons (i.e., pentane) at present as blowing agents [6], as they present lower thermal conductivity than other inert gases, while at the same time increasing the need for flame retardants, which are often toxic and hinder the later recycling of the material [7]. Another paradoxical example could be the research efforts placed on green polyurethane foams by deriving polyols from vegetable oils, such as palm [8–10], rapeseed [11], soybean [12,13] and linseed [14,15], while diisocyanates are still required for the polyurethanes’ synthesis, which are classified as suspected of causing cancer, as dermal and respiratory sensitizers, for acute toxicity following inhalation, as well as eye, skin and respiratory irritants [16] and have recently been restricted [17].

The Circular Economy (CE) is gaining momentum. Increasing focus on the development of circular buildings [18–20] and infrastructure [21–24] requires the availability of circular materials and products. The availability of circular, sustainable and recyclable insulation materials is reported to be particularly lacking [18], which shows the need for research and development in this direction. The fundamental distinctions between circular product design versus eco-design have been the focus of methodological research [3]. Circular Product Design requires a holistic approach to ‘closing the loop’ of product life cycles by extracting the maximum value of all raw materials and widespread recycling and reuse [25]. However, recycling and reuse can be hampered by the presence of certain chemicals because of technical barriers or because of their hazardous nature. Moving toward the CE will require a paradigm shift in the way things are produced, i.e., using less additives and eliminating toxic chemicals to enable mainstream recycling.

This paper takes the Cradle-to-Cradle framework [4] and will use the 12 Principles of Green Engineering [26] and the Inertia Principle [27] as guidelines to measure the fulfillment of Circular Design, as detailed in Section 2. Although sustainability and environmental concerns have supported different research lines in polymeric foaming, such as the elimination of CFCs [28–31], the use of inert gases as blowing agents [32–36], the foaming of thermoplastic materials [32,37–39], biobased [40–42] or biodegradable [33,43,44], and this typically involves only one aspect of the foam developed, and none of these works considers or consistently applies the principles of Green Engineering or Cradle to Cradle.

Reviews of the literature on recent trends in polymer foaming, including knowledge gaps, have been published in recent years [45–47]. These works provide a general overview of the state of the art and current technical challenges. The novelty of this work is that it presents a broad screening of the literature through a Circular Design filter, to answer the following questions: how can polymeric foams be developed while consistently applying the Cradle to Cradle framework? Which research gaps need to be addressed? The recycling possibilities of traditional polymeric foams is out of the scope of this paper.

2. Designing for the Circular Economy

As to develop an insulating foam that meets the requirements of the circular economy, the definition and criteria for this fulfillment need to be established.

The concept of CE is fed by different schools of thought, and a description of them can be found in [48]. This section summarizes the essential concepts and applicability of the selected frameworks and principles, which are Cradle to Cradle [4], the 12 Principles of Green Engineering [26] and The Inertia Principle [27]. In this paper, the term Cradle to Cradle design and circular product design will be used indistinctly. It should be stressed that Cradle to Cradle is here referred to as the design methodology, and not to the scope or boundaries of a Life Cycle Assessment (LCA). LCA is a tool for the assessment of environmental impacts associated with established products or processes, while this paper and the Cradle to Cradle design methodology is concerned with the design and development of products and processes. Discussions on the similarities and differences can be found in [49].

2.1. The Performance Economy and the Inertia Principle

With the objective of decoupling growth from resource consumption, the Performance Economy [27] proposes business models based on trading performance instead of goods. Through such business models, the internalization of waste costs is achieved and resource efficiency is rewarded. Walter Stahler introduced a guiding principle for circular design with the Inertia Principle: “Do not repair what is not broken, do not remanufacture something that can be repaired, do not recycle a product that can be remanufactured. Replace or treat only the smallest possible part to maintain the existing economic value of the technical system” [27]. The aim of the Inertia Principle is to maintain the integrity of the product for as long as possible, minimizing the environmental costs of the required processes to restore the economic value of the product. Transferring the concept to polymeric foams would

prioritize thermoplastic foams over chemically recyclable foams, for example, as a lower level of recycling is needed.

2.2. Cradle-to-Cradle Design

The cradle-to-cradle (C2C) design [4] antagonizes current recycling in that it starts from the beginning (design for recycling), rather than the current end-of-pipe approach (what to do with waste). It proposes a new approach towards sustainable design based on the intelligence of natural systems.

Three main tenets are proposed:

- Waste equals food;
- Use of current solar income;
- Celebrate diversity.

The first tenet brings the notion that waste is a human based concept, and by replicating nature, materials should be designed as nutrients that flow through the biological or technical cycle.

In the biological cycle, biobased materials would be used and composted after their lifecycle, serving as nutrients for crops to grow and allow the circular production of new biobased materials. The technical cycle is a closed-loop system in which non-harmful, valuable synthetic and mineral materials flow in manufacturing, use, recovery, and remanufacture cycles. This definition implies no preference for bio or non-bio materials, as long as they are fully recyclable and non-harmful. An important issue is to keep separate the biological and technical cycles, to enable the correct flow of materials. Hybrid bio/technical materials which cannot be later separated impeach their later recovery, as they cannot be composted nor technically recycled. This provides a first design criterion. Material safety plays a central role and is a fundamental criterion in the design. The second tenet sets renewable energy as a source to power any C2C product or process, as nature uses photosynthesis. Thus, by keeping materials in the circular economy and powering cycles with renewable energy, the number of cycles a product or process is subjected to would be irrelevant from the environmental impact perspective. However, the fact that today 100% renewable energy is not yet available to all, and the choice of energy source supply for i.e., manufacturing facility is not always in the scope of the engineer's work is a source of criticism towards the broad applicability of the framework [50]. The third tenet encourages to tailor designs to maximize their positive effects on the particular niche in which they will be implemented, or in McDonough and Braungart's words, ecoeffectivity vs. ecoefficiency.

2.3. The 12 Principles of Green Engineering

The 12 principles of Green Engineering [26] provide a guideline for scientists and engineers aiming to design new materials, products, processes, and systems that are benign to human health and the environment. The principles are envisaged for broad applicability, from the construction of chemical compounds to urban architecture. Some examples include 'designers need to strive to ensure that all material and energy inputs and outputs are as inherently nonhazardous as possible' (Principle 1), 'system components should be output pulled rather than input pushed through the use of energy and materials' (Principle 5), and 'multicomponent products should strive for material unification to promote disassembly and value retention' (Principle 9). In the context of polymer foaming, the application of Principle 1 would support the need to phase out polyurethane due to the toxicity of diisocyanates.

The application of Principle 5 can be exemplified using shear forces to promote cell nucleation, where the presence of high shear would "pull" the gas phase out of the solid cavity [51], as will be discussed in Section 4.3. Principle 9 aims to minimize the use of additives. For the full list of principles and their details, the reader is referred to Anastas and Zimmerman [26].

As stated by the authors of both frameworks [52], the C2C vision sets the course for 'what do I do?' while the 12 Principles of Green Engineering answer "How do I do it?" In

this sense, they will be used to define the research needs for developing insulating foams for the circular economy.

3. Methods

The objective of this paper is to identify the research needs and potential strategies for polymeric foam development from a circular economy perspective, where the meaning of a circular economy perspective is fulfilling the criteria described in Section 2. Data were retrieved through a literature search. As search engines, Google Scholar, Google Patents, and Espacenet were used. Used key words included foaming, polymeric foam, foamable, AND recyclable, recycled, thermoplastic, environmentally friendly, sustainable, high temperature, thermally stable, and insulation. Screened documents included peer reviewed journal articles, books and handbooks, dissertations, project reports, and patents. Relevant references identified in the evaluated pieces of literature were additionally included for completeness.

The retrieved literature was screened and the data were sorted to answer the following questions:

- What characteristics does a polymer need to have for successful foaming?
- Which are the main morphology–properties relationships of cellular plastics and the link to processing conditions?
- Which strategies can be followed to use these relationships and what research needs to arise when developing insulating polymeric foams according to circular product design?

Data collection, screening, and sorting was conducted in the period 2019–2022.

4. Results

The properties of polymeric foams are related to the properties of the polymer matrix and to the foam morphology, which in turn is connected to the relative density and the geometric structure of the foam [53]. At the same time, the final foam morphology itself is conditioned by the selection of polymer, blowing agent, and expansion techniques [6,54]. Developing a foam with target properties involves the selection of raw materials, process conditions, and foaming tooling and technology. The following sections evaluate each of these aspects and the research needs arising from them when following Circular Product Design.

4.1. Selection of Raw Materials: Need for Material Characterization

Material selection plays a central role, as it defines the properties of the final product and at the same time their nonhazardous and recyclable nature are at the heart of C2C design. The fulfillment of the full recyclability criteria implies no preference between bio-based or non-bio-based materials. A recent review comparing LCAs of fossil based and bio-based polymers found it was not possible to conclusively declare any polymer type as having the least environmental impact in any category [55]. Therefore, they will not be discussed separately in this paper. While the use of different additives is common in foaming, such as cell stabilizers [56–58], flame retardants [56,58,59], nucleating agents [32,58,59], and fillers [60,61], material diversity should be minimized to facilitate the later recycling of the product.

In line with the Inertia Principle [27], thermoplastics would be preferred to thermosets, as they retain greater product integrity, followed by chemically recyclable polymers. In line with the 12 principles of Green Engineering [26], the non-hazardous nature of the materials should be placed first. The requirement to replace commonly used foams because of their non-recyclability or hazardous nature of raw materials triggers the need for alternative foaming polymers. Insulating foams are often part of multi-functional sandwich structures. The application of circular product design to the complete structure may trigger the interest to foam particular polymers to match the other material layers [62]. However, the foamability performance assessment is not trivial. When comparing resin properties, PET can be expected to provide superior mechanical and thermal performance as well as

improved chemical and flame resistance than PS [63], leading to a reduction of additives requirement. However, PET has long been a challenge in foaming, related to its low melt strength [54,64,65]. Likewise, the IR-absorbing characteristics of PLA arising from the ester group anticipate it to have better insulating performance than PS foam [36], but its foaming has again been found to be problematic, due to its low melt strength [40]. Polybutene-1's high heat deflection temperature [66] and low thermal conductivity of 0.114 W/mK [67] make it a great candidate for insulation where heat resistance is required, such as district heating pipes. However, its foamability is only recently being explored [62].

The basic principles of foaming can be found in the literature [6,35,45,68] and involve the sorption of the blowing agent into the polymer matrix under pressure, and the nucleation and growth of bubbles, which can be induced through a reduction in pressure or an increase in temperature. There is mass transport from the blowing agent in the polymer–gas solution to the bubbles, which ends with the vitrification or crystallization of the polymer. This last stage is critical for the success of the foaming process, as it stabilizes the cellular structure. A schematic illustration of the process is presented in Figure 1. Delayed or slow vitrification or crystallization may result in a too large extensional elongation of the cell walls, resulting in cell wall rupture and coalescence.

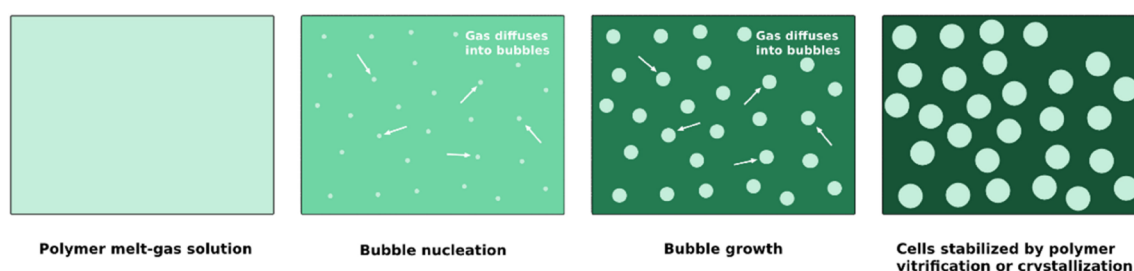


Figure 1. Cell nucleation, growth, and stabilization.

Blowing agents are a necessary constituent of polymeric foams. They may be divided into chemical (CBA) or physical blowing agents (PBA). Physical blowing agents are generally preferred for lower density foams, while CBAs are preferred for high- and medium-density foams [6,64]. Within PBA, chlorofluorocarbons (CFC), hydrochlorofluorocarbons (HCFC), hydrofluorocarbons (HFC), hydrocarbons (HC), and inert gases (N_2 , CO_2) have been used [6]. Before the mid-1980s, CFCs were preferred due to their soluble, volatile, and nontoxic nature [6]. However, their ozone depleting nature is well known, and the Montreal Protocol signed in 1987 [69] called for the phase out of their manufacturing and use, initially causing a shift to transition replacement HCFCs, and later to HFCs. These are now called to phase out due to their high global warming potential (GWP) by the Kigali Amendment to the Montreal Protocol [70] in force from 1 January 2019. The phase-out program is represented in Figure 2.

Today, hydrocarbons, despite flammable in nature, are the blowing agent of choice for extrusion foaming of insulating foams [6]. This flammable nature is a hazard [71,72], and typically requires further adding flame retardants, which are often toxic themselves [7]. Therefore, focus should be placed on the use of inert gases. There is currently increased interest in the use of CO_2 as a blowing agent due to the mentioned safety and environmental reasons, as well as cost considerations [36,43,73,74]. The main drawback of its use is its higher diffusivity than that of long-chain hydrocarbons such as pentane, which affects the maximum expansion ratio achievable [32], the thermal aging of the foam [75], and can cause post-foaming shrinkage [72,76,77]. Strategies to overcome this will be discussed in Section 4.2.2. An alternative is the use of hydrofluoroolefines (HFO), labeled 4th generation blowing agents or refrigerants [78,79]. The main advantage of these blowing agents is their very low global warming potential [79–81], ozone depletion potential [79,81], and flammability [79], while presenting thermal conductivity similar to that of HFCs [82]. They also have a low photochemical ozone creation potential [80]. This has motivated

their proposal [81,83] and evaluation [78,80,84] as blowing agents for polymer foaming, including PU [78,81,83], HDPE [81,83], PBT [81], phenolic resins [81], PP [81,83], PS [81,83], PTFE [81], PVC [81], PET [83] and cellulose acetate [84]. However, the toxicity of HFO is conflictive and depends on the particular HFO in question [80,85,86]. Some are reported to be toxic, such as HFO-1225 [85], while limited information prevents a conclusive statement for others, such as HFO-1234yf, which undergoes atmospheric degradation producing trifluoroacetic acid (TFA) [86]. There is reportedly no clear evidence of any HFO molecule being toxicologically innocuous [85]. Thus, further research on the use of HFOs as blowing agents for polymer foaming cannot be recommended.

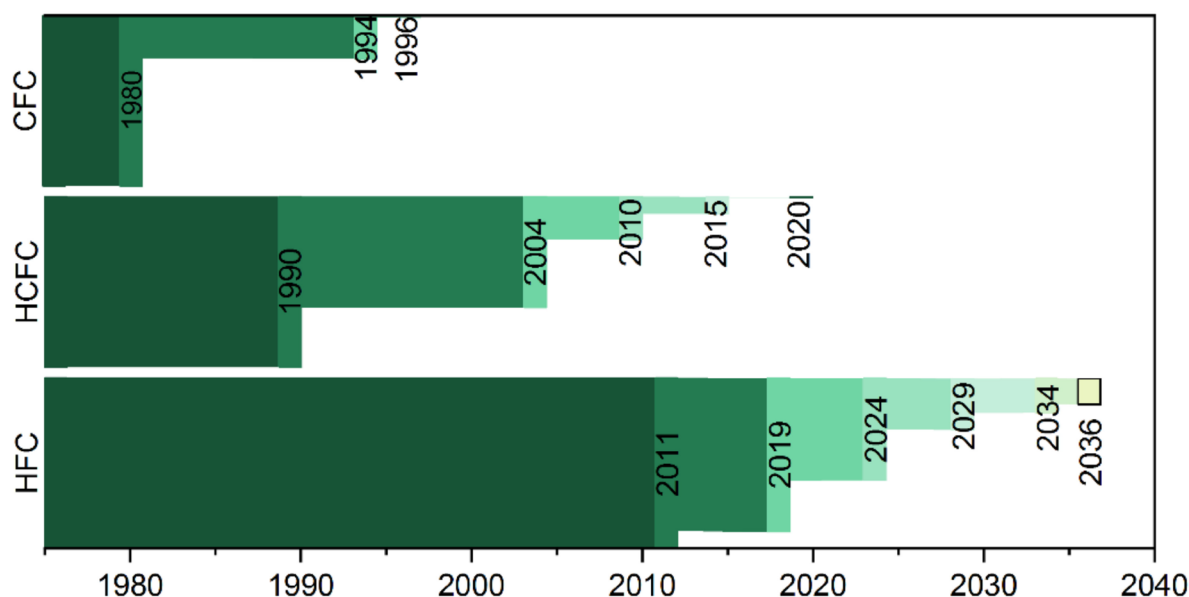


Figure 2. Sankey diagram representing blowing agents phase out for non-article 5 countries (industrialized) agreed in the Montreal Protocol and Kigali amendment.

The changes experienced and overcome by the foaming industry in the past 30 years demonstrate how a shift towards a more sustainable design and manufacturing of polymeric foams is possible when the right framework and R&D investments are in place. Since the number of inert gases is small and known, as for research needs concerning PBA, inert gases solubility and diffusivity in different polymer matrixes, the rheology of the polymer melt–gas solution and processing parameters can be cited and will be further discussed in the following section.

Chemical blowing agents are solid or liquid materials which decompose under certain conditions generating vapors [87]. An overview of the different blowing agents and their mechanisms of action can be found in [81]. In terms of Circular Economy, the innocuousness of the agent as well as of its decomposition products is a main selection criterion. Some of the solid residues from the decomposition of CBAs such as 5-Phenyltetrazol, azodicarbonamide or hydrazides are hazardous [88] and hence make these compounds ineligible. The CBA's masterbatch carrier should be compatible with the polymer matrix. Since it is typically impossible to use the same polymer as the matrix and master batch carrier, to eliminate the risk of decomposition during production [88], using CBA's involves polymer blending to some extent, and its impact on later recycling options, should be explored.

Concerning the polymer, the foamability of polymers is strongly related to their rheological behavior [74,89,90]. Characteristics commonly reported as required for successful foaming include high melt strength to withstand the elongational stresses acting during the bubble growth phase [32,33,40,64,65,91,92] and strain hardening as an enhancement of melt strength, contributing to the success of cell stabilization [43,89,90,93,94] and widening the processing window [90]. Strain hardening behavior would contribute to successful

foaming when it occurs at the strain rates relevant to the foaming process [95], which are reported to be between 1 and 5 s⁻¹ [74], although it has been suggested that the quantitative increase in the achieved expansion ratio might not remain when the process is scaled-up from laboratory to production scale [96]. Other important aspects include the size of the processing window, which is found between the melting temperature (T_m) and the crystallization temperature (T_c) for semicrystalline polymers or the glass transition temperature (T_g) for the case of amorphous polymers [45,97]. The processing window is schematically represented in Figure 3. It has recently been reported that the crystallization rate and processing window could be of higher importance towards the consecution of low-density foams with fine morphology [98].

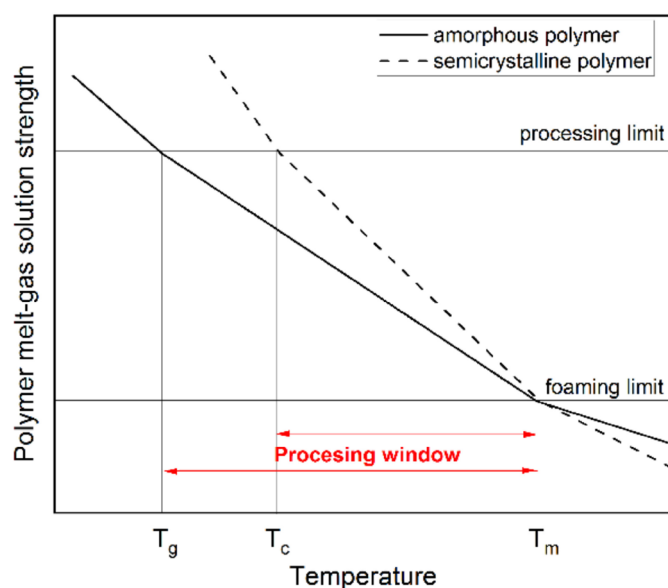


Figure 3. Schematic representation of the foaming processing window for semicrystalline and amorphous polymers, adapted from [6].

However, data on the extensional rheology of polymer melts are not readily available for all polymers [74].

Basic research is needed in polymer rheology characterization, to increase knowledge and widen the choice of foamable polymers. However, while the rheology of the polymer melt provides good starting information, the foaming process is determined by the rheology of the polymer melt–gas solution [74,99]. It is well known that the dissolution of the blowing agent can cause a plasticization effect on the polymer matrix [43,97,100,101], which results in depressing the T_g and T_m . During bubble growth, a rapid viscosity increase can occur as the gas dissolved in the melt diffuses into the cells if the processing temperature is in the vicinity of the glass transition temperature of an amorphous polymer [43,100]. In semicrystalline polymers, this is more complex, as the increase in free volume has an impact not only on the crystallization temperature but also on its kinetics [43]. The crystallization kinetics and T_c have been established as relevant factors for the foamability of semicrystalline polymers [43], and the knowledge of crystallization kinetics under the presence of blowing agent is pointed out as a knowledge gap to overcome for successful foaming optimization of each polymer–gas system under study [36]. It has significant effects both on cell nucleation mechanisms and cell growth [43,102], as well as on the cell stabilization step [36]. The semi-crystalline nature involves a sudden transition from a low viscosity material above the crystalline melting temperature (T_c) to a high viscosity polymer below the T_c [63]. This leads to a narrower processing window than for amorphous polymers.

Moreover, the gas does not dissolve in the crystals, resulting in lower gas solubility [36,43,102,103].

However, crystallization can also improve the foaming of low melt strength polymers by restricting cell coalescence [36], as schematically represented in Figure 4. An optimal crystallization degree during processing is needed to ensure that the foam has a high expansion ratio and a considerable cell density.

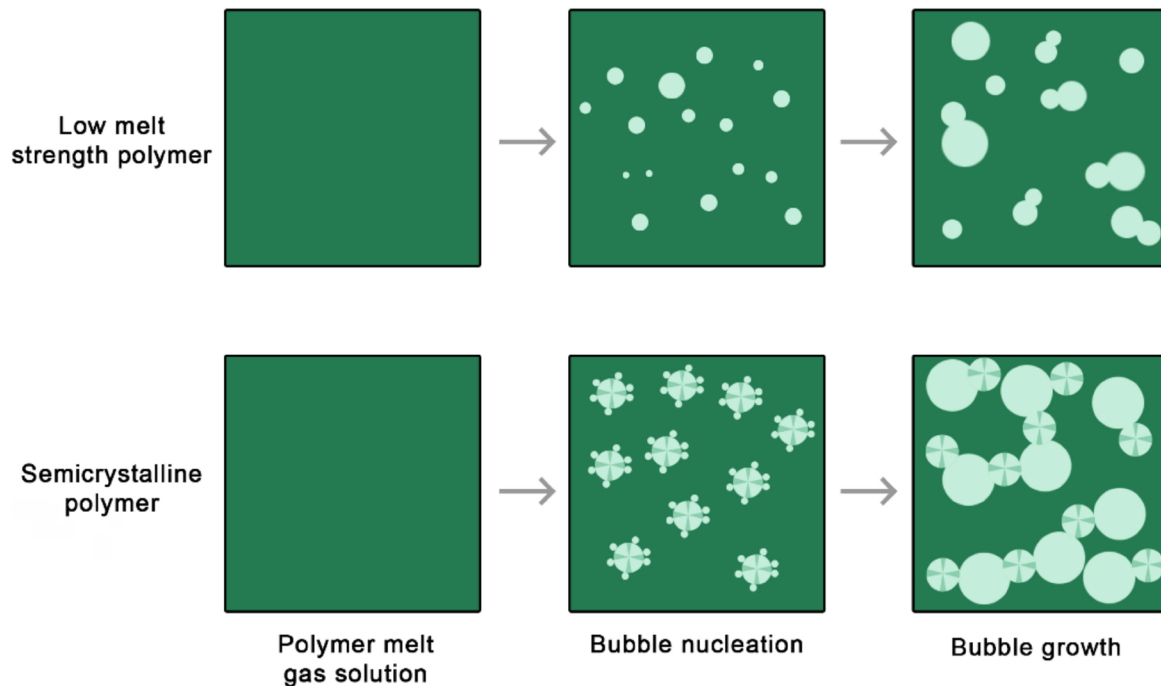


Figure 4. Low melt strength polymers do not yield foams with suitable morphology due to cell coalescence (**top** scheme). Crystal formation during the foaming of semicrystalline polymers can restrict cell coalescence (**bottom** scheme).

Lastly, the solubility and diffusivity of the gas in the melt [104] and the interfacial tension [45] condition the nucleation of the bubbles and the growth rate, hence the morphology of the foam [43,54]. The surface tension of a polymer–gas solution is lower than that of the pure polymer and intimately related to the gas concentration and polymer–gas system [33]. These data are not commonly available. For the case of extrusion foaming, the solubility limit at the given processing conditions marks the maximum mass of the blowing agent that can be added, to ensure a complete mixing and dissolution into the polymer, which would otherwise lead to premature bubble formation and inhomogeneous foam morphology [105]. This highlights the importance of determining the solubility of the blowing agent in the polymer at different pressures and temperatures.

Looking into the foam’s application, the characterization of the ageing of the foam is vital to confirm the fulfilment of the required properties during the required service life, which for insulation products spans decades. This reaches a further dimension from the circular economy perspective, as the different product lifecycle stages should be considered. While crystallinity challenges the foam processing, it could have positive consequences concerning the ageing of the foam, since the crystalline regions create a more restrictive pathway for the diffusing molecules, hence decreasing the diffusivity of the blowing agent [102] out of the cells. Together with the permeability, it can play a major role on the ageing of the thermal properties of the insulating foam. The thermal conductivity of a foam (λ_{foam}) is the sum of the thermal conductivity due to conduction in the polymer matrix (λ_{pol}), the thermal conductivity due to conduction in the gas (λ_{gas}) and the thermal conductivity due to radiation (λ_{rad}) [106,107]:

$$\lambda_{foam}(t) = \lambda_{gas}(t) + \lambda_{pol} + \lambda_{rad} \quad (1)$$

The contribution of convection is typically disregarded as it is reported to only occur when the cell size exceeds a few millimeters, with references stating the threshold at 3 mm [108], 4 mm [109] or 5 mm [110], the temperature is low, or the temperature gradient is very high [111]. Since the composition of the cell gas changes over time as the blowing agent diffuses out of the foam and ambient air diffuses in, so does the thermal conductivity of the foam. For reference, $\lambda_{\text{cyclopentane}} = 0.0110 \text{ W/mK}$, $\lambda_{\text{CO}_2} = 0.0165 \text{ W/mK}$ and $\lambda_{\text{N}_2} = 0.0258 \text{ W/mK}$, as compiled in [87].

Mangs [106] studied the ageing of the insulating capacity of PET and PU foams and determined the effective diffusion coefficients of CO_2 , N_2 and O_2 in PET and PU foams, and concluded they are 10 to 30 times lower in the PET foam, in the temperature range studied from 23 to 90 °C. This leads to a 10-times slower decrease in insulation capacity for PET than for PU foam [106]. Consistent with this, Ref. [111] reported effective diffusion coefficients of oxygen, nitrogen, and carbon dioxide in PET foams approximately 5–15 times lower than those in PU foam. With these data, a typical district heating pipe insulated with PU and a 3 mm polyethylene casing of dimensions DN 40/125 would decrease its insulation capacity by 16% after 30 years, while a pipe with PET foam with the same dimensions and a 1 mm PET casing would see a decrease of 3% [111]. Therefore, while the initial thermal conductivity of PET foam is higher than that of PU, associated with a larger cell size [106,111], the difference may be offset over time, as conceptually illustrated in Figure 5.

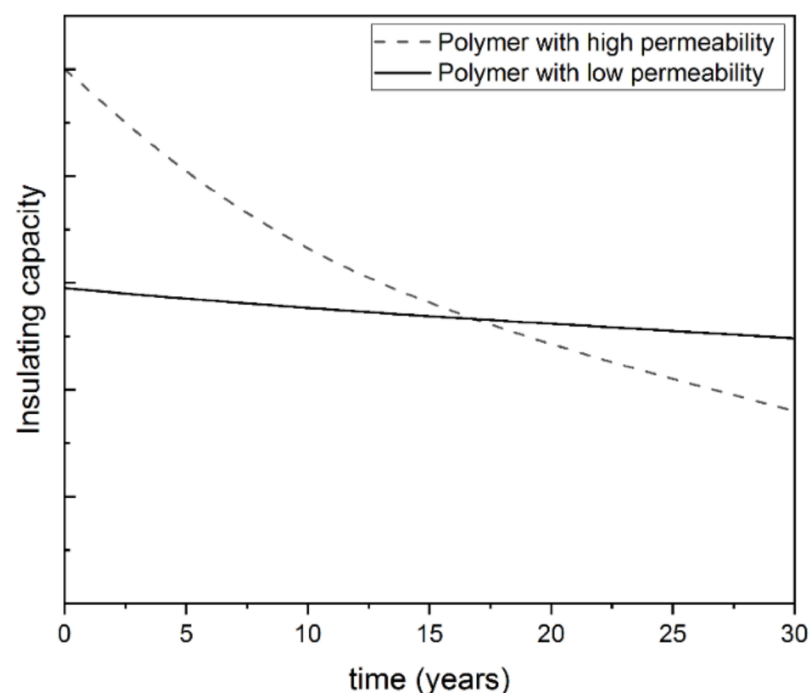


Figure 5. Conceptual representation of the long-term insulating capacity of foams depending on the permeability of the polymer.

Crystallinity can also be used to modify the mechanical properties and heat resistance of the produced foams. There is a strong relation between heat resistance and crystallinity of a material, since the crystalline regions could sustain the material stiffness past its T_g [112]. Modifications in crystallinity could be introduced during resin manufacturing. However, the foaming process itself can enhance crystallinity, due to the free volume allowed by the dissolved blowing agent and the biaxial stretching during bubble growth. This is reported to allow PLA foams to have a higher crystallinity than neat PLA, and consequently a higher temperature resistance [40]. Thermal annealing is also possible in some cases. In this line, an increase in the compression strength of PET foam of up to 130% at 100 °C has been obtained after an overnight temperature soak at that temperature [113], which extends the service temperature of the foam past its T_g .

In summary, all non-toxic and recyclable polymers and gases would meet the C2C criteria. The need to replace widely used foams based on hazardous or non-recyclable raw materials, or the integration of foams in multifunctional sandwich structures, triggers the need for foaming alternative polymers. Characterization data on (i) polymer melt–gas systems, including extensional rheology, solubility and diffusivity of the gas in the melt, superficial tension, plasticization effects, and crystallization kinetics, are required to assess foamability and optimize foaming, and (ii) ageing of foams, to assess their service life and benchmark foams according to their entire lifecycle, are not always available for polymers and polymer melt–gas systems which have not yet been foamed. Research on material characterization is needed to broaden the choice of foamable polymers.

4.2. Optimization of Polymer Foamability

The previous section discussed that the foamability of many polymers remains to be explored. Nevertheless, it is recognizable that the foaming of the most easily-foamed polymers has been achieved. However, how can properties equivalent to state-of-the-art polymeric foams be achieved, based on materials that are already ‘second choice’ in their foaming abilities? In this section, strategies to overcome the most commonly reported challenges are revised.

4.2.1. Overcoming Poor Melt Strength

As compiled in the previous section, the lack of suitable melt rheology is a common challenge. Melt rheology can generally be modified by additives [64,114], changes in molecular weight and molecular weight distribution [64,90] and cross-linking, either chemically [115–118] or by electron beam irradiation [119–121]. Extensive cross-linking turns the matrix into a thermoset, conditioning its recyclability [115]. Again, additive minimization is desired to facilitate broad recyclability. Therefore, the focus of this review is placed on modification of the polymer and processing:

- Reactive extrusion: branching and chain extending.

Branching polymers have been reported to have better foaming properties, as branches contribute to melt strain hardening as they prevent the macromolecules to disentangle at the same rate as exponential deformation during the bubble growth phase [74,94,122]. Therefore, resin rheology is reported to be improved through reactive branching or chain extension, resulting in successful foaming [58,65,122,123], adding branching agents or chain extenders during the extrusion process [54,122,124]. It may be argued that adding branching and chain extending agents is additivation, and modification of the matrix would complicate the later polymer sorting and recycling. There is a thin line between additives and reactants that could lead to a definitions debate. However, C2C does strive for tailor-made design in contraposition to “one-size-fits-all” through its Celebrate Diversity tenate [4] (see Section 2.2). At the same time, it should be highlighted that, even in thermoplastics, successive washing and reprocessing cycles lead to polymer degradation and chain scissoring, as well documentation for the case of PET [125,126]. Endless recycling in a fully closed loop cannot be achieved in practical terms. Therefore, reactive branching and chain extending can also be used to improve the rheology and allow the use of recycled resins.

However, care must be taken in the design and material selection for the branching process. As reported in [63], relatively high concentrations of the unreacted branching agent often remain in the final product, which may restrict certain uses or compromise its long-term stability. A certain level of cross linking may occur by using chain extenders [127], and its impact towards successive recycling loops needs to be assessed. Toxic chemicals like diisocyanates have been explored as chain extenders for PLA [128–131], overturning environmental benefit claims on the developed material, stemming from its bio-based and bio-degradable nature. Pyromellitic dianhydride, which has been found to successfully improve the rheology of PET and recycled PET as a chain extender [132–134], has recently been reported to be suspected of causing occupational asthma [135].

Chain extending and branching through reactive extrusion have been found a successful technique to improve the melt strength and enable successful foaming of polymers. Research and development efforts are required to identify and/or develop nontoxic chain extenders and branching agents:

- Improving foamability properties during the resin manufacturing phase.

With the knowledge on resin properties required for successful foaming, optimization could be conducted during the resin manufacturing phase, which will later reduce the need for additives. The development of high melt strength polypropylene (HMS-PP) has been an area of great industrial research activity in recent years and has enabled its foaming [32,89,136,137]. The better foam morphology obtained with HMS branched PP vs. linear PP can be visualized in Figure 6. Linear HMS-PP has been developed for foaming [138] but most HMS-PP arise from the addition of long branches, produced through gamma irradiation [139], Ziegler-Natta [140] or metallocene catalysis [141,142]. Metallocene catalysts [56] are promising to tailor the resin structure to fit foaming processes, as they allow better control on the monomer and molecular weight distribution [143,144]. Metallocene catalysts not only can allow for custom design and engineering of new polymeric materials but also offer environmental benefits as they allow for producing polyolefins with milder process conditions, do not contain toxic heavy metals, and the additional chemicals and compounds used for their heterogenization are chemically inert [144].

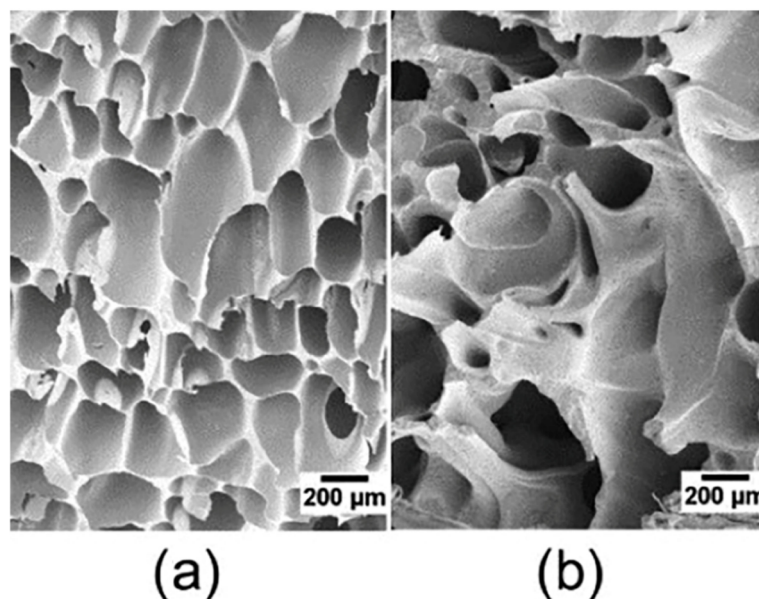


Figure 6. Foams produced with long-chain branched PP (a) and linear PP (b) under the same foaming conditions, reproduced from [89] with permission from Wiley.

The development of HMS-PP was demand driven, given the interest of foaming PP. Cited properties that justify this interest include higher rigidity compared to other polyolefins [89,136], higher strength than PE [32,136], superior impact strength compared to PS [32,136], higher service temperature range and good temperature stability [89] compared to PE and PS [32,136], and competitive material cost [32]. Interest in foaming other polymers may grow, sparked by the need to replace a material for environmental or regulatory aspects, as in the case of PU, or as a result of broader availability of properties data (Section 4.1). As the uptake of circular product design increases, another driver would be to match the foam's polymer with other material layers within sandwich structures [62].

It is expected that demand will drive the tailoring of resin properties as they become the focus of foaming research:

- Optimizing the processing tools.

Another strategy to overcome the low melt strength is the optimization of the processing tools. A success story is strand foam extrusion technology [139]. A multi-orifice die that produces several individual foam strands is used. These are then pressed together to yield low-density foam sheets, as represented in Figure 7. This tooling facilitates expanding and stabilizing low-melt strength polymers, allowed the development and commercialization of PP foam plank products [137] and is currently the state-of-the-art technology for commercial PET foam [145].

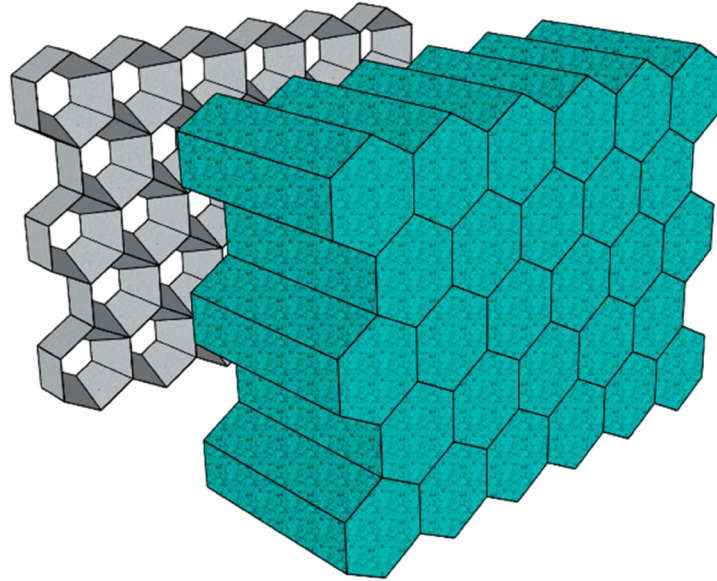


Figure 7. Collided foam strands exiting a multi-orifice die.

Optimization of processing tools is an effective strategy to advance polymer foaming. Significant research efforts are needed in this area, for example for the manufacturing of nanocellular foams.

4.2.2. Processing Strategies towards Cell Stabilization

Having addressed the melt strength optimization to support the bubble growth, the next stage for allowing successful foaming would be to support and optimize the cell stabilization step and dimensional stability of the obtained foam. CO₂ is a suitable blowing agent given its high solubility and produced plasticization, which allows to foam at lower temperatures and supports the stabilization step when the plasticization is lost upon desorption [45]. However, the shrinkage and collapse of the cellular structure of the resulting foams due to its high diffusivity in the hot polymer matrix are problematic, in particular with low rigidity [71,72] and elastomeric [76,77] polymers. A long-established strategy to overcome this has been the use of long chain hydrocarbons as blowing agents [57,136]. Long chain blowing agents have low volatility resulting in low diffusivity [138], while CO₂ has a higher diffusivity related to its smaller molecular size [146]. This slower gas diffusion contributes to a better control of the cell stabilization step. The flammable nature of these blowing agents [71,72] and the consecutive need for flame retardants trigger the need to move towards inert gases, as discussed in Section 4.1. Another common procedure is the addition of surfactants and permeability modifiers [56,57], examples of which are stearic acid amide, glycol monostearate, and glycine fatty acids [56]. Given the criteria to avoid the use of additives, a processing strategy to prevent or minimize gas escape is to reduce the temperature, thereby reducing the diffusivity [147]. Freezing extrudate skin by lowering the die temperature has been reported as a successful strategy to prevent gas escape and stabilize cell structure [136,148]. In a batch foaming study [33], reduction of saturation pressure is suggested as a strategy to prevent cell collapse due to gas escape. However, this comes together with a lower pressure drop rate, which has been identified as a parameter

that correlates with cell density [149]; therefore, a compromise between the two needs to be found.

A study on the effect of confined foaming of rubbery elastomers in a mold vs. free foaming with CO₂ has recently been published [76]. It concluded that, through confined foaming with permeable molds, dimensionally stable foams could be obtained with a higher cell uniformity but also density than in the case of free foaming. With impermeable molds, dimensionally stable foams with higher expansions could be achieved due to the restriction of the gas escape. However, post expansion and relaxation could occur after removal from the mold in some cases.

CO₂-N₂ mixtures have been reported to be used to tailor and optimize the resulting foam microstructure [33] and avoid post-foaming shrinkage while still using inert gases only [72,77], as a synergetic effect is achieved between cell nucleation enhanced by CO₂ solubility and minimized shrinkage due to lower diffusivity of N₂.

A novel proposed anti-shrinkage strategy is to reduce ambient pressure during the post-foaming ageing phase [77] to counterbalance the decrease in pressure inside foam cells due to CO₂ escape, as schematically represented in Figure 8. This is an excellent example of how creative use of physical and processing parameters can be used to avoid the use of additives or hazardous raw materials. The work [77] also modelled the effect of cell shape on the shrinkage, concluding that circular cells present better dimensional stability, followed by hexagonal and last square shaped cells. This would also be an interesting strategy, although the obtention of particular cell shapes in practical terms remains a challenge.

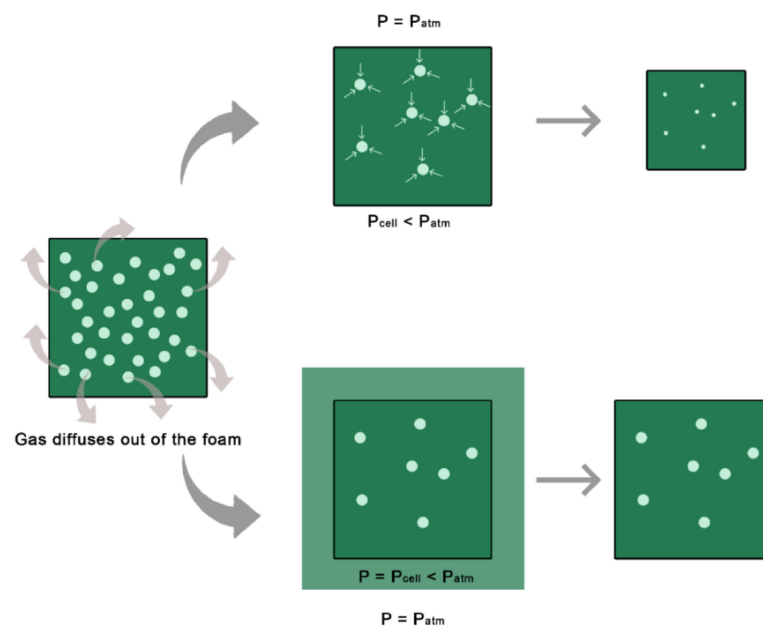


Figure 8. Negative pressure created within the cells as the gas diffused from the hot skin of the foam (top scheme). Lowering ambient pressure during the post-foaming ageing phase could counterbalance the pressure decrease inside the cells and prevent shrinkage.

Identified strategies to control the dimensional stability of cellular structures compatible with CE include optimizing the foaming pressure and temperature, reducing ambient pressure during post-foaming, and the use of molds. The impact of these strategies on the obtained foam morphology and skin formation and optimization and potential trade-offs between the different parameters in play need to be assessed and adjusted for each practical case.

4.3. Tailoring Properties through Foam Processing and Cellular Structure

The cellular structure has a decisive influence on the thermal and mechanical properties of foams [53,108]. The foam morphology is characterized by cell size, shape and

population density, cell size variability, existence and morphology of skin and foam bulk density, all of which are function of the selected polymer–gas system, the processing parameters and the processing tools.

As for thermal properties, the different contributors to the foam's effective thermal conductivity were presented in Equation (1). After considering the physical properties of the foam's raw materials, the thermal conductivity can be modified through the cell morphology as it affects the thermal radiation. It is influenced by both the cell size and cell shape.

Concerning the shape, increasing the cell isotropy is reported to reduce thermal conductivity, related to effects of polymer chain alignments in anisotropic foams [150]. Differently, a reduction of the thermal conductivity from 0.035 W/mK to 0.025 W/mK was achieved through the production of very elongated cells, with an aspect ratio ideally larger than 2 [151]. This highly anisotropic cellular structure was achieved through the choice of a multi-hole die geometry and high pulling speed during the extrusion process, together with a high melt strength resin [151].

The reduction of the cell size contributes to favorable insulating properties of the foam in different ways. On one hand, small cell size slows the diffusion of the blowing agent out of the foam [33], reducing the thermal aging of the foam with time. On the other hand, reducing the cell size has been experimentally proven as an effective way to reduce thermal conductivity of polymeric foams [150,152] irrespective of the blowing agent [153], and related to the radiative heat transfer within the foam [154]. This is explained by the higher number of reflections occurring in foams with smaller cell size [53]. This however no longer holds for highly expanded nanocellular foams, as the thin cell walls and struts may become highly transparent to thermal radiation, not being able to attenuate it [155,156]. An optimum between volume expansion and cell size needs to be reached to minimize thermal conductivity in cellular nanocellular foams [155]. A quantitative step forwards to reducing thermal conductivity would be by using the Knudsen effect, which would be achieved when the gas molecules do not interact with each other but collide with the molecules of the surrounding solid, reducing the energy transfer through the gas molecules [157]. That is, when cell size is comparable or smaller than the mean free path of the gas [107,158]. This has been demonstrated to occur in nanocellular polymeric foams, with cell diameter <700 nm [159]. While research on the foaming of nanocellular polymers is ongoing [159,160], so is the understanding of their structure–properties relationships. The effect of the cell size distribution on the thermal conductivity of nanocellular foams has been recently modelled [161], highlighting the interest on bimodal structures. This is because, while nanometric cells reduce the conductivity through the gas phase, microcellular pores reduce the conduction through the solid phase.

The cellular structure not only affects the thermal properties but also the mechanical ones, which is key in many multifunctional applications of cellular plastics. Early work by Gibson and Ashby [162] modeled the cell as a cube and related the Young's modulus (E) to the relative density of the foam and the E of the cell wall material. Modeling the mechanical behavior of foams has been progressively refined to adjust the cell shape to that of a Kelvin cell [163], account for cell anisotropy [164,165], account for cell size in addition to relative density [166] and, with the use of Laguerre tessellation models, variation of cell size and cell wall thickness [167]. These models are represented in Figure 9.

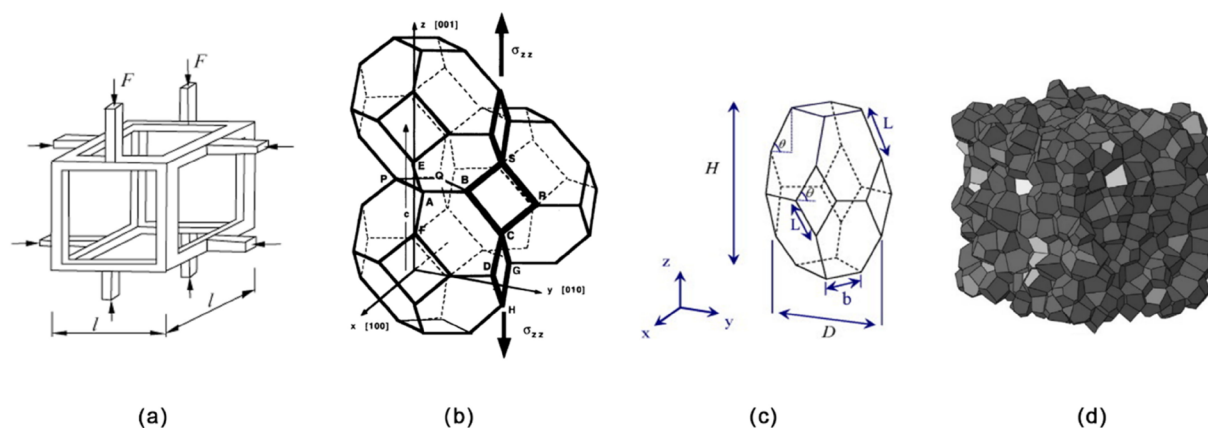


Figure 9. (a) Cube cell model, reproduced from [162] with permission; (b) Kelvin cell model, reproduced from [163] with permission; (c) Kelvin cell model, which accounts for cell anisotropy, reproduced from [165] with permission; (d) Laguerre tessellation model of a foam, reproduced from [167] with permission.

These models provide the indication that E scales with relative density [53], decreases with increasing cell size and variability of cell wall thickness [167], and can be maintained constant while reducing density if cell size is reduced [166]. In this line, a breakthrough in the mechanical properties of polymeric foams came with the development of microcellular foams pioneered at MIT during the 1980s [168–170]. They refer to those with cell size in the order of $10\ \mu\text{m}$ and a cell population density of the order of $10^8\ \text{cells}/\text{cm}^3$. Their development was aimed at reducing the amount of polymer used in mass produced products, as well as their transportation costs. The impact strength of the foams was found to be increased by 6 to 7 times versus that of solid polymers of the same linear dimensions, related to improved craze initiation and crack blunting [171], and appeared to have higher specific strength and improved fatigue life [170]. It appears clear that the reduction of the cell size results in improved mechanical and insulating performance of polymeric foams, and should be a design target. The nucleation step is key for the achievement of large numbers of small cells and as such has been the focus of research since early stages of microcellular foaming. According to classical nucleation theory, two mechanisms are possible for a second phase nucleation in a primary phase: homogeneous nucleation, which would occur when a second component reaches a critical amount, forming a stable second phase, or heterogeneous nucleation, when a third phase is formed in the interphase of two other phases [172], such as an additive in a polymer matrix. The activation energy for heterogeneous nucleation is lower, resulting in the earlier nucleation of heterogeneously nucleated bubbles than of homogeneously nucleated bubbles [173]. The number of nucleated bubbles is a function of the concentration of heterogeneous nucleation sites and their relative effect on the nucleation activation energy [173]. Additives can enhance nucleation by providing the presence of an interface, but also by reducing the surface tension of the polymer [174]. With additive minimization in the focus of this article, homogeneous nucleation can be enhanced by increasing the pressure drop, the driving force for bubble nucleation, as can be recognized from the following general expression for nucleation rate (N) [33]:

$$N = M \cdot B \exp \left[-\frac{16\pi\sigma^3}{3k_B T (P_v - P_L)^2} \right] \quad (2)$$

where M and B are increasing functions of the gas concentration and of the gas diffusivity, respectively. k_B is the Boltzmann constant, and P_v and P_L are the equilibrium gas pressure and the pressure in the liquid phase.

This effect is clearly observed in [175]. By modifying the foaming pressure drop, polybutene-1 foams with similar density were produced, but with very different microstructure: cell size reduction by a factor of 1/6 and cell population density increase by a factor 66 were achieved by increasing the foaming pressure from 50 to 100 bars. This is illustrated by the two micrographs in Figure 10.

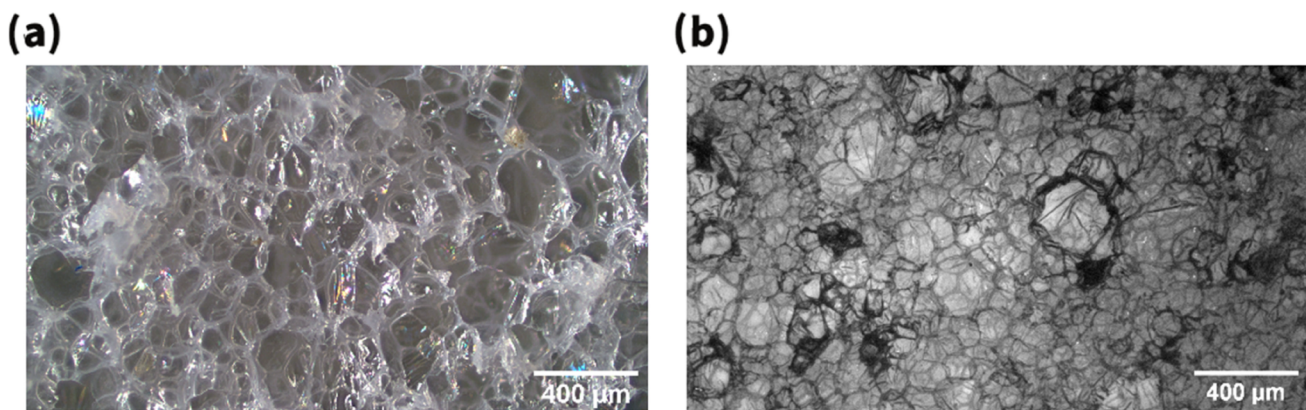


Figure 10. PB-1 foam obtained with a P drop of 49 bar (a) and of 99 bar (b).

A further parameter that affects the thermodynamic instability driving bubble nucleation is the pressure drop rate, as first proposed by Park et al. [149]. It affects the competition between cell nucleation and growth because the gas that contributes to cell growth is minimized by maximizing the pressure drop rate. The fundamental role of the pressure drop rate in the density of polymeric foam cell population has been confirmed by later authors [176], and efforts have been made to explore and understand the boundary conditions under which the number of nucleated cells can increase with increasing pressure drop rate. Using a miniature batch foaming apparatus that achieves pressure drop rates of up to 500 MPa/s [177], Tammaro et al. [178] report that the density of the cell population increases linearly with the pressure drop rate on a bi-logarithmic scale. Studies on the effect of maximizing the pressure drop rate have typically been carried out in batch apparatus [176,177,179], and R&D efforts are needed to expand the technology for commercial foam manufacturing under these process conditions.

A further parameter that plays a role in cell nucleation is the effect of shear forces in the melt, which occur at the die in an extrusion process. These forces have been reported to promote nucleation and are interpreted through a cavity model, where the presence of high shear would “pull” the gas phase out of the solid cavity [51]. They are found to have a greater impact on cell nucleation than the pressure drop rate, with particular relevance at low saturation pressures, when the pressure drop is an insufficient driving force [51,180]. This can be observed in Figure 11.

Although more recent studies generally confirm these observations [181], in this review of the literature, no mechanistic or phenomenological model has been found relating shear to cell nucleation.

A more comprehensive understanding of the mechanism is needed to fully use this parameter in morphology optimization. Acting shear forces are related to the polymer melt–gas solution rheology, highlighting the need for characterization data as presented in Section 4.1.

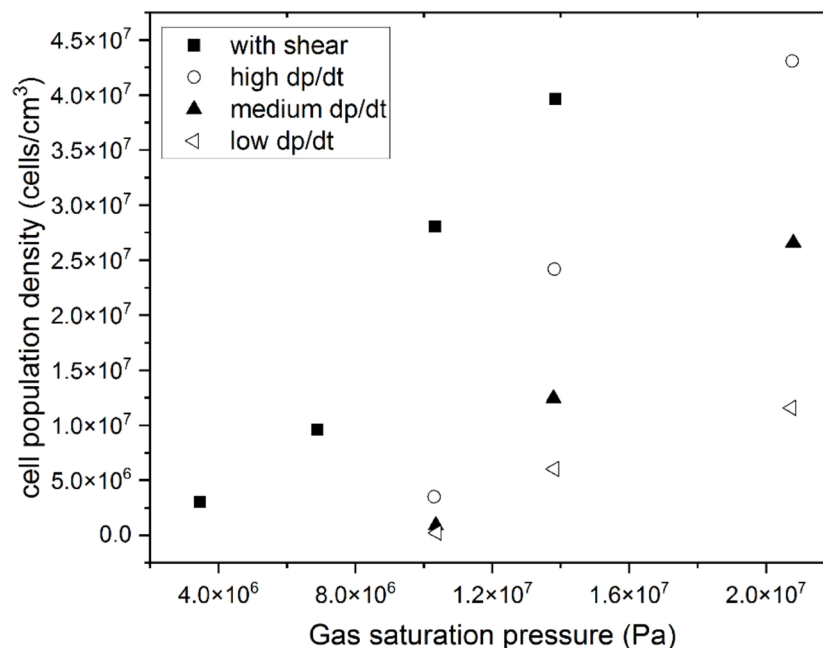


Figure 11. Cell population density as a function of gas saturation for HDPE foamed with different pressure drop rates and the application of shear [180].

Mechanical and thermal properties of polymeric foams are generally improved with the reduction of cell size, and can be tuned through cell size variability. Pressure drop rate and acting shear have been confirmed as processing parameters that contribute to the obtention of microcells, by promoting cell nucleation. Research is needed for a more detailed understanding of the effects of shear on cell nucleation. R&D efforts are needed to scale up manufacturing tools to obtain high pressure drop rates in commercial scale manufacturing.

5. Conclusions

For the development of polymeric foams consistent with circular product design, the following strategies and research needs have been identified during this review:

- To broaden the selection of polymeric foams, research on material characterization is needed, on (i) polymer melt–gas systems, including extensional rheology, solubility and diffusivity of the gas in the melt, superficial tension, plasticization effects and crystallization kinetics to assess foamability and optimize foaming, and (ii) ageing of foams, to assess their service life and benchmark foams according to their entire lifecycle;
- Chain extending and branching through reactive extrusion has been found a successful technique to improve the melt strength and enable successful foaming of polymers. Research and development efforts are required to identify and/or develop nontoxic chain extenders and branching agents;
- Polymer chain configuration could be tailored for foaming applications during the manufacturing phase. It is expected that the demand will drive the tailoring of resin properties of alternative polymers as they become the focus of foaming research;
- Optimizing the processing tools is an effective strategy to advance on polymer foaming. The breaker plate could be used for the foaming of low melt strength polymers. Significant research efforts are required in this area, to allow the commercial manufacturing of, i.e., nanocellular foams;
- Identified strategies to control the dimensional stability of cellular structures include the foaming pressure and temperature and the use of molds. The impact of these strategies on the obtained foam morphology and skin formation, and the optimization

and potential trade-offs between the different parameters in play need to be assessed and adjusted for each practical case;

- Mechanical and thermal properties of polymeric foams are generally improved with the reduction of cell size and can be fine-tuned through cell size variability. The pressure drop rate and acting shear have been confirmed as processing parameters that contribute to the obtention of microcells by promoting cell nucleation. Research is needed to gain a more detailed understanding of the effects of shear on cell nucleation. R&D efforts are needed to scale up manufacturing tools to obtain high pressure drop rates.

Author Contributions: Conceptualization, L.D.; methodology, L.D.; formal analysis, L.D.; investigation, L.D.; resources, I.W.; data curation, L.D.; writing—original draft preparation, L.D.; writing—review and editing, L.D., I.W. and E.D.M.; supervision, I.W. and E.D.M.; project administration, I.W. All authors have read and agreed to the published version of the manuscript.

Funding: This research received no external funding.

Institutional Review Board Statement: Not applicable.

Informed Consent Statement: Not applicable.

Data Availability Statement: Data available through the reported references.

Conflicts of Interest: The authors declare no conflict of interest.

References

1. Directive 2009/125/EC of the European Parliament and of the Council of 21 October 2009 Establishing a Framework for the Setting of Ecodesign Requirements for Energy-Related Product. Available online: <https://eur-lex.europa.eu/legal-content/EN/ALL/?uri=celex:32009L0125> (accessed on 1 September 2022).
2. Faber, N.; Jorna, R.; van Engelen, J. The Sustainability of “Sustainability”—A Study into the Conceptual Foundations of the Notion of “Sustainability”. *J. Environ. Assess. Policy Manag.* **2005**, *7*, 1–33. [CrossRef]
3. Den Hollander, M.C.; Bakker, C.A.; Hultink, E.J. Product Design in a Circular Economy: Development of a Typology of Key Concepts and Terms. *J. Ind. Ecol.* **2017**, *21*, 517–525. [CrossRef]
4. McDonough, W.; Braungart, M. *Cradle to Cradle: Remaking the Way We Make Things*, 1st ed.; North Point Press: New York, NY, USA, 2002; ISBN 978-0865475878.
5. Sprinckx, C. Exploratory Study with Regard to Ecodesign of Thermal Insulation in Buildings (Lot 36): MEErP Tasks 0, 1 and 7-MEErP Study on Insulation Materials, Brussels. 2014. Available online: https://www.eup-network.de/fileadmin/user_upload/Produktgruppen/MEErP_exploratory_study_insulation_materials_final_report.pdf (accessed on 1 September 2022).
6. Lee, S.-T.; Park, C.B. (Eds.) *Foam Extrusion*; CRC Press: Boca Raton, FL, USA, 2014; ISBN 9780429184703.
7. Leslie, H.A.; Leonards, P.E.G.; Brandsma, S.H.; Boer, J.D.; Jonkers, N. Propelling plastics into the circular economy—weeding out the toxics first. *Environ. Int.* **2016**, *94*, 230–234. [CrossRef]
8. Chian, K.S.; Gan, L.H. Development of a rigid polyurethane foam from palm oil. *J. Appl. Polym. Sci.* **1998**, *68*, 509–515. [CrossRef]
9. Pillai, P.K.; Li, S.; Bouzidi, L.; Narine, S.S. Metathesized palm oil & novel polyol derivatives: Structure, chemical composition and physical properties. *Ind. Crops Prod.* **2016**, *84*, 205–223. [CrossRef]
10. Tanaka, R.; Hirose, S.; Hatakeyama, H. Preparation and characterization of polyurethane foams using a palm oil-based polyol. *Bioresour. Technol.* **2008**, *99*, 3810–3816. [CrossRef]
11. Kairytė, A.; Vėjelis, S. Evaluation of forming mixture composition impact on properties of water blown rigid polyurethane (PUR) foam from rapeseed oil polyol. *Ind. Crops Prod.* **2015**, *66*, 210–215. [CrossRef]
12. Tan, S.; Abraham, T.; Ference, D.; Macosko, C.W. Rigid polyurethane foams from a soybean oil-based Polyol. *Polymer* **2011**, *52*, 2840–2846. [CrossRef]
13. Zhang, L.; Jeon, H.K.; Malsam, J.; Herrington, R.; Macosko, C.W. Substituting soybean oil-based polyol into polyurethane flexible foams. *Polymer* **2007**, *48*, 6656–6667. [CrossRef]
14. Khoe, T.H.; Otey, F.H.; Frankel, E.N. Rigid urethane foams from hydroxymethylated linseed oil and polyol esters. *J. Am. Oil Chem. Soc.* **1972**, *49*, 615–618. [CrossRef]
15. Akram, D.; Sharmin, E.; Ahmad, S. Synthesis and Characterization of Boron Incorporated Polyester Polyol from Linseed Oil: A Sustainable Material. *Macromol. Symp.* **2009**, *277*, 130–137. [CrossRef]
16. CLP Regulation: (EC) No 1272/2008. 2008. Available online: <https://eur-lex.europa.eu/legal-content/EN/TXT/?uri=celex%3A32008R1272> (accessed on 1 September 2022).

17. European Union. Commission Regulation (EU) 2020/1149 of 3 August 2020 amending Annex XVII to Regulation (EC) No 1907/2006 of the European Parliament and of the Council concerning the Registration, Evaluation, Authorisation and Restriction of Chemicals (REACH) as regards diisocyanates: (EU) 2020/1149. *Off. J. Eur. Union* **2020**. Available online: <https://eur-lex.europa.eu/legal-content/EN/TXT/?uri=CELEX:32020R1149> (accessed on 7 September 2020).
18. Attia, S.; Beney, J.F.; Andersen, M. Application of the Cradle to Cradle paradigm to a housing unit in Switzerland: Findings from a prototype design. In Proceedings of the PLEA 2013—29th Conference on Passive-Low Energy Architecture Conference—Sustainable Architecture for a Renewable Future, Munich, Germany, 10–12 September 2013.
19. Finch, G.; Marriage, G.; Pelosi, A.; Gjerde, M. Building envelope systems for the circular economy; Evaluation parameters, current performance and key challenges. *Sustain. Cities Soc.* **2021**, *64*, 102561. [CrossRef]
20. Minunno, R.; O’Grady, T.; Morrison, G.; Gruner, R.; Colling, M. Strategies for Applying the Circular Economy to Prefabricated Buildings. *Buildings* **2018**, *8*, 125. [CrossRef]
21. Ketekaars, M.; Venmans, A. Making Cradle-to-Cradle Work: First Steps for Dutch Infrastructure. 2010. Available online: <https://publications.deltares.nl/Deltares107.pdf> (accessed on 1 September 2022).
22. Giezen, M. Shifting Infrastructure Landscapes in a Circular Economy: An Institutional Work Analysis of the Water and Energy Sector. *Sustainability* **2018**, *10*, 3487. [CrossRef]
23. Mignacca, B.; Locatelli, G.; Velenturf, A. Modularisation as enabler of circular economy in energy infrastructure. *Energy Policy* **2020**, *139*, 111371. [CrossRef]
24. Jensen, P.D.; Purnell, P.; Velenturf, A.P. Highlighting the need to embed circular economy in low carbon infrastructure decommissioning: The case of offshore wind. *Sustain. Prod. Consum.* **2020**, *24*, 266–280. [CrossRef]
25. Communication from the Commission to the European Parliament, the Council, the European Economic and Social Committee and the Committee of the Regions on the Implementation of the Circular Economy Package: Options to Address the Interface between Chemical, Product and Waste Legislation (Text with EEA Relevance) Options to Address the Interface between Chemical, Product and Waste Legislation: COM (2018) 32 Final. 2018. Available online: <https://eur-lex.europa.eu/legal-content/en/TXT/?uri=CELEX%3A52018DC0032> (accessed on 1 September 2022).
26. Anastas, P.T.; Zimmerman, J.B. Design through the 12 principles of green engineering. *Environ. Sci. Technol.* **2003**, *37*, 94A–101A. [CrossRef]
27. Stahel, W.R. *The Performance Economy*, 2nd ed.; Palgrave Macmillan: Basingstoke, UK; New York, NY, USA, 2010; ISBN 978-0-230-58466-2.
28. Lamberts, W.M. 1,1,1,4,4,4 Hexafluorobutane, a New Non-Ozone-Depleting Blowing Agent for Rigid PUR Foams. *J. Cell. Plast.* **1992**, *28*, 584–595. [CrossRef]
29. Barthelemy, P.P.; Leroy, A.; Franklin, J.A.; Zipfel, L.; Krücke, W. 1,1,2-Trifluoroethane (HFC-143): Zero-ODP Blowing Agent for Rigid Polyurethane Foams Using Conventional Dispensing Equipment. *J. Cell. Plast.* **1995**, *31*, 513–531. [CrossRef]
30. Howard, P.; Tunkel, J. Identification of CFC and HCFC Substitutes for Blowing Polyurethane Foam Insulation Products, Washington, DC. 1995. Available online: https://cfpub.epa.gov/si/si_public_record_Report.cfm?Lab=NRMRL&dirEntryId=115653&CFID=3363171&CFTOKEN=40126298&jsessionid=3830744124ae48e33d8f4245575a1162753a (accessed on 1 September 2022).
31. Ohara, Y.; Tanaka, K.; Hayashi, T.; Tomita, H.; Motani, S. The Development of a Non-Fluorocarbon-Based Extruded Polystyrene Foam Which Contains a Halogen-Free Blowing Agent. *Bull. Chem. Soc. Jpn.* **2004**, *77*, 599–605. [CrossRef]
32. Kaewmesri, W.; Lee, P.C.; Park, C.B.; Pumchusak, J. Effects of CO₂ and Talc Contents on Foaming Behavior of Recyclable High-melt-strength PP. *J. Cell. Plast.* **2006**, *42*, 405–428. [CrossRef]
33. Di Maio, E.; Mensitieri, G.; Iannace, S.; Nicolais, L.; Li, W.; Flumerfelt, R.W. Structure optimization of polycaprolactone foams by using mixtures of CO₂ and N₂ as blowing agents. *Polym. Eng. Sci.* **2005**, *45*, 432–441. [CrossRef]
34. Reignier, J.; Gendron, R.; Champagne, M.F. Extrusion Foaming of Poly(lactic acid) Blown with CO₂: Toward 100% Green Material. *Cell. Polym.* **2007**, *26*, 83–115. [CrossRef]
35. Reverchon, E.; Cardea, S. Production of controlled polymeric foams by supercritical CO₂. *J. Supercrit. Fluids* **2007**, *40*, 144–152. [CrossRef]
36. Gong, P.; Zhai, S.; Lee, R.; Zhao, C.; Buahom, P.; Li, G.; Park, C.B. Environmentally Friendly Polylactic Acid-Based Thermal Insulation Foams Blown with Supercritical CO₂. *Ind. Eng. Chem. Res.* **2018**, *57*, 5464–5471. [CrossRef]
37. Nam, G.J.; Yoo, J.H.; Lee, J.W. Effect of long-chain branches of polypropylene on rheological properties and foam-extrusion performances. *J. Appl. Polym. Sci.* **2005**, *96*, 1793–1800. [CrossRef]
38. Petrone, G.; D’Alessandro, V.; Franco, F.; Mace, B.; Rosa, S.d. Modal characterisation of recyclable foam sandwich panels. *Compos. Struct.* **2014**, *113*, 362–368. [CrossRef]
39. Grünwald, J.; Parlevliet, P.; Altstädt, V. Manufacturing of thermoplastic composite sandwich structures. *J. Thermoplast. Compos. Mater.* **2017**, *30*, 437–464. [CrossRef]
40. Nofar, M.; Park, C.B. *Polylactide Foams: Fundamentals, Manufacturing, and Applications*; Elsevier/William Andrew: Oxford, UK, 2018; ISBN 9780128139912.
41. Chen, X.; Li, J.; Pizzi, A.; Fredon, E.; Gerardin, C.; Zhou, X.; Du, G. Tannin-furanic foams modified by soybean protein isolate (SPI) and industrial lignin substituting formaldehyde addition. *Ind. Crops Prod.* **2021**, *168*, 113607. [CrossRef]
42. Ye, X.; Capezza, A.J.; Gowda, V.; Olsson, R.T.; Lendel, C.; Hedenqvist, M.S. High-Temperature and Chemically Resistant Foams from Sustainable Nanostructured Protein. *Adv. Sustain. Syst.* **2021**, *5*, 2100063. [CrossRef]

43. Reignier, J.; Gendron, R.; Champagne, M.F. Autoclave Foaming of Poly (ϵ -Caprolactone) Using Carbon Dioxide: Impact of Crystallization on Cell Structure. *J. Cell. Plast.* **2007**, *43*, 459–489. [CrossRef]
44. Frerich, S.C. Biopolymer foaming with supercritical CO₂—Thermodynamics, foaming behaviour and mechanical characteristics. *J. Supercrit. Fluids* **2015**, *96*, 349–358. [CrossRef]
45. Di Maio, E.; Kiran, E. Foaming of polymers with supercritical fluids and perspectives on the current knowledge gaps and challenges. *J. Supercrit. Fluids* **2018**, *134*, 157–166. [CrossRef]
46. Jin, F.-L.; Zhao, M.; Park, M.; Park, S.-J. Recent Trends of Foaming in Polymer Processing: A Review. *Polymers* **2019**, *11*, 953. [CrossRef] [PubMed]
47. Sarver, J.A.; Kiran, E. Foaming of polymers with carbon dioxide—The year-in-review—2019. *J. Supercrit. Fluids* **2021**, *173*, 105166. [CrossRef]
48. Homrich, A.S.; Galvão, G.; Abadia, L.G.; Carvalho, M.M. The circular economy umbrella: Trends and gaps on integrating pathways. *J. Clean. Prod.* **2018**, *175*, 525–543. [CrossRef]
49. Björn, A.; Hauschild, M.Z. Cradle to Cradle and LCA. In *Life Cycle Assessment*; Hauschild, M.Z., Rosenbaum, R.K., Olsen, S.I., Eds.; Springer International Publishing: Cham, Germany, 2018; pp. 605–631. ISBN 978-3-319-56474-6.
50. Bakker, C.A.; Wever, R.; Teoh, C.; Clercq, S.d. Designing cradle-to-cradle products: A reality check. *Int. J. Sustain. Eng.* **2010**, *3*, 2–8. [CrossRef]
51. Lee, S.-T. Shear effects on thermoplastic foam nucleation. *Polym. Eng. Sci.* **1993**, *33*, 418–422. [CrossRef]
52. McDonough, W.; Braungart, M.; Anastas, P.T.; Zimmerman, J.B. Applying the principles of Green Engineering to cradle-to-cradle design. *Environ. Sci. Technol.* **2003**, *37*, 434A–441A. [CrossRef]
53. Gibson, L.J.; Ashby, M.F. *Cellular Solids*; Cambridge University Press: Cambridge, UK, 1997; ISBN 0 521 49911 9.
54. Di Maio, E.; Coccorullo, I.; Montesano, S.; Incarnato, L. Chain Extension and Foaming of Recycled PET in Extrusion Equipment. *Macromol. Symp.* **2005**, *228*, 185–200. [CrossRef]
55. Walker, S.; Rothman, R. Life cycle assessment of bio-based and fossil-based plastic: A review. *J. Clean. Prod.* **2020**, *261*, 121158. [CrossRef]
56. Van der Ven, E.; Bout, H.; De Bell, H.; Baars, G. Thermal Insulation Metallocene Polyethylene Foam and Manufacturing Method Therefor. European Patent EP1336064B1, 26 January 2005.
57. Knaus, D.A. Stability Control Agent Composition for Polyolefin Foam. U.S. Patent US005750584A, 12 May 1998.
58. Tabacchiera, A. Concentrate of Polyfunctional Compounds Usable for the Preparation of Foamed Polyester Materials. European Patent EP2009043A1, 31 December 2008.
59. Meller, M.; Li, J.; Dolega, J.; Graeter, H. Cellular Polyester Made of Post-Consumer Flakes and the Use F Products Made Thereof. European Patent EP2383309A1, 2 November 2011.
60. Laguna-Gutierrez, E.; Escudero, J.; Kumar, V.; Rodriguez-Perez, M.A. Microcellular foaming by using subcritical CO₂ of crosslinked and non-crosslinked LDPE/clay nanocomposites. *J. Cell. Plast.* **2018**, *54*, 257–282. [CrossRef]
61. Velasco, J.I.; Antunes, M.; Realinho, V.; Ardanuy, M. Characterization of rigid polypropylene-based microcellular foams produced by batch foaming processes. *Polym. Eng. Sci.* **2011**, *51*, 2120–2128. [CrossRef]
62. Doyle, L. Extrusion foaming behavior of polybutene-1. Toward single-material multifunctional sandwich structures. *J. Appl. Polym. Sci.* **2021**, *139*, 51816. [CrossRef]
63. Rotter, G.E.; Melquist, J.L.; Chiang, W.; Tsai, B.C.; Kelly, J.J. Increased Throughput in Foaming and Other Melt Fabrication of Polyester. European Patent EP0636158B1, 31 March 1999.
64. Xanthos, M.; Zhang, Q.; Dey, S.K.; Li, Y.; Yilmazer, U.; O’Shea, M. Effects of Resin Rheology on the Extrusion Foaming Characteristics of PET. *J. Cell. Plast.* **1998**, *34*, 498–510. [CrossRef]
65. Xanthos, M.; Dey, S.K.; Zhang, Q.; Quintans, J. Parameters Affecting Extrusion Foaming of PET by Gas Injection. *J. Cell. Plast.* **2000**, *36*, 102–111. [CrossRef]
66. Olabisi, O.; Adewale, K. *Handbook of Thermoplastics*; CRC Press: Boca Raton, FL, USA, 2016; ISBN 1466577223.
67. Wypych, G. *Handbook of Plasticizers*, 3rd ed.; Chemtec: Toronto, ON, Canada, 2017; ISBN 9781895198973.
68. Okolieocha, C.; Raps, D.; Subramaniam, K.; Altstädt, V. Microcellular to nanocellular polymer foams: Progress (2004–2015) and future directions—A review. *Eur. Polym. J.* **2015**, *73*, 500–519. [CrossRef]
69. Montreal Protocol on Substances That Deplete the Ozone Layer. Chapter XXVII Environment. 1987. Available online: https://treaties.un.org/Pages/ViewDetails.aspx?src=IND&mtdsg_no=XXVII-2-a&chapter=27&clang=_en (accessed on 1 September 2022).
70. Chapter XXVII 2.f Amendment to the Montreal Protocol on Substances That Deplete the Ozone Layer. 2016. Available online: https://treaties.un.org/Pages/ViewDetails.aspx?src=IND&mtdsg_no=XXVII-2-f&chapter=27&clang=_en (accessed on 1 September 2022).
71. Zhang, H.; Fang, Z.; Liu, T.; Li, B.; Li, H.; Cao, Z.; Jin, G.; Zhao, L.; Xin, Z. Dimensional Stability of LDPE Foams with CO₂ + i-C₄H₁₀ Mixtures as Blowing Agent: Experimental and Numerical Simulation. *Ind. Eng. Chem. Res.* **2019**, *58*, 13154–13162. [CrossRef]
72. Zhang, H.; Liu, T.; Li, B.; Li, H.; Cao, Z.; Jin, G.; Zhao, L.; Xin, Z. Foaming and dimensional stability of LDPE foams with N₂, CO₂, i-C₄H₁₀ and CO₂-N₂ mixtures as blowing agents. *J. Supercrit. Fluids* **2020**, *164*, 104930. [CrossRef]

73. Dey, S.K.; Natarajan, P.; Xanthos, M.; Braathen, M.D. Use of inert gases in extruded medium density polypropylene foams. *J. Vinyl Addit. Technol.* **1996**, *2*, 339–344. [[CrossRef](#)]
74. Gendron, R.; Daigneault, L.E. Rheology of Thermoplastic Foam Extrusion Process. In *Foam Extrusion*; Lee, S.-T., Park, C.B., Eds.; CRC Press: Boca Raton, FL, USA, 2014; pp. 56–99. ISBN 9780429184703.
75. Alsoy, S. Modeling of Diffusion in Closed Cell Polymeric Foams. *J. Cell. Plast.* **1999**, *35*, 247–271. [[CrossRef](#)]
76. Sarver, J.A.; Sumey, J.L.; Whitfield, R.M.; Kiran, E. Confined batch foaming of semi-crystalline rubbery elastomers with carbon dioxide using a mold. *J. Appl. Polym. Sci.* **2021**, *138*, 50698. [[CrossRef](#)]
77. Chen, Y.; Li, D.; Zhang, H.; Ling, Y.; Wu, K.; Liu, T.; Hu, D.; Zhao, L. Antishrinking Strategy of Microcellular Thermoplastic Polyurethane by Comprehensive Modeling Analysis. *Ind. Eng. Chem. Res.* **2021**, *60*, 7155–7166. [[CrossRef](#)]
78. Lee, Y.; Youngchul, Y. Properties of Polyurethane Foam Blown by Environment Friendly Blowing Agent. In Proceedings of the 28th (2018) International Ocean and Polar Engineering Conference, Sapporo, Japan, 10–15 June 2018; International Society of Offshore and Polar Engineers: Cupertino, CA, USA, 2018. ISBN 9781880653876.
79. Nair, V. HFO refrigerants: A review of present status and future prospects. *Int. J. Refrig.* **2021**, *122*, 156–170. [[CrossRef](#)]
80. Vo, C.V.; Fox, R.T. Assessment of hydrofluoropropenes as insulating blowing agents for extruded polystyrene foams. *J. Cell. Plast.* **2013**, *49*, 423–438. [[CrossRef](#)]
81. Wypych, G. *Handbook of Foaming and Blowing Agents*; ChemTec Publishing: Toronto, ON, Canada, 2017; ISBN 978-1-895198-99-7.
82. Yakushin, V.; Cabulis, U.; Fridrihsone, V.; Kravchenko, S.; Pauliks, R. Properties of polyurethane foam with fourth-generation blowing agent. *e-Polymers* **2021**, *21*, 763–769. [[CrossRef](#)]
83. Bowman, J.M.; Williams, D.J. Thermal Insulating Foam Comprising HFO-1233zd as Blowing Agent. European Patent EP2154223B3, 26 June 2006.
84. Hendriks, S.; Hopmann, C.; Zepnik, S. Extrusion foaming of thermoplastic cellulose acetate sheets with HFO-1234ze and co-blowing agents. *Polym. Eng. Sci.* **2018**, *58*, E182–E188. [[CrossRef](#)]
85. Lindley, A.A.; Noakes, T.J. Consideration F Hydrofluoroolefins (HFOs) as Potential Candidate Medical Propellants. 2010. Available online: <http://mexfluor.com/pdf/hfos-as-candidate-medical-propellants.pdf> (accessed on 26 May 2022).
86. Fleet, D.; Hanlon, J.; Osborne, K.; La Vendrine, M.L.; Ashford, P. Study on Environmental and Health Effects of HFO Refrigerants. Report Prepared for the Norwegian Environment Agency M-917/2017. 2017. Available online: <https://www.miljodirektoratet.no/globalassets/publikasjoner/M917/M917.pdf> (accessed on 26 May 2022).
87. Pontiff, T. Foaming Agents for Foam Extrusion. In *Foam Extrusion*; Lee, S.-T., Park, C.B., Eds.; CRC Press: Boca Raton, FL, USA, 2014; ISBN 9780429184703.
88. Wegner, J.-E.; Groeseling, M. Stable PET foaming. *Kunstst. Int.* **2010**, *9*, 144–146.
89. Laguna-Gutierrez, E.; van Hooghten, R.; Moldenaers, P.; Rodriguez-Perez, M.A. Understanding the foamability and mechanical properties of foamed polypropylene blends by using extensional rheology. *J. Appl. Polym. Sci.* **2015**, *132*. [[CrossRef](#)]
90. Spitael, P.; Macosko, C.W. Strain hardening in polypropylenes and its role in extrusion foaming. *Polym. Eng. Sci.* **2004**, *44*, 2090–2100. [[CrossRef](#)]
91. Park, C.B.; Cheung, L.K. A study of cell nucleation in the extrusion of polypropylene foams. *Polym. Eng. Sci.* **1997**, *37*, 1–10. [[CrossRef](#)]
92. Naguib, H.E.; Park, C.B.; Reichelt, N. Fundamental foaming mechanisms governing the volume expansion of extruded polypropylene foams. *J. Appl. Polym. Sci.* **2004**, *91*, 2661–2668. [[CrossRef](#)]
93. Gotsis, A.D.; Zeevenhoven, B.L.F.; Tsenoglou, C. Effect of long branches on the rheology of polypropylene. *J. Rheol.* **2004**, *48*, 895–914. [[CrossRef](#)]
94. Yamaguchi, M. Material Strength in Molten State for Foam. In *Foam Extrusion*; Lee, S.-T., Park, C.B., Eds.; CRC Press: Boca Raton, FL, USA, 2014; pp. 83–117. ISBN 9780429184703.
95. Xu, Z.; Zhang, Z.; Guan, Y.; Wei, D.; Zheng, A. Investigation of extensional rheological behaviors of polypropylene for foaming. *J. Cell. Plast.* **2013**, *49*, 317–334. [[CrossRef](#)]
96. Münstedt, H. Extensional Rheology and Processing of Polymeric Materials. *Int. Polym. Process.* **2018**, *33*, 594–618. [[CrossRef](#)]
97. Sarver, J.A.; Sumey, J.L.; Williams, M.L.; Bishop, J.P.; Dean, D.M.; Kiran, E. Foaming of poly(ethylene-co-vinyl acetate) and poly(ethylene-co-vinyl acetate-co-carbon monoxide) and their blends with carbon dioxide. *J. Appl. Polym. Sci.* **2018**, *135*, 45841. [[CrossRef](#)]
98. Weingart, N.; Raps, D.; Lu, M.; Endner, L.; Altstädt, V. Comparison of the Foamability of Linear and Long-Chain Branched Polypropylene—The Legend of Strain-Hardening as a Requirement for Good Foamability. *Polymers* **2020**, *12*, 725. [[CrossRef](#)] [[PubMed](#)]
99. Ma, C.-Y.; Dae Han, C. Measurement of the Viscosities of Mixtures of Thermoplastic Resin and Fluorocarbon Blowing Agent. *J. Cell. Plast.* **1982**, *18*, 361–370. [[CrossRef](#)]
100. Pasquali, I.; Comi, L.; Pucciarelli, F.; Bettini, R. Swelling, melting point reduction and solubility of PEG 1500 in supercritical CO₂. *Int. J. Pharm.* **2008**, *356*, 76–81. [[CrossRef](#)]
101. Takahashi, S.; Hassler, J.C.; Kiran, E. Melting behavior of biodegradable polyesters in carbon dioxide at high pressures. *J. Supercrit. Fluids* **2012**, *72*, 278–287. [[CrossRef](#)]
102. Doroudiani, S.; Park, C.B.; Kortschot, M.T. Effect of the crystallinity and morphology on the microcellular foam structure of semicrystalline polymers. *Polym. Eng. Sci.* **1996**, *36*, 2645–2662. [[CrossRef](#)]

103. Tang, L.; Zhai, W.; Zheng, W. Autoclave preparation of expanded polypropylene/poly(lactic acid) blend bead foams with a batch foaming process. *J. Cell. Plast.* **2011**, *47*, 429–446. [CrossRef]
104. Mouliné, P.; Simha, R. Statistical Thermodynamics of Gas Solubility in Polymers. In *Foam Extrusion*; Lee, S.-T., Park, C.B., Eds.; CRC Press: Boca Raton, FL, USA, 2014; ISBN 9780429184703.
105. Zhang, Q.; Xanthos, M. Material Properties Affecting Extrusion Foaming. In *Polymeric Foams: Mechanisms and Materials*; Lee, S.-T., Ramesh, N.S., Eds.; CRC Press: Boca Raton, FL, USA, 2004; ISBN 0-8493-1728-2.
106. Mangs, S. Insulation Materials in District Heating Pipes. Ph.D. Thesis, Chalmers University of Technology, Goteborg, Sweden, 2005.
107. Zauner, C.; Bettermann, M. Flexible Foam with Improved Insulation Properties. European Patent EP3372631A1, 12 September 2018.
108. Kurańska, M.; Prociak, A. Bio-Based Polyurethane Foams for Heat-Insulating Applications. In *Nano and Biotech Based Materials for Energy Building Efficiency*; Pacheco Torgal, F., Buratti, C., Kalaiselvam, S., Granqvist, C.-G., Ivanov, V., Eds.; Springer International Publishing: Cham, Switzerland, 2016; pp. 357–373. ISBN 978-3-319-27503-1.
109. Collishaw, P.G.; Evans, J.R.G. An assessment of expressions for the apparent thermal conductivity of cellular materials. *J. Mater. Sci.* **1994**, *29*, 2261–2273. [CrossRef]
110. Isberg, J. The Thermal Conductivity of Polyurethane Foam. Ph.D. Thesis, Chalmers University of Technology, Goteborg, Sweden, 1988.
111. Ramnäs, J. New Materials and Constructions for Improving the Quality and Lifetime of District Heating Pipes Including Joints-Thermal, Mechanical and Environmental Performance: Annex VIII Project 1. Final Report. 2008. Available online: <https://www.iea-dhc.org/the-research/annexes/2005-2008-annex-viii/annex-viii-project-01> (accessed on 1 September 2022).
112. Peelman, N.; Ragaert, P.; Ragaert, K.; Meulenaer, B.d.; Devlieghere, F.; Cardon, L. Heat resistance of new biobased polymeric materials, focusing on starch, cellulose, PLA, and PHA. *J. Appl. Polym. Sci.* **2015**, *132*. [CrossRef]
113. Doyle, L.; Weidlich, I. Sustainable insulation for sustainable DHC. *Energy Rep.* **2021**, *7*, 150–157. [CrossRef]
114. Antunes, M.; Velasco, J.I.; Realinho, V.; Solórzano, E. Study of the cellular structure heterogeneity and anisotropy of polypropylene and polypropylene nanocomposite foams. *Polym. Eng. Sci.* **2009**, *49*, 2400–2413. [CrossRef]
115. Rodríguez-Pérez, M.A. *Crosslinked Polyolefin Foams: Production, Structure, Properties, and Applications. Crosslinking in Materials Science*; Springer: Berlin/Heidelberg, Germany, 2005; pp. 97–126. ISBN 978-3-540-25831-5.
116. Abe, S.; Yamaguchi, M. Study on the foaming of crosslinked polyethylene. *J. Appl. Polym. Sci.* **2001**, *79*, 2146–2155. [CrossRef]
117. Yamaguchi, M.; Suzuki, K.-I. Rheological properties and foam processability for blends of linear and crosslinked polyethylenes. *J. Polym. Sci. B Polym. Phys.* **2001**, *39*, 2159–2167. [CrossRef]
118. Laguna-Gutierrez, E.; Pinto, J.; Kumar, V.; Rodriguez-Mendez, M.L.; Rodriguez-Perez, M.A. Improving the extensional rheological properties and foamability of high-density polyethylene by means of chemical crosslinking. *J. Cell. Plast.* **2018**, *54*, 333–357. [CrossRef]
119. Feng, J.-M.; Wang, W.-K.; Yang, W.; Xie, B.-H.; Yang, M.-B. Structure and Properties of Radiation Cross-Linked Polypropylene Foam. *Polym. Plast. Technol. Eng.* **2011**, *50*, 1027–1034. [CrossRef]
120. Danaei, M.; Sheikh, N.; Taromi, F.A. Radiation Cross-linked Polyethylene Foam: Preparation and Properties. *J. Cell. Plast.* **2005**, *41*, 551–562. [CrossRef]
121. Lopez-Gonzalez, E.; Salmazo, L.O.; Lopez-Gil, A.; Laguna-Gutierrez, E.; Rodriguez-Perez, M.A. Analysis of the foaming mechanisms of materials based on high-density polyethylene (HDPE) crosslinked with different irradiation doses. *J. Appl. Polym. Sci.* **2018**, *135*, 46276. [CrossRef]
122. Mihai, M.; Huneault, M.A.; Favis, B.D. Rheology and extrusion foaming of chain-branched poly(lactic acid). *Polym. Eng. Sci.* **2010**, *50*, 629–642. [CrossRef]
123. Khemani, K.C.; Mercer, J.W.; McConnel, R.L. Concentrates for Improving Polyester Compositions and Method of Making Same. U.S. Patent US5801206A, 9 September 1997.
124. Tang, H.; Dai, W.; Chen, B. A new method for producing high melt strength polypropylene with reactive extrusion. *Polym. Eng. Sci.* **2008**, *48*, 1339–1344. [CrossRef]
125. Frounchi, M. Studies on degradation of PET in mechanical recycling. *Macromol. Symp.* **1999**, *144*, 465–469. [CrossRef]
126. Badia, J.D.; Strömberg, E.; Karlsson, S.; Ribes-Greus, A. The role of crystalline, mobile amorphous and rigid amorphous fractions in the performance of recycled poly (ethylene terephthalate) (PET). *Polym. Degrad. Stab.* **2012**, *97*, 98–107. [CrossRef]
127. Standau, T.; Nofar, M.; Dörr, D.; Ruckdäschel, H.; Altstädt, V. A Review on Multifunctional Epoxy-Based Joncryl[®] ADR Chain Extended Thermoplastics. *Polym. Rev.* **2021**, *62*, 1–55. [CrossRef]
128. Zhong, W.; Ge, J.; Gu, Z.; Li, W.; Chen, X.; Zang, Y.; Yang, Y. Study on biodegradable polymer materials based on poly(lactic acid). I. Chain extending of low molecular weight poly(lactic acid) with methylenediphenyl diisocyanate. *J. Appl. Polym. Sci.* **1999**, *74*, 2546–2551. [CrossRef]
129. Li, B.-H.; Yang, M.-C. Improvement of thermal and mechanical properties of poly(L-lactic acid) with 4,4-methylene diphenyl diisocyanate. *Polym. Adv. Technol.* **2006**, *17*, 439–443. [CrossRef]
130. Ren, J.; Wang, Q.-F.; Gu, S.-Y.; Zhang, N.-W.; Ren, T.-B. Chain-linked lactic acid polymers by benzene diisocyanate. *J. Appl. Polym. Sci.* **2006**, *99*, 1045–1049. [CrossRef]

131. Gu, S.; Yang, M.; Yu, T.; Ren, T.; Ren, J. Synthesis and characterization of biodegradable lactic acid-based polymers by chain extension. *Polym. Int.* **2008**, *57*, 982–986. [[CrossRef](#)]
132. Incarnato, L.; Scarfato, P.; Di Maio, L.; Acierno, D. Structure and rheology of recycled PET modified by reactive extrusion. *Polymer* **2000**, *41*, 6825–6831. [[CrossRef](#)]
133. Forsythe, J.S.; Cheah, K.; Nisbet, D.R.; Gupta, R.K.; Lau, A.; Donovan, A.R.; O’Shea, M.S.; Moad, G. Rheological properties of high melt strength poly(ethylene terephthalate) formed by reactive extrusion. *J. Appl. Polym. Sci.* **2006**, *100*, 3646–3652. [[CrossRef](#)]
134. Wang, M.Y.; Guo, Z.Q.; Lei, B.Y.; Zhou, N.Q. Rheological and Thermal Behavior of Recycled PET Modified by PMDA. *Adv. Mater. Res.* **2011**, *391–392*, 688–691. [[CrossRef](#)]
135. Madsen, M.T.; Skadhauge, L.R.; Nielsen, A.D.; Baelum, J.; Sherson, D.L. Pyromellitic dianhydride (PMDA) may cause occupational asthma. *Occup. Environ. Med.* **2019**, *76*, 175–177. [[CrossRef](#)]
136. Naguib, H.E.; Park, C.B.; Panzer, U.; Reichelt, N. Strategies for achieving ultra low-density polypropylene foams. *Polym. Eng. Sci.* **2002**, *42*, 1481–1492. [[CrossRef](#)]
137. Park, C.P.; Garcia, G.A. Development of Polypropylene Plank Foam Products. *J. Cell. Plast.* **2002**, *38*, 219–228. [[CrossRef](#)]
138. Huovinen, P.; Harlin, A.; Jääskeläinen, P.; Kabasi, A.; Manner, N. High Melt Strength Polypropylene. U.S. Patent US6875826B1, 28 September 1998.
139. Lugão, A.B.; Artel, B.; Yoshiga, A.; Lima, L.; Parra, D.F.; Bueno, J.R.; Liberman, S.; Farrah, M.; Terçariol, W.R.; Otaguro, H. Production of high melt strength polypropylene by gamma irradiation. *Radiat. Phys. Chem.* **2007**, *76*, 1691–1695. [[CrossRef](#)]
140. Uzawa, T.; Goto, K.; Uozumi, T.; Sugano, T.; Zhu, W.; Mike Chung, T.C. Direct Synthesis of High-Melt-Strength Polypropylene Using the Fourth Generation Heterogeneous Ziegler–Natta Catalyst and Commercial Production Process. *ACS Appl. Polym. Mater.* **2020**, *2*, 1827–1838. [[CrossRef](#)]
141. Weng, W.; Hu, W.; Dekmezian, A.H.; Ruff, C.J. Long Chain Branched Isotactic Polypropylene. *Macromolecules* **2002**, *35*, 3838–3843. [[CrossRef](#)]
142. Langston, J.; Dong, J.Y.; Chung, T.C. One-Pot Process of Preparing Long Chain Branched Polypropylene Using C₂-Symmetric Metallocene Complex and a “T” Reagent. *Macromolecules* **2005**, *38*, 5849–5853. [[CrossRef](#)]
143. Kaminsky, W.; Laban, A. Metallocene catalysis. *Appl. Catal. A Gen.* **2001**, *222*, 47–61. [[CrossRef](#)]
144. Razavi, A. Metallocene catalysts technology and environment. *C. R. Acad. Sci. Ser. IIC. Chem.* **2000**, *3*, 615–625. [[CrossRef](#)]
145. Farthi, A. Mechanical Properties of Strand PET Foams at Different Length Scales. Ph.D. Thesis, University of Bayreuth, Bayreuth, Germany, 2018.
146. Klemptner, D.; Frisch, K.C. *Handbook of Polymeric Foams and Foam Technology*; Hanser: Munich, Germany, 1991; ISBN 3446150978.
147. Van Krevelen, D.W.; Nijenhuis, K.t. *Properties of Polymers: Their Correlation with Chemical Structure; Their Numerical Estimation and Prediction from Additive Group Contributions*, 4th ed.; Elsevier: Amsterdam, The Netherlands; Boston, MA, USA, 2009; ISBN 9780080915104.
148. Park, C.B.; Behraves, A.H.; Venter, R.D. Low density microcellular foam processing in extrusion using CO₂. *Polym. Eng. Sci.* **1998**, *38*, 1812–1823. [[CrossRef](#)]
149. Park, C.B.; Baldwin, D.F.; Suh, N.P. Effect of the pressure drop rate on cell nucleation in continuous processing of microcellular polymers. *Polym. Eng. Sci.* **1995**, *35*, 432–440. [[CrossRef](#)]
150. Prociak, A.; Pielichowski, J.; Sterzynski, T. Thermal diffusivity of rigid polyurethane foams blown with different hydrocarbons. *Polym. Test.* **2000**, *19*, 705–712. [[CrossRef](#)]
151. Meller, M.; Li, J.; Dolega, J. A foam Material with Very Low Thermal Conductivity and a Process for Manufacturing the Foam Material. European Patent EP2671911A1, 5 June 2012.
152. Kang, M.J.; Kim, Y.H.; Park, G.P.; Han, M.S.; Kim, W.N.; Park, S.D. Liquid nucleating additives for improving thermal insulating properties and mechanical strength of polyisocyanurate foams. *J. Mater. Sci.* **2010**, *45*, 5412–5419. [[CrossRef](#)]
153. Park, D.H.; Park, G.P.; Kim, S.H.; Kim, W.N. Effects of isocyanate index and environmentally-friendly blowing agents on the morphological, mechanical, and thermal insulating properties of polyisocyanurate-polyurethane foams. *Macromol. Res.* **2013**, *21*, 852–859. [[CrossRef](#)]
154. Roux, G.A.; Balme, A.L. The Improvement of the Effective R-Value of Rigid Polyurethane Foams. *J. Therm. Insul.* **1990**, *14*, 98–106. [[CrossRef](#)]
155. Buahom, P.; Wang, C.; Alshrah, M.; Wang, G.; Gong, P.; Tran, M.-P.; Park, C.B. Wrong expectation of superinsulation behavior from largely-expanded nanocellular foams. *Nanoscale* **2020**, *12*, 13064–13085. [[CrossRef](#)]
156. Wang, G.; Wang, C.; Zhao, J.; Wang, G.; Park, C.B.; Zhao, G. Modelling of thermal transport through a nanocellular polymer foam: Toward the generation of a new superinsulating material. *Nanoscale* **2017**, *9*, 5996–6009. [[CrossRef](#)] [[PubMed](#)]
157. Knudsen, M. *Kinetic Theory of Gases*; Methuen, Co.: London, UK, 1934.
158. Notario, B.; Pinto, J.; Solorzano, E.; Saja, J.A.d.; Dumon, M.; Rodríguez-Pérez, M.A. Experimental validation of the Knudsen effect in nanocellular polymeric foams. *Polymer* **2015**, *56*, 57–67. [[CrossRef](#)]
159. Martín-de León, J.; Bernardo, V.; Cimavilla-Román, P.; Pérez-Tamarit, S.; Rodríguez-Pérez, M.Á. Overcoming the Challenge of Producing Large and Flat Nanocellular Polymers: A Study with PMMA. *Adv. Eng. Mater.* **2019**, *21*, 1900148. [[CrossRef](#)]
160. Martín-de León, J.; Bernardo, V.; Rodríguez-Pérez, M.Á. Nanocellular Polymers: The Challenge of Creating Cells in the Nanoscale. *Materials* **2019**, *12*, 797. [[CrossRef](#)] [[PubMed](#)]

161. Bernardo, V.; Martin-de Leon, J.; Pinto, J.; Verdejo, R.; Rodriguez-Perez, M.A. Modeling the heat transfer by conduction of nanocellular polymers with bimodal cellular structures. *Polymer* **2019**, *160*, 126–137. [[CrossRef](#)]
162. Gibson, L.J.; Ashby, M. The mechanics of three-dimensional cellular materials. *Proc. R. Soc. Lond. A* **1982**, *382*, 43–59. [[CrossRef](#)]
163. Zhu, H.X.; Knott, J.F.; Mills, N.J. Analysis of the elastic properties of open-cell foams with tetrakaidecahedral cells. *J. Mech. Phys. Solids* **1997**, *45*, 319–343. [[CrossRef](#)]
164. Huber, A.T.; Gibson, L.J. Anisotropy of foams. *J. Mater. Sci.* **1988**, *23*, 3031–3040. [[CrossRef](#)]
165. Sullivan, R.M.; Ghosn, L.J.; Lerch, B.A. A general tetrakaidecahedron model for open-celled foams. *Int. J. Solids Struct.* **2008**, *45*, 1754–1765. [[CrossRef](#)]
166. Bureau, M.N.; Gendron, R. Mechanical-Morphology Relationship of PS Foams. *J. Cell. Plast.* **2003**, *39*, 353–367. [[CrossRef](#)]
167. Chen, Y.; Das, R.; Battley, M. Effects of cell size and cell wall thickness variations on the stiffness of closed-cell foams. *Int. J. Solids Struct.* **2015**, *52*, 150–164. [[CrossRef](#)]
168. Martini, J.E. The Production and Analysis of Microcellular Foam. Master's Thesis, Massachusetts Institute of Technology, Cambridge, MA, USA, 1981.
169. Martini-Vvedensky, J.E.; Suh, N.P.; Waldman, F.A. Microcellular Closed Cell Foams and Their Method of Manufacture. U.S. Patent US4473665A, 25 September 1984.
170. Kumar, V. Microcellular Polymers: Novel Materials for the 21st Century. *Prog. Rubber Plast. Technol.* **1993**, *9*, 54–70.
171. Waldman, F.A. The Processing of Microcellular Foam. Master's Thesis, Massachusetts Institute of Technology, Cambridge, MA, USA, 1982.
172. Colton, J.S.; Suh, N.P. The nucleation of microcellular thermoplastic foam: Process model and experimental results. *Adv. Manuf. Process.* **1986**, *1*, 341–364. [[CrossRef](#)]
173. Colton, J.S.; Suh, N.P. Nucleation of microcellular foam: Theory and practice. *Polym. Eng. Sci.* **1987**, *27*, 500–503. [[CrossRef](#)]
174. Colton, J.S.; Suh, N.P. The nucleation of microcellular thermoplastic foam with additives: Part I: Theoretical considerations. *Polym. Eng. Sci.* **1987**, *27*, 485–492. [[CrossRef](#)]
175. Doyle, L. A Circular Economy Approach to Multifunctional Sandwich Structures: Polymeric Foams for District Heating Pre-Insulated Pipes. Ph.D. Thesis, HafenCity University, Hamburg, Germany, 2022.
176. Guo, Q.; Wang, J.; Park, C.B.; Ohshima, M. A Microcellular Foaming Simulation System with a High Pressure-Drop Rate. *Ind. Eng. Chem. Res.* **2006**, *45*, 6153–6161. [[CrossRef](#)]
177. Tammaro, D.; Contaldi, V.; Carbone, M.P.; Di Maio, E.; Iannace, S. A novel lab-scale batch foaming equipment: The mini-batch. *J. Cell. Plast.* **2016**, *52*, 533–543. [[CrossRef](#)]
178. Tammaro, D.; Astarita, A.; Di Maio, E.; Iannace, S. Polystyrene Foaming at High Pressure Drop Rates. *Ind. Eng. Chem. Res.* **2016**, *55*, 5696–5701. [[CrossRef](#)]
179. Muratani, K.; Shimbo, M.; Miyano, Y. Correlation of Decompression Time and Foaming Temperature on the Cell Density of Foamed Polystyrene. *Cell. Polym.* **2005**, *24*, 15–27. [[CrossRef](#)]
180. Chen, L.; Sheth, H.; Wang, X. Effects of Shear Stress and Pressure Drop Rate on Microcellular Foaming Process. *J. Cell. Plast.* **2001**, *37*, 353–363. [[CrossRef](#)]
181. Wong, A.; Chu, R.K.; Leung, S.N.; Park, C.B.; Zong, J.H. A batch foaming visualization system with extensional stress-inducing ability. *Chem. Eng. Sci.* **2011**, *66*, 55–63. [[CrossRef](#)]



Received: 17 March 2020 | Revised: 14 August 2020 | Accepted: 20 August 2020

DOI: 10.1111/ffe.13347

ORIGINAL CONTRIBUTION



WILEY

Effects of thermal and mechanical cyclic loads on polyurethane pre-insulated pipes

Lucía Doyle | Ingo Weidlich

Department of Infrastructural Engineering, HafenCity University, Hamburg, Germany

Correspondence

Lucía Doyle, Department of Infrastructural Engineering, HafenCity University, Überseeallee 16, Hamburg, Germany.
Email: lucia.doyle@hcu-hamburg.de

Funding information

HafenCity University

Abstract

District heating (DH) pre-insulated pipes are a sandwich assembly composed by a steel heat service pipe, polyurethane (PU) foam and polyethylene casing. The foam acts as bond between the steel pipe and casing. The application has high constraints for the foam, as it is subjected to cyclic multiaxial stresses, high cyclic temperatures and long expected service life. In this study, we evaluate if and how cyclic loads affect the shear strength, shear modulus, toughness and failure behaviour of the PU foam in DH pipes sandwich assembly compared with unaged reference samples. We have found that the simultaneous application of mechanical and thermal loads weakens the strength and increases the stiffness of the foam and that this change is not caused by degradation of the molecular structure. Crack initiation and propagation along the pipe samples follow a very consistent pattern between samples, with cracks initiating in Mode II and propagating in Mode I. The consistent axial displacement of approximately 2 cm from each other suggests the formation of strain localizations.

KEYWORDS

cyclic loading, district heating, fatigue, foam, polyurethane, sandwich structure

1 | INTRODUCTION

District heating (DH) pre-insulated pipes sandwich assembly composed of a steel heat service pipe, insulating material (polyurethane [PU] foam) and polyethylene (PE) casing, which are bonded by the insulating material.¹ The pipe networks are directly buried underground. The DH system's start-up and shut downs, as well as fluctuations on heat demand and ambient temperature, subject the piping network to thermal and mechanical cycling due to the thermal expansion. The axial expansion of the pipes is partially counteracted by frictional forces acting between the ground and the casing, with

the shear stresses transferred through the PU foam bond. Therefore, the use of pre-insulated pipes has implied the simplification of the laying methods, employing cold laying instead of expansion facilities like compensators or U-bends, being more cost effective.² The PU foam layer needs to withstand the shear stresses without failure for the network lifetime to preserve its load bearing function. Knowledge on the ageing mechanisms of the PU foam is of great importance in order to ensure the pipe assembly performs as specified during its service life, as well as to assess if this service life could be extended.

The EN253:2019 standard¹ assumes that the failure of the PU bond and hence the service life is driven by

This is an open access article under the terms of the Creative Commons Attribution License, which permits use, distribution and reproduction in any medium, provided the original work is properly cited.

© 2020 The Authors. Fatigue & Fracture of Engineering Materials & Structures published by John Wiley & Sons Ltd

thermo-oxidative degradation of the PU, governed by an Arrhenius relationship. Studies on the accelerated ageing and thermal degradation of pre-insulated pipes^{3–6} show discrepancies between the results of the tests and the degradation process observed in the field. Cited explanations include that higher temperatures alter the degradation rather than accelerate it. Aspects like gas exchange with the environment are recently considered.

Previous projects and reports have dealt with the topic of thermal cycling and fatigue of DH systems.^{2,7} The studies however relate only to the steel service pipe, while the effects on the PU foam are insufficiently well known or studied.² The design guidelines for DH networks include fatigue check.⁸ However, again it relates to the steel pipe only, and stating the lack of knowledge, it assumes that fatigue does not occur on the foam within the limits of the permissible stresses. This highlights the research need for observing and understanding if and how cyclic loads could produce fatigue on the foam or facilitate debonding of the layers due to stresses at the interface.

2 | FATIGUE AND FRACTURE OF PU FOAM—STATE OF THE ART

The increasing use of PU sandwich composites as load bearing structures has triggered research on its fatigue and fracture behaviour in recent years. The most accepted mechanism for fatigue crack growth in cellular solids is the failure of a cell wall ahead of the crack tip after repeated flexure, causing a step-wise crack growth, one cell at a time.⁹ Empirical observations of crack propagation through cell walls and the adjacent struts confirm this.^{10,11} Huang and Lin¹² have proposed a model for fatigue crack growth rate consistent with this mechanism. They conclude that fatigue of cellular materials depends on cyclic stress intensity range, cell size, relative density and the fatigue parameters of the solid from which they are made. Zenkert et al.¹³ follow a different approach, assuming crack growth in closed cell polymeric foams to be continuous and not cell-size dependent. Their model relates crack propagation rate behaviour with their un-notched fatigue life. However, it is reported that crack propagation in foams is interrupted by crack bridging by cell edges,^{10,14} which differentiates crack propagation in foams from that in solids. In this regard, Olurin¹⁵ suggests that the fatigue crack growth rate in an aluminium alloy foam is controlled by the progressive degradation of crack bridging by fatigue failure of the cell edges behind the crack tip. In a previous work by the team, it was argued that the fatigue degradation mechanism is material ratcheting due to progressive strain accumulation, rather than cracking

events in the foam.¹⁶ This is in contrast with the report of Burman¹⁷ that fatigue crack nucleation appears over a large volume of the test specimen, later converging to a macroscopic crack. The governing mechanisms are therefore not yet fully understood.

Another followed approach is the experimental characterization of mechanical behaviour and the development of empirical failure criteria. Marsavina and coworkers have characterized the fracture of PU foams, comparing dynamic and static fracture toughness,¹⁸ the effects of density, anisotropy, loading speed and mix mode ratio,¹⁹ and Modes I and II fracture toughness for different types of specimens.²⁰ They have found that density exerts the main influence on the results, dynamic fracture toughness is higher than static, and increase in loading speed produces a decrease of Mode I but no effect on Mode II fracture toughness.

On fatigue tests of foam core sandwich structures under higher temperatures, Kanny et al.²¹ report that crosslinks provide mechanical stability of the PVC cores under temperature, extending their fatigue life, while an inverse behaviour is observed at room temperature.

The type of loading, constituent material properties and geometrical dimensions condition the initiation, propagation and interaction of failure modes.²² In a previous work, we have found that PU in pre-insulated pipes presents a much higher anisotropy in both the microstructure and the mechanical properties under compression than that previously reported for PU slabs, arising from the different geometry of the mould during the foaming process.²³ This, together with the different geometry of the sample, an annular pipe, and the effect of high temperature, highlights the need for specific evaluation of this element.

The focus of this work lies in observing and understanding if and how cyclic loads affect the shear strength (τ_{\max}), shear modulus (G), toughness (U) and failure behaviour of the PU foam in DH pipes sandwich assembly compared with unaged reference samples.

3 | MATERIALS AND METHODS

3.1 | Cyclic loading tests

Samples were machined out of commercial DN20 pipes with 28.5 mm insulation thickness and 6-m length (Logstor A/S, Denmark), following EN 253:2019.¹ All samples were produced with a length $L = 200$ mm and were individually accurately measured using a caliper and weighed prior to testing. The foam is cyclopentane-blown closed-cell PU with an average density of 76.2 kg/m³. Details on the microstructural

characterization have been presented in Doyle et al.²³ The ends of the pipe samples were not sealed and in direct contact with air. However, previous research from accelerated ageing of PU pre-insulated pipes under equivalent high ambient temperature have shown that changes in shear strength do not depend on the thermo-oxidation of PU at the temperatures under consideration²⁴ and therefore this should not have a relevant impact on the obtained results.

Three different cyclic loading trials were carried out, as summarized in Table 1.

3.1.1 | Trial T: Thermal cycles

For trial T, five specimens were subjected to thermal cycling inside a thermal chamber (Weiss WK1 340, Reiskirchen, Germany). Temperature was varied between 25°C and 100°C, which is the maximum operation temperature of the chamber and close to DH networks operation temperature. The number of cycles was set at 250, which is the number of cycles established for fatigue check for secondary effects for distribution lines according to AGFW e.V.⁸ Initial trials were conducted to measure the required time needed for the steel service pipe to reach thermal equilibrium at 100°C, which was

measured as 75 min. The heating and cooling ramp was established as 30 min, as it should not be as fast as to induce thermal shock, which would lead to a different type of stresses, and is the time length defined by EN 253:2019¹ to achieve the high temperature for axial shear strength at 140°C.

The specimens were allowed to freely expand and contract. Therefore, the stresses produced by these thermal cycles are due to the mismatch in coefficient of thermal expansion of the materials, which is higher for the PU foam than for the steel.

3.1.2 | Trial MT-wc: Thermal and mechanical cycles—Worst case conditions

Because the pipes under operating conditions do not freely expand but are subjected to axial shear stresses due to the soil friction forces, in this trial, axial shear stresses were mechanically induced in addition to the thermal cyclic loads described and applied in Trial T. For this, a specific test rig was designed in-house for the simultaneous testing of five samples inside of the thermal chamber. An axial force is exerted on the steel medium pipe by means of pneumatic valves (Festo AG, Esslingen am Neckar, Germany), while a ring at the base prevents movement of the casing, hence producing a shear stress along the foam. The electronic control of the mechanical cycling rig was coupled with a thermocouple placed in the middle specimen. This ensured that the maximum force was applied simultaneously to the maximum T°. A schematic of the test rig is presented in Figure 1.

For the selection of the applied force, a worst case scenario criterion was selected. Because EN 253:2019¹ establishes aged pipes should still withstand a shear stress of

TABLE 1 Parameters for the executed cyclic loading trials

Trial	T° interval (°C)	τ interval (MPa)	Number of cycles
T	25–100	0	250
MT-wc	25–100	0–0.12	250
MT-m	25–70	0–0.04	125

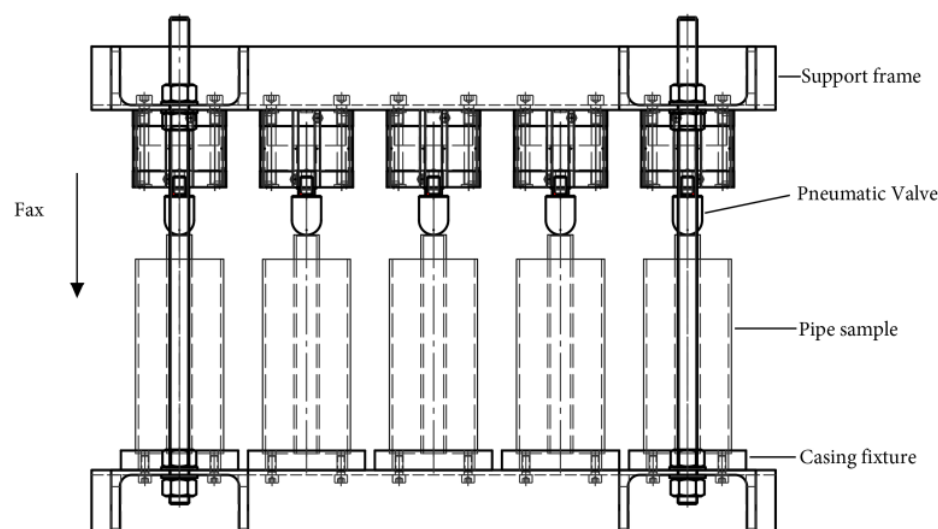


FIGURE 1 Test rig for mechanical cycling [Colour figure can be viewed at wileyonlinelibrary.com]

0.12 MPa at room temperature, this stress was selected, and the force to be applied is calculated as

$$F_{ax} = \tau \cdot L \cdot D_s \cdot \pi, \quad (1)$$

F_{ax} is the axial force

τ = shear stress

L = length of the pipe sample

D_s = diameter of the steel medium pipe.

This is a worst case scenario because

- The 0.12 MPa will be applied in the trial when the pipes are at 100°C and not at room temperature.
- According to the network design guidelines, the design shear stresses for operating conditions are 0.04 MPa.⁸

The number of cycles selected was again 250.

3.1.3 | Trial MT-m: Thermal and mechanical cycles—Mild conditions

In this trial, the mechanically applied shear stresses were set at 0.04 MPa. These stresses were applied in cycles from 0 to 0.04 MPa with the same frequency as in the previous trials. This value was selected as it is the acting shear stress under the network design point.⁸ The temperature was cycled between 25°C and 70°C, because buckling of the PE casing was experienced in trial MT-wc, as 100°C is too close to its heat deflecting temperature (Section 4). The number of cycles conducted was 125, representing half of the established number of cycles for fatigue check of DH pipes.

3.2 | Static tests

The test setup was chosen according to EN 253. The axial force was applied on the steel medium pipe until failure of the foam with a crosshead displacement controlled speed of 5 mm/min. The force was measured with a 20-kN load cell, accuracy class 0.5 (HBM, Darmstadt, Germany). Because the casing is fixed, the relative displacement between the steel medium pipe and the casing produces shear strain on the foam. The shear strain was calculated as

$$\gamma = \frac{u}{a}, \quad (2)$$

where u is the displacement of the steel medium pipe relative to the pipe casing and a is the thickness of the foam, equal to 28.5 mm.

The displacement was measured by three-dimensional (3-D) digital image correlation (DIC)²⁵ using an ARAMIS 5M adjustable stereo camera system (GOM mbH, Braunschweig, Germany) with a resolution of 2448 × 2051 pixels. The images were acquired at frequency of 1 Hz. Reference point markers were used to measure and track the 3D coordinates during the tests. Figure 2 presents a sketch of the test setup.

Five unaged samples were tested to obtain the reference values of strength, stiffness and toughness. For samples aged under cyclic loading, careful examination of possible damage or failure was undertaken and photographically documented prior to the execution of the static tests. Reweighing and remeasuring was undertaken. Seventy-two hours was allowed between the finalization of the cycles and the axial shear test to ensure stable conditions of the samples.

Additional static tests of unaged specimens were conducted under temperature, as to derive the acting stresses during the cyclic loading trials. For this, an environmental chamber (Weiss WK3-180/70/5-UKA, Reiskirchen, Germany) was placed around the universal testing machine. Samples were temperature soaked overnight to ensure stable conditions prior testing. Five specimens were tested at 70°C. Only one sample was tested at 100°C as it was decided to stop the tests after observing the buckling in the casing due to softening of the PE casing at that temperature.

Engineering stress–strain curves were derived from the obtained data. As per EN253, the shear stress is calculated from Equation 1.

The standard assumes that the maximum axial stresses are acting in the area continuous to the steel pipe. This is because it is the smallest area of the foam in the pipe section subjected to shear stresses. Our results show that indeed this is the area where the crack initiates (see Section 4). The shear strength is taken as the maximum value of the curve.

The G modulus is determined for each case from the slope of the initial linear segment of the curves.

The toughness (U) was calculated from the integral under the stress–strain curve until the strain upon failure is reached, at maximum value of the curve

$$U = \int_0^{\gamma_f} \tau \cdot d\gamma, \quad (3)$$

where

γ is the shear strain

γ_f is the shear strain upon failure

τ is the shear stress.

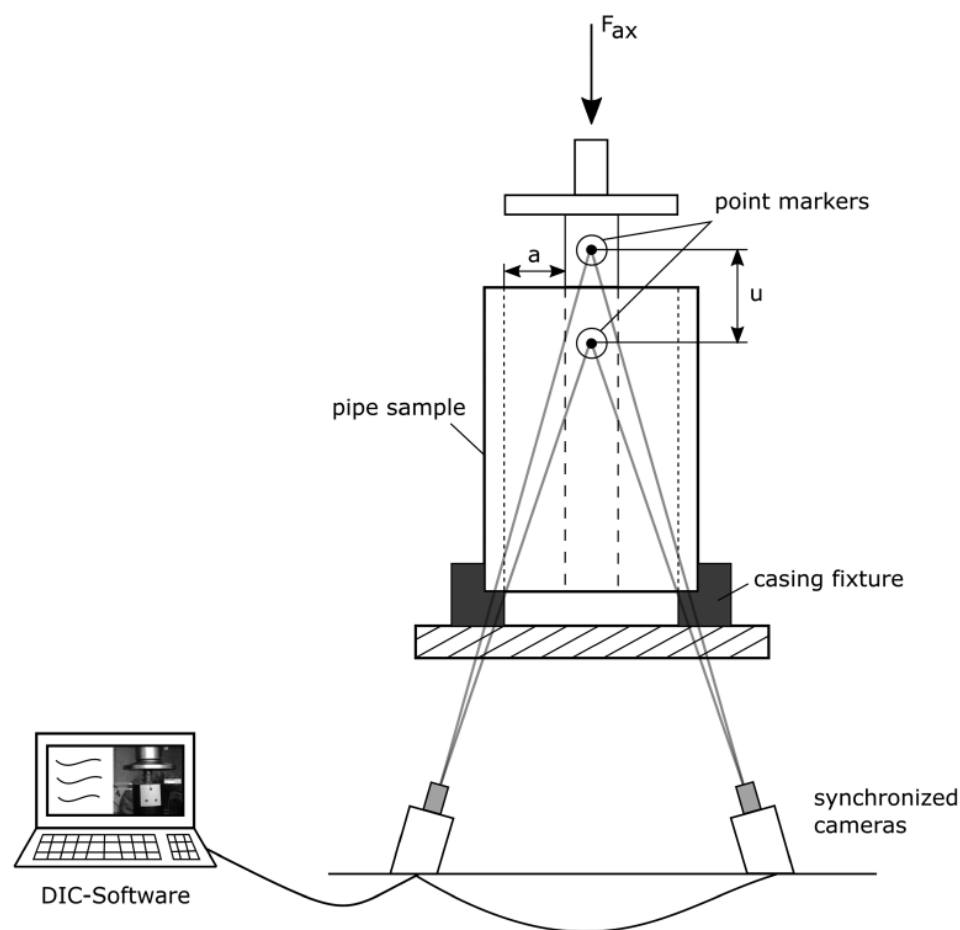


FIGURE 2 Schematic drawing of the static test setup. DIC, digital image correlation

3.3 | Evaluation of alterations in the chemical structure of the PU foam

Possible alterations in the chemical structure of the PU foam were evaluated through Fourier transform infrared spectroscopy (FTIR) in attenuated total reflection (ATR) mode^{3,26–29} using a Thermo Scientific Nicolet is 10 FTIR spectrometer with a diamond ATR Smart Orbit accessory (Dreieich, Germany). Infrared spectra were collected in transmission mode from 32 co-added scans and 6 cm^{-1} spectral resolution and converted to absorption as to allow linear correspondence between concentration and peak area. Spectra were baseline corrected, and the integrated absorbance for selected peaks were normalized using the C=C stretching vibration in the aromatic ring at 1595 cm^{-1} to correct for sample thickness differences. For each evaluated pipe, five foam samples were analysed, taken along the axial direction of the pipe, from the area in the vicinity of the steel medium pipe. Because the foam from unaged pipes presents a higher variability in their mechanical behaviour, foam from three unaged pipes was analysed, and one from each ageing trial. Assignments for many PU absorption bands can be found

in several publications.^{3,27,30} The focus was placed on observing potential post curing through changes on the concentration of non-reacted isocyanates (2270 cm^{-1}) and urethane linkages (1714 cm^{-1}), thermo-oxidative degradation and chain scissoring through changes in urethane linkages (1714 cm^{-1}) and CH_2 groups (peaks between 2975 and 2872 cm^{-1}) and changes in the strength of H bonds through the stretching vibration of the N-H groups (3302 cm^{-1}), and shift between H-bonded urea (1640 cm^{-1}) and monodentate urea (1650–1680 cm^{-1}).

3.4 | Documentation of crack propagation

In order to gain knowledge on the fracture and failure of the pre-insulated pipes, the resulting cracks from the static tests were photographically documented with a digital camera. The tested pipes were axially cut as to observe the crack propagation through interior of the foam. Prior to the cutting, a coloured epoxy resin was introduced through the cracks as to highlight them and evaluate their interconnections through the length of the pipe.

4 | RESULTS

4.1 | Effects of cyclic loads on the mechanical behaviour of the pre-insulated pipes

After the finalization of the programmed load cycles no weight change detected in any of the tested specimens, nor damage or geometry change for specimens from trials T or MT-m. A yellowing of the specimens after ageing was observed for the samples aged with 250 cycles (T and MT-wc), which is as a sign for thermo-oxidative degradation.³ After later observation of the fractured pipes, it could be seen that this phenomenon was only superficial.

For the MT-wc trial, 24 of the 250 cycles were conducted with a constant stress of 0.12 MPa due to a malfunction of the control system. In this case, all five specimens exhibited compression and buckling of the casing at the bottom of the samples, as well as failure of the foam close to the steel interface, as can be seen in Figure 3. This caused a length reduction of the casing from 200 to approximately 196 mm. This can be related to the vicinity of the 100°C test T° to the melting T° of high-density PE (HDPE), which is in the range 118°C–146°C depending on molecular weight and crystallization conditions.³¹ Because the cycles were load controlled, we

do not know in which cycle the failure occurred. However, from the static test performed on an unaged sample at 100°C (see Section 3.4), the buckling occurred at 0.34 MPa, which is higher than the applied 0.12 MPa during the cyclic loading test. The failure at this load is therefore a consequence of the cyclic loading.

Figure 4 shows the obtained engineering stress–strain curve obtained through Trials T (A), MT-wc (B) and MT-m (C). Curves for the unaged samples tested at room conditions are added in all plots for reference. For the MT-wc trial, the damaged section of one of the specimens was removed before testing as to assess the impact of the pre-existing failure on the obtained results. The obtained max shear strength (τ_{\max}), stiffness (G) and toughness (U) are presented in Table 2 and Figure 5.

4.2 | Effects of temperature on the mechanical behaviour of the pre-insulated pipes

The obtained stress–strain curves for unaged samples tested at different temperatures are shown in Figure 6, and obtained values for strength, stiffness and toughness presented in Table 3.

FIGURE 3 Buckling and compression of the casing (A) and failure of the foam at the foam–steel interface (B) after MT-wc trial [Colour figure can be viewed at wileyonlinelibrary.com]

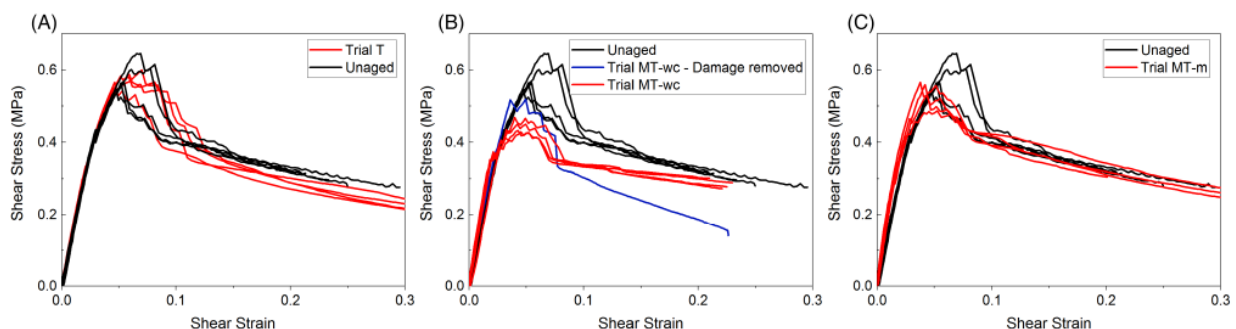
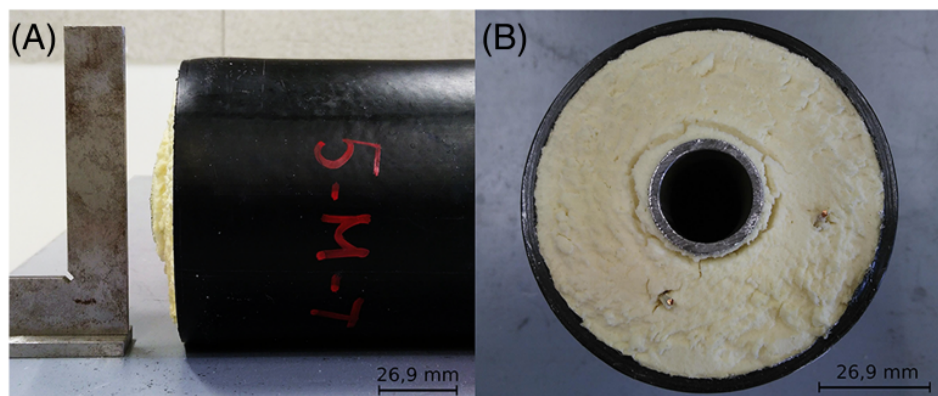


FIGURE 4 Stress–strain curves for static tests, unaged and after Trails T (A), MT-wc (B) and MT-m (C) [Colour figure can be viewed at wileyonlinelibrary.com]

TABLE 2 Results from static tests for different cycling trials

Cycling trials	τ_{max} (MPa)	G (MPa)	U (MJ/m ³)	γ_f
Unaged	0.58 ± 0.04^a	16.55 ± 0.51^a	0.019 ± 0.003^a	0.081 ± 0.063^a
MT-wc	0.45 ± 0.02^a	17.71 ± 2.34	0.013 ± 0.003^a	0.046 ± 0.003^a
MT-wc (damage removed)	0.52	16.52	0.010	0.035
T	0.58 ± 0.01^a	16.80 ± 0.51^a	0.022 ± 0.005^a	0.058 ± 0.0097^a
MT-m	0.54 ± 0.01^a	20.44 ± 0.77^a	0.015 ± 0.002^a	0.043 ± 0.0062^a

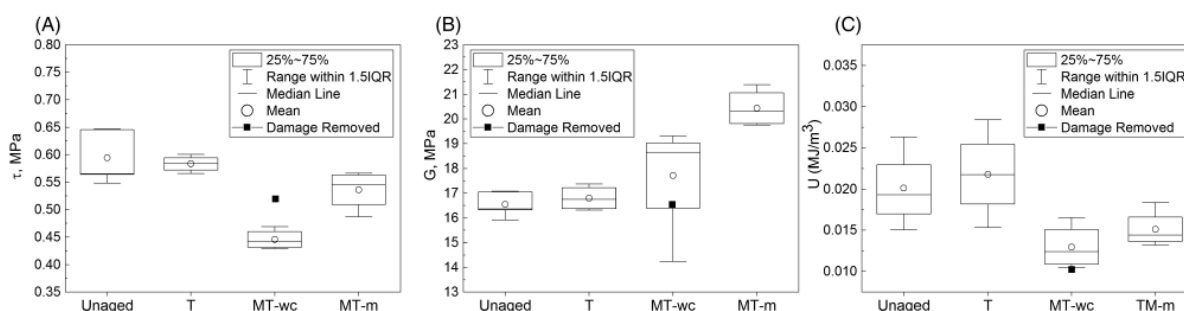
^aStandard deviation.

FIGURE 5 Obtained shear strength (A), stiffness (B) and toughness (C) for the conducted trials

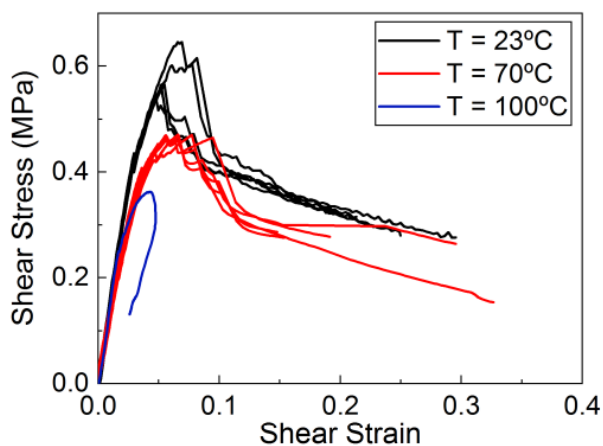


FIGURE 6 Stress–strain curve of unaged samples under different temperatures [Colour figure can be viewed at wileyonlinelibrary.com]

As previously indicated, for the test at 100°C, only one sample was tested. Due to the buckling, the strain is reduced after reaching a maximum, as the casing is no longer holding the applied load. However, through careful observation of the obtained stress–strain curve and the test digital images, valuable information towards the understanding of the failure of the specimens from trial MT-wc (see Section 3.1). While the maximum is reached at 0.36 MPa stress and 0.043 strain, the compression of the casing starts practically from the beginning of the test, although buckling is only evident starting at a loading of approximately 0.34 MPa. A first peak is observed at 0.25 MPa in the stress–strain curve, which could be the offset on which the failure of the foam and the buckling of the casing started. The buckling failure in the static test occurred at a higher stress than the 0.12 MPa applied in the cyclic loading, which is the point taken as the end

TABLE 3 Results from static tests conducted at different temperatures

T (°C)	τ_{max} (MPa)	G (MPa)	U (MJ/m ³)	γ_f
23	0.58 ± 0.04^a	16.55 ± 0.51^a	0.019 ± 0.003^a	0.081 ± 0.063^a
70	0.46 ± 0.003^a	13.42 ± 1.43^a	0.020 ± 0.004^a	0.063 ± 0.008^a
100	0.36	16.34	—	0.043

^aStandard deviation.

of the linear elastic region, showing that the failure at this stress was due to the effects of the cyclic loads.

As it can be seen, the shear strength is reduced by 20% and the modulus is reduced by 18% when testing at 70°C compared with 23°C. From these tests, we can derive that the acting strain during the cyclic loading tests was 0.008 for trial MT-wc and between 0.001 and 0.003 for trial MT-m.

4.3 | Evaluation of alterations in the chemical structure of the PU foam

PU presents a segmented structure, consisting of a soft segment originating from the polyol chain, and a hard segment, mainly composed of aromatic rings bonded together through urea linkages. The urethane bond chemically links both segments covalently. When the diisocyanate is in excess, further chemical cross linking can occur through the creation of allophanate linkages. The hard segments are strongly hydrogen bonded, which act as physical crosslinks²⁶ and are reported to have a significant impact on the PU's physical behaviour, increasing its mechanical properties,^{32,33} and also, the inhomogeneity of the material.²⁶ A degradation of the links, chemical and/or physical, would lead to a degradation in the PU foam's mechanical properties.

A typical spectrum obtained for an unaged sample with the identified peaks is shown in Figure 7.

The obtained normalized integrated absorbance for the selected peaks can be found in Figure 8.

Unreacted isocyanates were not detected in the obtained spectra. An increase in peak 1712 cm^{-1} would imply further curing of the PU from its unreacted components, while its decrease would imply scissoring of the chain. Thermo-oxidative degradation is reported to occur mainly in the soft segment³ and a decrease of the concentration of C–H links through the band at 2975–2872 cm^{-1} (evaluated through the peaks at 2928 and 2868 cm^{-1}) would be a sign of this. A decrease in the N–H stretch band at 3305 cm^{-1} and a shift from the bidentate urea at 1640 cm^{-1} to monodentate urea at 1650–1680 cm^{-1} would be a sign of weakening of the H bonds. The bidentate urea peak was not visible in the obtained spectra. Peak deconvolution was not attempted.

As it can be seen, the differences in the normalized absorbance for the selected peaks after cyclic loading are within the variability found in unaged samples. From this analysis, we can conclude that the applied cyclic loading did not produce changes in the molecular structure of the polymer matrix.

4.4 | Crack propagation

After sectioning the tested pipes, it was seen that the same crack pattern occurred consistently in all specimens, independently of aged or unaged. Seven to nine cracks appear through the axial length of the pipe, with a constant distance of 2–2.5 cm between them. They span from the area close to the foam–steel interface to approximately 2 cm away from the PE casing, in an

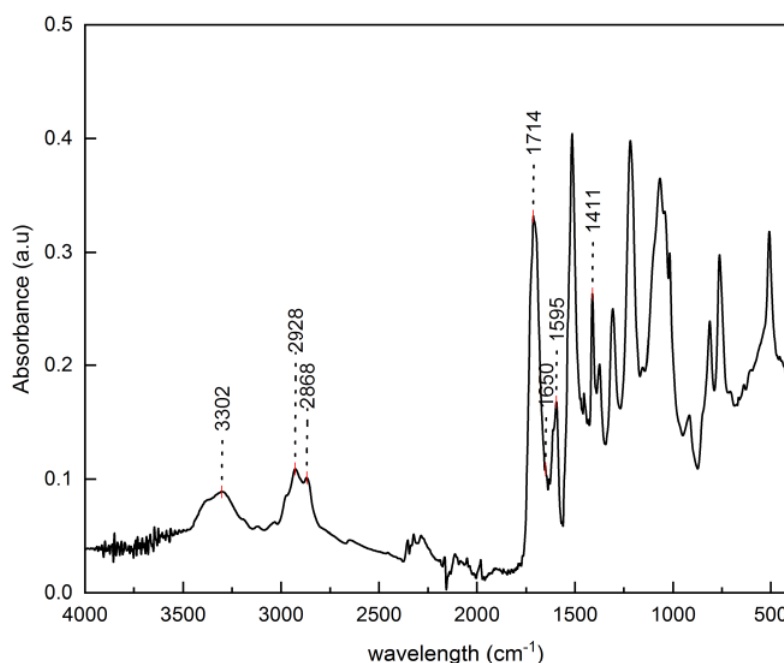


FIGURE 7 Obtained Fourier transform infrared spectroscopy (FTIR) for the foam of an unaged pipe [Colour figure can be viewed at wileyonlinelibrary.com]

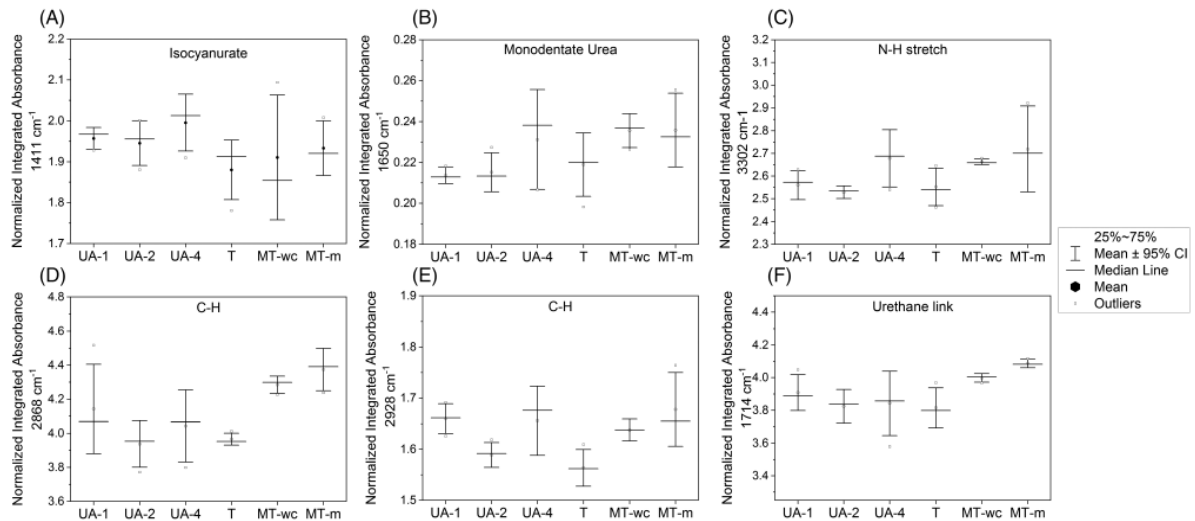


FIGURE 8 Normalized integrated absorbance for selected peaks (A–F), for unaged (UA) pipes, T, MT-wc and MT-m cyclic pipes. CI, confidence interval

approximately 45° angle with the horizontal. Only the bottom crack reaches the PE casing, which could be the result of the stress concentrations by the test fixture on the casing. From this pattern, we can derive that the cracks initiate in Mode II fracture close to the steel interface, which is the area where the shear stresses are maximum, and then kink and propagate in Mode I fracture.

For the MT-wc specimens (Figure 9A), different colours were used for the initial failure near the foam–steel interface due to the cyclic loads (red) and that close to the foam–casing due to the static test (blue). It could be seen that the initial failure propagated through the foam–steel interface approximately 1/3 or the pipe length, interconnecting the first and third cracks.

As for the fracture type, from the evaluation of the specimens after shear tests, it can be observed that for the 18 specimens tested at room temperature, aged and unaged, cohesive fracture occurred in the foam, except for one case where both failure of the adhesion of the PU–steel bond and cohesive fracture of the foam occurred. For the specimens tested at 70°C (Figure 9B and C), both adhesive and cohesive failure occurred in three out of five specimens. This could be easily observed as the coloured epoxy resin introduced through the cracks at the bottom of the specimens flowed until exiting at the steel–foam interface and colouring all cracks, showing they are interconnected, while for the case of specimens sheared at room

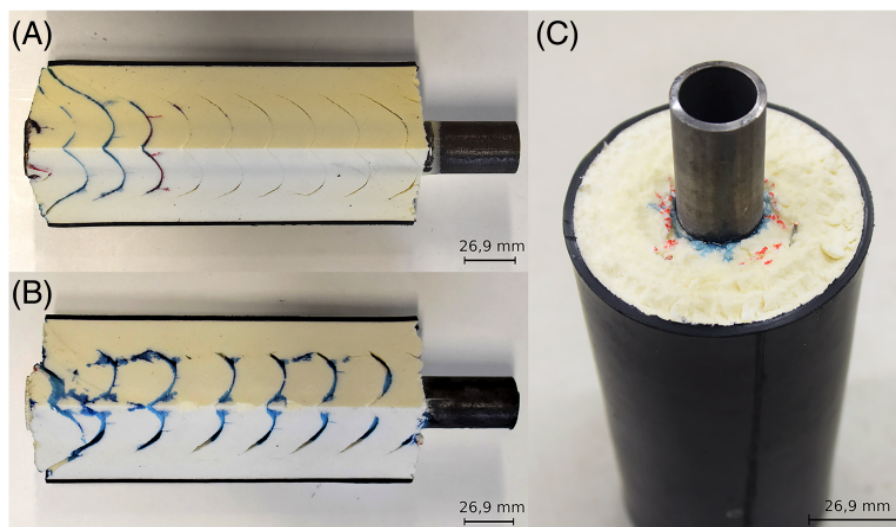


FIGURE 9 (A) Specimen tested at room temperature (MT-wc), (B) specimen tested at 70°C where the coloured resin flowed through the foam–steel interphase along the pipe, (C) detail of the foam–steel interface for the specimen tested at 70°C . The coloured resin proves loss of adhesion between them [Colour figure can be viewed at wileyonlinelibrary.com]

temperature, the colour only flowed through the first layers of cracks (see Figure 9).

5 | DISCUSSION

The main objective of this study is the evaluation of the impact of cyclic loads on the mechanical properties of the pre-insulated pipes. From Figure 5, we can observe that the combination of cyclic mechanical and thermal loads has a stronger effect on the mechanical properties of the pre-insulated pipes than the thermal loads on their own. Because the samples of the T series are under free expansion conditions, the caused strain is limited to the mismatch of thermal expansion between the material layers. From the obtained values of strength and stiffness, we can conclude that these strains are not enough to deteriorate the structure within the number of cycles under consideration. The main effect of the temperature loads is a homogenization of the behaviour between specimens, reducing the standard deviation of the measured strength values while maintaining the average values similar to the unaged control series. Foam-filled composites produced in batches for structural applications in the building sector present a higher variability in material properties than those manufactured in bulk and under tightly controlled curing conditions for applications such as shipping and aerospace.^{34,35} Therefore, the temperature could produce a post-curing effect on the PU, leading to a higher homogeneity between specimens. The post-curing would increase the number of links in the polymer matrix, which is consistent with the slight increase in toughness observed (Figure 5C), as more energy is required to fracture a larger number of links. Previous authors have reported an increase in strength^{3,6} and stiffness³⁵ of PU foam after an initial thermal ageing and related it to post-curing of the PU. However, this was not confirmed by our FTIR analysis (see Figure 8F).

A degradation of the strength and toughness of the pre-insulated pipes due to the combined thermal and mechanical loads can be observed from Figure 5A,C. The degradation is more severe for the MT-wc cycles, with an average 24% loss of strength versus 8.5% loss for the cycles under milder conditions. If we consider the strength obtained for the sample tested after removal of the damaged section, the strength reduction for the MT-wc trial is of approximately 11%. While this is the result of one sample only, it is very likely that test setup fixture caused stress concentration on the lower section of the pipes, leading to premature failure. It was observed during the execution of the tests that the fitting of the pipe in the fixture was tight, as the casing buckling had increased the sample diameter in that area. Influence of setup-

induced stress concentrations on results in shear tests is often encountered and reported.^{36,37}

From Figure 6B, we can observe a reduction of the experimental scatter in the G modulus with similar mean values between the control specimens and the T cycled specimens and an increase in the modulus for the thermal and mechanically cycled samples. This indicates that the mechanical cycles have a strain hardening effect on the foam. This would be caused by the orientation of the PU segments during extension,³⁸ facilitated as the higher temperature increases the mobility of the polymer chains. Our results show a higher increase of the stiffness for the MT-m trial than the MT-wc, which was subjected to higher stress and number of cycles. Previous authors have reported that the hardening effect is confined to the first several cycles.³⁸ This could imply that the initial cycles produce a hardening effect, as obtained in trial MT-m, and that the additional cycles conducted in trial MT-wc would produce a degradation of the stiffness from the hardened state.

As for the effects of temperature on the static tests, the mechanical properties of the foam decrease with increasing temperature, as expected. As can be seen from Tables 2 and 3, the effect of temperature on the mechanical behaviour of the foam is stronger than the effect of the ageing itself. The glass transition temperature (T_g) of PU is set around 200°C–250°C.⁹ Below this T_g , the polymer is in the glassy regime, being the modulus directly linked with the Van-der-Waals intermolecular bonds, which are influenced by T_g , causing the stiffness to decrease with increasing temperature.²¹ As mentioned earlier, a source of strength in the PU foam are the H bonds in the hard segment. Previous studies have shown that these H bonds in PU foam are disrupted at temperatures starting around 40°C^{28,39} and this disruption is the most probable cause of loss of strength for our tests under temperature. These H bonds would reform as the temperature is brought back to ambient temperature. Permanent bond disruption could take place if an H bond is replaced by a water molecule, as proposed by Herrington and Klarfeld.⁴⁰ These water to water H bonds could break upon compression of the foam, allowing for chain slippage. França de Sá et al.²⁷ propose that the elimination of some bonded interactions would enable the penetration of further water molecules as well as the interaction of oxidation products into the free space between the hard segment chains, leading to the formation of new H-bonding interactions between these compounds and the urea group. Because the relative humidity inside both environmental chambers used was close to zero, permanent H-bond disruption or replacement would be unlikely, as confirmed through our FTIR analysis of the post-cycled samples (see Figure 8B).

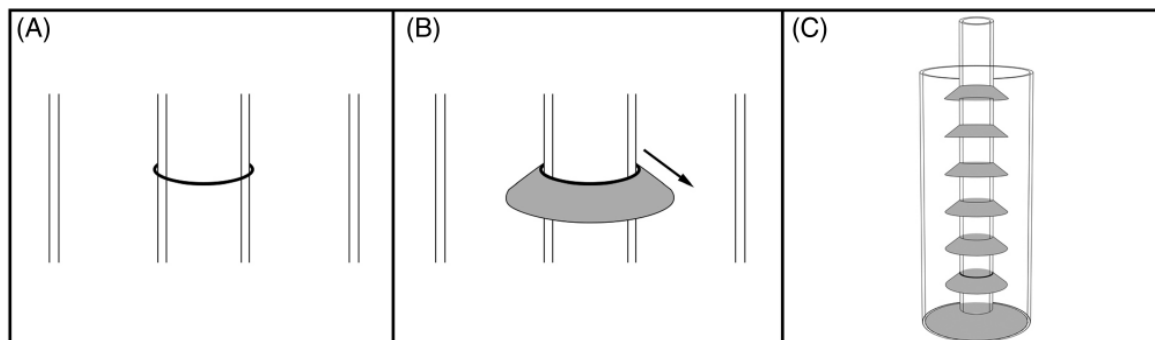


FIGURE 10 (A–C) Crack initiation and propagation in the polyurethane (PU) foam. Shaded areas represent crack planes

Thermal oxidation PU was not found to have occurred during the applied cycles, consistent with the findings of previous authors given the maximum applied temperature of 100°C.^{3,24,41} This means that the loss of mechanical properties as a consequence of the applied cyclic loads is not due to molecular changes on the polymer matrix, but could be related to other phenomenon as stress relaxation or fatigue.

As for crack propagation through the foam, propagation in Mode I is observed. Previous experimental studies indicate that this is the most common crack propagation mode in foam sandwich structures.^{37,42} The consistent distance between cracks indicate that the foam experiences strain localizations in the axial direction, displaced by approximately 2-cm intervals, which are the main driver for the crack nucleation. Pre-existing voids or other defects would produce cracks located randomly. This provides interesting information for the failure evaluation of the piping networks. A schematic drawing of the crack initiation, propagation and resulting fracture pattern is presented in Figure 10.

Concerning the fracture type, previous research on the cohesive laws between PU and galvanized steel⁴³ concluded that the fracture energy of the interface for Mode I tests appeared similar than that of the PU foam, with similar energy release rates for both interfacial failure and fracture of the foam cells adjacent to the interface, suggesting failure of the foam. But the adhesive bond strength at the interface also decreases with the increase in temperature. Fatigue studies on PU sandwich structures⁴⁴ report that debonding occurs when testing at higher frequencies due to increase in temperature at the mating surfaces. This suggests that, when conducting the shear tests at elevated temperatures, the strength of the adhesive bond between the foam and the steel is reduced, facilitating failure at the interface, while at room temperature, the predominant failure mechanism is cohesive fracture of the foam.

6 | CONCLUSIONS AND OUTLOOK

The main conclusions of our work are as follows:

- The combined cyclic thermal and mechanical loads evaluated in our trials have an effect on the PU foam, reducing its shear strength and increasing its stiffness. Despite this reduction, all the aged samples of the three executed trials would comply with the minimum shear strength requirement of EN253.
- Temperature has an important influence on the mechanical behaviour of the PU foam. The change in mechanical properties at the operating conditions of DH networks for the PU foam is significantly higher than for steel. Therefore, calculations for the steel pipe cannot be assumed to be valid for the sandwich composite.
- Crack initiation and propagation along the pipe samples follow a very consistent pattern between samples, with cracks initiating in Mode II and propagating in Mode I. The consistent axial displacement of approximately 2 cm from each other suggest the formation of strain localizations.
- At room temperature, cohesive fracture of the foam is obtained, while at higher temperatures, both adhesive failure at the foam–steel interface and cohesive fracture of the foam are found.

The presented work is limited to the investigated pipe dimensions representing household connections. The evaluation of the transferability of the results to distribution and main DH pipelines with larger dimensions requires further investigation.

ACKNOWLEDGEMENTS

The authors would like to express their gratitude to Logstor A/S (Løgstør, Denmark) and in particular Peter Jorsal and Tobias Langer for providing the district

heating pipes and discussions about the foam formulation. Assistance by Marcus Illguth for the design of the mechanical cyclic test rig, Jens Ohlendieck for the execution of the static tests, and Erik Borrs for the acquisition of the FTIR spectra are gracefully acknowledged.

This research was self-funded by the Hafencity University. Open access funding enabled and organized by Projekt DEAL.

CONFLICT OF INTEREST

The authors declare to have no conflict of interest.

AUTHOR CONTRIBUTION

I. W. was responsible for the study conceptualization and supervision of the research project. L. D. was responsible for the design of experiments, data collection and analysis and chiefly responsible for preparing the manuscript. Both authors contributed with the critical discussion of results and editing of the manuscript.

NOMENCLATURE

a	foam thickness
D_s	diameter of steel medium pipe
F_{ax}	axial force
G	shear modulus
L	pipe sample length
T_g	glass transition temperature
U	toughness
u	displacement
γ	shear strain
γ_f	shear strain at failure
τ	shear stress
τ_{max}	shear strength

ORCID

Lucia Doyle  <https://orcid.org/0000-0001-8697-8621>

Ingo Weidlich  <https://orcid.org/0000-0003-2653-0133>

REFERENCES

- EN 253:2019. District heating pipes. Bonded single pipe systems for directly buried hot water networks. Factory made pipe assembly of steel service pipe, polyurethane thermal insulation and a casing of polyethylene.
- Christensen. Fatigue analysis of district heating systems. *Netherlands Agency for Energy and the Environment* 1999
- Yarahmadi N, Vega A, Jakubowicz I. Accelerated ageing and degradation characteristics of rigid polyurethane foam. *Polym Degrad Stab.* 2017;138:192-200.
- Leuteritz A, Döring K-D, Lampke T, Kuehnert I. Accelerated ageing of plastic jacket pipes for district heating. *Polym Test.* 2016;51:142-147.
- Vega A, Yarahmadi N, Jakubowicz I. Optimal conditions for accelerated thermal ageing of district heating pipes. *Energy Procedia.* 2018;149:79-83.
- Vega A, Yarahmadi N, Jakubowicz I. Determination of the long-term performance of district heating pipes through accelerated ageing. *Polym Degrad Stab.* 2018;153:15-22.
- Randlov P, Hansen KE, Penderos M. Temperature variations in preinsulated DH pipes low cycle fatigue. <http://www.leadhc.org/the-research/annexes/1993-1996-annex-iv/annex-iv-project-06.html>
- AGFW e.V, ed. Installation and calculations of preinsulated bonded pipes for district heating networks. *Static design; basics of stress analysis*
- Gibson LJ, Ashby MF. *Cellular Solids*. Cambridge: Cambridge University Press; 1997.
- Cotgreave T, Shortall JB. Failure mechanisms in fibre reinforced rigid polyurethane foam. *J Cell Plast.* 1977;13(4):240-244.
- Ridha M. Mechanical and Failure Properties of rigid Polyurethane Foam Under Tension. *PhD Dissertation*, National University of Singapore, 2007
- Huang JS, Lin JY. Fatigue of cellular materials. *Acta Mater.* 1996;44(1):289-296.
- Zenkert D, Shipsha A, Burman M. Fatigue of closed cell foams. *J Sandw Struct Mater.* 2006;8(6):517-538.
- McCullough KYG, Fleck NA, Ashby MF. Toughness of aluminium alloy foams. *Acta Mater.* 1999;47(8):2331-2343.
- Olurin O. Fatigue crack propagation in aluminium alloy foams. *Int J Fatigue.* 2001;23(5):375-382.
- McCullough KYG, Fleck NA. The stress-life fatigue behaviour of aluminium alloy foams. *Fatigue Fract Eng Mater Struct.* 2000;23(3):199-208. <https://doi.org/10.1046/j.1460-2695.2000.00261.x>
- Burman M. Fatigue Crack Initiation and Propagation in Sandwich Structures. *PhD. Dissertation*, Royal Institute of Technology, Sweden, 1998
- Marsavina L, Linul E, Voiconi T, Sadowski T. A comparison between dynamic and static fracture toughness of polyurethane foams. *Polym Test.* 2013;32(4):673-680.
- Marsavina L, Constantinescu DM, Linul E, Apostol DA, Voiconi T, Sadowski T. Refinements on fracture toughness of PUR foams. *Eng Fract Mech.* 2014;129:54-66.
- Marsavina L, Constantinescu DM, Linul E, Voiconi T, Apostol DA. Shear and mode II fracture of PUR foams. *Eng Fail Anal.* 2015;58:465-476.
- Kanny K, Mahfuz H, Thomas T, Jeelani S. Temperature effects on the fatigue behavior of foam core sandwich structures. *Polym Polym Compos.* 2004;12(7):551-559.
- Linul E, Marsavina L. Assessment of sandwich beams with rigid polyurethane foam core using failure-mode maps. *Proceedings of the Romanian Academy*, 2015
- Doyle L, Weidlich I, Illguth M. Anisotropy in Polyurethane Pre-Insulated Pipes. *Polymers.* 2019;11:2074. <https://doi.org/10.3390/polym11122074>
- Yarahmadi N, Sällström JH. Improved maintenance strategies for district heating pipe-lines. *IEA-DHC final report, Annex X*, Stockholm, Sweden, 2014
- Peters WH, Ranson WF. Digital Imaging Techniques In Experimental Stress Analysis. *Opt Eng.* 1982;21(3):427-431. <https://doi.org/10.1117/12.7972925>

26. Kontou E, Spathis G, Niaounakis M, Kefalas V. Physical and chemical cross-linking effects in polyurethane elastomers. *Colloid Polym Sci*. 1990;268(7):636-644.
27. França de Sá S, Ferreira JL, Pombo Cardoso I, Macedo R, Ramos AM. Shedding new light on polyurethane degradation: assessing foams condition in design objects. *Polym Degrad Stab*. 2017;144:354-365.
28. Senich GA, MacKnight WJ. Fourier transform infrared thermal analysis of a segmented polyurethane. *Macromolecules*. 1980;13(1):106-110.
29. Cole KC, van Gheluwe P, Hébrard MJ, Leroux J. Flexible polyurethane foam. I. FTIR analysis of residual isocyanate. *J Appl Polym Sci*. 1987;34:395-407.
30. Hepburn C. *Polyurethane Elastomers*. Dordrecht: Springer Netherlands; 2000.
31. Mark JE (Ed). *Polymer Data Handbook*. New York: Oxford University Press; 1999.
32. Petrović ZS, Ilavský M, Dusek K, Vidaković M, Javni I, Banjanin B. The effect of crosslinking on properties of polyurethane elastomers. *J Appl Polym Sci*. 1991;42:391-398.
33. Smith TL. Strength of elastomers, a perspective. *Polym Eng Sci*. 1977;17(3):129-143.
34. Banerjee B, Kraus B, Das R. Characterization of an anisotropic low-density closed-cell polyurethane foam: Unpublished, 2015
35. Tuwair H, Volz J, ElGawady M, Mohamed M, Chandrashekhara K, Birman V. Behavior of GFRP bridge deck panels infilled with polyurethane foam under various environmental exposure. *Structure*. 2016;5:141-151.
36. Gdoutos EE, Daniel IM, Wang K-A. Failure of cellular foams under multiaxial loading. *Compos A: Appl Sci Manuf*. 2002;33(2):163-176.
37. Gibson RF. A mechanics of materials/fracture mechanics analysis of core shear failure in foam core composite sandwich beams. *J Sandw Struct Mater*. 2011;13(1):83-95.
38. Kim BK, Lee SY, Xu M. Polyurethanes having shape memory effects. *Polymer*. 1996;37(26):5781-5793.
39. Teo L-S, Chen C-Y, Kuo J-F. Fourier transform infrared spectroscopy study on effects of temperature on hydrogen bonding in amine-containing polyurethanes and poly (urethane-urea)s. *Macromolecules*. 1997;30(6):1793-1799.
40. Herrington RM, Klarfeld DL. Humid aged compression set phenomena in water blown Hr molded foams. *J Cell Plast*. 1984;20(1):58-63.
41. Yarahmadi N, Vega A, Jakubowicz I. Determination of essential parameters influencing service life time of polyurethane insulation in district heating pipes. *Energy Procedia*. 2017;116:320-323.
42. Carlsson L, Matteson R, Aviles F, Loup D. Crack path in foam cored DCB sandwich fracture specimens. *Compos Sci Technol*. 2005;65(15-16):2612-2621.
43. Kraus B, Das R, Banerjee B. Characterization of Cohesive Laws for Foam-Metal Interfaces. *Int J Appl Mech*. 2014;6:1450072-1-1450072-31. <https://doi.org/10.1142/s1758825114500720>
44. Sharma SC, Murthy HNN, Krishna M. Interfacial studies in fatigue behavior of polyurethane Sandwich structures. *J Reinf Plast Comp*. 2004;23(8):893-903.

How to cite this article: Doyle L, Weidlich I. Effects of thermal and mechanical cyclic loads on polyurethane pre-insulated pipes. *Fatigue Fract Eng Mater Struct*. 2021;44:156-168. <https://doi.org/10.1111/ffe.13347>

Annex VIII. Publication [BJ2]



Article

Anisotropy in Polyurethane Pre-Insulated Pipes

Lucía Doyle , Ingo Weidlich *  and Marcus Illguth 

Infrastructural Engineering, HafenCity University, 20457 Hamburg, Germany;
lucia.doyle@hcu-hamburg.de (L.D.); marcus.illguth@hcu-hamburg.de (M.I.)

* Correspondence: ingo.weidlich@hcu-hamburg.de

Received: 15 November 2019; Accepted: 9 December 2019; Published: 12 December 2019



Abstract: The polyurethane foam in district heating pre-insulated pipes has a critical role to play both as thermal insulation and as load bearing element, as it serves as bond between the medium pipe and the casing. Hence, knowledge on how the foam behaves under multiaxial stresses is of great importance for the design as well as for aging predictions of the network. It is known that cell shape anisotropy in polymeric foams leads to anisotropy in its mechanical properties. In this study, we evaluate and quantify the microstructural anisotropy of PU foam from pre-insulated pipes as well as its mechanical behaviour under compression in the three orthogonal directions. We cover rigid and flexible PU foam, batch and continuous manufacturing, and different pipe diameters. The results were compared with those predicted by available rectangular and Kelvin cell shape models. We have found that PU from pre-insulated pipes is orthotropic and present stronger anisotropy than that typically found in PU slabs. The traditional bonded pipes under consideration behaved in a similar way. However, when comparing the two flexible pipes in this study, despite no significant differences in cell shape anisotropy were found, a significantly different behaviour for the E modulus ratio was observed. This shows that while the manufacturing process exerts the main influence on cell shape anisotropy, to explain the difference in stiffness behaviour other factors need to be taken into consideration, such as cell size and cell size variability.

Keywords: cell anisotropy; polyurethane foam; sandwich structure; district heating; multiaxial loading

1. Introduction

District heating (DH) pre-insulated pipes are composed of an inner medium pipe, polyurethane (PU) insulating foam, and a polyethylene (PE) casing. The PU foam bonds the medium pipe and the casing. The medium pipe can be steel or plastic (i.e., PEX) depending on the network operating temperature. Available PU pre-insulated bonded pipes can be manufactured with different processes and PU formulations. Rigid bonded steel pipes are the most widely used. They are manufactured in batch, where the PU is injected between the service pipe and the casing. Service pipe and casing are manufactured in a separate process. The flexible pipes, which have appeared in the market more recently, are manufactured in a continuous process where the PU is poured into a moving casting mould, and the PU material flows around the moving pipe. Then, the PE outer casing is extruded in place [1]. Pre-insulated flexible pipes are available, presenting different degrees of flexibility achieved through different formulations of the PU foam and with corrugated and smooth casing. Figure 1 presents a cross-section of a pre-insulated pipe.

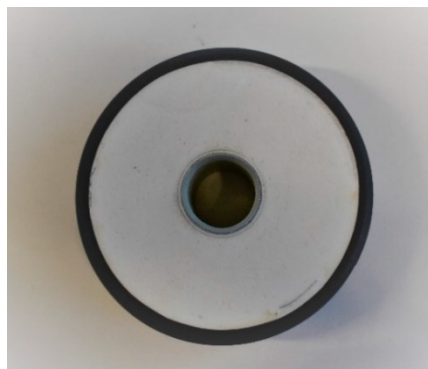


Figure 1. Cross-section of a PU pre-insulated pipe.

DH pipe networks are usually buried underground. They are subjected to multiaxial loading, as the operation temperature produces an expansion of the pipe, which is partially restrained by the surrounding soil. This expansion leads to axial shear stress on the foam, as the axial expansion is partially counterbalanced by the soil friction, and in compression of the foam in the radial direction due to the earth pressure. Hence, the polyurethane foam in this application has a critical role to play both as thermal insulation and as load bearing element, minimizing the heat losses of the network, critical for the sustainability of the whole district heating system, while serving as bond between the medium pipe and the casing. Therefore, knowledge on how the foam behaves under multiaxial stresses is of great importance both for the design as for aging predictions of the network, which is key as this infrastructure's lifecycle is expected to last for over 30 years. However, details on the microstructure and behaviour of the PU foam in DH pre-insulated pipes are insufficiently well known, and therefore design standards and calculation methods used in the sector relate mainly to the steel medium pipe [2,3]. While aging of PU foam in district heating pipes has been a subject of research during recent years, the focus has been placed mainly on oxidation and thermal degradation [4–6], but details on the microstructure and its relation to the bonded pipe's mechanical behaviour remain mostly unexplored. In order to optimize structural design, detailed understanding of the mechanical behaviour of the elementary materials is required. There is a need for better characterization of the PU foam used in DH pipes, which would allow the development of material models and numerical simulations that could support the design process.

The mechanical properties of cellular solids are greatly influenced by the microstructure of the foam, as well as the properties of the solid material constituting it. Key structural features are [7]:

- The relative density.
- The degree to which cells are open or closed.
- The geometric anisotropy of the foams.

It is a noted phenomenon that the cells of polymeric foams tend to be elongated in the foam rise direction of the mould due to the acting viscous forces during the foaming process, and are hence anisotropic. This phenomenon and its impact on the material's properties is well described in [7].

The PU foam used in DH pipe insulation presents closed-cells. The first model relating the shape-anisotropy to the mechanical properties of cellular foams is proposed by Huber and Gibson [8] as an extension of the model proposed by Gibson and Ashby [9]. This model is based on a simple cubic cell geometry. The cell aspect ratio R , would influence the elastic modulus of the cell foam according to:

$$\frac{E_3}{E_2} = \frac{E_3}{E_1} = \frac{2R^2}{1 + \left(\frac{1}{R}\right)^3}, \quad (1)$$

where E_3 is the elastic modulus in the rising direction, E_1 and E_2 in the perpendicular direction to the foam rise, and R is the anisotropy ratio, defined as the ratio of the largest cell dimension to the smallest.

This expression assumes axisymmetric cells. For the case of orthotropic cells, where all three dimensions of the cell differ, the different values of R are needed to characterize it:

$$\frac{E_1}{E_2} = (R_{12})^2 \left[\frac{1 + (R_{32})^3}{1 + (R_{31})^3} \right], \quad (2)$$

$$\frac{E_2}{E_3} = (R_{23})^2 \left[\frac{1 + (R_{13})^3}{1 + (R_{12})^3} \right], \quad (3)$$

$$\frac{E_3}{E_1} = (R_{31})^2 \left[\frac{1 + (R_{21})^3}{1 + (R_{23})^3} \right] \quad (4)$$

For closed cell foams, an additional term should be considered [7]:

$$(1 - \phi) \frac{2R}{1 + \left(\frac{1}{R}\right)}, \quad (5)$$

where Φ is the fraction of solid material located in the cell's struts, which for open cell foams is $\phi = 1$. However, closed-cell foams tend to mechanically behave similar to open-cell ones when the membranes across the cell faces are thin in relation to the cell edges [8]. Since measurement of cell wall thickness is difficult [10], we will assume the PU under study behaves mechanically, such as an open cell foam.

Later models relating the mechanical properties to the cell anisotropy have been developed for open cell foams using an elongated tetrakaidecahedron Kelvin model [11] as the repeating unit cell, such as those from Gong et. al. [12], Ridha et. al. [13] and Sullivan et al. [14]. This geometry more closely represents the cellular structure observed in polymer foams than the rectangular cell. The fundamental difference between the Kelvin model developed by Sullivan et al. from those by previous authors is that the geometry and size of the repeating unit cell is defined by three independent dimensions, allowing to account for additional variation in the unit cell shape. The equivalent expression to Equation (1) with this model would be:

$$\frac{E_3}{E_1} = \frac{E_3}{E_2} = \frac{R}{4} \left[\frac{\left(2\tilde{Q}R^2 + \frac{64Q^3}{\sqrt{16+\tilde{Q}^2R^2}} \right) C_1 + \frac{8R\tilde{Q}^3 C_2 (32+4Q\sqrt{16+\tilde{Q}^2R^2})}{(4Q+2\sqrt{16+\tilde{Q}^2R^2})(16+\tilde{Q}^2R^2)} \left(\frac{\rho_f}{\rho_s} \right)}{1 + \left(\sqrt{3} - \pi/2 \right) + \frac{8R^3\tilde{Q}^5 \left(\frac{20\sqrt{3}-11\pi}{2\sqrt{3}-\pi} \right)}{(4Q+2\sqrt{16+\tilde{Q}^2R^2})(16+\tilde{Q}^2R^2)} \left(\frac{\rho_f}{\rho_s} \right)} \right] \quad (6)$$

where

$$\tilde{Q} = 2 + \sqrt{2}Q,$$

ρ_f = density of the foam

ρ_s = density of the basis solid material

for an hypocycloid:

$$C_1 = \sqrt{3} - \frac{\pi}{2},$$

$$C_2 = \frac{20\sqrt{3} - 11\pi}{2\sqrt{3} - \pi},$$

$$Q = b/(L \cos \theta),$$

where b , L and θ are dimensions describing the cell shape. For more insights on the geometric description of the elongated tetrakaidecahedron unit cell, the reader is referred to [14]. It should be noted that this unit cell is axisymmetric.

The anisotropy of polyurethane foams and its impact on their mechanical properties has been extensively studied [8,15–20]. However, significant differences and variability of the foam and the obtained results are expected between these studies and the case of PU pre-insulated pipes, due to:

- (a) The foam manufacturing process can have a great influence on the resulting microstructure of the foam [21]. All previous studies have been conducted with PU slabs foamed in rectangular moulds, where the distance between the mould walls is significantly larger than in pre-insulated pipes. Since cell anisotropy in foams is caused by the acting viscous forces between the liquid and the mould walls during the foaming process [7], it is expected that the narrower distance between mould walls in the case of the pre-insulated pipes will have a higher impact on the anisotropy of the cells. Moreover, the geometry of the mould, annular in the case of pipes, could have an influence on the cell's microstructure. Furthermore, the effects of manufacturing in a continuous process remains to be explored.
- (b) PU foams can be tailored through modifications in the chemical formulation [22–24]. However, details on the chemical formulation of the PU are rarely documented in the studies found in the literature and they may or may not match those of PU insulated pipes.
- (c) Not all studies cover the three orthogonal directions.

This paper seeks to address some of the challenges faced in the network design, damage accumulation and aging modeling for district heating piping systems by closing the knowledge gap on the microstructure and mechanical anisotropic behavior of the PU insulating foam from batch-produced bonded pipes and continuously produced flexible pipes.

2. Materials and Methods

In this study, three different types of pipes were investigated: traditional bonded pipes with steel medium pipe, rigid PU foam and smooth PE casing, flexible bonded pipes with PEX medium pipe, flexible PU foam and PE corrugated casing (denoted FC-DN40 in this study), and flexible bonded pipe with PEX medium pipe, flexible PU and PE smooth casing (denoted FS-DN40). For the traditional bonded pipe, three nominal diameters were evaluated: DN20 (denoted B-DN20), DN40 (B-DN40) and DN100 (B-DN100). The flexible pipes' nominal diameter was DN40. All pipes were insulation series 1 (insulation thickness 28.5 mm) manufactured by Logstor.

The traditional bonded pipes used in this study were manufactured in a batch process by injecting the PU insulating foam between the service pipe and the outer casing. The casing is manufactured in a previous process and one pipe is manufactured at a time [25]. The PU foam is blown with cyclopentane, with properties as required by EN 253 [26]. Further information about the PU formulation is not provided by the manufacturer.

The flexible pipes are manufactured in a continuous process, where the PU is poured in a moving casting mould, hence the PU material flows around the moving pipe. Then, the PE outer casing is melted in place in an extruder station [1], manufactured according to EN 15632-1 [27] and EN 15632-2 [28]. The formulation of the PU from the two flexible pipe types included in this study is visibly different, however further information about the chemical formulation is not provided, as it is proprietary data from the manufacturer. Flexible pipes are supplied in coils of up to 200 m length, which makes the laying of the pipes faster and more economical. Flexible pipes with smooth casing are typically used for branches. The flexible pipes with corrugated casing have a small bend radius as to allow for laying of the pipe on difficult sites and around obstacles. This extra flexibility is achieved through the geometric design of the corrugated casing and the chemical formulation of the PU [25].

2.1. Sample Preparation

Samples were machined out of the pipes following [26] as far as possible. The pipes were stored at 23 °C for at least 72 h prior removal of the casing. After discarding 500 mm of the pipe ends, cuboids were cut out of the pipe's insulation according to Figure 2 with different orientations, in order to

mechanically test the foam along the three orthogonal directions X_1 (red), X_2 (blue) and X_3 (green). Sample size was $30 \times 30 \times 20$ mm for the B-DN100 and ca. $25 \times 25 \times 20$ mm for the other pipes, since the smaller diameter prevented the extraction of larger specimens. However, successful testing of samples this size under uniaxial compression can be found in studies in the literature [19,29], and given the obtained 1000 times cell size to sample size difference, it can be assumed that the used sample size will have no impact on the results [30]. While it was foreseen in the design of experiments to extract three samples of each case equally distributed around the circumference, this was not possible as the tolerances in pipe dimensions from the manufacturing process made the pipes slightly oval, preventing the extraction samples of the same size from all segments of the circumference.

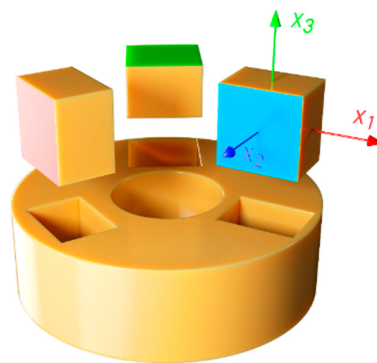


Figure 2. Sample extraction procedure.

2.2. Microstructural Characterization

The cross sections of all five pipe foams were examined in an optical microscope (Leica DMLP, Wetzlar, Germany). Slices of the PU foam were cut along the three orthogonal directions under study for each pipe with a cutter (planes 1-2, green; 1-3, blue and 2-3, red, see Figure 2). As to facilitate the view of the cells through the microscope, two sample preparation procedures were followed and compared: the first was infiltrating the samples with a blue coloured epoxy resin under vacuum. After curing the resin, the samples were polished until reaching the cell walls. The second procedure consisted in shading the surface of the foam with a black felt tip pen. While both procedures resulted valid, the simplicity of the second favoured this technique.

The cell size and shape were then measured from the obtained micrographs by adjusting the cells to an ellipse using Fiji [31]. The shape anisotropy R can then be calculated as the ratio from the largest dimension to the shortest. The rotation angle of the ellipse was measured in order to confirm a preferential direction of the cell elongation. Around 100 cells were measured per cross section and pipe.

2.3. Mechanical Characterization

Standard [32] was followed as far as possible. The main deviation is in the smaller sample size used, as described and justified in Section 2.1. Five specimens per pipe type and orientation were tested for compression using a universal testing machine, under a displacement controlled rate of 2 mm/s. The force was measured with a 20 kN load cell, accuracy class 0.5 (HBM, Darmstadt, Germany). The strain was measured by 3D digital image correlation (DIC) [29,33] using an ARAMIS 5M adjustable stereo camera system (GOM mbh, Braunschweig, Germany) with a resolution of 2448×2051 pixels. The images were acquired at frequency of 1 Hz. The strain measured by the ARAMIS optical system's software is based on a stochastic pattern recognition analysis. Therefore, a stochastic pattern was painted on one side.

Samples were individually accurately measured using caliper and weighed prior testing.

Engineering stress-strain curves were derived from the obtained data. The E modulus is obtained for each case from the slope of the initial linear segment of the curves. Given that the E modulus is the property most sensitive to cell shape [7], ratios of E_3/E_1 and E_3/E_2 are related to the shape anisotropy

ratio R for each pipe type and compared with the available models. For completeness of the study, the compressive stress at 10% strain (σ_{10}) was obtained, as its value is a requirement included in EN 253 [26].

3. Results

3.1. Microstructure of the PU Foam

Micrographs of the three sections of the PU foam for the five pipes under consideration are presented in Figure 3. The obtained average cell size and shape anisotropy ratio R is presented in Table 1, as well as the obtained cell symmetry.

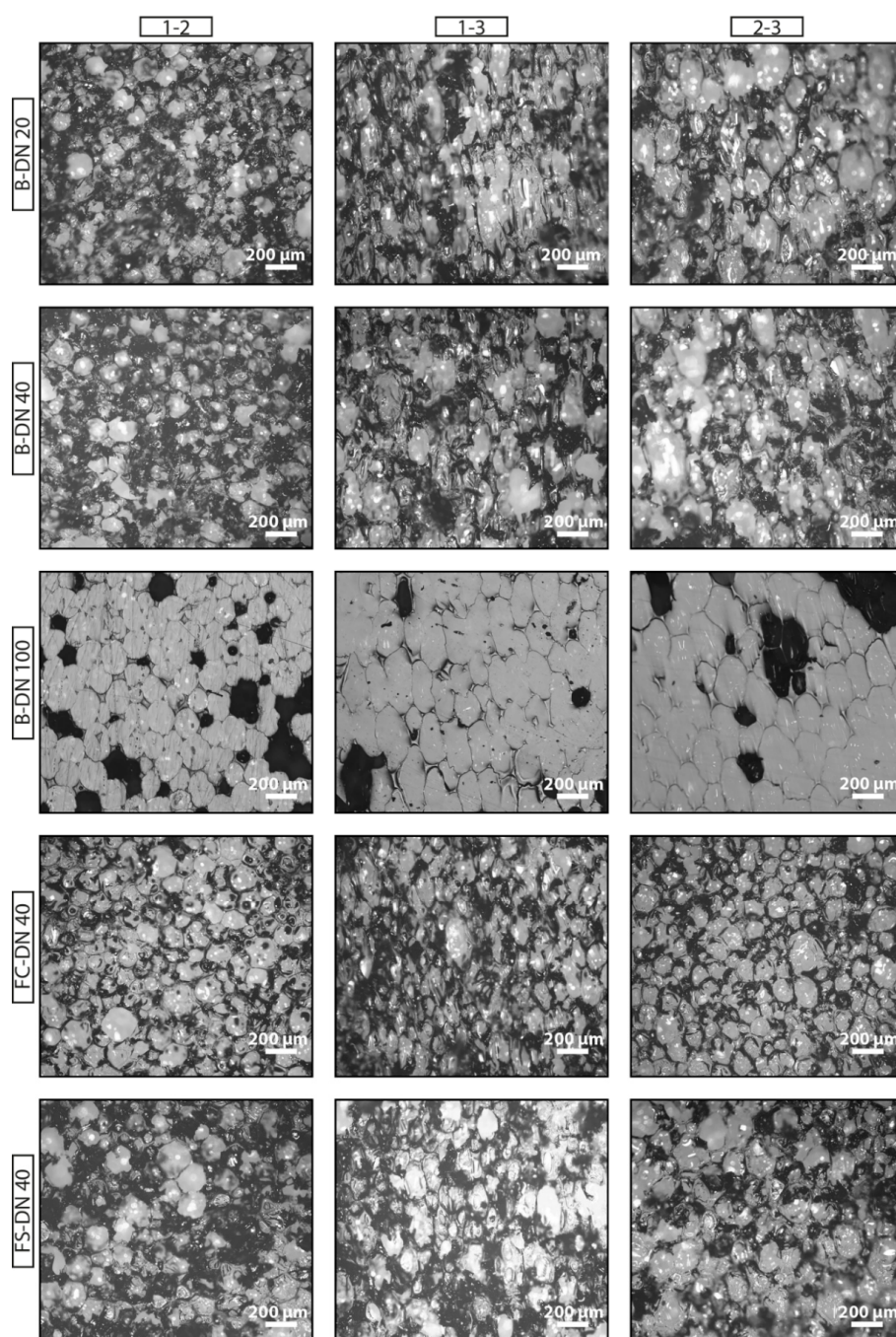
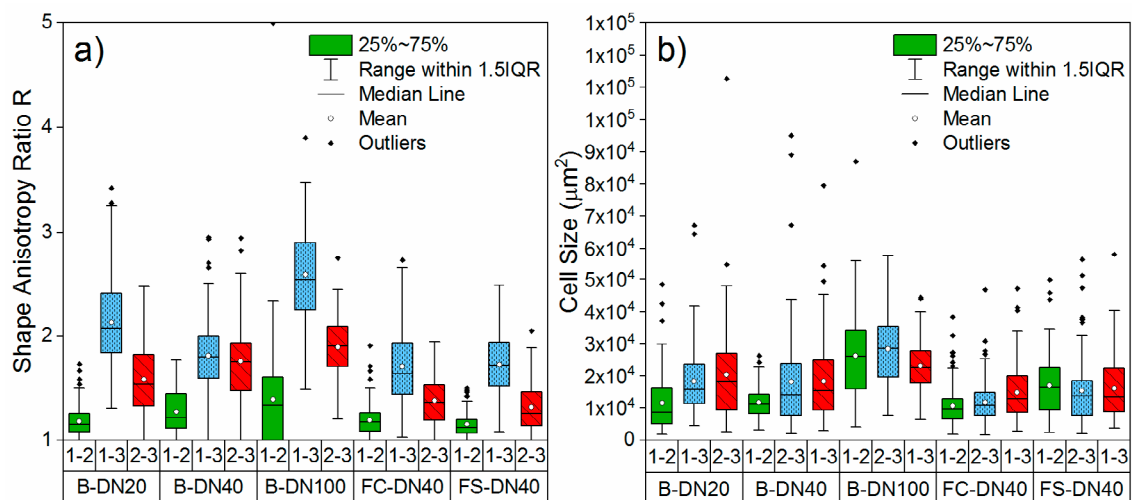


Figure 3. Foam micrographs. Pipe types are displayed in the different rows and the three orthogonal planes in columns.

Table 1. Mean cell area and R per plane and pipe type and resulting symmetry.

Pipe	Plane	Number of Measured Cells	Mean Cell Area (mm ²)	Cell Area Std. dev (mm ²)	Mean R	R Standard Deviation	Symmetry
B-DN20	1-2	103	0.012	0.009	1.18	0.15	orthotropic
	1-3	108	0.018	0.010	2.13	0.46	
	2-3	100	0.020	0.015	1.58	0.35	
B-DN40	1-2	114	0.012	0.005	1.27	0.19	axisymmetric
	1-3	103	0.018	0.013	1.81	0.38	
	2-3	101	0.018	0.015	1.75	0.38	
B-DN100	1-2	79	0.026	0.013	1.39	0.54	orthotropic
	1-3	81	0.023	0.008	2.58	0.52	
	2-3	74	0.028	0.011	1.89	0.31	
FC-DN40	1-2	130	0.011	0.006	1.19	0.15	orthotropic
	1-3	107	0.015	0.008	1.70	0.35	
	2-3	137	0.012	0.007	1.37	0.23	
FS-DN40	1-2	100	0.017	0.010	1.15	0.12	orthotropic
	1-3	100	0.016	0.010	1.72	0.30	
	2-3	101	0.015	0.010	1.32	0.24	

The obtained R distribution and cell size for each plane is plotted in Figure 4 for each case.

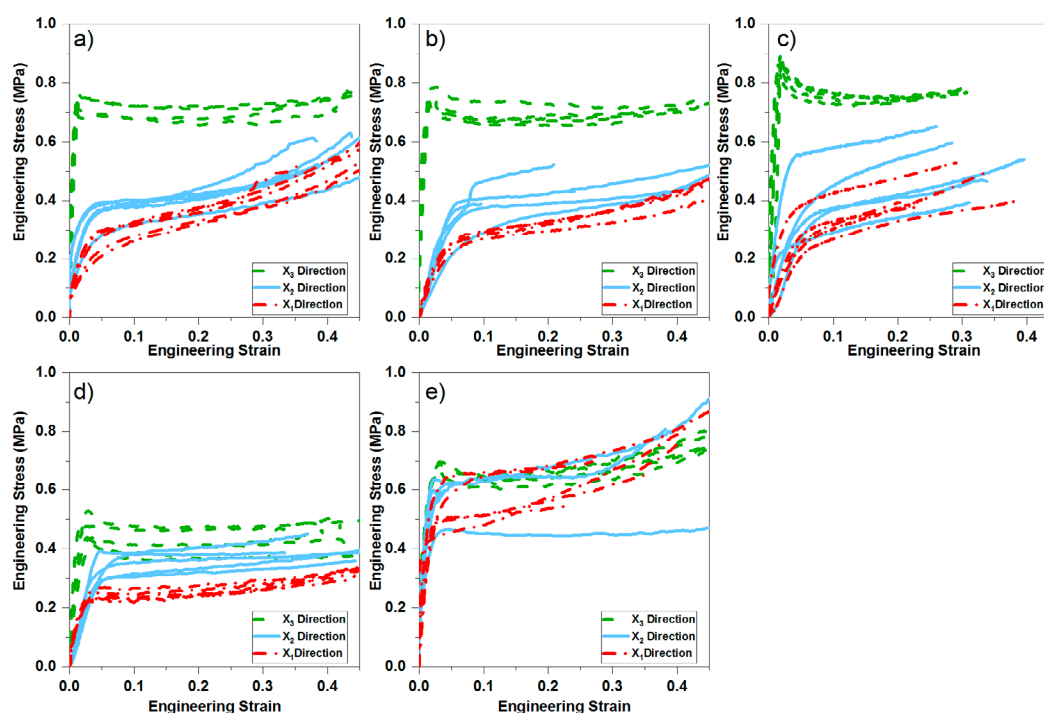
**Figure 4.** Distribution of measured R (a) and cell size (b) per plane and pipe type.

3.2. Mechanical Behaviour of the PU Foam

The obtained E modulus and σ_{10} per pipe type and compression direction is presented in Table 2. The resulting engineering stress-strain curves for the PU foams tested under uniaxial compression in the three orthogonal directions are presented in Figure 5a–e. The shape of the obtained curves corresponds well with those expected for polymeric foams: an initial linear elastic region, which is controlled by cell wall bending of the cells, followed by a plateau associated with the collapse of the cells [7].

Table 2. Obtained density, E modulus, and σ_{10} per pipe type and compression direction.

Pipe	(kg/m ³)	Direction	E (MPa)	E Std dev (MPa)	σ_{10} (MPa)	σ_{10} St. dev (MPa)
B-DN20	76.2	X3	52.1	1.9	0.72	0.05
		X2	8.4	1.6	0.38	0.03
		X1	6.1	1.5	0.30	0.03
B-DN40	76.2	X3	51.5	8.6	0.68	0.03
		X2	7.4	2.1	0.39	0.06
		X1	5.5	0.7	0.28	0.01
B-DN100	75.6	X3	53.6	4.2	0.75	0.02
		X2	7.7	0.8	0.41	0.11
		X1	5.2	0.8	0.33	0.06
FS-DN40	67.9	X3	15.7	1.8	0.63	0.01
		X2	8.2	1.1	0.57	0.11
		X1	6.6	1.0	0.56	0.08
FC-DN40	99.2	X3	27.4	0.8	0.42	0.05
		X2	20.5	5.1	0.35	0.04
		X1	17.9	5.2	0.24	0.02

**Figure 5.** Stress–Strain curves for (a) B-DN20 (b) B-DN40 (c) D-DN100 (d) FS-DN40, and (e) FC-DN40.

Significant differences can be found between the samples deformed in the three orientations. Curves from samples deformed in the X_3 direction (rising of the foam) present a pronounced peak in the stress at the outset of plastic instability, followed by a stress drop and a flat plateau region. The shape curves from samples deformed in the X_1 and X_2 directions do not present this pronounced peak. The shape of the curves from pipes B-DN20, B-DN40, B-DN100 and FS-DN40 agree with the typical load-deflection curves for rigid polyurethane foam, and the FC-DN40 for elastomeric polyurethane [7]. Hence the foam from FS-DN40 could be classified as semi-rigid. It can be seen from Figure 5a–c that the three traditionally bonded pipes behave in a similar way, with a much higher compressive strength in the X_3 direction, followed by X_2 and X_1 , while FS-DN40 (Figure 5d) presents a less pronounced difference between the compressive strength for the different directions, although following the same tendency. Comparing the two flexible pipes through Figure 5d,e, a different behaviour is observed.

The stress strain curves in the three directions overlap for FC-DN40, despite having no significantly different shape anisotropy ratio than FS-DN40.

The Young's modulus E where obtained from the initial slope of the stress-strain curve for each tested specimen and are presented in Figure 6a. The compressive strength at 10% strain is presented in Figure 6b.

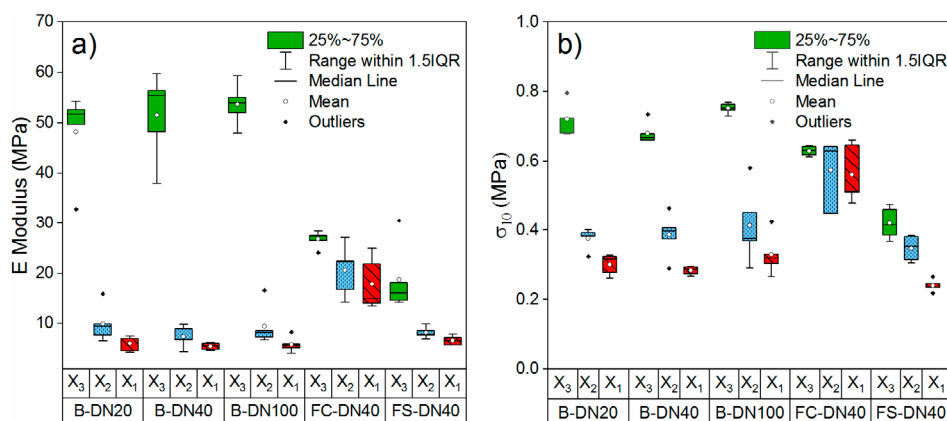


Figure 6. Distribution of the obtained E modulus (a) and σ_{10} (b) per direction and pipe type.

All pipes present mechanical anisotropy in the E modulus under compression and the compressive strength between the X_3 direction and X_1 and X_2 .

4. Discussion

4.1. Microstructure of the PU Foam

Elongation of the cells in the rise direction is easily observed from Figures 3 and 4. For the plane 1-2, despite diverging from circularity (which would correspond with an aspect ratio of 1), the percentage of cells elongated in the same direction is in the range 56% to 74%, while in the 2-3 and 1-3 planes they are in the range 97% to 100% in the case of the bonded pipes. Therefore, it is clear that the aspect ratio of plane 1-2 shows irregularity of the cells' shape, while in the planes 2-3 and 1-2 shows strong anisotropy in the foam rise direction, which is axial to the pipe length (X_3). As for the flexible pipes, in which due to the continuous manufacturing process the foam expands both around the pipe diameter as well as axial to the pipe length as the pipe is pulled through the extruder, we find anisotropy of the cells in the axial direction (X_3), showing that this is the predominant expansion direction. However, statistical evaluation of the cell geometries shows that the extent of the anisotropy is lower for both flexible pipes than for the traditional bonded pipes. Given that both flexible pipes have different PU formulations, densities and casing geometry but present no significant difference in R , we can conclude that the manufacturing process exerts the main influence on the observed shape anisotropy ratio.

Literature reports a typical R for polymeric foams of around 1.3 [7]. The study on PU by [8] yielded an R between 1.2 and 1.6, while that of [20] ranged from 1.34 to 1.72. In our study, we have obtained an R from 1.31 for the case of FS-DN40 up to 2.58 for the B-DN100 bonded pipe. This shows that the PU foam in pre-insulated pipes presents a much stronger anisotropy than PU slabs. This can be explained by the geometry of the mould, the annular section of the pipe in this case. When foaming from a liquid in a mould, viscous forces act between the mould walls and the foaming melt as the volume expansion leads it to rise in one direction, provoking an elongation of the cells [7]. The distance between walls in the bonded pipe is of roughly 28 mm, while the foam expands along the 6 m length of the pipe. Therefore, the acting viscous forces are higher than those in a rectangular mould where the distance between walls is larger in relation to the rise direction. This shows the importance

of evaluating foams manufactured under representative conditions and how sandwich materials may have different properties and behaviour than their individual constituents.

In order to determine if the foams present axisymmetric or orthotropic behaviour, a series of *t*-tests with 0.05 significance level were run comparing *R* in the 1-3 and 2-3 planes for each pipe type. The results are shown in Table 1. With the exception of B-DN40, all pipes were found to present orthotropic shape anisotropy in the microstructure. Shape anisotropy ratio was found higher in the 1-3 plane, corresponding to the X_2 direction. In this direction, the distance between the mould walls, which would be the outer diameter of the medium pipe and the inner diameter of the PE casing is smaller than in the X_1 direction, which would be casing to casing.

4.1.1. Effect of Pipe Diameter

The effect of increasing pipe diameter on the microstructural anisotropy of the cells was evaluated between the three traditionally bonded pipes under consideration. The hypothesis was that anisotropy would increase with the pipe diameter for the same insulation thickness, as the surface of the pipes increases with the diameter, and with it, the friction forces between the liquid and the mould during the foaming process, contributing to the shape anisotropy. The three pipe diameters were compared one to one in the 1-3 and 2-3 planes, using a *t*-test with 0.05 significance level. *R* was found to be significantly higher in B-DN100 compared to B-DN40 and B-DN20 in both directions, while B-DN40 was higher than B-DN20 in direction 2-3, but not in 1-3. One possible explanation is that the pipe surface difference between the DN20 and DN40 pipes would not be significant enough as to produce an increase in *R*. However, we cannot conclude that there is an evident correlation between the pipe diameter and the cell shape anisotropy for the diameter range under study.

4.1.2. Comparison between Smooth and Corrugated Flexible Pipes

After running the *t*-test, no significant difference was found between the FSDN40 and FCDN40 pipes in any of the three orthogonal directions. Therefore, we can conclude that the manufacturing process has a larger impact on cell shape anisotropy than the foam formulation.

4.2. Mechanical Behaviour of the PU Foam and Relation to the Cell Shape Anisotropy

The PU foam of the five pipe types under study present mechanical anisotropy on the E modulus and σ_{10} under compression. The three traditional bonded pipes under study present similar E modulus and E modulus ratios. The three traditional bonded pipes and flexible pipe FS-DN40 present similar E for the X_1 and X_2 direction, which is the X_3 , which varies and increases with the shape anisotropy.

It is interesting to compare the two flexible pipes. While they present no significant difference in cell shape anisotropy, their mechanical behaviour under compression is very different. The modulus ratio for FC-DN40 is roughly 50% lower than that of FS-DN40. While the difference in E modulus for the same directions can be explained by the different chemical formulation, the difference in ratio does not relate to the shape anisotropy ratio in the same way than the other PU foams under study, showing that other effects come into play. One possible explanation is the effect of cell size and cell size variability. It has been noted that the Young modulus decrease with increasing cell size variations [10]. From Figure 4b and Table 1 we can see that the variability in cell size for FC-DN40 is ~35% lower than that of FS-DN40 in planes 1-2 and 2-3, which could explain the lower E modulus for FS-DN40. It could be however argued that, since the cell sizes have been determined from 2D micrographs and cells have different sizes at different altitudes, the measured sizes might diverge from the real values. This effect would however appear equivalently in all measured planes. While the most rigorous indicator for cell size is cell volume, as applied by [34], its measurement implies 3D reconstruction and complex image processing to obtain the polyhedral profile of each cell [10]. 2D micrographs are commonly used for the determination of cell size [8,10,19,20] and the obtained cell size has been reported to be close to that measured with 3D reconstruction [35]. Another variable that can affect the E modulus is the variability in cell wall thickness [10,36], which is out of the scope of our study.

In Figure 7 the modulus ratio vs. shape anisotropy R is plotted for the five pipe types under study, as well as values from the literature. The rectangular cell model [1] for both open-cell and closed-cell (assuming $\Phi = 0.8$) as well as the Kelvin cell model [2] under the scenarios $Q = 2$, $Q = \sqrt{2}$ and $Q = 1$ and $\rho_f/\rho_s = 0.056$ and $\rho_f/\rho_s = 0.082$ (corresponding to the foam densities 67.9 kg/m^3 and 99.2 kg/m^3 , see Table 2, and $\rho_s = 1200 \text{ kg/m}^3$ [3]). Since the literature data corresponds to axisymmetric foams and the Kelvin cell model assumes axisymmetric, only the ratios between X_3/X_1 are plotted to facilitate the comparison. From this graph we can observe, firstly that the shape anisotropy and the modulus anisotropy present in the traditional bonded pipes is significantly higher than the cases previously reported in the literature. This shows how foams in sandwich structures present different morphologies and behaviour than stand-alone foams and the need to characterize them individually obtained under real manufacturing conditions. As for the relation between the modulus ratio and R , the obtained results could be best fitted to the Kelvin cell model using different values of Q . Foam cells with similar shape anisotropy but different modulus ratio could be explained by differences in the cell shape. Still, caution needs to be taken given the experimental variability in R and modulus ratio. The fact that the cells in PU from DH pipes are orthotropic, and that this involves a deviation from the idealized Kelvin cell, needs to be highlighted. While unit-cell based models can yield important results, real foams are typically non-uniform presenting variations in size and shape in the struts and in the cells, limiting their accuracy.

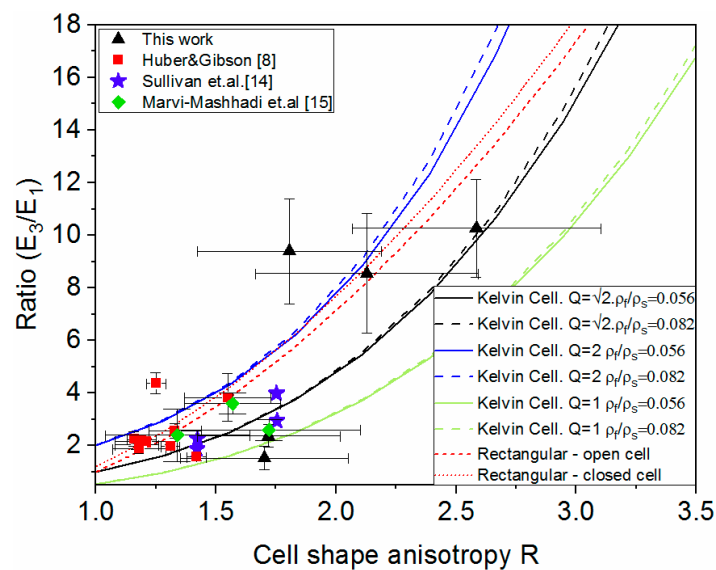


Figure 7. Modulus ratio vs. shape anisotropy.

5. Conclusions

Polyurethane foam in pre-insulated bonded pipes for district heating applications present strong cell shape, elastic modulus and compressive strength anisotropy, higher than that reported for PU foam slabs especially for the traditional bonded pipes. This is due to the geometry of the mould, the annular section between the medium pipe and the pipe casing, where the distance between the walls is much smaller than that of rectangular moulds for the production of slabs. This highlights the importance of the foam manufacturing in the resulting cell microstructure and how foams in sandwich structures present different properties and behaviour than foam slabs. The cells have been found to be mainly orthotropic, with different dimensions in the three orthogonal directions.

The three traditional bonded pipes under consideration behaved in a similar way. However, when comparing the two flexible pipes under consideration, no significant difference in cell shape anisotropy was found, but significantly different behaviour as for E modulus ratio. The equivalent

shape anisotropy is due to the same manufacturing process. To explain the difference in stiffness behaviour other factors need to be taken into consideration, such as cell size and cell size variability.

Author Contributions: Conceptualization, I.W.; methodology, L.D.; M.I.; validation, L.D.; formal analysis, L.D.; investigation, L.D.; M.I.; resources, I.W.; M.I.; data curation, L.D.; writing—original draft preparation, L.D.; writing—review and editing, I.W.; M.I.; L.D.; visualization, L.D.; supervision, I.W.; project administration, I.W.

Funding: This work was self-funded by the HafenCity University.

Acknowledgments: The authors would like to express their gratitude to Logstor and in particular Peter Jorsal and Tobias Langer for providing the district heating pipes and discussions about the manufacturing process. Assistance by Jens Ohlendieck, Jens Eidenberg and Diego Robles Lara is gracefully acknowledged. Editorial support and drawing of graphical abstract is thankfully acknowledged to Michelle Claas.

Conflicts of Interest: The authors declare no conflict of interest.

References

1. Logstor. New Standards for Production. Available online: <https://www.logstor.com/about-us/hseq/production> (accessed on 9 September 2019).
2. Christensen, R. Fatigue Analysis of District Heating Systems. *Neth. Agency Energy Environ.* **1999**, *7*, 8.
3. EN 13941-1: District Heating Pipes—Design and Installation of Thermal Insulated Bonded Single and Twin Pipe Systems for Directly Buried Hot Water Networks—Part 1: Design; European Committee for Standardization: Brussels, Belgium, 2016.
4. Vega, A.; Yarahmadi, N.; Jakubowicz, I. Determination of the long-term performance of district heating pipes through accelerated ageing. *Polym. Degrad. Stab.* **2018**, *153*, 15–22. [[CrossRef](#)]
5. Yarahmadi, N.; Vega, A.; Jakubowicz, I. Accelerated ageing and degradation characteristics of rigid polyurethane foam. *Polym. Degrad. Stab.* **2017**, *138*, 192–200. [[CrossRef](#)]
6. Yarahmadi, N.; Vega, A.; Jakubowicz, I. Determination of essential parameters influencing service life time of polyurethane insulation in district heating pipes. *Energy Procedia* **2017**, *116*, 320–323. [[CrossRef](#)]
7. Gibson, L.J.; Ashby, M.F. *Cellular Solids*; Cambridge University Press: Cambridge, UK, 1997; ISBN 9781139878326.
8. Huber, A.T.; Gibson, L.J. Anisotropy of foams. *J. Mater. Sci.* **1988**, *23*, 3031–3040. [[CrossRef](#)]
9. Gibson, L.J.; Ashby, M.F. The Mechanics of Three-Dimensional Cellular Materials. *Proc. R. Soc. Lond. A Math. Phys. Sci.* **1982**, *382*, 43–59. [[CrossRef](#)]
10. Chen, Y.; Das, R.; Battley, M. Effects of cell size and cell wall thickness variations on the stiffness of closed-cell foams. *Int. J. Solids Struct.* **2015**, *52*, 150–164. [[CrossRef](#)]
11. Thomson, W. LXIII. On the division of space with minimum partitional area. *Lond. Edinb. Dublin Philos. Mag. J. Sci.* **1887**, *24*, 503–514. [[CrossRef](#)]
12. Gong, L.; Kyriakides, S.; Jang, W.-Y. Compressive response of open-cell foams. Part I: Morphology and elastic properties. *Int. J. Solids Struct.* **2005**, *42*, 1355–1379. [[CrossRef](#)]
13. Ridha, M.; Shim, V.P.W.; Yang, L.M. An Elongated Tetrakaidecahedral Cell Model for Fracture in Rigid Polyurethane Foam. *KEM* **2006**, *306*, 43–48. [[CrossRef](#)]
14. Sullivan, R.M.; Ghosn, L.J.; Lerch, B.A. A general tetrakaidecahedron model for open-celled foams. *Int. J. Solids Struct.* **2008**, *45*, 1754–1765. [[CrossRef](#)]
15. Linul, E.; Marsavina, L.; Voiconi, T.; Sadowski, T. Study of factors influencing the mechanical properties of polyurethane foams under dynamic compression. *J. Phys. Conf. Ser.* **2013**, *451*, 012002. [[CrossRef](#)]
16. Marsavina, L.; Constantinescu, D.M.; Linul, E.; Apostol, D.A.; Voiconi, T.; Sadowski, T. Refinements on fracture toughness of PUR foams. *Eng. Fract. Mech.* **2014**, *129*, 54–66. [[CrossRef](#)]
17. Marsavina, L.; Constantinescu, D.M.; Linul, E.; Voiconi, T.; Apostol, D.A. Shear and mode II fracture of PUR foams. *Eng. Fail. Anal.* **2015**, *58*, 465–476. [[CrossRef](#)]
18. Marsavina, L.; Linul, E.; Voiconi, T.; Sadowski, T. A comparison between dynamic and static fracture toughness of polyurethane foams. *Polym. Test.* **2013**, *32*, 673–680. [[CrossRef](#)]
19. Hamilton, A.R.; Thomsen, O.T.; Madaleno, L.A.O.; Jensen, L.R.; Rauhe, J.C.M.; Pyrz, R. Evaluation of the anisotropic mechanical properties of reinforced polyurethane foams. *Compos. Sci. Technol.* **2013**, *87*, 210–217. [[CrossRef](#)]

20. Marvi-Mashhadi, M.; Lopes, C.S.; LLorca, J. Effect of anisotropy on the mechanical properties of polyurethane foams: An experimental and numerical study. *Mech. Mater.* **2018**, *124*, 143–154. [[CrossRef](#)]
21. Kurańska, M.; Prociak, A. Bio-Based Polyurethane Foams for Heat-Insulating Applications. In *Nano and Biotech Based Materials for Energy Building Efficiency*; Pacheco Torgal, F., Buratti, C., Kalaiselvam, S., Granqvist, C.-G., Ivanov, V., Eds.; Springer International Publishing: Cham, Switzerland, 2016; pp. 357–373. ISBN 978-3-319-27503-1.
22. Akindoyo, J.O.; Beg, M.D.H.; Ghazali, S.; Islam, M.R.; Jeyaratnam, N.; Yuvaraj, A.R. Polyurethane types, synthesis and applications—A review. *RSC Adv.* **2016**, *6*, 114453–114482. [[CrossRef](#)]
23. Gama, N.V.; Ferreira, A.; Barros-Timmons, A. Polyurethane Foams: Past, Present, and Future. *Materials* **2018**, *11*, 3390. [[CrossRef](#)]
24. Orzel, R.A.; Womble, S.E.; Ahmed, F.; Brasted, H.S. Flexible Polyurethane Foam: A Literature Review of Thermal Decomposition Products and Toxicity. *J. Am. Coll. Toxicol.* **1989**, *8*, 1139–1175. [[CrossRef](#)]
25. *Logstor Product Catalogue*; LOGSTOR: Løgstør, Denmark, 2019.
26. *EN 253: District Heating Pipes—Preinsulated Bonded Pipe Systems for Directly Buried Hot Water Networks—Pipe Assembly of Steel Service Pipe, Polyurethane Thermal Insulation and Outer Casing of Polyethylene*; European Committee for Standardization: Brussels, Belgium, 2009.
27. *EN 15632-1: District Heating Pipes—Pre-Insulated Flexible Pipe Systems—Part 1: Classification*; European Committee for Standardization: Brussels, Belgium, 2015.
28. *EN 15632-2: District Heating Pipes—Pre-Insulated Flexible Pipe Systems—Part 2: Bonded Plastic Service Pipes*; European Committee for Standardization: Brussels, Belgium, 2015.
29. Jin, H.; Lu, W.-Y.; Scheffel, S.; Hinnerichs, T.D.; Neilsen, M.K. Full-field characterization of mechanical behavior of polyurethane foams. *Int. J. Solids Struct.* **2007**, *44*, 6930–6944. [[CrossRef](#)]
30. Tekoğlu, C.; Gibson, L.J.; Pardoën, T.; Onck, P.R. Size effects in foams: Experiments and modeling. *Prog. Mater. Sci.* **2011**, *56*, 109–138. [[CrossRef](#)]
31. Schindelin, J.; Arganda-Carreras, I.; Frise, E.; Kaynig, V.; Longair, M.; Pietzsch, T.; Preibisch, S.; Rueden, C.; Saalfeld, S.; Schmid, B.; et al. Fiji: An open-source platform for biological-image analysis. *Nat. Methods* **2012**, *9*, 676–682. [[CrossRef](#)] [[PubMed](#)]
32. *ISO 844: Rigid Cellular Plastics—Determination of Compression Properties*; International Organization for Standardization: Geneva, Switzerland, 2014.
33. Peters, W.H.; Ranson, W.F. Digital Imaging Techniques in Experimental Stress Analysis. *Opt. Eng.* **1982**, *21*, 427–432. [[CrossRef](#)]
34. Montminy, M.D.; Tannenbaum, A.R.; Macosko, C.W. The 3D structure of real polymer foams. *J. Colloid Interface Sci.* **2004**, *280*, 202–211. [[CrossRef](#)]
35. Fischer, F.; Lim, G.T.; Handge, U.A.; Altstädt, V. Numerical Simulation of Mechanical Properties of Cellular Materials Using Computed Tomography Analysis. *J. Cell. Plast.* **2009**, *45*, 441–460. [[CrossRef](#)]
36. Li, K.; Gao, X.-L.; Subhash, G. Effects of cell shape and strut cross-sectional area variations on the elastic properties of three-dimensional open-cell foams. *J. Mech. Phys. Solids* **2006**, *54*, 783–806. [[CrossRef](#)]



© 2019 by the authors. Licensee MDPI, Basel, Switzerland. This article is an open access article distributed under the terms and conditions of the Creative Commons Attribution (CC BY) license (<http://creativecommons.org/licenses/by/4.0/>).



ELSEVIER

Available online at www.sciencedirect.com**ScienceDirect**

Energy Reports 7 (2021) 150–157

www.elsevier.com/locate/egy

17th International Symposium on District Heating and Cooling, 6–9 September 2021, Trent, UK

Sustainable insulation for sustainable DHC

Lucía Doyle, Ingo Weidlich*

HafenCity University, Hamburg 20457, Germany

Received 15 August 2021; accepted 22 August 2021

Abstract

The piping network is the essence of DHC. Its insulation is fundamental for its correct and efficient functioning. State of the art DHC networks are insulated with polyurethane (PU) foam, which presents outstanding mechanical and insulating properties. However, the high toxicity of the diisocyanates (European Chemical Agency, 2008) required for its production and the recently approved European Restriction on their Use (European Commission, 2020) highlight the need for sustainable alternatives.

Polyethylene terephthalate (PET) foam has been previously identified as a promising candidate for DHC given its mechanical properties (Ramnäs, 2008) and high insulation capacity retention, due to slow gas diffusion (Mangs, 2005). However, its behavior upon ageing remains unexplored. Without this knowledge, the material cannot be reliably introduced in the market. The objective of this work is to experimentally investigate PET foam's ageing behavior, with a focus on the effects of thermal cycling, thermally induced crystallinity and hygrothermal degradation on its mechanical properties.

Different ageing trials were conducted in an environmental chamber. The effects on the mechanical properties and crystalline structure were evaluated. No degradation was found in the scenarios covered by this study. Service temperature over 100 °C is found possible thanks to thermally induced crystallization.

© 2021 The Authors. Published by Elsevier Ltd. This is an open access article under the CC BY-NC-ND license (<http://creativecommons.org/licenses/by-nc-nd/4.0/>).

Peer-review under responsibility of the scientific committee of the 17th International Symposium on District Heating and Cooling, 2021.

Keywords: PET foam; Insulation; Circular economy

1. Introduction

District Heating (DH) networks are called to bring sustainability through the decarbonization of the heating sector. But as we curve towards a circular economy, the term sustainable expands from carbon neutral to additionally recyclable and non-toxic.

The energy efficiency of state-of-the art DH pipelines is warranted with polyurethane foam (PU), which presents outstanding thermal conductivity values as well as the necessary load bearing capacity to support the acting stresses on buried pipelines. However, the recently approved restriction on diisocyanates [1], required for the PU manufacturing, highlights its toxicity [2] and the urge to look for more sustainable materials. The lower operating

* Corresponding author.

E-mail address: ingo.weidlich@hcu-hamburg.de (I. Weidlich).

<https://doi.org/10.1016/j.egy.2021.08.161>

2352-4847/© 2021 The Authors. Published by Elsevier Ltd. This is an open access article under the CC BY-NC-ND license (<http://creativecommons.org/licenses/by-nc-nd/4.0/>).

Peer-review under responsibility of the scientific committee of the 17th International Symposium on District Heating and Cooling, 2021.

Nomenclature

DSC	Differential Scanning Calorimetry
$\sigma_{c,10}$	compression strength at 10% strain
$\sigma_{f,max}$	maximal flexural strength
ε_f	strain at break
r.H	relative humidity
ΔH_f	enthalpy of fusion, measured at the melting point
ΔH_f^0	enthalpy of fusion of the 100% crystalline polymer, measured at the equilibrium melting point
T_g	glass transition temperature
U	toughness
X_c	weight degree of crystallinity

temperature of the 4th generation DH [3] opens up the possibility, not only to include renewable and waste heat sources in the system, but to use alternative polymeric foams.

A promising candidate is polyethylene terephthalate (PET) foam. PET is non-toxic and recyclable, and its current wide use across sectors and established recycling processes allows for a cascading-use of the material, as well as a competitive price. PET foam has been previously explored for DH applications [4,5]. Results showed excellent thermal resistance ageing behavior due to very low gas diffusion rates, which would allow long-term energy efficiency of the system. In terms of mechanical properties, PET foam showed outstanding creep behavior, as well as possessing a compression strength over 0,3 MPa required by EN 253, under temperatures up to 80 °C, after which a reduction of the strength occurs due to the transition from the glassy to the rubbery state [5].

However, for successful commercial implementation, knowledge on its ageing behavior is needed to confirm the attainment of the required service life. In this paper we summarize our efforts to close this knowledge gap.

Previous research has shown that thermal and thermoxidative degradation of PET occurs at or above the melting temperature of PET (~250 °C) and the reaction rate at lower temperatures is very low [6,7] and hence not an issue for DH applications. The temperature fluctuations of the system however expose the pipeline's materials to mechanical and thermal cyclic loading. We have found that this causes degradation of the mechanical properties of PU pre-insulated pipes [8] and could also be the case for PET. The vicinity of the operation temperature with the materials T_g and hence fluctuation around it could also lead to changes in crystallinity, impacting on the mechanical properties. Therefore, the effects of thermal cycling were evaluated.

Another source of degradation could be moisture. Buried DH pipelines can be located below the groundwater level and damage due to moisture is reported to be frequently encountered in the field [9]. Though the HDPE casing protects the insulation from water ingress, it has been recently reported that moisture penetrates the casing [10]. While an aluminum layer is an efficient diffusion barrier [11], moisture can still penetrate through the pipe ends and joints [9,11]. Moisture can degrade the mechanical properties of polymeric foams due to plasticization and swelling [12]. Further degradation risk involves hydrolysis, which has been widely reported for PET, above T_g [i.e. 13,14]. Therefore, hygrothermal ageing was the second degradation pathway investigated.

2. Materials and methods

2.1. Materials

Commercial closed cell cyclopentane-blown PET foam boards (Gurit Kerdyn Green) of two densities were examined: 80 and 100 kg/m³.

2.2. Thermal cycling ageing trials and evaluation

Specimens of approx. 50 × 50 × 50 mm were subjected to thermal cycling inside an environmental chamber (Weiss WK1 340, Reiskirchen, Germany). Three trials were conducted according to the following profiles:

- Thermal Cycling A.

Temperature was varied between 25 °C and 100 °C. The upper temperature was chosen above PET's T_g to examine the potential changes in the crystalline structure. The duration of the temperature ramps was 30 min, and the set points were held for 75 mins. This was kept equal for all trials. The number of cycles was set to 250, which is the number of cycles established for fatigue check for secondary effects for distribution lines according to [15].

- Thermal Cycling B.

Temperature was varied between 25 °C and 75 °C, as to assess the effects of cycling below PETs T_g . The number of cycles was set at 125, which is half of the number of cycles established for fatigue check for secondary effects for distribution lines according to [15].

- Thermal Cycling C.

Temperature was varied between 25 °C and 75 °C, and the number of cycles was set at 250 for the same reason as in A.

Evaluation:

Reference (unaged) and aged samples were tested under compression at room temperature in a universal testing machine following standard [16] as far as possible. The samples were tested in the direction perpendicular to the extrusion, which would correspond to the radial direction of the pipes.

Five specimens were tested per condition, under a displacement-controlled rate of 2 mm/s. The force was measured with a 20 kN load cell, accuracy class 0.5 (HBM, Darmstadt, Germany). The strain was measured by 3D digital image correlation (DIC) [17] using an ARAMIS 5M adjustable stereo camera system (GOM mbh, Braunschweig, Germany). The images were acquired at frequency of 1 Hz. Samples were individually accurately measured using calliper and weighed prior testing.

Engineering stress–strain curves were derived from the obtained data. The E modulus is obtained for each case from the slope of the initial linear segment of the curves. The compressive stress at 10% strain ($\sigma_{c,10}$) was obtained, and both parameters were used to assess the changes in mechanical properties.

Crystallinity of the 80 kg/m³ foam unaged and after A ageing was assessed through DSC following [18] standard with a heating rate of 10 k/min. This analysis was conducted in duplicate. The degree of crystallinity is calculated as:

$$X_c = \frac{\Delta H_f}{\Delta H_f^0} \quad (1)$$

where ΔH_f^0 is taken as 140 J/g [19].

2.3. Behavior under temperature

Additional compression tests of unaged specimens were conducted under temperature. For this, an environmental chamber (Weiss WK3-180/70/5-UKA, Reiskirchen, Germany) was placed around the universal testing machine. Samples were tested at 70 °C and 100 °C after ~2 h of temperature stabilization. Additional samples were temperature soaked overnight at 100 °C and then tested at 100, 70 or 85 °C. Ca. 2 h of temperature stabilization at the testing T was applied prior the test.

2.4. Hygrothermal ageing trials and evaluation

Samples were aged at 40 °C and 80% r.H inside an environmental chamber (Mettmert ICH-C, Schwabach, Germany) for up to six months. The selected temperature corresponds to an accelerated ageing from the ground moisture temperature (around 10 °C), but with a comfortable ΔT of 20 °C from T_g , considering the depression in T_g caused by the moisture [20]. Ageing above T_g would alter the degradation mechanisms. The selected relative humidity is the maximal allowed by the chamber.

Specimens of approx. 200 × 25 × 25 mm before and after ageing were subjected to a 3-point bending test under a displacement-controlled rate of 1.5 mm/min. The force was measured with a 2 kN load cell, accuracy class 0.5 (HBM, Darmstadt, Germany) and the strain with DIC as described in the previous section.

Engineering stress–strain curves were derived from the obtained data. The maximum flexural stress ($\sigma_{f,max}$) and strain at break (ε_f) were obtained from the curves. The E modulus is derived for each case from the slope of

the initial linear segment of the curves. The toughness was calculated as the integral under the stress–strain curve, according to (2):

$$U = \int_0^{\varepsilon_f} \sigma_{f,\max} \cdot d\varepsilon \quad (2)$$

Degradation was assessed in terms of the changes in mechanical properties.

3. Results

3.1. Thermal cycling ageing

Fig. 1 presents the engineering stress–strain curves for the samples tested under compression, in unaged condition and after thermal cycling trials A, B and C for the foam 80 kg/m³ (a) and 100 kg/m³ (b). The E modulus and σ_{10} obtained from the curves are summarized in Table 1.

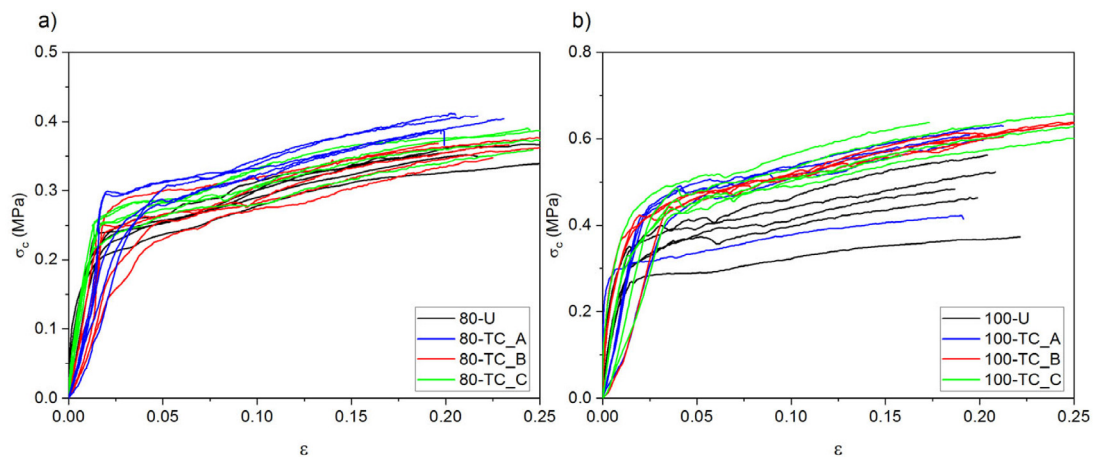


Fig. 1. Compression stress–strain curves for foam 80 (a) and 100 (b) unaged (U) and after thermal cycling ageing A, B and C trials.

Table 1. Mechanical Properties derived from compression tests, unaged and after thermal cyclic ageing.

	E modulus (MPa)				σ_{10} (MPa)			
	Unaged	TC-A	TC-B	TC-C	Unaged	TC-A	TC-B	TC-C
80	15.83 ± 2.15	12.5 ± 4.71	10.83 ± 3.99	15.3 ± 2.57	0.30 ± 0.01	0.33 ± 0.01	0.29 ± 0.02	0.31 ± 0.02
100	24.02 ± 1.84	20.09 ± 3.39	27.08 ± 8.77	23.16 ± 7.71	0.41 ± 0.05	0.49 ± 0.07	0.51 ± 0.02	0.52 ± 0.03

As can be seen in Fig. 1(a) and (b) and Table 1, the applied thermal cycles did not produce a significant change in the mechanical properties. An increase in the strength for foam 100 after trials B and C can be noted. Given the variability between samples, this increase should be taken with care.

No significant change in weight or dimensions was detected after the ageing trials.

A representative DSC curve for foam 80 unaged and after trial TC-A is presented in Fig. 2. The presented curves correspond to the second heating ramp. From the curves and Eq. (1) a weight % crystallinity of 33.8% for unaged and 31.3% for aged foam 80 can be derived.

3.2. Behavior under temperature

Fig. 3 presents the engineering stress–strain curves from compression tests conducted at different temperatures. The left column presents the results of tests conducted after a short stabilization time of approx. 2 h, for foam 100 (a) and foam 80 (c). As can be seen, the strength is progressively reduced as the temperature is increased. The

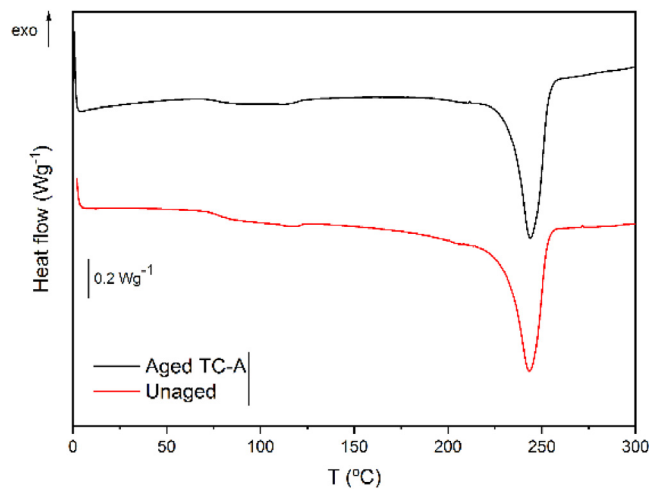


Fig. 2. DSC curves for unaged and TC-A aged 80 kg/m^3 PET foam.

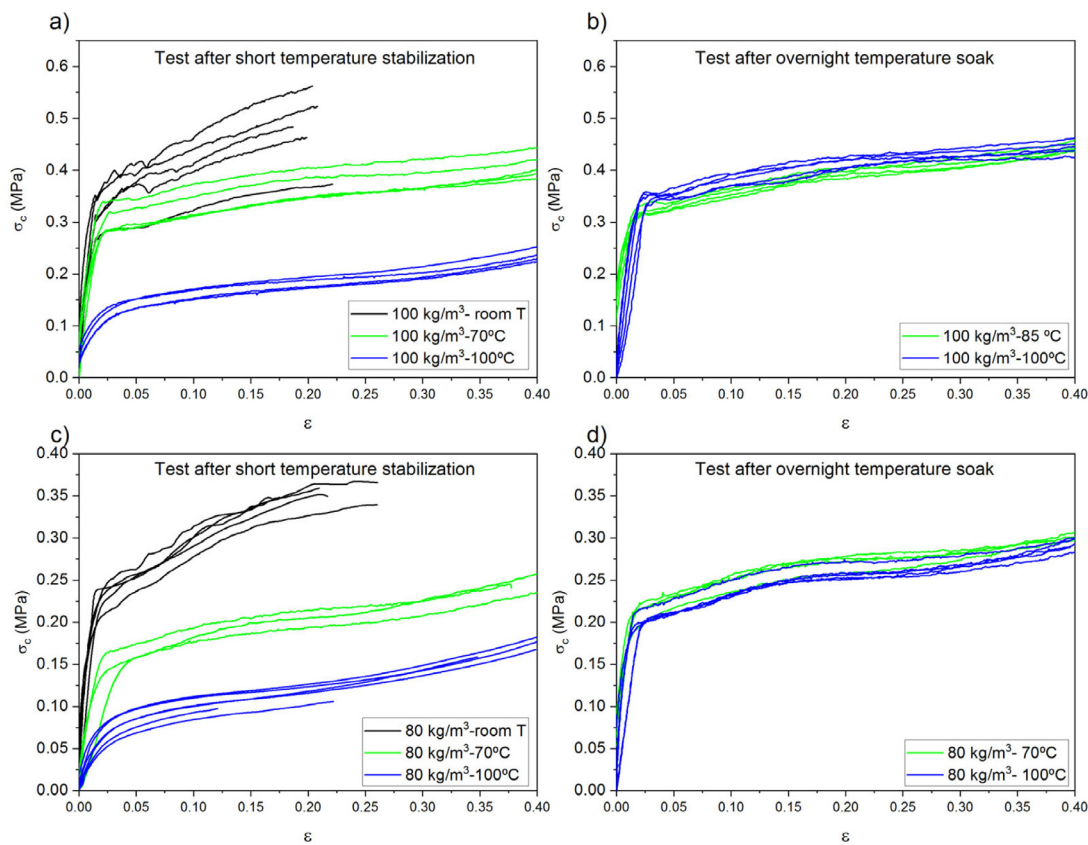


Fig. 3. Stress–Strain curves for samples tested under temperature for foam 100 (a) and 80 (c). Samples tested under temperature after an overnight $100 \text{ }^\circ\text{C}$ temperate soak are presented in (b) (foam 100) and (d) (foam 80).

graphs on the right column present the foams tested at the same temperatures, but after an overnight temperature soak at $100 \text{ }^\circ\text{C}$. The strength is significantly increased, from $0.1 \pm 0.01 \text{ MPa}$ to $0.23 \pm 0.009 \text{ MPa}$ for the 80 foam and from $0.16 \pm 0.01 \text{ MPa}$ to $0.38 \pm 0.01 \text{ MPa}$ for the 100 PET foam when testing at $100 \text{ }^\circ\text{C}$ after overnight

soak, meaning a 130% strength increase. This significantly reduces the gap with the behavior at room temperature. The implication on this regarding the selection of the design values at the network operation point and possible service temperatures will be discussed in Section 4.

3.3. Hygrothermal ageing

Fig. 4 presents the bending stress–strain curves for foam 80 (a) and 100 (b). Foam 80 was tested in both the extrusion (E) and parallel (P) directions, unaged (FU) and aged (FA) after 6 months. Foam 100 was tested in the E direction, unaged and after 3 and 6 months ageing. One of the FU-80 P samples did not break during the test, marked with a cross at the end of the curve. The values of toughness, maximum strength and strain at break are presented in Table 2.

Despite a decrease in the mean for most properties of aged samples can be seen for most properties, a two-sample t-test with a significant level of 0.05 was undertaken for all toughness aged/unaged pairs, which showed that the results are not statistically different.

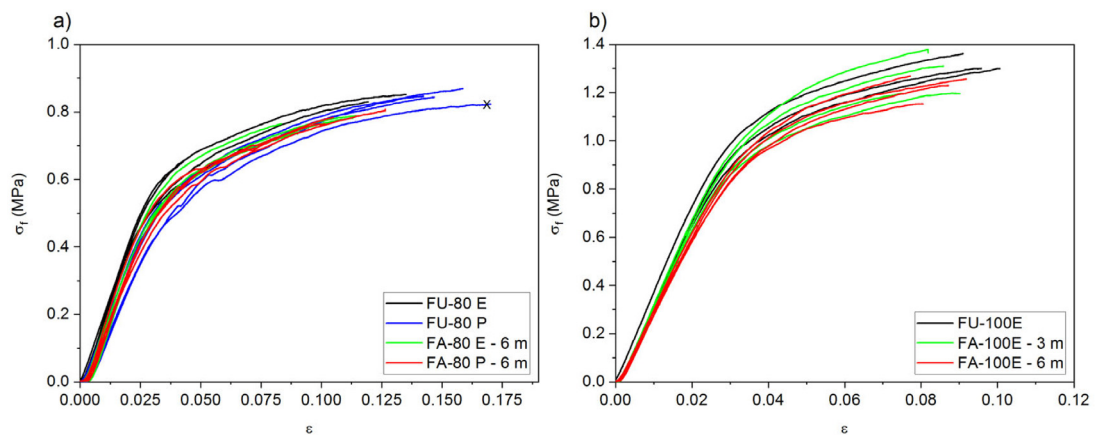


Fig. 4. Bending stress–strain curves for foam 80 (a) and 100 (b).

Table 2. Mechanical Properties derived from flexural tests.

	$\sigma_{f,max}$ (MPa)	U (MJ/m ³)	ϵ at break	E modulus (MPa)	$\Delta\sigma_{f,max}$ (%)	ΔU (%)	$\Delta\epsilon$ at break (%)	ΔE modulus (%)
FU-80E	0.76 ± 0.10	0.05 ± 0.03	0.091 ± 0.04	21.84 ± 1.30	n.a	n.a	n.a	n.a
FU-80P	0.78 ± 0.14	0.07 ± 0.04	0.12 ± 0.06	18.9 ± 1.78	n.a	n.a	n.a	n.a
FU-100E	1.28 ± 0.07	0.08 ± 0.01	0.092 ± 0.01	35.00 ± 3.05	n.a	n.a	n.a	n.a
FU-100P	1.29 ± 0.08	0.1 ± 0.02	0.106 ± 0.02	33.52 ± 1.85	n.a	n.a	n.a	n.a
FA100E - 3 m	1.27 ± 0.09	0.07 ± 0.01	0.083 ± 0.01	35.32 ± 1.50	−1.1	−11.7	−10.3	0.9
FA100E - 6 m	1.23 ± 0.05	0.07 ± 0.01	0.084 ± 0.01	32.46 ± 1.13	−4.9	−14.1	−8.6	−7.2
FA80E - 6 m	0.77 ± 0.02	0.05 ± 0.01	0.1 ± 0.02	20.99 ± 0.55	1.5	4.2	9.5	−3.9
FA80P - 6 m	0.76 ± 0.05	0.05 ± 0.02	0.101 ± 0.02	19.87 ± 2.59	−2.6	−24.3	−15.8	5.1

4. Discussion

The acting cyclic loads in DH pipes could be a cause of fatigue for the constituent materials. While this is widely considered for the steel pipe, only a few studies evaluate its effect on the insulating foam [8,21]. A foam is not a material, but a structure, and repetitive expansion and contraction and related flexure of the cell walls could lead to cracking events [22]. Cell anisotropy [23] and hysteresis intrinsic to polymers may exacerbate irreversible changes in the cellular structure. A previous study with PU foam at high temperature reports that the cell expansion is wider

in the direction parallel to the foam direction and original shape is only partly recovered [24]. One contributor to the foam thermal expansion is the expansion of polymer itself. The second contributor is the expansion of the gas inside the cells, applying pressure to the cell walls [24]. With increasing temperature, the expansion of the gas coincides with the reduction of the strength of the polymer matrix. We have found no effect of the applied cycles on the mechanical properties of the PET foam. This is related to the low thermal expansion of PET, of $9.1 \cdot 10^{-5} \text{ K}^{-1}$ [25] vs $15 \cdot 10^{-5} \text{ K}^{-1}$ for PU [22]. Due to the semicrystalline nature of PET, a further change in the mechanical properties could arise from temperature induced changes in crystallinity. No significant changes in crystallinity were detected after the applied thermal cycles. The results from the static tests under temperature (Section 3.2) suggest that the 75 min temperature hold time was not long enough to allow for thermal crystallization. The hold time was selected in order to achieve a manageable trial duration for the 250 cycles, which ascended to 8 weeks.

It is seen in Fig. 3(a) and (c) that the strength and E modulus decrease with increasing temperature, consistent with previous observations in PET [5] and other polymeric foams [22,26]. However, it can be seen that the strength at 100 °C can increase by 130% with time under temperature. This indicates that during this period the crystallinity degree increased. The intermolecular bonding is higher in the crystalline phase than in the amorphous, increasing the strength of the polymer [27]. This effect is expected to occur in DH networks, which are held at high temperature for long periods of time. Therefore, limiting the PET foam for networks operating below 100 °C due to the softening of the foam at its T_g (~80 °C) [5] is proven conservative, as the $\sigma_{10} = 0.3 \text{ MPa}$ required by EN 253 can be exceeded at 100 °C (Fig. 3b). It should be noted that in any case the standard requires this σ_{10} at room temperature. Foaming semicrystalline polymers is a recent development, and its particularities i.e. crystallinity degree changes with time and temperature should be taken into account when selecting the materials properties at the design point of the piping network.

As for moisture-induced ageing, no effects have been found after 6 months accelerated ageing. While the obtained data does not allow us to predict long term behavior, at the ground temperature all involved processes will be slower. It should be noted that the samples were left to stabilize at ambient conditions prior mechanical testing, since the focus of the study was to evaluate irreversible degradation. Therefore, loss of mechanical properties due to the plasticization effect of moisture would not be detected in this experimental plan. Equivalently only permanent effects related to swelling. i.e. deformation of the cells, would be detected. It has been seen during the study that moisture uptake by PET foam is very low, reaching only 0.3% weight increase after over 2600 h of 80% moisture exposure at 40 °C. The details on the moisture uptake and its in-situ and long-lasting effects will be discussed in another publication [28]. This very low moisture uptake limits to a great extent the degradation. It is known that PET is susceptible to hydrolysis at temperatures above its T_g and has been widely studied [13,14]. The chain scission produced by hydrolysis leads to embrittlement, conditioning the service life of the material. Therefore, bending tests were selected to better detect embrittlement, which was not found after the applied 6 months hygrothermal ageing. We have found that the cellular structure of the foam produces no deviation in the hydrolysis reaction rate from that occurring in films [29]. According to models developed by previous authors based of PET films [14], service life at 40 °C and 50% r. H would be 30 years, assuming an Arrhenius relationship. Since all the experimental data is collected above T_g , it is likely that deviations are encountered in the glassy state, leading to an underestimation of the service life below T_g [14]. Since the temperature gradient through the insulation thickness keeps the insulation in contact with the medium pipe dry, high humidity levels would only be found at low temperatures. Degradation through hydrolysis is hence not foreseen an issue for steel PET-insulated pipes.

5. Conclusions

The ageing of PET foam has been studied, in order to confirm its suitability as insulation for DHC pipes. No degradation due to thermal cycling or hygrothermal exposure has been detected, related to the low coefficient of thermal expansion and moisture sorption of PET. Previously determined service temperature limit to PET's T_g at around 80 °C has been proven conservative, due to the thermally induced crystallinity increase and its impact on the material's strength. Therefore, PET foam could be a sustainable replacement for PU, eliminating the use of toxic chemicals in the DH piping manufacturing and supporting the transition to the Circular Economy.

CRedit authorship contribution statement

Lucía Doyle: Study design and conception, Data collection and analysis, Preparing the manuscript, Critical discussion of the results, Editing of the manuscript. **Ingo Weidlich:** Scientific supervision, Critical discussion of the results, Editing of the manuscript.

Declaration of competing interest

The authors declare that they have no known competing financial interests or personal relationships that could have appeared to influence the work reported in this paper.

References

- [1] Commission regulation (EU) 2020/1149 of 3 2020 amending annex XVII to regulation (EC) no 1907/2006 of the European parliament and of the council concerning the registration, evaluation, authorisation and restriction of chemicals (REACH) as regards diisocyanates. (EU) 2020/1149. 2020,
- [2] European Chemical Agency. CLP regulation: (EC) No 1272/2008. 2008.
- [3] Lund H, Werner S, Wiltshire R, Svendsen S, Thorsen JE, Hvelplund F, Mathiesen BV. 4th generation district heating (4GDH). *Energy* 2014;68:1–11.
- [4] Mangs S. Insulation materials in district heating pipes [Ph.D. thesis], Sweden: Chalmers University of Technology; 2005.
- [5] Ramnäs J. New materials and constructions for improving the quality and lifetime of district heating pipes including joints - thermal, mechanical and environmental performance: Annex VIII. 2008.
- [6] Marshall I, Todd A. The thermal degradation of polyethylene terephthalate. *Trans Faraday Soc* 1953;49(67).
- [7] McMahon W, Birdsall HA, Johnson GR, Camilli CT. Degradation studies of polyethylene terephthalate. *J Chem Eng Data* 1959;4(1):57–79.
- [8] Doyle L, Weidlich I. Effects of thermal and mechanical cyclic loads on polyurethane pre-insulated pipes. *Fatigue Fract Eng Mater Struct* 2021;44(1):156–68.
- [9] Sällberg SE, Nilsson S, Bergström G. Leakage ways for ground-water in PUR-foam. In: 10th international symposium on district heating and cooling. 2006.
- [10] Hay S, Huther H, Grimm S, Heiler D, Dony J, Nielsen H-J, Schuchardt GK, Grage T, Blesl M, Wendel F, Achmus M, Gerlach T, Terceros M, Below H, Thölert M, Leuteritz A. EnEff: Wärme - Technische Gebrauchsdaueranalyse von Wärmenetzen unter Berücksichtigung Volatiler Erneuerbarer Energien: Teil I: Untersuchungsergebnisse zur Materialdegradation. Frankfurt am Main: AGFW-Projektgesellschaft für Rationalisierung, Information; 2020.
- [11] Larsen CT, Togeskov P, Leuteritz A. Analyses of diffusion rates through pe and impact on ageing, vol. 6 II. English ed.. *EuroHeat & Power*; 2009.
- [12] Edge M, Allen NS, He JH, Derham M, Shinagawa Y. Physical aspects of the thermal and hydrolytic ageing of polyester, polysulphone and polycarbonate films. *Polym Degrad Stab* 1994;44(2):193–200.
- [13] Ballara A, Verdu J. Physical aspects of the hydrolysis of polyethylene terephthalate. *Polym Degrad Stab* 1989;26(4):361–74.
- [14] Dubelley F, Planes E, Bas C, Pons E, Yrieix B, Flandin L. Predictive durability of polyethylene terephthalate toward hydrolysis over large temperature and relative humidity ranges. *Polymer* 2018;142:285–92.
- [15] EN13941-1:2019. District heating pipes - Design and installation of thermal insulated bonded single and twin pipe systems for directly buried hot water networks - Part 1: Design; EN13941-1:2019.
- [16] ISO 844. Rigid cellular plastics – Determination of compression properties No. 2014.
- [17] Peters WH, Ranson WF. Digital imaging techniques in experimental stress analysis. *Opt Eng* 1982;21(3).
- [18] DIN EN ISO 11357. Plastics - differential scanning calorimetry (DSC) No. 11357. 2014th ed. Beuth.
- [19] Mehta A, Gaur U, Wunderlich B. Equilibrium melting parameters of poly(ethylene terephthalate). *J Polym Sci Polym Phys Ed* 1978;16(2):289–96.
- [20] Langevin D, Grenet J, Saiter JM. Moisture sorption in pet influence on the thermokinetic parameters. *Eur Polym J* 1994;30(3):339–45.
- [21] Vega A, Yarahmadi N, Sällström JH, Jakubowicz I. Effects of cyclic mechanical loads and thermal ageing on district heating pipes. *Polym Degrad Stab* 2020;182:109385.
- [22] Gibson LJ, Ashby MF. Cellular solids. Cambridge: Cambridge University Press; 1997.
- [23] Doyle L, Weidlich I, Ilguth M. Anisotropy in polyurethane pre-insulated pipes. *Polymers* 2019;11(12).
- [24] Lerch BA, Sullivan RM. Thermal expansion of polyurethane foam. In: 43rd annual technical meeting of the society of engineering science. 2006.
- [25] Mark JE. The polymer data handbook. second ed.. New York, Oxford: Oxford University Press; 2009.
- [26] Doyle L, Weidlich I. Mechanical behaviour of polylactic acid foam as insulation under increasing temperature. *Environ Clim Technol* 2019;23(3):202–10.
- [27] Balani K, Verma V, Agarwal A, Narayan R, editors. Biosurfaces: A Materials Science and Engineering Perspective. Hoboken: Wiley; 2015.
- [28] Doyle, et al. Moisture uptake and effects of hygrothermal exposure on semicrystalline PET foam. 2021 [in preparation].
- [29] Doyle L. Hydrolytic degradation of closed cell PET foams. 2021 [in preparation].



Proceedings

Recyclable Insulating Foams for High-Temperature Applications [†]

Lucía Doyle ^{*} and Ingo Weidlich

Infrastructural Engineering, HafenCity University, 20457 Hamburg, Germany; ingo.weidlich@hcu-hamburg.de

^{*} Correspondence: lucia.doyle@hcu-hamburg.de; Tel.: +49-40-42827-4590

[†] Presented at the First International Conference on “Green” Polymer Materials 2020, 5–25 November 2020;

Available online: <https://sciforum.net/conference/CGPM2020>.

Abstract: The recently approved restriction on diisocyanates highlights the health and safety issues concerning polyurethane manufacturing and the relevance of developing sustainable insulating polymeric foams. This is particularly challenging for applications where the foam is subjected to high temperatures (>80 °C) and bear loads, such as insulating and bonding material for district heating pipes. As part of a PhD project concerning pre-insulated district heating pipes for the circular economy, polybutylene (PB-1) has been identified as a promising candidate for the application, due to its low thermal conductivity, high-temperature mechanical properties, retention, excellent environmental stress cracking resistance (ESCR) and outstanding creep resistance. It is a recyclable thermoplastic and of non-toxic nature, pre-requisites for circular product development. On the contrary to other polyolefins, PB-1 is reported to strain-harden and has high melt strength, required properties for foaming. The purpose of the study is to assess the foamability of PB-1 through extrusion foaming experiments. A twin-screw extruder was used with varying concentrations of a chemical blowing agent. The obtained samples have been characterised for density, expansion ratio and microstructure. Foams with a volume expansion ratio of 1.8 were achieved. The results confirm the foamability of this polymer. The increase of the die pressure and its contribution to strain hardening were identified as key parameters for successful foaming. Further research will include improving the expansion ratio with a physical blowing agent and mechanical characterization of the foam.

Keywords: polymeric foam; polybutylene; district heating; insulation; thermoplastic; circular economy

Citation: Doyle, L.; Weidlich, I. Recyclable Insulating Foams for High Temperature Applications. *2021*, *65*, 29. <https://doi.org/10.3390/CGPM2020-07200>

Published: 4 November 2020

Publisher’s Note: MDPI stays neutral with regard to jurisdictional claims in published maps and institutional affiliations.



Copyright: © 2020 by the authors.

Licensee MDPI, Basel, Switzerland.

This article is an open access article distributed under the terms and conditions of the Creative Commons Attribution (CC BY) license (<http://creativecommons.org/licenses/by/4.0/>).

1. Introduction

District heating (DH) infrastructure is called to be a cornerstone element towards decarbonizing the heating sector. Thanks to a district heating network, the use of decentralized renewable and waste heat sources is enabled. For its technical and economic feasibility, correct insulation of district heating pipes is critical. As for state of the art, all district heating pipes are insulated with polyurethane foam (PU) [1].

PU foams present the lowest thermal conductivity among foamed polymers used commercially [2]. While PU has excellent thermal and mechanical properties, it has important environmental and toxicity drawbacks, which trigger the need for research in new and alternative insulating foams.

PU is produced from a ca. 50/50 mix of a polyol and either TDI (toluene diisocyanate) or MDI (methylene diphenyl diisocyanate). TDI and MDI are classified as suspected of causing cancer, as dermal and respiratory sensitizers, for acute toxicity following inhalation, as well as eye, skin and respiratory irritants under the EU’s CLP Regulation [3]. The European Commission has approved to restrict the use of diisocyanates to a concentration limit of 0.1% by weight under REACH on 4 August 2020 [4].

There is a need for developing environmentally friendly insulating foams following a holistic approach: conceptualized from the beginning out of non-toxic and recyclable materials and a safe manufacturing process. In this context, the foamability of PB-1 is explored. Promising properties for the application are its low thermal conductivity of 0.114 W/mK [5], good mechanical property retention under high temperature, excellent environmental stress cracking resistance (ESCR) and outstanding creep resistance [6]. It is a recyclable thermoplastic and of non-toxic nature, pre-requisites for circular product development. In contrast to other polyolefins, PB-1 is reported to strain harden and has high melt strength [6], required properties for foaming [7]. However, its foaming behaviour has not been found reported in the open literature. In this study, the foamability of PB-1 is studied through extrusion foaming experiments with a chemical blowing agent. The obtained samples have been characterised for density, expansion ratio and microstructure. Foamability is assessed in terms of achieved volume expansion ratio, microstructure and processing window using available extrusion equipment. Optimization of the foaming process is out of the scope of this study. The presented results are part of a larger screening of commercial PB-1 grades.

2. Experiments

2.1. Materials

Toppyl PB0110M PB-1 from LyondellBasell was extrusion foamed using Hydrocerol CT 550 chemical blowing agent (CBA), kindly provided by Clariant.

2.2. Extrusion Foaming Process

The extrusion process was undertaken with a twin screw ZSE 27 MAXX extruder (Leistritz Extrusionstechnik GmbH, Nürnberg, Germany), with $D = 28.3$ mm, $L/D = 48$, and 12 modular barrels with 2.1 kW heating power each and water cooling. A strand die with three strands of 4 mm diameter each was used. The feeding temperature was set as low as possible as to create a melt seal and avoid premature degassing of the CBA, which was set at 140 °C. The temperature was progressively increased to 175 °C after the CBA dosing point, which as to allow its complete decomposition, and then progressively lowered. The amount of dosed CBA was varied from 4.2 to 10% wt., for die exit temperatures of 110 and 115 °C. Screw speed rate and feed rate were kept constant to 100 rpm and 4 kg/h respectively.

2.3. Foam Characterization

The foam samples were randomly collected at each processing condition after achieving the steady state and characterized for density, volume expansion, cell size and cell density.

The density was determined with a 100 mL glass pycnometer, distilled water and a Sartorius AC 211 S (Goettingen, Germany) balance.

Foam volume expansion ratio is often determined as the ratio between the density of the polymer and the density of the foam. However, since a CBA is used—for which the effective foaming components amount to 70% wt., and up to 10% wt.—CBA was dosed, resulting in the addition of 3.3% wt. of the decomposition products. It was found to be more accurate to determine the volume expansion ratio V_{exp} as

$$V_{\text{exp}} = \frac{\text{diameter foam extrudate}}{\text{diameter polymer extrudate}} \quad (1)$$

in an analogous method to the one used by [8].

The diameter of the obtained foam samples and neat polymer extrudates were obtained from photographs taken using a Nikon D700 camera and a tripod. Photographs were recorded from immediately after collection (max. time between collection and initial photo 20 s) up to over 2 h after extrusion, in 20 s time-lapse intervals. The diameter of each

strand was measured in five different locations of each strand once its dimension was stable using Fiji [9]. The average of the five measurements is presented in each case.

The morphology of the foams was examined in an optical microscope (Leica DMLP, Wetzlar, Germany). Cell size was measured from the obtained micrographs using Fiji [9]. Cell population density (N_0), defined as the number of cells per unit volume of the original unfoamed polymer, was calculated as [10,11]:

$$N_0 = \left(\frac{n}{A}\right)^{3/2} \cdot V_{\text{exp}} \quad (2)$$

where (N_0) is the cell population density (cell/cm³), n is the number of cells in the micrograph and A the area of the micrograph (cm²).

3. Results and Discussion

The density of the obtained samples is presented in Table 1.

Table 1. Density for samples under different process conditions.

Die T (°C)	CBA% wt.	Density (g/mL)
110	4.2	0.740 ± 0.032 *
110	7.1	0.5 ± 0.017 *
110	8.50	0.598 ± 0.031 *
110	10	0.53 ± 0.034 *
115	4.2	0.508 ± 0.122 *
115	7.1	0.508 ± 0.036 *
115	8.50	0.488 ± 0.178 *
115	10	0.601 ± 0.089 *

* Standard deviation.

The determined volume expansion ratio, cell population density and cell size and their relation to the process conditions can be found in Figure 1.

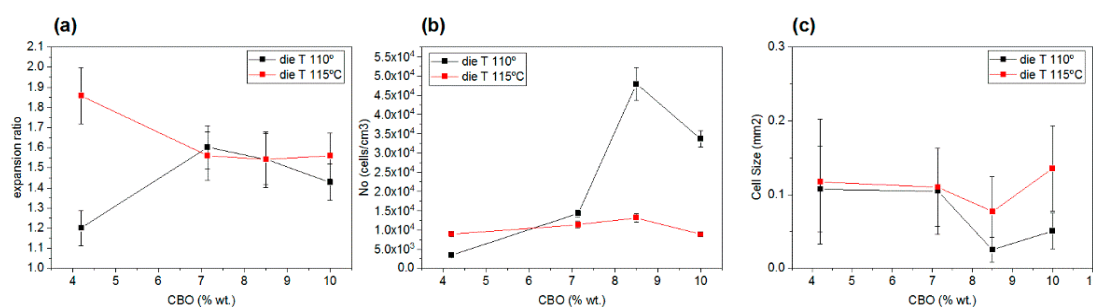


Figure 1. (a) Expansion ratio vs. introduced amount of CBA. (b) Cell population density vs. introduced amount of CBA. (c) Cell size vs. introduced amount of CBA.

Representative micrographs for each process condition can be found in Figure 2.

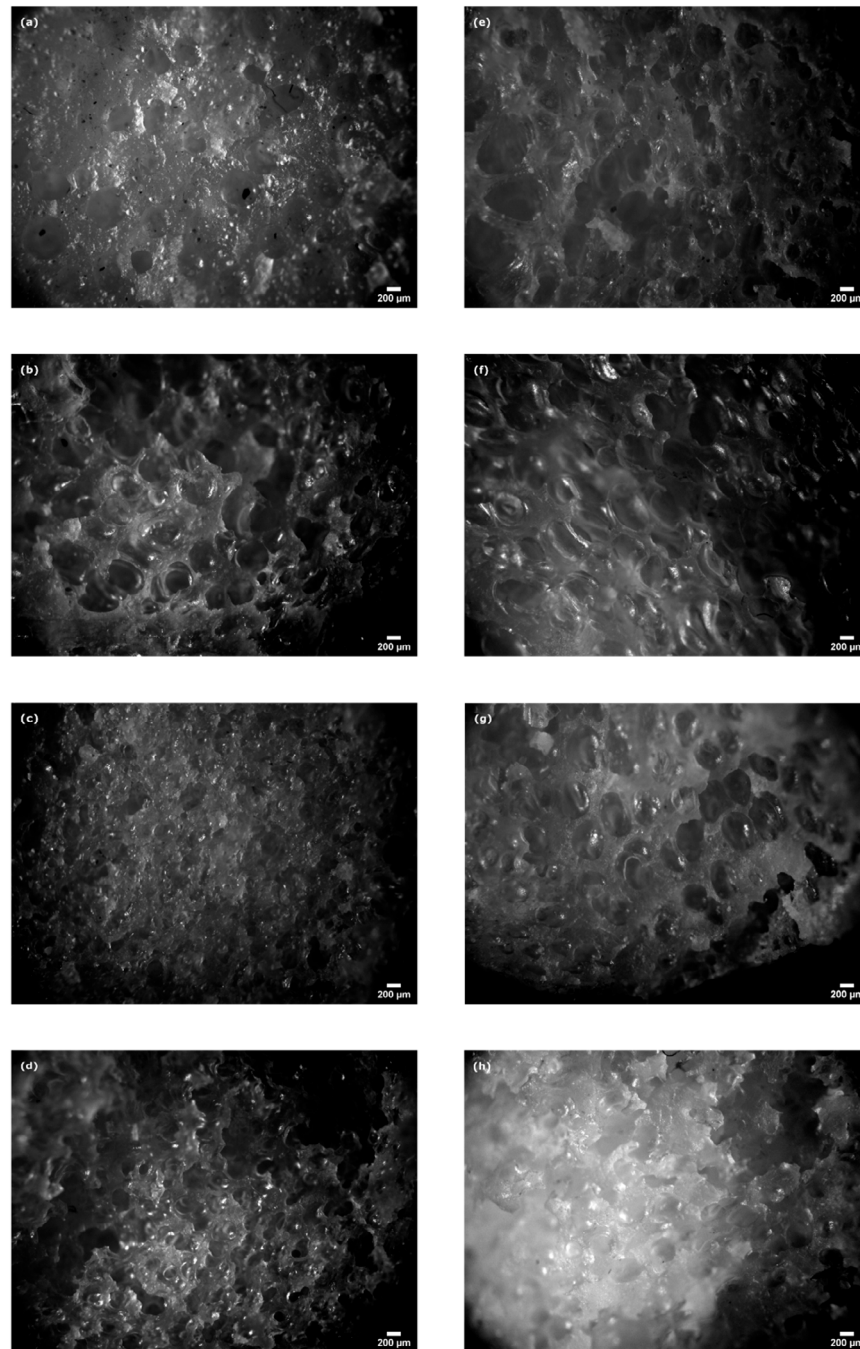


Figure 2. Micrographs of obtained foams under different process conditions: die $T^\circ = 110\text{ }^\circ\text{C}$ and 4.2% CBA (a); 7.1% CBA (b); 8.5% CBA (c) and 10% CBA (d) die $T^\circ = 115\text{ }^\circ\text{C}$ and 4.2% CBA (e); 7.1% CBA (f); 8.5% CBA (g) and 10% CBA (h).

3.1. Microstructural Characterization and the Relationship with the Process Conditions

As can be seen in Figures 1c and 2, foams present large pores with significant cell size variability. The two die temperatures used did not produce any difference in the obtained cell size for CBA concentrations of 4.2 and 7.1% wt. Cell size decreased for 8.5% wt. as cell population density increased. This inverse trend has been previously reported [12]. This effect is particularly significant for the $110\text{ }^\circ\text{C}$ die T° trial, where the average cell size was

reduced by more than 50%. After this point N_0 decreased again and cell size increased. This can be explained as the increase of CBA provides more available gas for cell nucleation, until a maximum is reached. With further gas increase and cell growth, cells collide against each other, reducing the n° of cells and increasing their size [13], as can be observed by the trends in Figure 1b,c.

3.2. Effect of Process Conditions on the Volume Expansion Ratio

The two die temperatures tested were selected as a result of a preliminary process parameter screening. With die T° over 120 °C, limited expansion was achieved. This is an indication for low melt strength, which prevents the polymer melt from withstanding the stretching forces of the bubble growth, leading to cell collapse, and of high gas diffusion out of the polymer matrix. The lower processing temperature was conditioned by viscosity, being 110 °C the lowest temperature at which the melt would flow out of the extruder.

As can be seen in Figure 1a, with the die T° of 110 °C, the expansion ratio increased until a maximum and then decreased. This indicated that at this temperature the expansion behaviour is governed by the polymer melt's stiffness. Expansion increases with increasing CBA concentration due to the plasticisation effect of the gas [12]. After reaching a maximum, the gas starts diffusing out of the polymer's hot skin. For the 115 °C die temperature series, the maximum expansion was achieved with the lowest concentration of CBA tested. Since the cell size and cell population density of the samples obtained at the lowest concentration (4.2%) was not higher than those obtained with increasing CBA dosages, we can conclude that from that dosage the increased level of gas just increased the diffusion out of the hot skin of the extrudates, thus the volume expansion remained at constant levels.

During the execution of the trials, a transient situation was encountered where the die pressure was increased from the 45 bar of the reported trials up to 75 bar. Under these conditions, a higher volume expansion was obtained, and strain hardening was observed on the extrudates. The relationship between strain hardening and successful foaming is known in the field [7], as well as the relation between pressure drop and cell population density [14]. The data of this obtained foam are not included due to the non-reproducible process conditions (transient), but show the potential of improved foaming of this resin under optimal process conditions. As mentioned in the introduction, process optimization is out of the scope of this study, which aims at screening foamability.

4. Conclusions

An experimental study on the extrusion foaming behaviour of a commercial PB-1 resin was presented. Foamability of the resin was confirmed. High-density foams were produced, with a volume expansion of 1.8. The processing window was screened and the influence of process conditions on the microstructure and volume expansion of the obtained foams was studied, indicating that PB-1 foam of medium density can be produced when the foaming process is optimized.

Author Contributions: L.D. was responsible for the study design and conception, performing the experiments, analysing the data, and chiefly responsible for preparing the manuscript. I.W. provided scientific supervision of the study. Both authors contributed to the critical discussion of the results and editing of the manuscript. All authors have read and agreed to the published version of the manuscript.

Acknowledgments: The work reported is self-funded by the HafenCity University. Xihua Hu and Irina Smirnova, from the Technical University of Hamburg, are gratefully thanked for making the extruder available. The Hamburg Energy Research Network (EFH) is kindly acknowledged for facilitating the cooperation.

Conflicts of Interest: The authors declare no conflict of interest.

Abbreviations

The following abbreviations are used in this manuscript:

PB-1	Polybutylene
ESCR	Environmental stress cracking resistance
DH	District heating
PU	Polyurethane
TDI	Toluene diisocyanate
MDI	Methylene diphenyl diisocyanate
EU	European Union
CLP Regulation	Classification, labelling and packaging of substances and mixtures regulation
REACH	Registration, evaluation, authorisation and restriction of chemicals
CBA	Chemical blowing agent
wt.	Weight
T°	Temperature

References

1. Nilsson, S.F. New developments in pipes and related network components for district heating. In *Advanced District Heating and Cooling (DHC) Systems*; Elsevier: Amsterdam, The Netherlands, 2016; pp. 191–214, ISBN 9781782423744.
2. Kurańska, M.; Prociak, A. Bio-Based Polyurethane Foams for Heat-Insulating Applications. In *Nano and Biotech Based Materials for Energy Building Efficiency*; Pacheco Torgal, F., Buratti, C., Kalaiselvam, S., Granqvist, C.-G., Ivanov, V., Eds.; Springer International Publishing: Cham, Switzerland, 2016; pp. 357–373, ISBN 978-3-319-27503-1.
3. The European Parliament and the Council of the European Union. CLP Regulation; (EC) No 1272/2008. *Off. J. Eur. Union* **2008**.
4. Commission Regulation (EU). 2020/1149 of 3 August 2020 Amending Annex XVII to Regulation (EC) No 1907/2006 of the European Parliament and of the Council Concerning the Registration, Evaluation, Authorisation and Restriction of Chemicals (REACH) as Regards Diisocyanates: (EU) 2020/1149. *Off. J. Eur. Union* **2020**.
5. Wypych, G. *Handbook of Plasticizers*, 3rd ed.; Chemtec: Toronto, ON, Canada, 2017; ISBN 9781895198973.
6. Olabisi, O.; Adewale, K. *Handbook of Thermoplastics*; CRC Press: Boca Raton, FL, USA, 2016; ISBN 1466577223.
7. Lee, S.-T.; Park, C.B. (Eds.) *Foam Extrusion. Principles and Practice*, 2nd ed.; CRC Press: Boca Raton, FL, USA, 2014; ISBN 9781439898598.
8. Jeong, B.; Xanthos, M.; Seo, Y. Extrusion Foaming Behavior of PBT Resins. *J. Cell. Plast.* **2006**, *42*, 165–176.
9. Schindelin, J.; Arganda-Carreras, I.; Frise, E.; Kaynig, V.; Longair, M.; Pietzsch, T.; Preibisch, S.; Rueden, C.; Saalfeld, S.; Schmid, B.; et al. Fiji: An open-source platform for biological-image analysis. *Nat. Methods* **2012**, *9*, 676–682, doi:10.1038/nmeth.2019.
10. Liu, H.; Wang, X.; Liu, W.; Liu, B.; Zhou, H.; Wang, W. Reactive Modification of Poly(ethylene terephthalate) and its Foaming Behavior. *Cell. Polym.* **2014**, *33*, 189–212, doi:10.1177/026248931403300402.
11. Reignier, J.; Gendron, R.; Champagne, M.F. Autoclave Foaming of Poly(ϵ -Caprolactone) Using Carbon Dioxide: Impact of Crystallization on Cell Structure. *J. Cell. Plast.* **2007**, *43*, 459–489, doi:10.1177/0021955x07079591.
12. Kaewmesri, W.; Lee, P.C.; Park, C.B.; Pumchusak, J. Effects of CO₂ and Talc Contents on Foaming Behavior of Recyclable High-melt-strength PP. *J. Cell. Plast.* **2006**, *42*, 405–428, doi:10.1177/0021955x06066995.
13. Matuana, L.M.; Faruk, O.; Diaz, C.A. Cell morphology of extrusion foamed poly(lactic acid) using endothermic chemical foaming agent. *Bioresour. Technol.* **2009**, *100*, 5947–5954, doi:10.1016/j.biortech.2009.06.063.
14. Guo, Q.; Wang, J.; Park, C.B.; Ohshima, M. A Microcellular Foaming Simulation System with a High Pressure-Drop Rate. *Ind. Eng. Chem. Res.* **2006**, *45*, 6153–6161, doi:10.1021/ie060105w.



Environmental and Climate Technologies

2019, vol. 23, no. 3, pp. 202–210
doi: 10.2478/rtuct-2019-0090
<https://content.sciendo.com>

Mechanical Behaviour of Polylactic Acid Foam as Insulation Under Increasing Temperature

Lucia DOYLE^{1*}, Ingo WEIDLICH²

^{1,2} *HafenCity University, Uberseeallee 16, Hamburg, 20457, Germany*

Abstract – Measures to increase the share of renewables in heat generation, combined with increased energy efficiency provide a direct emissions reduction on the heating sector. Energy efficiency measures, as well as the role-out of sustainable heating technologies such as district heating networks have one key actor: insulation. However, state of the art insulating materials such as polyurethane or polystyrene have severe environmental drawbacks incompatible with today's transition to the circular economy, and are the Achilles' heel of the sector in terms of sustainability. Biobased and biodegradable polylactic acid (PLA) foam could be a promising replacement for fossil-based polymeric insulating foams. This study provides data on the mechanical behaviour of expanded PLA foam under different temperatures, which will help to assess its potential use as insulation where the foam is subject to heat.

Keywords – Circular economy; insulating foam; Polylactic Acid (PLA); thermal behaviour

Nomenclature		
σ_{10}	Compressive Stress at 10 % strain	MPa
E	Young Modulus	MPa
T	Temperature	°C
T_g	Glass transition temperature	°C
a	Sample width	mm
b	Sample depth	mm
h	Sample height	mm

1. INTRODUCTION

Energy efficiency measures combined with sustainable renewable sources of heat would significantly reduce global CO₂ emissions and contribute to the achievement of goals such as the EU 2020 climate and energy package.

The 4th generation District Heating [1] aims in this direction: by reducing the network's temperature, up to now non-used waste and renewable heat sources can be introduced in the system, significantly contributing to the decarbonisation of the sector, as well as contributing to higher air quality in urban areas. Decreasing the operating temperature will bring higher energy efficiency of the system, and its effects on the system's elements such as the heat

* Corresponding author.

E-mail address: lucia.doyle@hcu-hamburg.de

©2019 Lucia Doyle, Ingo Weidlich.

This is an open access article licensed under the Creative Commons Attribution License (<http://creativecommons.org/licenses/by/4.0>), in the manner agreed with Sciendo.

exchangers have been studied [2]. But the temperature reduction additionally opens up new possibilities in materials selection. This potential remains still untapped.

Today's insulation materials are to a big extent petroleum-based polymeric materials. Polyurethane (PU) and Polystyrene (PS) accounted for 42 % of the European thermal insulation market in 2012 [3], and PU is the standard insulation for District Heating Pipes [4]. However, the environmental profile of these materials makes insulation the weakest point of the sustainability efforts these energy efficiency measures intend to bring.

While PU is chemically inert [5] and non-toxic, its base material isocyanates are toxic and present a number of health and safety issues and harmful effects in varying degrees [5]–[8]. PU is produced from either TDI (toluene diisocyanate) or MDI (methylene diphenyl diisocyanate). TDI and MDI isomers and mixes thereof are classified as suspected of causing cancer, as dermal and respiratory sensitizers, for acute toxicity following inhalation, as well as eye, skin and respiratory irritants [8]. The residual styrene in the PS matrix is carcinogenic, and thus threatening human health [9]. None of these foams is recyclable.

There is an urgent need for developing alternative insulation materials which are nontoxic and fully recyclable, which would support the transition from eco-efficiency to a circular economy.

Within the frame of an exploratory research project aiming at identifying polymeric foams suitable for the insulation of 4th generation district heating networks, the mechanical behavior of PLA foam under different temperatures has been studied in order to obtain information on if and how the foams could be used as insulation in applications where they are subjected to or in contact with higher temperature.

Poly(lactide acid) (PLA) is a thermoplastic aliphatic polyester derived from biomass such as corn starch and sugarcane. It is the best-developed commercially available biopolymer [10] and is currently produced at low cost and commercialized in large quantities [11]. Given its physical properties and biodegradable nature, its first application niche has been biomedical applications, followed by disposable packaging. However, interest and applications concerning the building sector are under development. In 2016 Dutch plastic pipe manufacturer DYKA presented a PLA piping system for housing rain water collection at the VSK trade show (NL), claiming similar properties to PVC and long service life [12]. Previous work on PLA foams have reported comparable behavior with polystyrene foams in terms of mechanical and thermal properties [9], [13]. The PLA foam's intrinsic IR absorbing characteristics, acted via the ester group in the PLA molecular chain, sets this polymer matrix as a good candidate for insulation applications and further enhances its environmental impact [9].

One of the limitations of PLA is its low service temperature, due to its low crystallinity because of its inherently low crystallization kinetics [10], and with a glass transition temperature (T_g) set around 60 °C. T_g signals the transition from a hard and relatively brittle state into a rubber like state [14]. There is no clear protocol or parameter to define the heat resistance of a polymer, however, T_g can give an indication of the heat resistance for amorphous or low crystalline polymers [15], [16]. The heat resistance of a material is strongly linked to its crystallinity. A higher degree of crystallinity implies a higher temperature resistance, since the crystalline regions should maintain material stiffness past the T_g [15]. Literature reports the potential of PLA foams to be used at elevated temperatures above its T_g , as a higher crystallinity is obtained due to the foaming process, and as a result, the PLA foam products can exhibit ductile and tough behaviour without easy deformation above T_g [10].

With the basis of the above stated quote, the aim of this study is to observe the mechanical behaviour of readily produced PLA foams above the material's T_g , in order to obtain

information on how and if the foams could be used in applications where they are subjected to or in contact with higher temperature.

2. METHODS AND PROCEDURES

Samples of molded expanded bead PLA foam were provided by *BEWiSynbra*. Samples were tested for compression in a universal testing machine at a constant strain rate of 2 mm/s. The plates were placed inside a thermal chamber, where different temperatures can be set. The applied force was a direct output from the testing machine. The strain was optically measured using an *ARAMIS* adjustable stereo camera system.

The selected test temperatures were 22 °C, 55 °C, 65 °C and 75 °C. Samples at 22 °C were tested after storage for several days at the laboratory's room conditions: 22 °C and 30 % humidity. Samples tested at higher temperatures were previously temperature soaked inside the thermal chamber. Relative humidity inside the chamber could not be measured or modified and is thought to be very low.

In order to evaluate the impact of the duration of temperature conditioning, a thermocouple was inserted in one sample to measure the time needed to reach 75 °C. It was achieved within minutes. A batch of three samples were tested at 75 °C after 2 h temperature conditioning, and 5 further samples after 48 h of temperature conditioning, showing no difference in behaviour. Therefore, in order to optimize the test execution timing, temperature soaking was 2 h for the samples at 65 °C and over night for the samples at 55 °C.

The presented results correspond to the mean of five probes tested for each of the selected temperatures: 22 °C, 55 °C, 65 °C and 75 °C.

Samples for the 22 °C and 75 °C test series were provided as cut cubes (approx. 48·48·48 mm) by the supplier. Samples for the 55 °C and 65 °C were cut out of a slab with the same dimensions as the previous samples using a wire cutter.

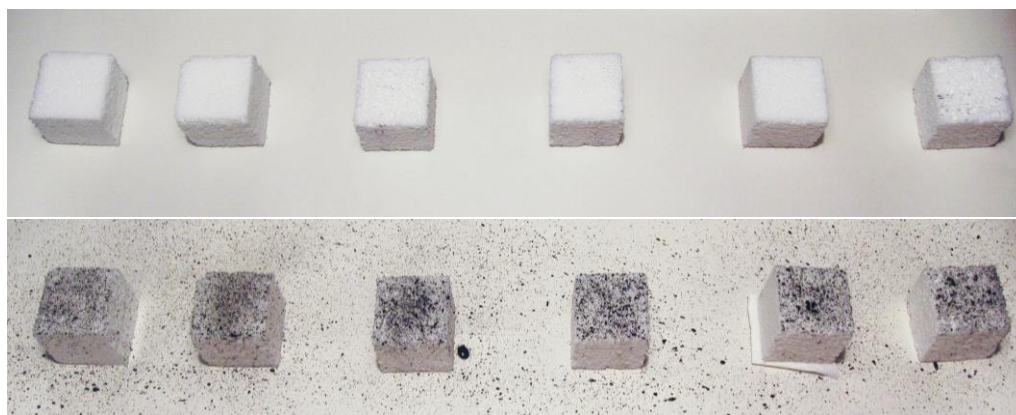


Fig. 1. Sample Preparation: before and after the painting of a stochastic pattern.

Samples were individually accurately measured using caliber and weighed prior testing. After observing shrinkage at 75 °C, samples at 55 °C and 75 °C were re-measured after being temperature soaked and immediately before testing. Dimensions of samples tested at 65 °C were re-evaluated from the images taken from the *ARAMIS* stereocamera. The strain measured by the *ARAMIS* optical system's software is based on a stochastic pattern recognition analysis.

Therefore a stochastic pattern was painted on one side, using canned black spray paint and a toothbrush.

IR spectroscopy has been reported as an appropriate technique to qualitatively and quantitatively determine the degree and nature of crystalline and non-crystalline order and has been previously been used in the study of PLA [16]–[18]. Hence in order to observe changes in the crystallinity structure due to the heating, foam tested under room temperature and under 75 °C where analysed using a Thermoscientific *Nicolet iS 10 FTIR* spectrometer.

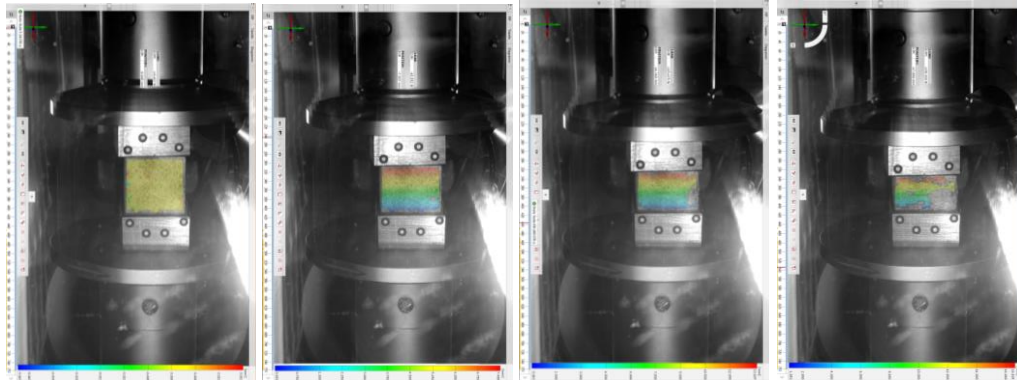


Fig. 2. Visualization of the compression test of sample 75-2. From left to right after 54 s, 272 s, 465 s and 563 s.

3. RESULTS

Table one presents the weight and dimensions of each sample, at room and at test temperature.

As can be derived from the data, samples tested at 55 °C experimented an average volumetric shrinkage of 0.8 % at 55 %, of 3.6 % at 65 °C and of 14.4 % at 75 °C. Shrinkage is typically observed when the gas inside the foam cells diffuses out of the foam in a faster rate as air diffuses in, creating a negative pressure in the closed cells [11].

TABLE 1. SAMPLES WEIGHT AND DIMENSIONS

Sample	Test T°	Weight, g	At room T, °C			At test T, °C		
			a, mm	b, mm	h, mm	a, mm	b, mm	h, mm
22-1	22	3.44	48.3	47.9	48.7	48.3	47.9	48.7
22-2	22	3.52	48.49	48.5	48.6	48.49	48.5	48.6
22-3	22	3.75	48.1	50.2	48.7	48.1	50.2	48.7
22-4	22	3.41	48.16	48.12	48.03	48.16	48.12	48.03
22-5	22	3.65	48.12	48.2	48.2	48.12	48.2	48.2
55-1	55	3.55	48.04	48.13	48.06	48.8	47.96	47.84
55-2	55	3.35	47.99	48.2	45.85	47.96	47.85	45.88
55-3	55	3.29	48.7	48.12	45.94	48.06	48.06	45.74

Sample	Test T°	Weight, g	At room T, °C			At test T, °C		
			a, mm	b, mm	h, mm	a, mm	b, mm	h, mm
55-4	55	3.63	47.83	48.03	48.11	47.81	47.9	47.97
55-5	55	3.7	48.01	48.33	47.94	47.92	47.98	47.61
65-1	65	3.58	48.37	48.7	47.78	47.70	48.02	47.12
65-2	65	3.77	48.58	48.1	49.6	47.91	47.43	48.91
65-3	65	3.47	48.85	48	48.12	48.12	47.29	47.41
65-4	65	3.52	48.35	47.9	48.8	48.30	47.86	48.75
65-5	65	3.7	48.25	48.6	48.2	47.39	47.73	47.34
75-1	75	3.49	48.22	48.23	48	45.68	45.67	45.55
75-2	75	3.58	48.09	48	48.1	46.2	45.39	45.04
75-3	75	3.46	48.34	48.29	48.05	46	45.79	47.7
75-4	75	3.64	48.02	47.97	48.1	45.25	45.23	45.36
75-5	75	3.6	47.98	48.1	48.04	45.35	45.54	45.42

The average density for the foam samples is 31 kg/m^3 .

Fig. 3 presents the stress strain curves for each sample tested. A clear grouping per test temperature can be observed.

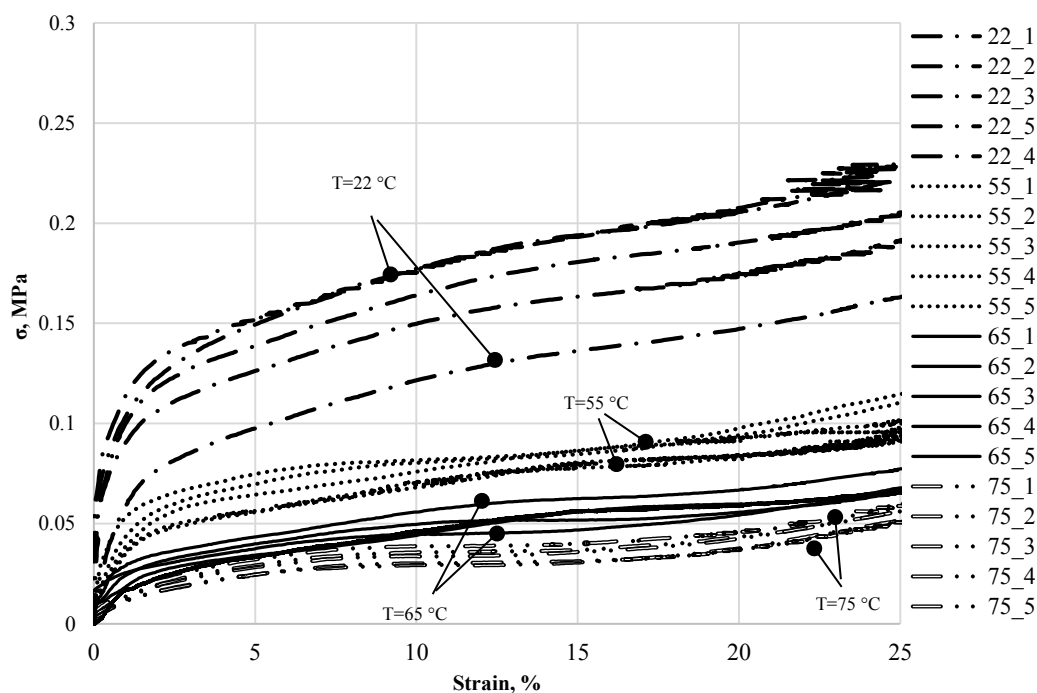


Fig. 3. Stress vs Strain curves for the tested PLA foam samples under different T .

Compressive strength at 10 % strain and E modulus were calculated for each sample. E modulus was determined for the zone between 25 % and 75 % of F_{10} , as per EN ISO 844:2014 [19]. Average values per test temperature and their variance are presented in Table 2.

TABLE 2. CALCULATED COMPRESSIVE STRENGTH AT 10 % STRAIN AND E MODULUS FOR EACH T°

$T, ^\circ\text{C}$	σ_{10}, MPa	Variance σ_{10}	E, MPa	Variance E
22	0.158	$5.4 \cdot 10^{-4}$	0.591	$4.01 \cdot 10^{-3}$
55	0.075	$4.2 \cdot 10^{-5}$	0.298	$5.23 \cdot 10^{-4}$
65	0.048	$2.2 \cdot 10^{-5}$	0.249	$7.79 \cdot 10^{-4}$
75	0.034	$1.5 \cdot 10^{-5}$	0.228	$4.20 \cdot 10^{-4}$

The relationship of σ_{10} and E with the test temperature can be observed in Fig. 4 and Fig. 5.

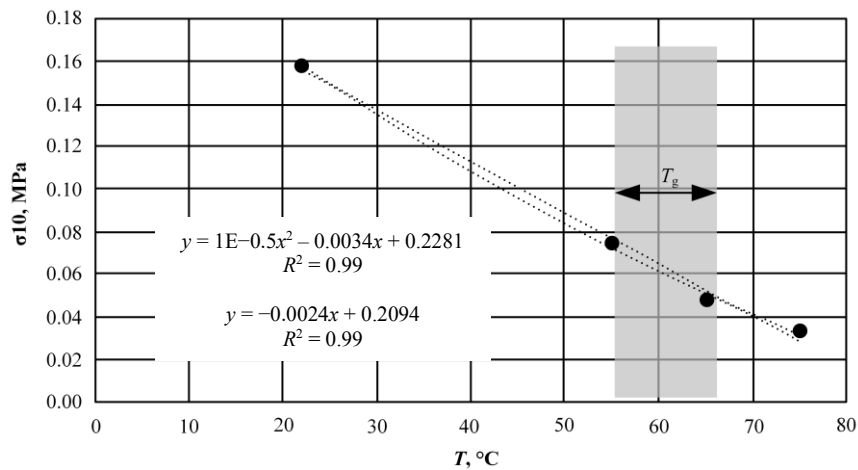


Fig. 4. Relationship of compressive strength with test T° .

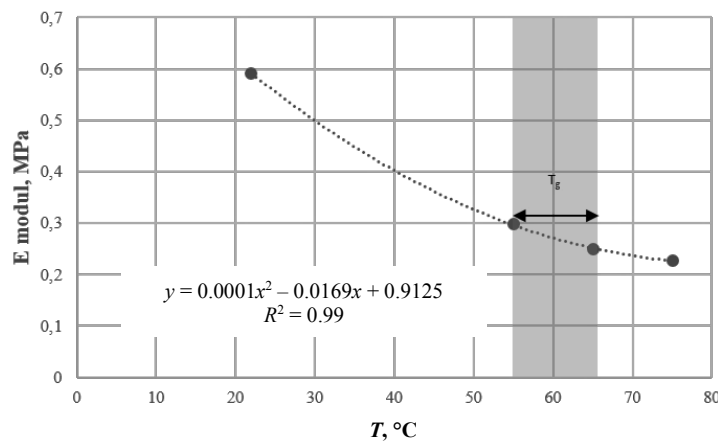
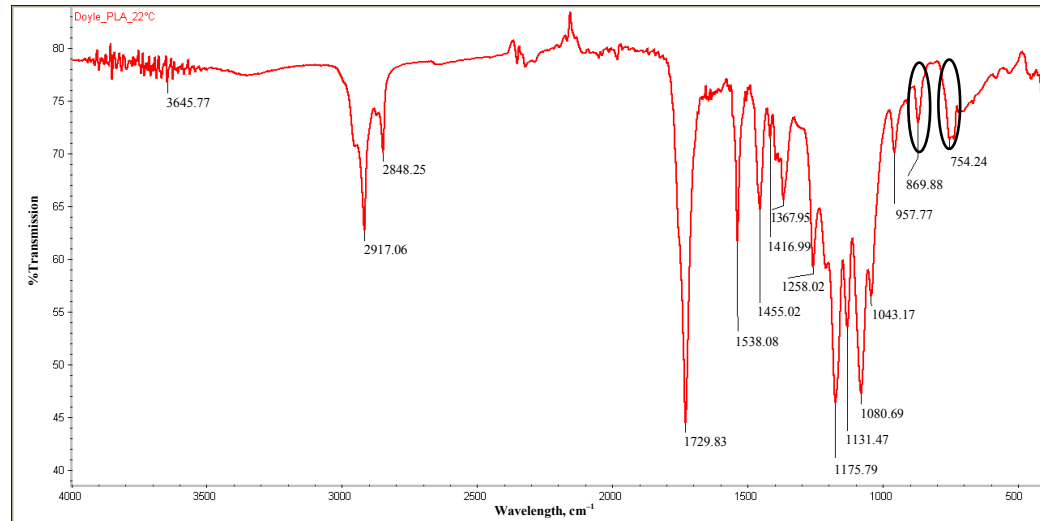
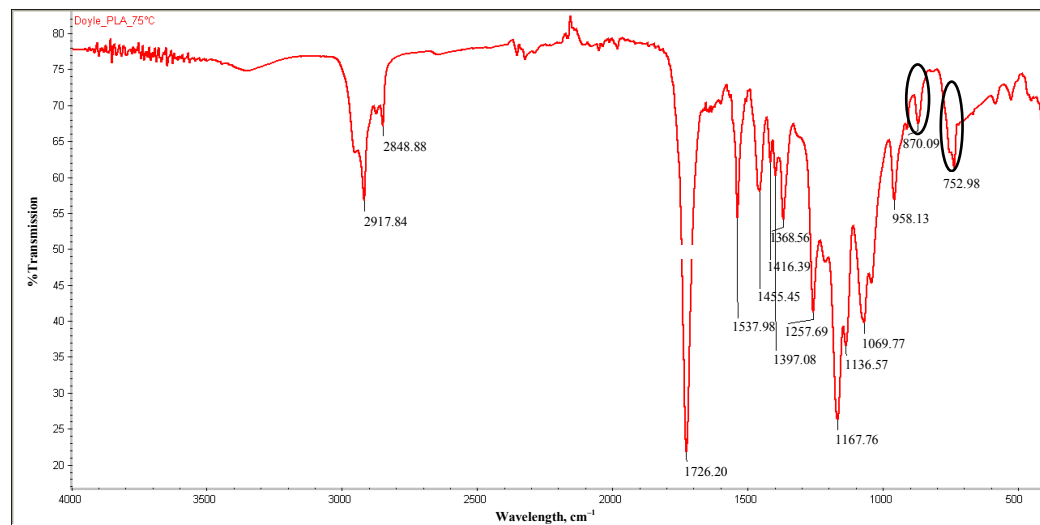


Fig. 5. Relationship of E modulus with test T° .

The obtained IR Spectra of foam samples stored at room temperature (22 °C) and after soaking at 75 °C is presented in Fig. 6.



(a)



(b)

Fig. 6. IR spectra of PLA foam samples after storage at (a) 22 °C and (b) 75 °C.

The peaks corresponding to the amorphous and crystalline phases are marked.

4. DISCUSSION

The investigation was carried out with PLA bead foams. Because of the manufacturing process of pre-insulated pipes, the use of bead foam it is not expected, but of extruded foam. However, extruded PLA foams are still under R&D and not commercially available. Hence, this study intends to provide qualitative data rather than quantitative data as for district heating applications. The generated data is however valuable for other insulating applications requiring foam sheets. Extruded foams would be expected to have a higher density and higher mechanical strength than bead foams. Compared to insulation foams according to district heating standards (PU), the tested material has a half the density, which has an influence on the mechanical properties.

Thus PLA foams would be useful for district heating application operating in the lower temperature levels. In the case of lower temperature, the mechanical strength of the material plays a minor role, since temperature induced stresses and displacements are less significant [20].

The compressive strength at 10 % strain obtained at room temperature is equivalent to that reported by Parker et al [13]. As expected for a thermoplastic, compression strength and E modulus steadily decreased with the testing temperature. However no sudden drop in properties was observed around the T_g . Two correlations are presented for σ_{10} , linear and quadratic polynomial, as a similar best fit was obtained.

As for the stress strain curve (Fig. 3), an interesting result is that the different samples tested for each temperature presented a larger deviation at room temperature and behaved closer alike as we went up with temperature.

The original crystallinity of the provided foam samples would be between 20 and 30 % according to the manufacturer. Work from Auras et al. [16] and Younes and Cohn, compiled in [21], report a peak related to the crystalline phase, at 755 cm^{-1} in [21] and 756 cm^{-1} in [16], and to the amorphous phase, at 869 cm^{-1} in [21] and 871 cm^{-1} in [16]. Consistent with these studies, both peaks were found and identified in our work. Crystallization of the amorphous but thermally crystallizable PLA copolymers is reported to be initiated by annealing at temperatures starting at $75\text{ }^\circ\text{C}$ [16]. Since this temperature corresponds to the higher testing temperature of this work, determining if further crystallization occurs due to the operation temperature the insulation is subjected to would provide valuable information about the aging of the foam. Further work on the preparation of a standard curve is needed to allow for quantitative determination of each phase. Further research is needed to evaluate the potential impact of thermal cycling.

Since the processing of PLA is still in its infancy, an increase of heat and mechanical stability is possible through further research and control on crystallization kinetics.

5. CONCLUSIONS

This study provides data that can be used for the simulation of systems where the insulating foam is subject or in contact with temperature, in order to assess the suitability of PLA for given applications. As expected for a thermoplastic, compression strength and E modulus steadily decreased with the testing temperature. However no sudden drop in properties was observed around the T_g .

Further research is needed to determine the effects of thermal cycling on PLA insulating foam.

This study is based on a limited number of specimens. Further research is necessary to get a more profound insight in the thermal behaviour of this biodegradable insulation material.

ACKNOWLEDGEMENT

Assistance provided by Marcus Illguth and his staff at HCU on the execution of the experiments is greatly appreciated. Jürgen de Jong at *BEWiSynbra* is gratefully acknowledged for providing the PLA bead foam samples.

AUTHOR CONTRIBUTION

L. Doyle was responsible for the study design and conception, data collection and analysis and chiefly responsible for preparing the manuscript. I. Weidlich provided scientific supervision of the study. Both authors contributed with the critical discussion of the results and editing of the manuscript.

REFERENCES

- [1] Lund H., et al. 4th Generation District Heating (4GDH) Integrating smart thermal grids into future sustainable energy systems. *Energy* 2014;68:1–11. doi:10.1016/j.energy.2014.02.089
- [2] Vigants, E., et al. Modelling of Technological Solutions to 4th Generation DH Systems. *Environmental and Climate Technologies* 2017;20(1):5–23. doi:10.1515/rtuect-2017-0007
- [3] IAL Consultants. The European Market for Thermal Insulation Products. Press Release, 2013.
- [4] EN 253:2009 District heating pipes – Preinsulated bonded pipe systems for directly buried hot water networks – Pipe assembly of steel service pipe, polyurethane thermal insulation and outer casing of polyethylene.
- [5] Dernehl C. U. Health hazards associated with polyurethane foams. *Journal of Occupational Medicine* 1966;8(2):59–62.
- [6] Zapp Jr. J. A. Hazards of Isocyanates in Polyurethane Foam Plastic Production. *Archives of Industrial Health* 1957;15(4):324–330.
- [7] US Department of Labor [Online]. [Accessed 19.11.2018]. Available: <https://www.osha.gov/SLTC/isocyanates/>
- [8] Annex XV Restriction Report – Proposal for a restriction to ECHA by BAuA. Vers 2.1, 2017.
- [9] Gong P., et al. Environmentally-friendly Poly(lactic acid)-based Thermal Insulation Foams Blown with Supercritical CO₂. *Industrial and Engineering Chemistry Research* 2018;57(15):5464–5471. doi:10.1021/acs.iecr.7b05023
- [10] Nofar M., Park C. B. *Poly(lactide) Foams. Fundamentals, Manufacturing and Applications*. Elsevier, 2018. doi:10.1016/C2017-0-00939-4
- [11] Reigner J., Gendron R. Champagne M. F. Extrusion Foaming of Poly(Lactic acid) Blown with CO₂: Toward 100% Green Material. *Cellular Polymers* 2007;26(2):83–115. doi:10.1177/026248930702600202
- [12] Bioplastics Magazine. DYKA premieres world's first plastic pipe system from renewably-sourced plant-based material [Online]. [Accessed 03.02.2016] Available: <https://www.bioplasticsmagazine.com/en/news/meldungen/2016-02-03-DYKA-lauches-bioplasic-pipe-system.php>
- [13] Parker K., Garancher J. P., Shah S., Fernyhough A. Expanded polylactic acid – an eco-friendly alternative to polystyrene foam. *Journal of Cellular Plastics* 2011;47(3):233–243. doi:10.1177/0021955X11404833
- [14] ISO 11357-2:2013 Plastics – Differential scanning calorimetry (DSC) – Part 2: Determination of glass transition temperature and glass transition step height.
- [15] Peelman N., et al. Heat resistance of new biobased polymeric materials, focusing on starch, cellulose, PLA and PHA. *Journal of Applied Polymer Science* 2015;132(48): 42305. doi:10.1002/app.42305
- [16] Auras R., Harte B., Selke, S. An overview of Poly(lactides) as Packaging Materials. *Macromolecular Bioscience* 2004;4(9):835–864. doi:10.1002/mabi.200400043
- [17] Kister G., Cassanas G., Vert M. Effects of morphology, conformation and configuration on the IR and Raman spectra of various poly(lactic acids)s. *Polymer* 1998;39(2):267–273. doi:10.1016/S0032-3861(97)00229-2
- [18] Kister G., et al. Vibrational Analysis of Poly(L-lactic acid). *Journal of Raman Spectroscopy* 1995;26(4):307–311. doi:10.1002/jrs.1250260409
- [19] EN ISO 844:2014 Rigid cellular plastics – Determination of compression properties.
- [20] Weidlich I. Sensitivity analysis on the axial soil reaction due to temperature induced pipe movements. Presented at the 15th International Symposium on District Heating and Cooling, Seoul, South Korea, 2016.
- [21] Garlotta D. A Literature Review of Poly(Lactic Acid). *Journal of Polymers and the Environment* 2001;9(2):63–84. doi:10.1023/A:1020200822435

Annex XII. Publication [B1]

Determination of the melting point depression of PB-1-CO₂ solutions through image analysis

Lucía Doyle
lucia.doyle@hcu-hamburg.de

HafenCity University, Hamburg

Abstract

In the context of replacing polyurethane foam in DH pre-insulated pipes due to the toxicity of the diisocyanates, and facilitating recycling by eliminating the need to separate material layers of the sandwich structure, the foaming of PB-1 with CO₂ is being studied. The assessment of the plasticization effect induced by CO₂ in the polymer melt and determination of the melting point depression is required for the establishment and optimization of the foaming processing window. In this paper, a method for the determination of the melting point through image analysis is presented, validated and used for the study of PB-1 – CO₂ solutions. The obtained results through image analysis agree with those obtained with differential scanning calorimetry, validating the method. The CO₂ - induced melting point depression of PB-1 was determined as $\Delta T = 14^\circ\text{C}$.

Introduction

Heating accounted for 50% of the global energy consumption in 2018, being so the largest energy end-use (IEA, 2019). The integration of renewable energy and waste heat sources could be largely facilitated by District Heating and Cooling (DHC). The backbone of DHC is the piping network, which enables the distribution and exchange of heat and cold between different producers and consumers. The use of polyurethane (PU) pre-insulated pipes has been a fundamental element for the transition from the 2nd to the 3rd Generation DHC (Lund et al., 2014). The PU acts both as insulation, ensuring and significantly increasing the energy efficiency of the system, and as bond between the heat medium pipe and the casing. The toxicity of the diisocyanates (ZAPP, 1957) required for the PU manufacturing and the recently approved restriction on their use (European Commission, 2020) challenge the continuity of PU pre-insulated pipes. With this background, the team of Technical Infrastructure Management HCU opened a research line on alternative polymeric foams which could replace PU in DHC pipelines in 2019 (Doyle, 2021; Doyle & Weidlich, 2019; Doyle & Weidlich, 2020; Doyle & Weidlich, 2021). This includes both the evaluation of commercial foams for the application as well as the foaming of other polymers. With the final goal of developing a pre-insulated pipe made out of a single material, as to facilitate recycling by eliminating the problematic of layer separation in sandwich constructions, the foaming of semicrystalline polybutene-1 (PB-1) is being studied. As for blowing agents, inert gases, mainly CO₂, are considered for environmental reasons.

The success of the foaming process and the morphology of resulting foams is strongly related to the foaming temperature. The foaming temperature window is found between the melting temperature (T_m) and the glass transition temperature (T_g) in the case of amorphous polymers, and between T_m and the crystallization temperature (T_c) for the case of semicrystalline polymers (Di Maio & Kiran, 2018; Sarver et al., 2018). The obtained expansion ratio and cell morphology are conditioned by the relative distance of the foaming temperature from the melting and crystallization temperatures of the polymer-CO₂ dissolution under equilibrium (Sarver et al., 2018). It is well known that the dissolution of CO₂ in a polymer matrix can cause a plasticization effect (Pasquali, Comi, Pucciarelli, & Bettini, 2008; Reignier, Gendron, & Champagne, 2007; Sarver et al., 2018; Takahashi, Hassler, & Kiran, 2012) resulting in a depression of T_m, T_g and T_c, causing a shift on the processing window. Energy savings also arise from the possibility to process at lower temperatures (Frerich, 2015). The determination of these temperatures under CO₂ environment is of great importance for the correct setting and optimization of the process parameters.

Different techniques have been used for the determination of the melting point depression of polymer – CO₂ mixes. Reignier et al. (2007) used high pressure differential scanning calorimetry (HP-DSC) with Poly-ε-Caprolactone (PLC) and CO₂. Kelly et al (2013) used infrared spectroscopy in a high pressure cell with PLC and CO₂. Takebayashi et al. (2014) used near infrared spectroscopy (NIR) with a high-pressure cell for biphenyl and naphthalene under high-pressure CO₂. Frerich (2015) studied the melting behavior of PLA, PBS and PLA-PHS and CO₂ with a scanning transitiometer in a high-pressure cell. Lian et al. (2006) measured the carbon dioxide-induced melting point depression of PCL and PBS though the light transmission change through a view cell. A lamp was placed on one end of the view cell and images captured on the other end via a borescope attached to a videocamera. The polymer chip was placed in the optical path blocking the light, the melting was observed by the sudden light transmission through the cell. It could not be derived if the change detection was human based or computer based. Analogously, Takahashi et al. (2012) studied the melting behavior of biodegradable polyesters in CO₂ at high pressures through changes in the light intensity through the polymer with a view cell, using a photodetector for measuring the light intensity change. Pasquali et al. (2008) studied the meting point reduction of PEG 1500 in supercritical CO₂ via photographs through a view cell. The temperature was fixed and pressure increased until the polymer melting onset, defined as the appearance of the first liquid drop. However, it is not specified how the first drop is detected.

Aside from common the high-pressure cell, the presented methods require complex equipment or rely on human decision to detect a change on a set of images. However, human-scored image analysis is qualitative (Carpenter et al., 2006), and may be exposed to subjectivity and bias, leading to non-reproducible results. Therefore, automated image analysis is preferred. In this paper, a method for the determination of the melting point of polymer CO₂ mixes through digital image analysis and processing is presented and used for the characterization of Polybutene-1 – CO₂ solutions. Tests were undertaken in an autoclave with sapphire windows which allowed for image acquisition.

Data on the melting point depression of PB-1 CO₂ binary system has not been found available in the open literature. Its determination provides valuable information for the optimization of the foaming temperature.

Methods

As materials, PB-1 kindly provided by LyondellBasell, and CO₂ of >99.8% purity purchased from Westfalen were used.

Melting experiments were conducted in an autoclave having two windows opposite each other (Eurotechnica GmbH, Bargteheide, Germany). The autoclave is heated with a heat jacket and CO₂ is injected with a piston pump. The autoclave's inner environment is monitored with a temperature sensor type K with a precision of ±1 °C and a digital pressure sensor with a precision of 0,5%. A light source with variable intensity is placed by one of the windows and a camera (Fastcam SA-X2, Photron Limited, Japan) on the opposite window. The trigger of the camera is coupled to the autoclave control system, so that pressure and temperature are logged simultaneously to the image acquisition. A sketch of the system is provided in Fig.1

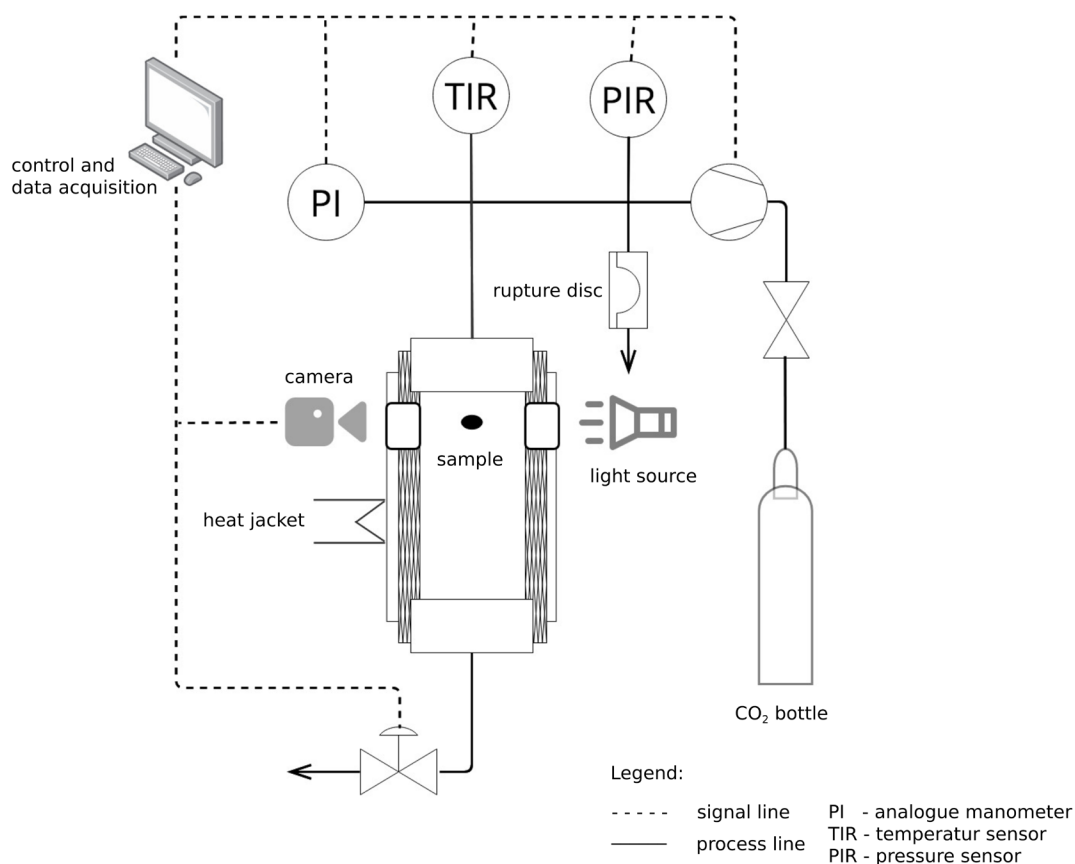


Fig. 1: Schematic representation of the autoclave with coupled image acquisition system

After reaching the required temperature, a pellet is placed centred in the optical path, on an optical glass support. The autoclave is purged 3 times with CO_2 before each trial. CO_2 is then introduced with a stepwise increase in pressure. Images are acquired in 20 s intervals and data logged accordingly. Trials were conducted in triplicate.

An image processing and analysis pipeline was developed using the open-source software Cell Profiler (Carpenter et al., 2006; Kamensky et al., 2011) version 4.1.3. The main steps included converting each image to greyscale, inverting image intensities, identifying the pellet (segmentation) and measuring the pellet. The full list of parameters measured is presented in Table 1. The pipeline is available at https://github.com/LuciaDoyle/MeltingPoint_ImageAnalysis.git

Area	Eccentricity	Median Radius
Bounding Box Area	Equivalent Diameter	Min Feret Diameter
Bounding Box Maximum X	Euler Number	Minor Axis Length
Bounding Box Maximum Y	Extent	Orientation
Bounding Box Minimum X	Form Factor	Perimeter
Bounding Box Minimum Y	Major Axis Length	Solidity
Center X	Max Feret Diameter	Center X
Center Y	Maximum Radius	Center Y
Compactness	Mean Radius	Center Z

Tab. 1: Parameters measured for the pellet in each image

Reproducibility was evaluated by running multiple sets of experiments and comparing the results. The method was validated through comparing the results of melting under atmospheric conditions obtained from the image analysis with the typical differential scanning calorimetry (DSC) curve provided by the manufacturer. For the tests under pressure, the duration of the intervals was established after running successive trials with increasing interval duration to confirm the attainment of equilibrium conditions.

Once the method was validated, the melting point depression of PB-1 was determined by executing successive runs at different temperatures. In each run the temperature would be fixed, and CO₂ pressure increased in 5 bar steps. Reported results were executed with an initial stabilization time of 2 h at the first pressure level and the successive pressure increases conducted in 1 h intervals.

Results

Method Validation

In order to validate the method, the relationship between geometrical deformation measured through the image analysis and polymer melting was proven. For this, a pellet was placed in the view cell and progressively heated up to 150 °C, which is above the melting point of PB-1, reported in the data sheet as 131°C.

The obtained sequence of image measurements is compared with the typical PB-1 DSC curve provided by the manufacturer in Fig. 2. For ease of analysis, eccentricity and major axis length were selected as reference parameters. Eccentricity is defined as the ratio of the distance between the foci of the ellipse and its major axis length, corresponding $e=0$ to a circle. Major axis length is length of the major axis of the ellipse that has the same normalized second central moments as the region, given in pixels (Rocha, Velho, & Carvalho, 2002).

It should be noted that PB-1 is polymorphic and undergoes crystal–crystal transformation at room temperature. When cooling from the melt, it crystallizes into Form II, which is metastable and characterized by a tetragonal unit cell. It then undergoes transformation into Form I stable crystals (Boor & Mitchell, 1963; Jones, 1963; Natta, Corradini, & Bassi, 1960), a process reported to have a duration of around 10 days depending on the storage conditions (Hadinata et al., 2007). Data reported corresponds to the melting of Form I.

Figure 2. (a) presents the parameters eccentricity and major axis length measured through the images (b) the DSC heating ramp, (c) the first image of the sequence, corresponding to the pellet in the solid state and (d) the last image of the sequence, corresponding to the pellet in the molten state.

A very good correlation between graphs (a) and (b) can be observed, showing how the selected geometrical parameters correlate unequivocally with the melting event. Fig. 2 (c) shows the first image of the sequence, and (d) the last, where the change in geometry can be observed. The change is not abrupt enough as to determine the onset with ease through the naked eye. It can be observed that the major axis length decreases during the melting event, which seems counterintuitive. It should be noted that when the region is fitted to an ellipse, it does not necessarily have its major axis parallel to the x axis. Moreover, since the best fit ellipse is found per image, it may change its orientation between images. Indeed it does change orientation during the melting event, causing the effect of the major axis length decreasing.

For the determination of the melting point of the polymer-CO₂ solution, the selected procedure was to fix a temperature and progressively increase the pressure, which was conducted in 5 bar steps, given the constant volume of the autoclave. The melting point depression is explained in terms of solubility effect, with the CO₂ acting as diluent in the melt (Lian et al., 2006). In order to ensure equilibrium conditions, care was taken in establishing the pressure increase duration steps. Trials were conducted with increasingly longer time steps, from 30 minutes to 2 hours. Procedure was fixed at 1 h time steps after a 2 h stabilization period at the initial conditions.

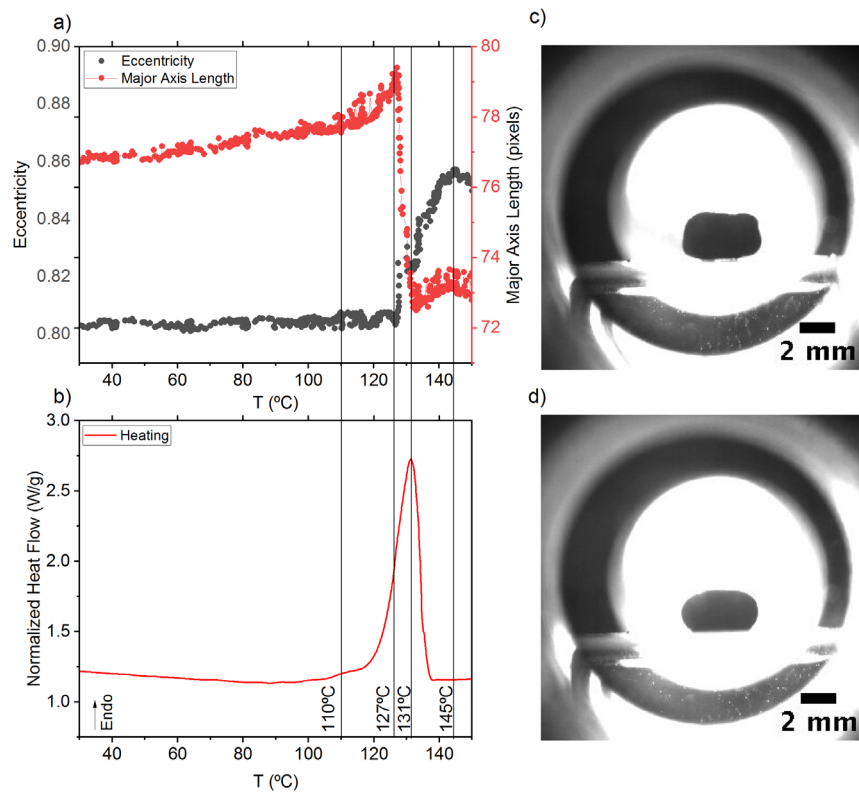


Fig. 2: (a) pellet deformation measured from the images during temperature increase. (b) DSC heating ramp. (c) initial pellet image. (d) last pellet image (molten)

Determination of melting point depression of PB-1 under CO₂

Representative runs for different set temperature are presented in Fig. 3. Additional trials at 112°C and 105°C were executed, where no melting was achieved with the pressures run up to 110 bar. The arrows highlight the melting point.

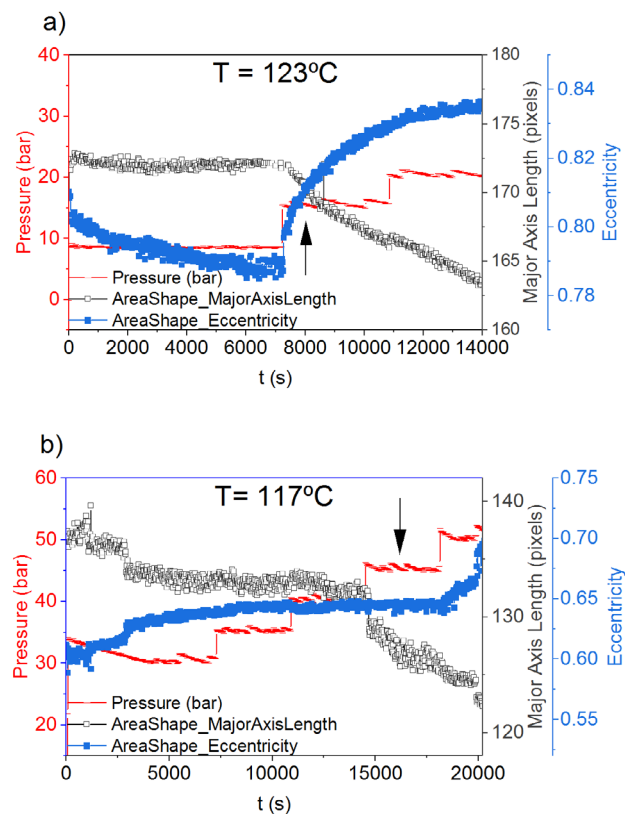


Fig. 3: Representative runs conducted at T = 123°C (a) and 117°C (b)

The obtained melting points as a function of pressure are given in Fig. 4. As can be seen, the melting point of PB-1 decreases linearly down to 117°C, with a pressure of 45 bar. This represents a ΔT_m depression of 14°C.

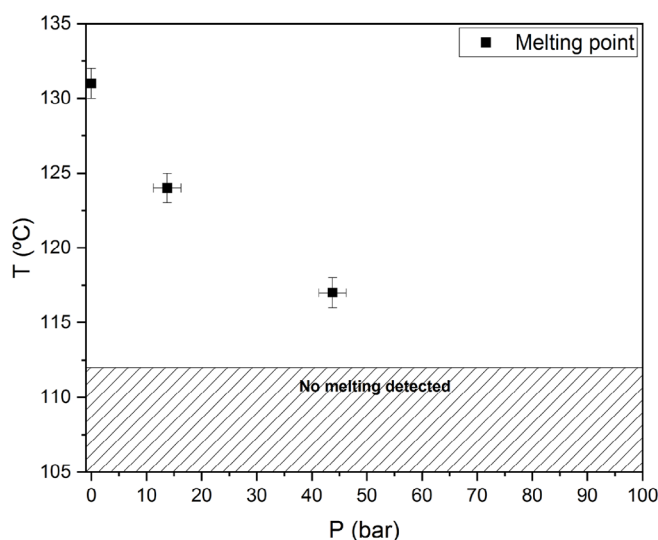


Fig. 4: Melting point of PB-1 in the presence of CO₂ at different pressures

The shape of the plot corresponds to that typically encountered in other polymer-CO₂ solutions, where the melting point decreases linearly with P until an abrupt change in slope occurs, from which the melting point remains more or less constant (Lian et al., 2006; Pasquali et al., 2008; Sarver et al., 2018; Takahashi et al., 2012). This change in behaviour is explained through solubility effects at low pressures, as the addition of low concentrations of a diluent in a melt depresses the pure component melting point, and by hydrostatic pressure effect increasing the melting temperature at higher pressures (Swaan Arons & Diepen, 1963). In order to measure the values after the kink point, a variable cell would be required, as to fix a temperature and progressively increase the pressure. The extent of the melting point depression can be correlated to the amount of absorbed CO₂ (Fukné-Kokot, König, Knez, & Škerget, 2000; Pasquali et al., 2008; Sarver et al., 2018), which is dependent on the applied pressure at a given temperature.

The CO₂ – induced plastitization effect observed in PB-1 is consistent with that reported by (Shi, Wu, Li, Liu, & Zhao, 2009) through the reduction of T_c. In their study, they report a depression of T_c from 90°C under atmospheric conditions to 60°C under supercritical CO₂ at 8 MPa when free cooling from the melt at 170°C, as detected with in-situ FTIR. This data also complements our findings towards the establishment of the processing window, since T_c cannot be detected through the here presented method. It should be however noted that unlike T_m, T_c is a second order transition and its value dependent on the cooling rate applied during the measurement (van Krevelen & Nijenhuis, 2009). The cooling rate at which the “free-cooling” occurred in the experiments by (Shi et al., 2009) is not reported. Data from the manufacturer provides a T_c of 71°C at a rate of 10°C/min, suggesting a much slower rate in the study by Shi et al.

Conclusion

This work demonstrates that the measurement of a sample’s geometrical features through image analysis is a powerful technique for the determination of the melting point in polymers and polymer-CO₂ solutions.

The melting point depression of PB-1-CO₂ mixtures was observed and quantified to $\Delta T = 14^\circ\text{C}$. This provides useful information for the study and optimization of PB-1 foaming with CO₂.

Acknowledgement

The author would like to thank Werner Rothhöft (Lyondellbasell) for providing the PB-1 and Marcus Illguth (HCU) for programming the autoclave control software and Easter Egg hunt.

Literature

Boor, J., & Mitchell, J. C. (1963). Kinetics of crystallization and a crystal-crystal transition in poly-1-butene. *Journal of Polymer Science Part A: General Papers*, 1(1), 59–84.

Carpenter, A. E., Jones, T. R., Lamprecht, M. R., Clarke, C., Kang, I. H., Friman, O., et al. (2006). CellProfiler: image analysis software for identifying and quantifying cell phenotypes. *Genome biology*, 7(10), R100.

Di Maio, E., & Kiran, E. (2018). Foaming of polymers with supercritical fluids and perspectives on the current knowledge gaps and challenges. *The Journal of Supercritical Fluids*, 134, 157–166.

Doyle, L., & Weidlich, I. (2019). Mechanical Behaviour of Polylactic Acid Foam as Insulation Under Increasing Temperature. *Environmental and Climate Technologies*, 23(3), 202–210.

Doyle, L., & Weidlich, I. (2020). Recyclable Insulating Foams for High Temperature Applications. In *Proceedings of The First International Conference on Green Polymer Materials 2020* (p. 7200).

Doyle, L. (2021). Extrusion foaming behavior of polybutene-1. Toward single-material multifunctional sandwich structures. *Journal of Applied Polymer Science*, 15, 51816.

Doyle, L., & Weidlich, I. (2021). Sustainable insulation for sustainable DHC. *Energy Reports*, 7, 150–157.

European Commission (2020). Commission Regulation (EU) 2020/1149 of 3 August 2020 amending Annex XVII to Regulation (EC) No 1907/2006 of the European Parliament and of the Council concerning the Registration, Evaluation, Authorisation and Restriction of Chemicals (REACH) as regards diisocyanates: (EU) 2020/1149. In *Official Journal of the European Union*.

Frerich, S. C. (2015). Biopolymer foaming with supercritical CO₂—Thermodynamics, foaming behaviour and mechanical characteristics. *The Journal of Supercritical Fluids*, 96, 349–358.

Fukné-Kokot, K., König, A., Knez, Ž., & Škerget, M. (2000). Comparison of different methods for determination of the S–L–G equilibrium curve of a solid component in the presence of a compressed gas. *Fluid Phase Equilibria*, 173(2), 297–310.

Hadinata, C., Boos, D., Gabriel, C., Wassner, E., Rüllmann, M., Kao, N., & Laun, M. (2007). Elongation-induced crystallization of a high molecular weight isotactic polybutene-1 melt compared to shear-induced crystallization. *Journal of Rheology*, 51(2), 195–215.

IEA (2019). *Renewables 2019*. IEA. Retrieved October 29, 2021, from <https://www.iea.org/reports/renewables-2019>.

Jones, A. T. (1963). Polybutene-1 – type II crystalline form. *Journal of Polymer Science Part B: Polymer Letters*, 1(8), 455–456.

Kamentsky, L., Jones, T. R., Fraser, A., Bray, M.-A., Logan, D. J., Madden, K. L., et al. (2011). Improved structure, function and compatibility for CellProfiler: modular high-throughput image analysis software. *Bioinformatics (Oxford, England)*, 27(8), 1179–1180.

Kelly, C. A., Harrison, K. L., Leeke, G. A., & Jenkins, M. J. (2013). Detection of melting point depression and crystallization of polycaprolactone (PCL) in scCO₂ by infrared spectroscopy. *Polymer Journal*, 45(2), 188–192.

Lian, Z., Epstein, S. A., Blenk, C. W., & Shine, A. D. (2006). Carbon dioxide-induced melting point depression of biodegradable semicrystalline polymers. *The Journal of Supercritical Fluids*, 39(1), 107–117.

Lund, H., Werner, S., Wiltshire, R., Svendsen, S., Thorsen, J. E., Hvelplund, F., & Mathiesen, B. V. (2014). 4th Generation District Heating (4GDH). *Energy*, 68, 1–11.

Natta, G., Corradini, P., & Bassi, I. W. (1960). Crystal structure of isotactic poly-alpha-butene. *Il Nuovo Cimento*, 15(S1), 52–67.

Pasquali, I., Comi, L., Pucciarelli, F., & Bettini, R. (2008). Swelling, melting point reduction and solubility of PEG 1500 in supercritical CO₂. *International journal of pharmaceuticals*, 356(1-2), 76–81.

Reignier, J., Gendron, R., & Champagne, M. F. (2007). Autoclave Foaming of Poly(ε-Caprolactone) Using Carbon Dioxide: Impact of Crystallization on Cell Structure. *Journal of Cellular Plastics*, 43(6), 459–489.

Rocha, L., Velho, L., & Carvalho, P. (2002). Image moments-based structuring and tracking of objects. In L. M. G. Gonçalves & S. R. Musse (Eds.), *15th Brazilian symposium on computer graphics and image processing* (pp. 99–105). IEEE Comput. Soc.

Sarver, J. A., Sumey, J. L., Williams, M. L., Bishop, J. P., Dean, D. M., & Kiran, E. (2018). Foaming of poly(ethylene -co- vinyl acetate) and poly(ethylene -co- vinyl acetate -co- carbon monoxide) and their blends with carbon dioxide. *Journal of Applied Polymer Science*, 135(7), 45841.

Shi, J., Wu, P., Li, L., Liu, T., & Zhao, L. (2009). Crystalline transformation of isotactic polybutene-1 in supercritical CO₂ studied by in-situ fourier transform infrared spectroscopy. *Polymer*, 50(23), 5598–5604.

Swaan Arons, J. de, & Diepen, G. A. M. (1963). Thermodynamic study of melting equilibria under pressure of a supercritical gas. *Recueil des Travaux Chimiques des Pays-Bas*, 82(3), 249–256.

Takahashi, S., Hassler, J. C., & Kiran, E. (2012). Melting behavior of biodegradable polyesters in carbon dioxide at high pressures. *The Journal of Supercritical Fluids*, 72, 278–287.

Takebayashi, Y., Sue, K., Furuya, T., Hakuta, Y., & Yoda, S. (2014). Near-infrared spectroscopic solubility measurement for thermodynamic analysis of melting point depressions of biphenyl and naphthalene under high-pressure CO₂. *The Journal of Supercritical Fluids*, 86, 91–99.

van Krevelen, D. W., & Nijenhuis, K. t. (2009). *Properties of polymers: Their correlation with chemical structure ; their numerical estimation and prediction from additive group contributions / D.W. van Krevelen (4th, completely rev. ed. / rev. by K. te Nijenhuis)*. Amsterdam, Boston: Elsevier.

ZAPP, J. A. (1957). Hazards of isocyanates in polyurethane foam plastic production. *A.M.A. archives of industrial health*, 15(4), 324–330.

